



HAL
open science

Synthèse de matériaux monolithiques pour la séparation et la catalyse en phase liquide : problématiques environnementales et du développement durable

Seydina Ibrahima Kebe

► **To cite this version:**

Seydina Ibrahima Kebe. Synthèse de matériaux monolithiques pour la séparation et la catalyse en phase liquide : problématiques environnementales et du développement durable. Recherche opérationnelle [math.OC]. Université Paris-Est, 2016. Français. NNT : 2016PESC1127 . tel-01668547

HAL Id: tel-01668547

<https://theses.hal.science/tel-01668547>

Submitted on 20 Dec 2017

HAL is a multi-disciplinary open access archive for the deposit and dissemination of scientific research documents, whether they are published or not. The documents may come from teaching and research institutions in France or abroad, or from public or private research centers.

L'archive ouverte pluridisciplinaire **HAL**, est destinée au dépôt et à la diffusion de documents scientifiques de niveau recherche, publiés ou non, émanant des établissements d'enseignement et de recherche français ou étrangers, des laboratoires publics ou privés.

Université Paris EST

Ecole Doctorale Sciences, Ingénierie et Environnement



THESE DE DOCTORAT

Présentée par:

SEYDINA IBRAHIMA KEBE

Pour obtenir le grade de Docteur de l'Université Paris EST

Spécialité : Chimie et Sciences des Matériaux

Sujet de Thèse :

***Synthèse de matériaux monolithiques pour la
séparation et la catalyse en phase liquide:
Problématiques environnementales et du
développement durable***

Soutenance le 9 décembre 2016

Devant la commission d'examen formée de :

K. Faure : Chargée de recherche, CNRS	Rapporteur
T. Tran-Maignan : Maître de conférences	Rapporteur
F. Le Derf : Professeur	Examineur
A. Elaissari : Directeur de recherche, CNRS	Examineur
A. Bressy : Chargée de recherche, CNRS	Membre invité
M. Guerrouache : Ingénieur de recherche	Membre invité
B. Carbonnier : Professeur	Directeur de thèse

Thèse réalisée au sein de l'équipe Systèmes Polymères Complexes, ICMPE, CNRS, Thiais France

Remerciements

Je tiens à profiter de ce rapport pour exprimer mes plus grands et chaleureux remerciements envers tous ceux qui ont, en leur manière, contribué à la réussite de cette thèse

Cette thèse a pu être réalisée grâce à l'accueil Madame Valérie LANGLOIS adjointe directrice de l'ICMPE, directrice du SPC professeur et chercheuse à l'Université Paris Est Créteil (UPEC). Je lui témoigne ma reconnaissance.

Je n'aurais jamais commencé sans exprimer tout particulièrement mes plus grands remerciements et à témoigner toute ma reconnaissance à Benjamin CARBONNIER mon directeur de thèse, professeur des universités à l'UPEC pour l'expérience enrichissante qu'il m'a fait vivre. De simples mots, ne sauraient décrire ma satisfaction à son égard.

Je tiens à remercier Mohamed GUERROUCHE, ingénieur, pour son temps consacré à me donner des explications et à me guider. Son aide a comblé mes espérances.

Je remercie aussi Sami MAHOUCHE-CHERGUI pour ses explications et sa gentillesse.

Je n'oublie pas de formuler des remerciements en vers Sabrina BELBEKOUICHE maître de conférences à l'UPEC pour son soutien, son assistance et les nombreuses discussions scientifiques et autres☺.

Je tiens bien sûr à remercier également toute l'équipe du SPC pour leur accueil, leur disponibilité, leur écoute et leur bonne humeur tout au long de ma thèse. Je n'oublie jamais la table de midi partagée avec Tina Modjinou, Carine Mangeon « Chérie coco », Erica Rodi Géa, Pierre Pubellier, Mohamed Ghazi Ayari, Antoine Benlahoues, Romain Poupart « le petit », Etienne Dessauw et Guillaume Péréra ATER.

Je n'oublie pas de remercier le jury : examinateurs et rapporteurs pour leur temps passé à juger mes travaux ainsi que tout le public présent lors de la présentation orale de cette thèse.

Je remercie aussi Rémy Pires pour toutes ses analyses microscopiques et Léon Preira responsable de l'atelier mécanique.

Merci à toute ma famille plus particulièrement à ma charmante maman, Mariama THIAM. Je lui souhaite une longue vie saine et riche. Merci mon bonheur, ma femme Fatima DIANKHA.

A la mémoire de mon père. Paix à son âme !!

Sommaire

Introduction générale 1

Chapitre I:

Article 1: Surface Engineering of Porous Monoliths via Click Chemistry: Towards functional materials for Flow Chemistry Applications 8

Chapitre II:

Article 2: Thiol-Ene Click Chemistry for the Design of Diol Porous Monolith with hydrophilic Surface Interaction Ability: A Capillary Electrochromatography Study 57

Article 3: Novel monolithic stationary phase with surface-grafted triphenyl selector for reversed-phase capillary electrochromatography 75

Article 4: Using capillary electrophoresis and electrochromatography for *in situ* detection of diverse organic molecules in space 92

Chapitre III:

Article 5: Aniline-grafted monolith as electrochromatographic and nano-gold catalyst supports: New implementation of diazonium salt chemistry 110

Chapitre IV:

Article 6: Metal nanoparticles @ monolithic supports as continuous- microreactor for the catalytic reduction of mono and disubstituted nitroaromatics, oxydation of benzyl alcohol and Suzuki-Miyaura carbon-carbon coupling reactions 133

Chapitre V :

Article 7 : 169

Annexes

Introduction générale

Les problématiques environnementales sont devenues une préoccupation majeure des pays développés depuis la deuxième moitié du XX^{ème} siècle avec la prise de conscience du rôle de l'environnement dans le développement des sociétés et les dégradations induites par notre système économique.¹ Au cœur des débats, se trouvent notamment les questions liées au développement des villes, aux modes de vie, à la mobilité, à la consommation..., et leur impact sur la santé et l'environnement.

La chimie a joué un rôle moteur dans tous ces domaines. Même si la tendance actuelle est nettement à la « chimie verte », elle ne doit pas masquer l'utilisation toujours plus abondante de produits chimiques. Parmi les divers produits chimiques utilisés en quantités considérables, on peut en citer la famille des phénols, des dérivés chlorés dont les polychlorobiphényles, des chlorophénols, des anilines, des dérivés nitrés dont les pesticides, des hydrocarbures aromatiques polycycliques, des parabènes. Ces produits ont été déclarés toxiques par plusieurs agences gouvernementales, nationales et internationales et ajoutés à la liste des substances les plus préoccupantes dont l'utilisation devrait être éliminée dans le futur.^{2,3} A titre d'exemple, l'aniline, toxique par inhalation et contact est susceptible d'induire des anomalies génétiques et de provoquer le cancer.

Evaluer et réduire l'impact de la chimie sur l'environnement nécessite une vision globale, allant de la chimie analytique, aux traitements d'effluents contaminés et vers l'optimisation des procédés de synthèse respectueux de l'environnement. Cette démarche s'inscrit dans un contexte socio-économique, où acteurs privés et publics ont bien souvent des intérêts divergents.

Les progrès scientifiques et technologiques spectaculaires enregistrés récemment non seulement dans le domaine de la chimie analytique mais également des procédés catalytiques ont été possibles, en partie, grâce à l'émergence des nouvelles technologies, avec pour enjeu la conception, l'élaboration et le contrôle d'objets de plus en plus petits, jusqu'à atteindre une taille microscopique et même nanométrique aujourd'hui. En effet, une des tendances actuelles des technologies appliquées aux sciences séparatives est la miniaturisation à l'échelle micrométrique des systèmes chromatographiques. De la même façon, l'utilisation de catalyseurs version « nanométrique » a connu un succès non démenti jusqu'à présent.

Cette thèse a visé l'élaboration de nouveaux outils pour, non seulement, l'analyse de polluants organiques par voies chromatographique et spectroscopique, mais également leur traitement par voie catalytique. La stratégie générale repose sur la technologie des adsorbants monolithiques organiques qui sont au cœur de ce projet de thèse. Les monolithes à base de polymères organiques ont vu le jour dans les années 90. Ils ont été proposés comme matériaux hautement perméable pour la préparation de phases stationnaires pour la chromatographie liquide. Dans notre cas, le squelette monolithique a été préparé en une seule étape par photopolymérisation radicalaire d'un mélange introduit dans un capillaire sous forme liquide. Le mélange est composé de monomère porteur d'un greffon latéral (N-acryloxysuccinimide ou NAS) dont les unités N-hydroxysuccinimides confèrent une réactivité de surface au monolithe, d'un réticulant (éthylène glycol diméthacrylate ou EDMA) qui assure la tenue mécanique du matériau final, un agent porogène (toluène, dodécanol, diméthylsulfoxyde, diméthylformamide) qui après extraction donne lieu à une porosité (macroporosité) élevée et indispensable à l'écoulement sans perte de charge élevée de la phase mobile, et un amorceur de polymérisation radicalaire (2,2'-azobisisobutyronitrile, ou AIBN). Pour conférer au squelette monolithique des propriétés séparatives, une étape de modification chimie de surface a été envisagée. Cette dernière a été réalisée soit directement par substitution nucléophile des unités N-hydroxysuccinimides par des amines fonctionnelles (triphenylmethylamine, 3,3-diphenylpropylamine) soit en deux étapes impliquant une substitution nucléophile dans le but d'immobiliser des liaisons doubles carbone-carbone, suivie d'une réaction de chimie Click avec un thiol fonctionnel. La réaction de chimie Click entre des fonctions alcènes et des thiols est connue sous le nom de réaction thiol-ène qui est en fait une réaction d'addition radicalaire. Ainsi, il a été possible d'introduire à la surface des monolithes des segments moléculaires (diol, di- et tri-phényle) qui contrôlent globalement les propriétés de surfaces desdits monolithes notamment en termes de degré d'hydratation, de balance hydrophile/hydrophobe, de mécanisme d'interaction en milieu liquide et de propriétés chélatantes.

Durant cette thèse nous nous sommes intéressés à deux techniques d'analyse. D'une part, l'électrochromatographie capillaire et d'autre part la diffusion Raman exaltée de surface, plus communément appelées CEC et SERS pour leurs acronymes anglais (Capillary ElectroChromatography et Surface-Enhanced Raman Spectroscopy). Ces méthodes ont été appliquées à la séparation (CEC) et la détection (SERS) de molécules organiques dont des polluants.

Pour ces deux méthodes, des matériaux monolithiques ont été mis en œuvre soit sous la forme d'objets 3D, colonnes monolithiques avec des diamètres micrométriques, et 2D, films monolithiques d'épaisseur micrométriques.

L'électrochromatographie combine certains des avantages des techniques plus classiques que sont la chromatographie liquide et l'électrophorèse capillaire. L'électrochromatographie repose en effet sur l'utilisation combinée d'une phase stationnaire, apportant la sélectivité au système séparatif et d'un flux électroosmotique assurant la migration de la phase mobile et des analytes. La sélectivité est contrôlée par la chimie de surface des monolithes peut facilement être ajustée à la séparation de composés polaires, apolaires, chiraux...

L'autre technique d'analyse de polluants développée dans ce travail est la spectroscopie de Raman exaltée de surface. La spectroscopie Raman est basée sur la diffusion inélastique de la lumière, permettant d'obtenir des informations vibrationnelles et des signatures spectrales caractéristiques des molécules sondées. La technique Raman souffre de la faiblesse de l'intensité du signal de diffusion. Cependant, il est possible d'induire une exaltation dite "de surface" en utilisant des substrats métalliques nanostructurés ou des supports décorés par des nanomatériaux métalliques. C'est cette seconde approche que nous avons suivie en décorant des monolithes successivement par des groupements chélatants puis par des nanostructures d'or.

Après avoir identifié et détecté des molécules polluantes, une autre question se pose, celle de la réduction de leur impact dans l'environnement. Pour le traitement des polluants organiques, la voie catalytique a été choisie. La catalyse est un procédé chimique découvert au 19^{ème} siècle par le danois Jöns Jakob Berzélius. Il s'agit d'une action par laquelle une substance, utilisée en faible quantité, accélère une réaction chimique, en se retrouvant intacte à l'issue de celle-ci. L'étude et le développement de procédés catalytiques, bien que très anciens, connaissent toujours un fort engouement tant sur les plans académique qu'industriel.

L'une des préoccupations majeures concerne la récupération et le recyclage des catalyseurs. Plusieurs approches sont possibles telles que la catalyse diphasique et la catalyse supportée. Dans notre cas, nous avons envisagé le thème de la catalyse supportée, utilisant des catalyseurs nanométriques. Notre objectif consistait à immobiliser des nanocatalyseurs métalliques (Au, Pd, Ag...) de tailles ajustables à la surface d'un support monolithique

préalablement synthétisé et fonctionnalisé en vue de permettre l'ancrage robuste et la stabilisation des nanoparticules à la surface de monolithes. En effet, en solution les nanoparticules présentent de fortes activités catalytiques mais restent très sensibles à l'agrégation, un phénomène qui est souvent néfaste aux propriétés catalytiques. Les nanocatalyseurs utilisés dans ce travail se présentent sous deux morphologies : des nanoparticules sphériques et des nanofleurs.

Ici, la synergie entre les propriétés intrinsèques des deux partenaires, à savoir haute perméabilité pour les supports monolithiques, et haute activité catalytique pour les nanoparticules, a été mise à profit pour l'élaboration de microréacteurs à base de monolithes modifiés par des nanostructures métalliques pour la réalisation de réactions catalytiques, telles que la réduction de groupements nitro, l'oxydation de fonction alcool, et le couplage carbone-carbone en flux continu. Les propriétés catalytiques ont été discutées en fonction de la méthode d'immobilisation et la taille des nanoparticules, du débit et de la température.

Cette stratégie a été finalement transposée à l'élaboration de films monolithiques nanostructurés et servant de substrats actifs vis-à-vis de la réduction et la détection SERS de pesticides.

L'ensemble de ces travaux est présenté dans la suite de cette contribution sous la forme de cinq chapitres.

Le premier chapitre de ce manuscrit, intitulé *Surface Engineering of Porous Monoliths via Click Chemistry: Towards Functional Materials for Flow Chemistry Applications* qui a été accepté pour une parution comme chapitre dans l'ouvrage *Click Chemistry, Approaches, Applications and Challenges*, édité par NOVA Publishers, propose une mise au point bibliographique des méthodes récentes utilisées pour l'élaboration ou la modification chimique de monolithes. Cette contribution montre l'importance grandissante des approches par Chimie click dans le domaine des matériaux monolithiques dédiés aux sciences séparatives et à la catalyse. Les mécanismes des réactions de chimie Click mises en œuvre sont brièvement présentés.

Le deuxième chapitre de ce manuscrit est consacré aux résultats expérimentaux obtenus dans le cadre de l'élaboration de monolithes pour l'électrochromatographie capillaire. Nous présentons dans cette section l'élaboration et la caractérisation de monolithes modifiés par des sélecteurs de type diol ou phényle. Différentes familles de molécules ont été étudiés (phénols,

anilines, bases pyrimidiques, hydrocarbures aromatiques polycycliques) afin de parfaitement illustrer les propriétés séparatives et l'efficacité des microsystemes séparatifs mis en œuvre, et de prouver que les mécanismes mis en jeu sont dictés par la nature des greffons. Nous avons aussi appliqué ces monolithes à l'étude de matrices réelles, telles que des parabènes dans des crèmes cosmétiques commerciales ou des hydrocarbures aromatiques polycycliques dans des sols.

Le troisième chapitre présente une nouvelle méthode d'immobilisation de nanoparticules d'or à la surface de monolithes *via* la chimie interfaciale des sels de diazonium. Cette partie présente aussi la transition de l'application de monolithes depuis l'électrochromatographie vers la catalyse supportée en flux continu. L'intermédiaire clé est un monolithe modifié en surface par des groupements aniline. Ces derniers servent de sélecteur dont les propriétés de séparation sont fortement guidées par la nature riche en électrons du cycle aromatique du fait de l'effet mésomère donneur de la fonction amine primaire et de site réactif pour la formation *in situ* d'un sel de diazonium et donc, *in fine*, de site d'ancrage pour des nanoparticules d'or.

Le quatrième chapitre de ce document traite des microréacteurs monolithiques modifiés par des nanosphères d'or ou de palladium et des nanofleurs d'or pour la catalyse en flux continu de la réduction de nitroarènes, de l'oxydation de l'alcool benzylique et du couplage entre le bromobenzène et l'acide phénylboronique. La réduction du paranitrophénol a été utilisée comme réaction modèle pour étudier divers paramètres tels que le débit et la taille des nanoparticules sur les propriétés catalytiques.

Le cinquième chapitre de ce travail présente nos travaux concernant l'élaboration de matériaux monolithiques décorés par des nanofleurs d'or pour la catalyse et la détection par spectroscopie Raman exaltée de surface de molécules toxiques utilisées dans la vie quotidienne, à savoir des pesticides.

Le chapitre 6 présente une conclusion et les perspectives à ce travail.

En annexe, nous présentons une mise au point bibliographique publiée dans la revue *Surface Innovations* et intitulée *Monoliths bearing hydrophilic surfaces for in vitro biomedical samples analysis*, par Mohamed Guerrouache, Ahmed M. Khalil, Seydina Ibrahima Kebe, Benjamin Le Droumaguet, Samia Mahouche-Chergui, Benjamin Carbonnier 3 (2015) 84–102 DOI: <http://dx.doi.org/10.1680/sufi.14.00011> ainsi que des travaux traitant de microréacteurs

monolithiques dédiés à la catalyse de dérivés nitrés. Dans cette dernière contribution, l'effet de la taille de nanoparticules d'or sur leur état de dispersion en surface est étudié en détail.

(1) <http://www.un.org/french/events/wssd/pages/cnued.html>.

(2) <https://www.ec.gc.ca/lcpe-cepa/default.asp?lang=Fr&n=0DA2924D-1>.

(3) Vincent GRAMMONT, C. B., Hiérarchisation des substances : Identification des listes existantes de substances prioritaires, Rapport d'étude 15/12/2009 N° DRC-09-104007-10463A, <http://www.ineris.fr/centredoc/rapport-drc-09-104007-10463a-1352824865.pdf>.

CHAPITRE I

Objectifs

Proposer une mise au point bibliographique des avancées récentes portant sur l'utilisation de la chimie click pour l'élaboration de monolithes perméables et fonctionnels.

Présenter une introduction à la chimie Click utiles aux novices et aux experts.

Mettre en évidence les apports de la chimie Click pour d'une part la préparation de monolithes hybrides organiques-inorganiques et d'autre part la fonctionnalisation de surface de monolithes réactifs.

Limites

Le choix des références a été guidé par le titre de l'ouvrage dans lequel sera publiée cette contribution.

A ce titre, les méthodes autres que celles faisant appel à la chimie Click ne sont pas passées en revue.

Surface Engineering of Porous Monoliths via Click Chemistry: Towards Functional Materials for Flow Chemistry Applications

Seydina Ibrahima Kebe,¹ Hela Kammoun,^{1,2} Mohamed Guerrouache,¹ Samia Mahouche-Chergui,¹ Sabrina Belbekhouche,¹ Benjamin Le Droumaguet,¹ Yosra Dridi-Zrelli,² Benjamin Carbonnier¹

¹ Université Paris-Est, ICMPE (UMR7182), CNRS, UPEC, F-94320 Thiais, France.

² Département de Génie Chimique-Université Libre de Tunis, 32 Avenue Kheireddine Pacha 1002 Tunis, Tunisie.

Keywords: Capillary column, Chromatography, Click chemistry, Micro-reactor, Monolith, Surface functionalization.

1. Introduction

Control at the molecular-level of the chemical nature of pores surface is of utmost importance for predicting the overall behavior of porous materials with potential flow-through uses.¹ This is notably true for monoliths which are defined as single continuous pieces of highly cross-linked and porous materials. Monoliths of organic, inorganic and hybrid nature, have continuously gained interest over the last quarter of century as stationary phases for capillary chromatographic and electrochromatographic applications, as solid sorbents for extraction and preconcentration purposes.^{2,3} Monoliths exhibit unmatched intrinsic properties as they offer, for instance, highly efficient mass transfer kinetics in contrast to their particulate counterparts. Monoliths can be prepared via different synthetic strategies as the traditional free radical polymerization and vinyl-like monomers and the inorganic polymerization, i.e. sol-gel process, of silane precursors.^{4,5} With the aim to combine both properties of organic and inorganic materials, hybrid monoliths have also met great success. In this regard, many research efforts have been devoted to implement easy elaboration methods with a special focus over the last 15 years on using click chemistry. The copper I-catalyzed Huisgen and Diels-Alder implementations are cycloaddition reactions involving 6π (4+2) electrons ended up with the formation of 5- and 6-membered cycles, respectively. In contrast, the addition of thiols on unsaturated carbon-carbon double and triple bonds is mediated by thiyl radicals, formed in the presence or not of a hydrogen abstractor and leading to the formation of thioether bridge. Alkaline-catalyzed thiol-epoxy click reaction is a well-established polymerization method to prepare linear polymer chains substituted with free hydroxyl groups.⁶ Indeed, beside its high efficiency, this synthetic method leads to the formation of a reactive OH upon upon ring opening. Such reactive polymers can be further functionalized through simple one-step chemistry. Commercial availability, at low cost, of a large range of di-epoxide and bis-sulfur reactants that can serve as comonomers, are additional attributes of this strategy which proved powerful for industrial and biomedical applications. As the reader will discover, or simply remember, by browsing the hereafter sections, these reactions have been implemented either as unique synthesis step, or in combination with other chemical process such as sol-gel, or even as functionalization method of clickable surface for the design of functional monoliths. Much has been said about click reaction in the general domain of organic synthesis and materials science, however their applications to separation and catalysis sciences is incipient, hence the motivation for this contribution. We are presenting a detailed

overview of the Click chemistry strategies recently implemented for the both aspects of the monolithic matrices elaboration and surface modification of monoliths is discussed with respect to the type of the click reaction, nature of the surface grafts and the resulting flow-through applications in the context of analytical sciences for separation, extraction and preconcentration purposes and catalysis technology for the stabilization of nanometals.^{7,8,9,10,11,12} Considering the monolith and Click chemistry pair, it will be shown that while the copper(I)-catalyzed Huisgen 1,3-dipolar cyclo-addition and the thiol-ene addition reaction have been mainly applied, successful achievement of thiol/yne, Diels-Alder 4+2 cycloaddition and thiol-maleimide Michael Addition remains challenging. This work conclusively highlights the synergy of surface Click chemistry and porous monolithic materials for the design of highly permeable materials with specific and selective surface interaction ability. Both fundamental and applied issues are of utmost importance to our ongoing research aiming at developing monolith-based microsystems allowing on-line catalytic reactions and monitoring of the said chemical processes.

2. Scope and aim

In this contribution, general overview about monolithic supports with a specific focus on synthetic routes exploiting the multifaceted toolbox of click chemistry for either the synthesis or surface functionalization of the monolithic skeleton is proposed. Application of the as-prepared monoliths for flow-through processes, namely (electro)chromatographic separation, on line solid phase extraction or preconcentration, as well as enzymatic and heterogeneous catalysis is also discussed and rationalized on the basis of the chemical nature of the used click-compatible partners. The discussion encompasses the field of organic, inorganic and hybrid monolithic materials and includes also a rapid discussion about major characteristics of monolithic materials and click reactions. This chapter is mainly intended to provide a condensed vision of the potential of the monolith & click chemistry tandem to providing functional materials with high potential in flow-chemistry. Hence, the deliberate choice from the authors to discuss well-selected studies independently of chronological considerations but mainly guided by relevance and benefits allowing scientific breakthrough in monolithic materials-related technological fields. This contribution is meant to provide the necessary scientific background to postgraduate students in chemistry and materials science as well as to illustrate very recent developments in the area of monoliths for senior scientists.

3. Key features of monoliths

A monolith, also referred to as a “continuous rod”, can be described as a single large solid particle that does not contain interparticular voids.¹³ In their original variants, in the early 1960s, polymer monoliths were proposed in the form of hydrogel-like materials with loose crosslinking density featuring high compressibility and limited flow rate resistance.¹⁴ The studies reported by the group of Hjertén,^{15,16,17} further complemented by the impressive contribution of Svec^{18,19,20} and his collaborators marked definitively the enshrinement of monoliths as a new generation of stationary phases for liquid-phase separation applications. Tanaka's group^{21,22} has played a major role in the development and reduction to practice of silica-based monolithic columns for separation science. Such columns were proved to provide high-speed, high-efficiency and operation methods allowing significant enhancement of chromatographic performances. Success of monolithic materials in separation science can be rationalized by the presence of large separation pores network providing high permeability and enhanced convective flow-driven mass transfer characteristics.²³ **Figure 1** presents scanning electron microscopy images of polymeric monolithic structures. In contrast to particles filled chromatographic media, for which mass transfer is primarily controlled by diffusion effects and speed is detrimental to resolution, monoliths offer high-resolution separations and no peaks broadening even at high-flow velocity. To date, organic and inorganic monoliths have been applied to reversed-phase,²⁴ charge-transfer,^{25,26} hydrophilic interaction,^{27,28} ion exchange^{29,30} chromatographic modes demonstrating their potential for the separation of amino acids, peptides, proteins, nucleic acids, nitrogenous bases, enantiomers, polar and apolar species with a large panel of molar mass.^{3,31,32}

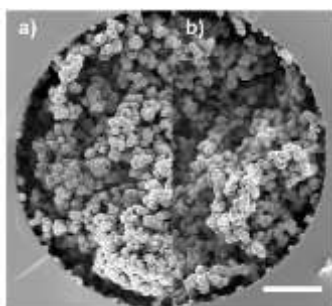


Figure 1. Scanning electron microscopy images showing typical morphology of polymer-based monolith. The two monoliths were prepared within fused-silica capillaries through UV-initiated free radical polymerization with different monomer/crosslinker ratios. The white bar in the figure represents size of 10 μm . Reproduced from ref 31 by permission of Wiley.

Low backpressures, outstanding reproducibility, large loading capacity, stability over a broad range of pH and adjustable surface chemistry are other positive features of monolithic materials. The latter is particularly true for polymeric monoliths whose synthesis can be easily performed through thermal or photochemical free radical polymerization in/on varied substrates such as glass slides, fused silica capillaries as well as PDMS and COC chips.^{33,34} The large variety of readily available (meth)acrylate/styrenic monomers and crosslinkers allows the preparation of monolithic structures with nearly endless possibilities in terms of surface functionality. Through judicious choice of the synthesis conditions, pore size and surface area can be easily tuned. Although the in-microchannel synthesis of silica monoliths is a more complex operation, inorganic-organic monoliths can be easily obtained through various preparation methods.³⁵ All these reasons explain why application features of monoliths are today far beyond separation science and have been generalized to the domain of flow chemistry.

4. Key features of click chemistry

“Click” chemistry including radical addition, cycloaddition, ring opening addition has emerged as an efficient and versatile tool for the synthesis of functional materials.^{36,37} Among the numerous relevant scientific and technological fields, one may cite (i) environmental sciences with chelating magnetic copolymer composites for the removal of metal ions,^{38,39} (ii) life sciences with boronic acid functionalized nanomagnets for glycoproteins enrichment⁴⁰ and enzyme immobilized on magnetic beads for proteomics,⁴¹ (iii) heterogeneous catalysis with magnetic nanoparticle-supported palladium catalysts for Suzuki-Miyaura coupling reactions⁴² bifunctional gold nanoparticles and monolith-immobilized copper nanoparticles for nitrophenol reduction,¹² (iv) sensing with electro-active PEDOT electrodes for label-free electrochemical DNA sensing⁴³, molecularly imprinted polymers grafted onto electrodes for the detection of antioxidant⁴⁴ and bifunctional gold nanoparticles for warfare agent analogues detection,⁴⁵ to mention but a few...

Click chemistry, term originally employed by Sharpless and coworkers to describe the copper-catalyzed azide-alkyne Huisgen dipolar cycloaddition reaction (also shortened as CuAAC), is now generally used to refer to a restricted pool of particular organic reactions that shared together a certain number of synthetic features. Indeed, according to Sharpless, such click reactions should be regio- (and even stereo-) selective, carried out in mild conditions and afford thermodynamically stable products with high yields without the need for tedious

purification procedures.⁴⁶ Additionally, they should only produce very few inoffensive byproducts and be wide in scope. In this context, different reactions have been classified within this conceptual click chemistry toolbox. Thus, in the last 15 years, a particular attention has been paid by the scientific community to a restricted pool of chemical reactions that notably encompass the CuAAC, the thiol-ene and thiol-yne, the thiol-(meth)acrylate Michael addition, the thiol-epoxyde and the Diels-Alder reactions, as shown on **Figure 2**.

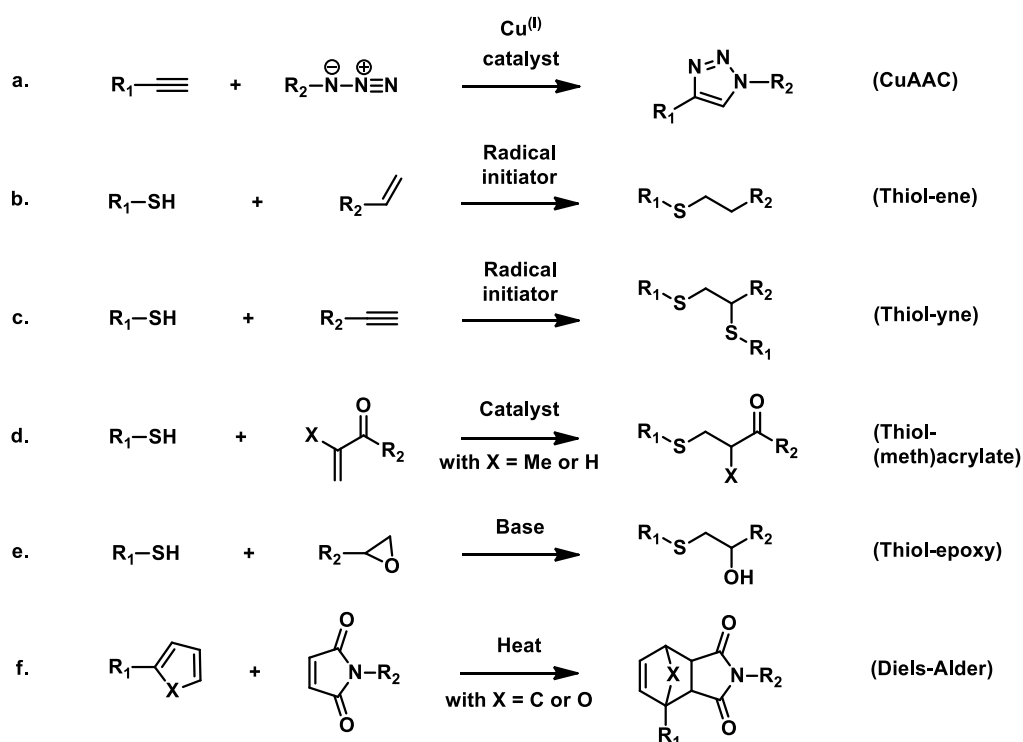


Figure 2. General scheme of the most commonly implemented reactions of the ‘click’ type so far developed for the synthesis and functionalization of monoliths.

Implementation of these click reactions in organic, but more importantly in polymer, materials and surface chemistry has flourished and even exploded in the literature, especially for the design and synthesis of macromolecular architectures (**Figure 3**). Numerous reviews in the field already gave a rather exhaustive overview of all possible applications of this click chemistry toolbox in such research area.^{47,48,49,50,51} It is worth mentioning that most of these click reactions have been discovered a long time ago but so far neglected by scientists that only found them a limited synthetic interest.

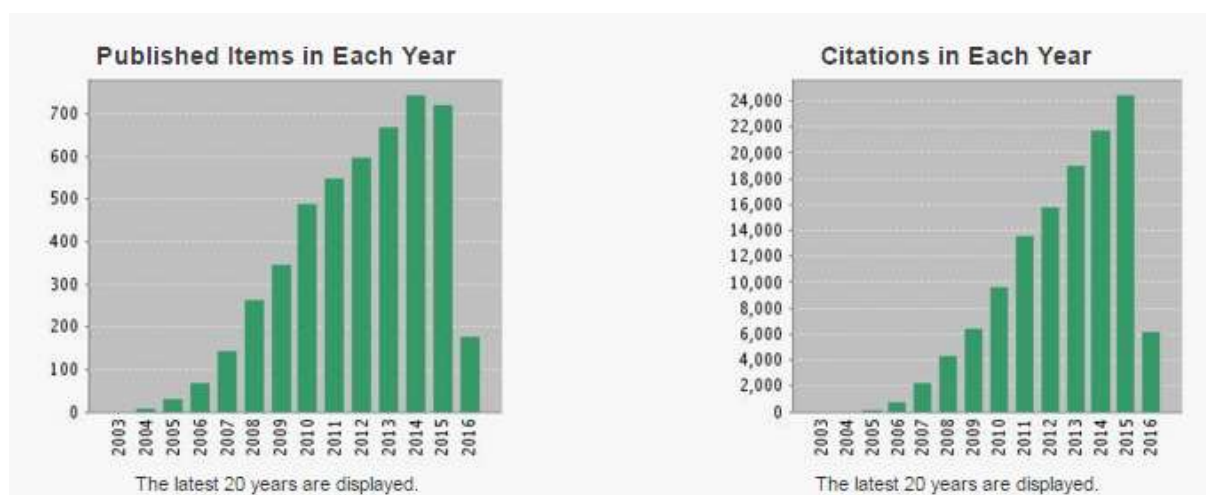


Figure 3. Histograms obtained from Web of ScienceTM displaying the number of published items in each year and the number of citations for each year when searching for “click chemistry” and “polymer” topics on the 2016, April 12th. Figure reproduced from Web of ScienceTM.

This section will emphasize on the particular features of these reactions that make them appealing for material scientists regarding the conception and functionalization of inorganic, hybrid and polymer-based monolithic materials. First of all, considering the topic of this book chapter, it is worth mentioning that chemical functions involved in click chemistry reactions can be easily installed both on organic/inorganic compounds, to be grafted, and onto surfaces, to be functionalized, regardless to the reaction yield. Additionally, some of these starting compounds, and notably a large variety of thiols, alkynes, (meth)acrylates or even alkenes and dienes are rather cheap and generally easy to purchase from chemical providers. On the other hand, such installed clickable functions are chemically inert in various environmental conditions, which is a crucial point regarding the stability in time of such starting materials. More importantly, they are inert under a large variety of reaction conditions, allowing for sequential click reactions to be easily envisioned in both one-pot and orthogonal fashion for instance.^{52,53,54,55,56,57} All these click reactions also give really better yields than more classical coupling ligation strategies, *i.e.* amidation, esterification, *etc.* Last but not least, monitoring of such click chemistry reactions, realized either in solution or at the surface of engineered materials is quite easy to investigate as the consumption of most of the starting materials but also the formation of the resulting products can be easily followed using diverse characterization techniques such as NMR, FT-IR, XPS and Raman spectroscopy for instance. Indeed, clickable functions generally possess particular chemical functions, *e.g.* azides, alkynes, alkenes, thiols, *etc.* that have very specific signature as examined using such physico-chemical techniques.

All these above-mentioned click reactions have been extensively implemented during the last 15 years in macromolecular engineering and for the conception of smart advanced materials and nanomaterials⁵⁸ and especially for the design and synthesis of chromatographic supports based on inorganic, hybrid or polymeric monoliths.

4.1 Copper-catalyzed azide-alkyne Huisgen dipolar cycloaddition reaction (CuAAC)

First discovered by Rolf Huisgen⁵⁹ in 1963 and considered in the early 2000's as the *cream of the crop* of the click reactions, CuAAC reaction has since been fallen into disuse when compared to other click reactions. Its reaction mechanism has not been elucidated for a long time. Recent studies notably bring to light two distinct possible routes to this mechanism, thanks to the isolation of CuAAC reaction intermediates.^{60,61} In a general manner, it involves the regioselective copper(I)-catalyzed cycloaddition between an azide and a terminal alkyne, as shown on **Figure 2a**. More precisely, two concomitant pathways can lead to the formation of the triazole ring (**Figure 4**). While the first one, slow, involves mononuclear catalytic species, the second one, underpinned by the isolation of bis(copper) key intermediates, relies on a fast and thus kinetically favoured synthetic route.

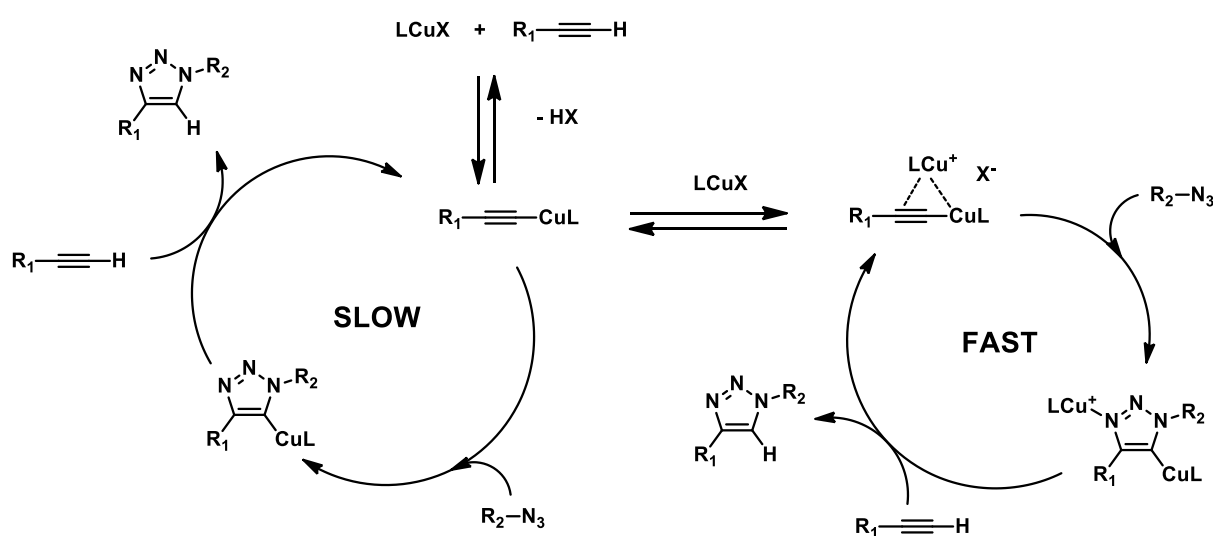


Figure 4. Two synthetic pathways, underpinned by the isolation of copper-based key intermediate species, proposed for the CuAAC click reaction.

However, this reaction is more and more abandoned because of the potential toxicity of the required copper catalyst, even though it is generally removed from the products in a nearly quantitative fashion. Nevertheless, a strain promoted version of the CuAAC reaction⁶² has

been since developed especially by Bertozzi and collaborators⁶³ that implemented the strain-promoted azide-alkyne cycloaddition (SPAAC) reaction that is a copper-free version of the CuAAC, involving in this case cyclooctyne-based compounds. The main advantage in that particular version relies in the absence of the copper catalyst that notably allows for using such click reaction for biofunctionalization and modification of biomolecules in living systems notably. Nevertheless, it has been extensively implemented for the functionalization of monoliths with selectors of interest for applications in separation sciences notably, as reported by different reviews in the field.^{64,65}

4.2 Thiol-Ene (TEC) and thiol-yne (TYC) Coupling chemistries

Thiol-based chemistries and especially radical-based version of this reaction class has re-emerged in the late 2000's.⁶⁶ Since, they have been applied to various research area and notably in the chemical, biological, physical, materials and engineering fields.⁶⁷ Originally discovered by Posner in 1905,⁶⁸ the thiol-ene click reaction is a step-growth radical-mediated organic reaction coupling between a thiol and an alkene to form the corresponding thioether (**Figure 2b**). As showed on **Figure 5**, it involves the formation of a thiyl radical that can be achieved *via* either photo-triggered, thermal or redox activation pathway in the presence of a suitable radical initiator (benzophenone (BP) and dimethoxyphenylacetophenone (DMPA) or azobisisobutyronitrile (AIBN) as photoinitiators or thermal initiator, respectively) during the initiation step. The photochemical initiation strategy generally affords, in such surface chemistry reactions, for spatially controlling the coupling reaction as photomasks can be in this particular case easily implemented.⁸ Further, the thiyl radical undergoes a radical addition onto the alkene function in an anti-Markovnikov fashion during the propagation step. The regioselectivity of this thiol-ene reaction can be easily explained by the enhanced stability of the intermediate carbon-centered radical upon addition to the less substituted alkene carbon.⁶⁹ The radical-mediated formation of such thioethers from unsaturated alkenes can also be achieved from disulfide-containing compounds. Termination reactions can occur rapidly with a bimolecular reaction between any of the radical species generated during the reaction. Electron rich and strained alkenes, like vinyl ethers, react more rapidly.

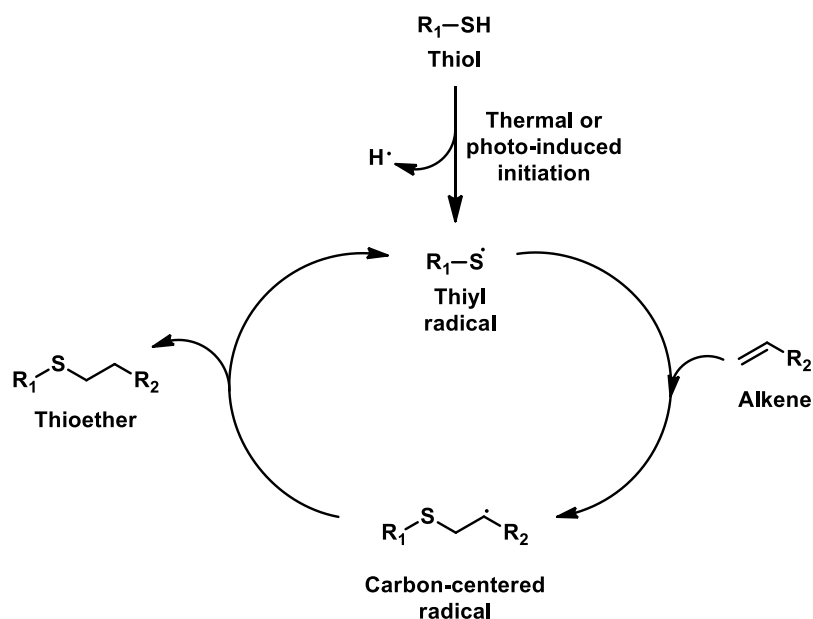


Figure 5. Commonly accepted mechanism of the radical thiol-ene addition reaction between a thiol and an olefin.

The alkyne-based version of the thiol-ene reaction, *i.e.* the thiol-yne click reaction, operates in the same conditions but allows in that particular case for the grafting of two thiol-containing compounds per alkyne moiety (**Figure 2c**).^{70,71} In surface chemistry area, this is actually an important parameter to take into consideration when one wants to obtain a denser surface functionalization with the thiol-containing compound, provided that steric hindrance is limited. It is worth mentioning that in such an attempt of denser surface functionalization, the supports should bear alkyne functions.

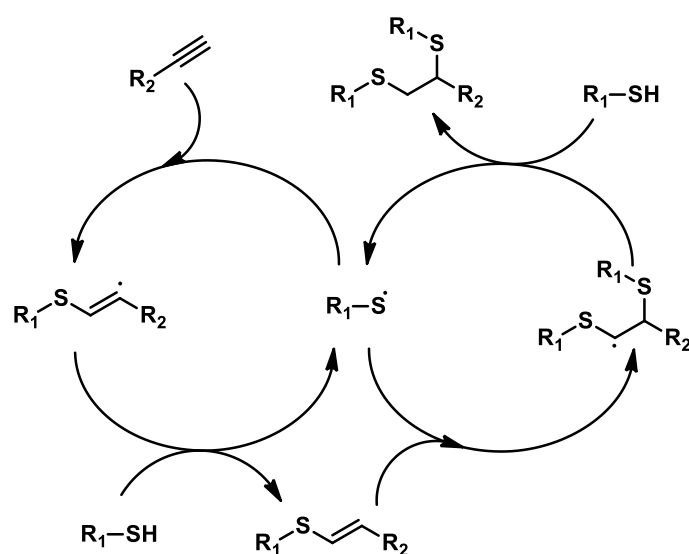


Figure 6. Reaction mechanism for addition of thiols to alkynes.

The mechanism is similar to that of the thiol-ene reaction, as depicted on **Figure 6**. Upon addition of the thiyl radical to the triple bond and abstraction of a hydrogen from another thiol molecule, the as-obtained vinyl thioether undergoes in the same way a radical addition of another thiyl radical to form the resulting carbon-centered radical that abstracts a hydrogen from another thiol of the reaction medium to finally generate a bithioether. Similarly to the thiol-ene reaction, the first thiyl addition is regioselectively achieved on the less substituted carbon of the alkyne function so as to produce the more stable radical. The second addition of the thiyl radical occurs on the other carbon of the unsaturation as the obtained carbon-centered radical is stabilized by electron-donating mesomer effect of the thioether moiety.

4.3 Thiol-(meth)acrylate reaction

Oppositely to the thiol-ene and thiol-yne reaction, the thiol-(meth)acrylate click coupling relies on a chemical process involving ionic species. It is generally catalyzed by Lewis bases such as amines and phosphines, for instance (**Figure 2d**). The mechanism notably involves the addition of the catalyst onto the less substituted carbon of the activated C-C double bond *via* a 1,4-Michael type addition. The zwitterionic intermediate then abstracts a hydrogen from a thiol molecule in the medium. Finally the as-formed thiolate substitutes the catalyst, thus generating the corresponding thioether (**Figure 7**). In order for this reaction to proceed, the alkene-containing substrate requires an electron-withdrawing group (generally an ester, a ketone or an aldehyde) directly conjugated to the C-C double bond to proceed.

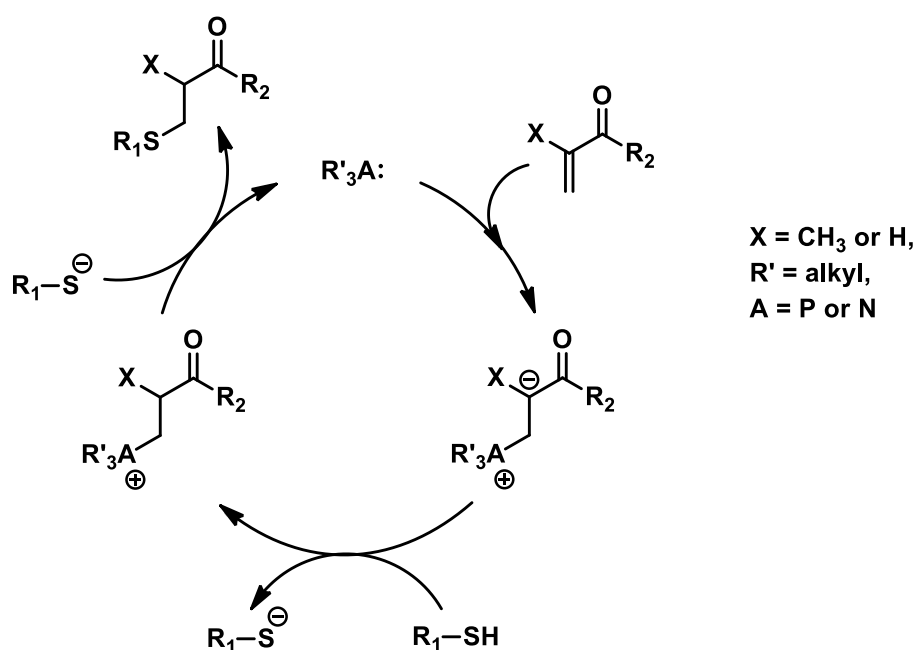


Figure 7. Mechanism of the Lewis acid-catalyzed thiol-(meth)acrylate click reaction.

4.4 Thiol-epoxy click coupling

This reaction operates *via* ring opening of epoxide moieties in the presence of rather strong nucleophiles. In the case of the addition of thiols to the epoxy group, it requires the presence of a base in the medium as thiols are not enough nucleophiles to undergo such addition reaction (**Figure 2e**).^{72,73} Bases can be directly added to the reaction medium or formed *in situ* by using photobase generators, depending whether the reaction is realized under its ionic or photo-initiated version, respectively. In such conditions the thiolate active species is generated by proton abstraction in the presence of the base and can then achieve the nucleophilic addition, as shown on **Figure 8**. The last step of the reaction involves hydrogen abstraction from another thiol molecule in the medium to afford the final α -mercaptoalcohol.

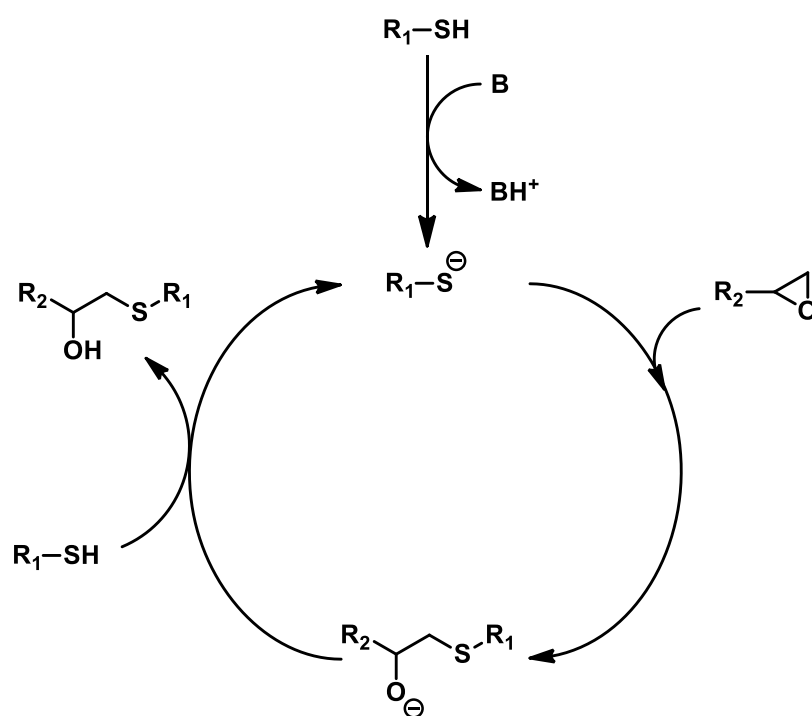


Figure 8. Generally accepted mechanism for the thiol-epoxy click coupling.

4.5 Diels-Alder click coupling

Diels-Alder click coupling generally occurs upon thermal process and has the advantage to be reversible. The mechanism, discovered by Diels and Alder⁷⁴ and awarded from the chemistry Nobel Prize in 1950, is based on the $[4\pi + 2\pi]$ cycloaddition between diene and dienophile (*i.e.* alkene). It generally involves alkene-based maleimide derivatives and diene-based

cyclopentadiene-, furan- or anthracene-functionalized compounds to afford cycloadduct products with high yield via photochemical or thermal pathways.^{75,76,77}

5. Click chemistry applied to monolith technology

Monoliths can be fully regarded as complex polymeric systems in the sense that their overall properties result from a delicate balance between interface and bulk characteristics. As discussed above, monolithic structures made of a network of together-fused solid nodules with in-between tortuous pore channels accounts for the flow-through properties and efficient fluid transport through monolithic elements, while interaction ability originates from the chemical functionality on the monolith surface. Such an interaction can be based on partitioning or adsorption for chromatographic processes, biomolecular recognition for separation, extraction and purification purposes, electrostatic forces for nanoparticulate elements immobilization...

Here below, we discuss specific cases where click chemistry was implemented towards either the synthesis or surface chemical modification of monoliths. Both organic, inorganic and organic-inorganic hybrid monolithic skeletons are considered. The following section is segmented in three parts describing successively Click chemistry for the preparation of monoliths, the synthesis of clickable monoliths and Click chemistry for the surface functionalization of monoliths.

5.1 Click chemistry for the preparation of monoliths

Radical-mediated addition of enes and thiols is a well-established method in the field of polymer science and engineering to design crosslinked materials.^{78,79} In the context of monolith, thiol-ene click reactions have found their way for the preparation of organic and hybrid structures.^{80,81} Photo-triggered ($\lambda = 365 \text{ nm}$, 120 mJ/cm^2) thiol-ene click polymerization of 1,2,4-trivinylcyclohexane (TVCH) and pentaerythritol tetra(3-mercaptopropionate) (4SH) was implemented for the fast (6 min) preparation of monoliths.⁸² The monolith was synthesized within UV-transparent capillary using 2,2-dimethoxy-2-phenylacetophenone (DMPA) as initiator and a mixture of diethyl ether (DEGDE) and polyethylene glycol 200 (PEG200) as binary porogenic solvent. Commonly used porogens (toluene/dodecanol and cyclohexanol/decanol) did not provide monolith-filled and permeable capillary column. Interestingly, the authors did not discuss only the effect of porogen mixture composition on permeability but they also clearly highlighted effects of photoinitiator content

and UV irradiation time. Permeability was found to decrease from 5.3 to $2.8 \times 10^{-14} \text{ m}^2$ when the DMPA content was increased from 0.19 to 1.87% while it decreased from 6.1 to $4.2 \times 10^{-14} \text{ m}^2$ while the UV irradiation time increased from 2 to 15 min. The group of Feng described an efficient method for the one-step preparation of organic-inorganic hybrid monoliths through a synthetic method based on polycondensation and thiol-ene click reaction (**Figure 9**).⁸³ To this end, homogeneous mixture made of vinyl-end organic monomers, azobisisobutyronitrile (AIBN), hydrolyzed tetramethoxysilane (TMOS) and 3-mercaptopropyltrimethoxysilane (MPTMS) was maintained at 40°C during 12h within fused-silica capillary providing monolithic materials. Depending on the chemical nature of the organic monomer, namely [2-(methacryloyloxy)ethyl]trimethylammonium (META) and acrylamide (AA), monoliths with anion exchange and hydrophilic interaction ability were obtained, respectively. Although polycondensation and thiol-ene occurred simultaneously, the latter reaction can be considered as mainly contributing to the surface functionalization of the monolith as, in some way, it performed end-capping of the SH groups arising from silane-like monomers. In other words, surface functionality of monoliths was dictated by the chemical nature of the vinyl monomers in the course of thiol-ene reaction.

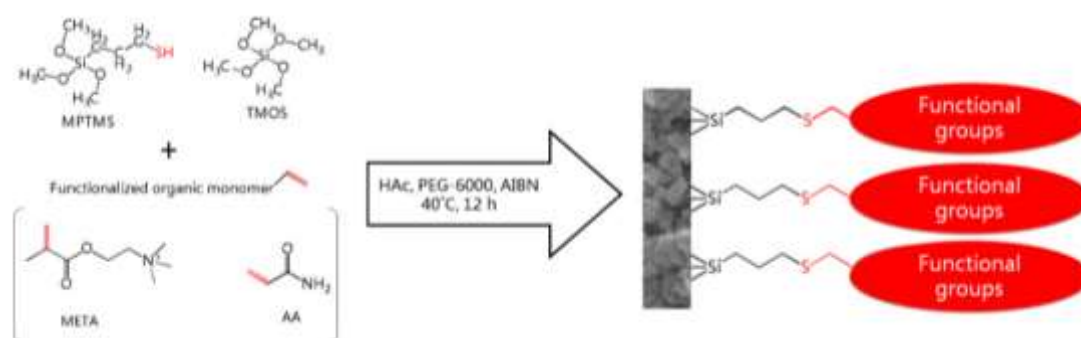


Figure 9. Schematic illustration of the synthetic path developed to synthesize hybrid monolith versatile surface functionality through thiol-ene click chemistry. Reproduced from ref 83 by permission of Elsevier.

In 2014, the group of Zou reported on the successful synthesis of macroporous hybrid monoliths via thiol-ene polymerization meant for cLC application (**Figure 10**).⁸⁴ The polymerization of vinyl monomers – 2,4,6,8-tetramethyl-2,4,6,8-tetravinylcyclotetrasiloxane (TMTVS) or tetravinylsilane (TVS) – with thiol – 1,6-hexanedithiol (dithiol) or pentaerythritol tetrakis(3-mercapto-propionate) (tetrathiol) – was initiated by UV light irradiation at 365 nm using 2,2-dimethoxy-2-phenylacetophenone (DMPA) and (diethylene glycol diethyl ether

(DEGDE) as a photoinitiator and good solvent, respectively. Fourier-transform infrared spectroscopy (FT-IR) revealed the almost disappearance of signals assigned to the vinyl (1592 cm^{-1}) and also thiol (2555 cm^{-1}) groups confirming occurrence of the thiol-ene reaction in high yields.

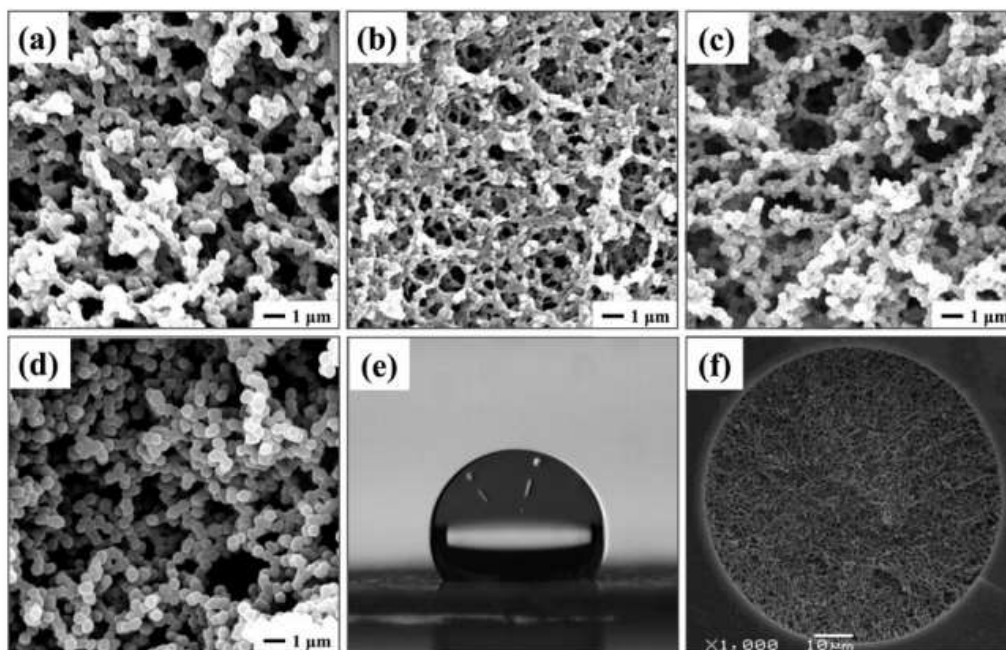


Figure 10. Scanning electron microscopy images showing the morphology of hybrid monolith prepared by through photodriven thiol-ene click chemistry using different tetra-vinyl monomers and multi-thiols. Reproduced from ref 84 by permission of Royal Society of Chemistry.

The same group applied thiol-yne click chemistry type in the area of monolithic materials.⁸⁵ Dual-process for the preparation of organic-inorganic monolith, involving simultaneous polycondensation and thiol-mediated radical addition, has also been exploited by the group of Huanghao Yang from the Fuzhou University.⁸⁶ Glutathione, a molecular combination of three proteins building blocks, namely cysteine, glycine and glutamine, was used in mixture with 2,2-azobisisobutyronitrile (AIBN), hydrolyzed tetramethyloxysilane (TMOS) and γ -methacryloxypropyltrimethoxysilane (γ -MAPS) to provide multifunctional monoliths (**Figure 11**). A two-step thermal treatment involving, initial heating at 40°C for 12 h and additional treatment at 70°C for another 12 h was applied with success. Such gradual temperature treatment can be easily rationalized by the intrinsic nature of the reaction mechanisms. Indeed radicals-forming decomposition of AIBN is known to occur efficiently in a temperature range 60°C - 85°C . As such, we may assume that thiol-ene reaction occurs mainly in the second half, i.e. in the higher temperature regime, of the synthesis process. This

is of course beneficial to the overall design of monolith with surface-controlled properties as the thiol-ene, in the present case, leads to the incorporation of glutathione that should occur on the surface of the inorganic skeleton to provide its chemical functions, $-\text{COOH}$, $-\text{NH}_2$, $-\text{CO}-\text{NH}_2-$, available for interacting with molecular targets. Silica network of GSH-hybrid monolith exhibited remarkable mechanical stability under pressure up to 18.6 MPa, the permeability and surface area were quantitatively determined to be $1.47 \times 10^{-14} \text{ m}^2$ and $273.5 \text{ m}^2/\text{g}$, respectively. Pore size analysis revealed a narrow mesoporous distribution centered at about 3.6 nm.

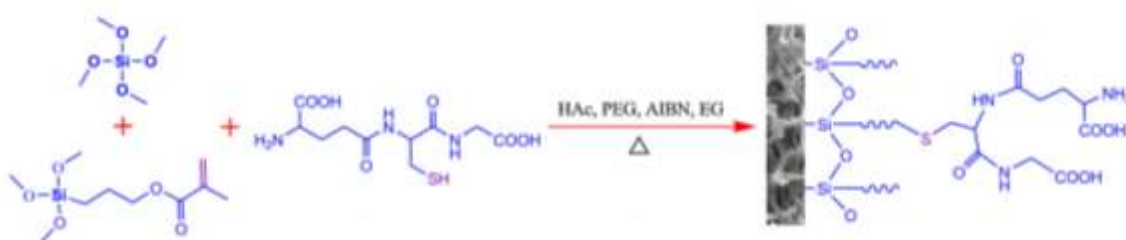


Figure 11. Schematic illustration of the synthetic path developed to synthesize hybrid monolith zwitterionic surface functionality through thiol-ene click chemistry. Reproduced from ref 69 86 by permission of elsevier.

Although vinyl-POSS derivatives have gained great interest over the last years for the preparation of organic polymer-based materials they suffer from low reactivity of the tightly tethered vinyl group in free radical polymerization. Radical-mediated step-growth process in the presence of thiol and initiator has been exploited to the chemical cross-linking of POSS precursors in an efficient and controlled way.⁸⁷ Thiol-methacrylate Michael addition click reaction between multi-methacrylate polyhedral oligomeric silsesquioxane and multi-thiols was reported as a facile strategy for the direct preparation of hybrid monolithic capillary columns.⁸⁸ Methacrylate-polyhedral oligomeric silsesquioxane (POSS-MA) (cage mixture, $n = 8, 10, 12$, POSS-MA) was allowed to react with different multi-thiol crosslinkers – 1,6-hexanedithiol (HDT), trimethylolpropane tris(3-mercaptopropionate) (TPTM) and pentaerythritol tetrakis(3-mercaptopropionate) (PTM) – in a two component (n-propanol and PEG 200) porogenic system. The Michael addition was efficiently catalyzed by adding 2, 4 or 6 wt% of dimethylphenylphosphine (DMPP) as catalyst as suggested by spectroscopic evidences such as increase in peak intensity of carbon sulfur bonds (697 cm^{-1}) and almost disappearance of peaks typical for stretching vibrations of $-\text{C}=\text{C}-$ (1637 cm^{-1}) and $-\text{S}-\text{H}$ (2569 cm^{-1}) groups. Such an increase in the DMPP content was accompanied by an increase in the permeability (by nearly one order of magnitude) leading to value of $3.12 \times 10^{-14} \text{ m}^2$.

Such a dependence is related to the fact that large feeding amount of catalyst induces faster rate of polymerization and the resulting formation of oligomers promotes early phase separation and large macropores. In 2014, a contribution from Shufen Shen et coll. described the elaboration of novel organic-inorganic hybrid monoliths based on POSS via thiol-ene click reaction between polyhedral oligomeric silsesquioxane methacryl substituted (POSS-MA) and 1,4-bis(mercaptoacetoxy) butane (BMAB) (**Figure 12**).⁸⁹ Influence of monomers ratio (POSS-MA–BMAB from 1:1.0 to 1:3 mol:mol), composition (toluene vs. dodecanol) of porogenic solvents and temperature (50, 55 and 60°C) on monoliths morphology and permeability were thoroughly investigated. Differences in morphology, as observed with different BMAB crosslinker content, were assumed to result from change in local degree of polymerization. For high crosslinker density, i.e. high degree of polymerization, crosslinked nanoglobular polymers are formed and separate from the solvent phase.

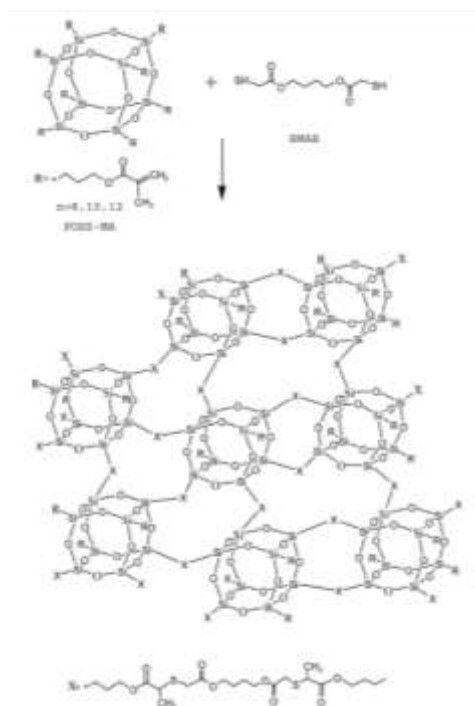


Figure 12. Schematic illustration of the synthetic path developed to synthesize POSS-based hybrid monolith through thiol-ene click chemistry. Reproduced from ref 72,89 by permission of Royal Society of Chemistry.

These hybrid materials are very appealing alternatives to organic and silica monoliths as they combine advantages of both partners without the inherent drawbacks. Hybrid monoliths were also synthesized through initial alkaline-catalyzed thiol-epoxy click polymerization. A multi-

epoxy monomer, octaglycidyl dimethylsilyl polyhedral oligomeric silsesquioxane (POSS-epoxy) was copolymerized with either trimethylolpropane tris(3-mercaptopropionate) (TPTM) or pentaerythritol tetrakis(3-mercaptopropionate) (PTM), as multi-thiols precursors (**Figure 13**).⁹⁰

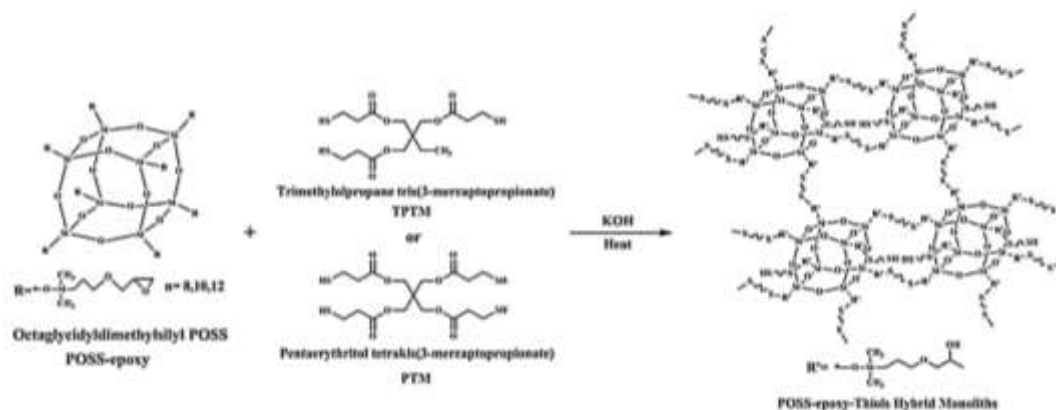


Figure 13. Schematic illustration of the synthetic path developed to synthesize POSS-based hybrid monolith through thiol-epoxy click chemistry. Reproduced from ref 73 90 by permission of Elsevier.

Assuming high efficiency of thiol-epoxy click reaction, i.e. almost equal consumption of epoxy and thiol groups, the mole ratio of the two functional groups was kept equal to 1. This assumption was confirmed to a large extent through FT-IR characterization as the authors observed significant decrease in the characteristic absorption peaks of epoxy group (in the range from 725 to 910 cm^{-1}) together with an almost disappearance of the absorption peak of the thiol group at 2570 cm^{-1} . Typical 3D skeleton with well-controlled microstructures and high thermal, mechanical and chemical stabilities were obtained for both, POSS-epoxy-TPTM and POSS-epoxy-PTM, hybrid monoliths. Permeability values as calculated according to Darcy's law were found in the range 0.19 – 60.51 $\times 10^{-14} \text{ m}^2$ for the POSS-epoxy-PTM hybrid monoliths depending on the composition of the binary porogenic mixture (EtOH/PEG 10,000) and catalyst (KOH) content. The same research team extended successfully the thiol-epoxy approach to other multi-epoxy monomer – *tetraphenylethane glycidyl ether* – and multi-thiol monomer – *trimethylolpropane tris(3-mercaptopropionate)* and *pentaerythritol tetrakis(3-mercaptopropionate)* – using ternary porogenic system – *DMSO/PEG200/H₂O* – as ascertained by systematic characterizations of the obtained monoliths by complementary methods including SEM, FT-IR spectroscopy, pore size measurement, thermal gravimetric analysis and nitrogen adsorption/desorption measurement.⁹¹ In another implementation,

methacrylate-silica monolithic columns of hybrid nature and bearing sulfonic acid surface groups were newly synthesized within capillary columns through a one pot approach.⁹² To establish the method, organic monomer (3-sulfopropyl methacrylate potassium) and initiator (2,2'-azobis (2-methyl propionamide) dihydrochloride) were simply added to the hydrolysis solution of TMOS and mercaptopropyltrimethoxysilane (MPTS) so that polycondensation and thiol-ene click reaction occurred simultaneously between the precondensed siloxanes and organic monomers. The reaction was conducted in presence of urea, PEG and acetic acid at low temperature (35 –55°C) for 12h. Monolithic materials with both homogeneous structure and good permeability, and referred to as ideal monoliths by the authors, were obtained only using an intermediate temperature of 45°C. The morphology was found to be highly dependent on the amount of added porogen. Low and high PEG amounts led to monoliths with poor permeability and weak attachment onto the silica wall, respectively. A multi-step and elegant preparation approach was implemented by Cuicui Liu with the aim to design two-dimensional monoliths within capillary columns for biomolecules analysis.^{93,94} The 1st dimension acted as pre-concentration segment. The corresponding monolithic structure was *in situ* prepared in a single step *via* Michael addition reaction and radical polymerization. Such mechanism combination involved thiol graphene (500 m²/g), 4-vinylphenylboronic acid (VPBA), ethylene dimethacrylate (EDMA), 1-vinyl-3-octylimidazolium chloride (ViOcIm⁺Cl⁻) and was initiated at 70°C in presence of 2, 2'-azobis(isobutyronitrile) (AIBN). Extensive ultra-sonication was required to dissolve the graphene derivative in a N,N-dimethylformamide and 1,4-butanediol solvent mixture.

5.2 Synthesis of clickable monoliths

In contrast to the historical one-step synthetic pathway applied to produce permeable polymeric monoliths, post-polymerization chemical modification of monoliths prevents tedious and time-consuming steps required for the concomitant optimization of both surface chemistry and flow-through properties.⁹⁵ Indeed, change in the nature of the functional monomer, i.e. monomer bearing as a side chain a selector/ligand for further flow-chemistry uses, requires tedious re-optimization of the polymerization conditions. Porogen or porogenic mixture, a crucial parameter in the design of monolithic structures, has to be well-fitted to solubility parameters of both monomers and polymers. Post-polymerization approach, enables tuning of these two characteristics independently. For generic monoliths, mechanical stability and porous structure, resulting from the polymerization kinetics and related phase separation process, can be initially optimized in the course of the free radical polymerization step

independently of the ultimate desired surface chemical nature.⁹⁶ In a further step, monoliths with very different surface characteristics can be prepared through simple grafting of functional molecules without troubles inherent to the reactivity or solubility of the corresponding functional monomer. Two strategies can be envisioned for each type of click reaction. Restricting the discussion to the case of copper(I)-catalyzed (3 + 2) azide-alkyne cycloaddition, either azide or alkyne units can be surface-grafted on the solid supports.^{97,98} Then, the surface with surface yne groups can subsequently react with a selector/ligand bearing an azide unit and *vice versa*. This allows a variety of combination taking advantage of the numerous and commercially available functional thiols, alkenes, alkynes, azides, epoxy, methacrylates... Extended this introductory section to silica-based monoliths, alkynyl- or azido-hybrid monoliths can be prepared through condensation of the hydrolyzed silane precursors tetramethoxysilane and (3-iodopropyl)-trimethoxysilane in the presence of neutralized functional amine, propargylamine or 11-azido-3,6,9-trioxaundecan-1-amine, respectively.⁹⁸ Using ethylene dimethacrylate (EDMA), as a crosslinker, and glycidyl methacrylate, as monomer, P(GMA-EDMA) monoliths carrying epoxy surface groups have proved very useful to serve as generic platforms for the preparation of monolithic materials with a variety of functionality (hydrophobic, hydrophilic, anion/cation exchange, chiral, affinity)⁵ including, more recently, clickable groups. P(GMA-EDMA) can be prepared by free radical polymerization using heavy alcohol (cyclohexanol/dodecanol mixtures) as porogen. Svec *et al.* reported on the synthesis of thiol monoliths by one-^{99,100} and two-step^{101,102} surface modification of GMA-based monoliths. Surface thiols were obtained by direct aminolysis of epoxy groups with 2-aminoethanethiol while the grafting of **2,2'-dithiobis(ethylamine)** required additional treatment under reducing conditions to provide disruption of the S-S bonds. Considering the surface modification of generic P(GMA-co-EDMA) with cystamine, the same group of authors showed that repeating the grafting twice (1.0 mol/L cystamine dihydrochloride in 2.0 mol/L aqueous sodium hydroxide at RT for 1 h and subsequent heating at 50°C for 1 h) enables increasing the sulfur content from 2.6% to 3.7%. Such monolith with enriched sulfur, i.e. thiol, content can serve as versatile clickable platform for efficient grafting of methacrylate monomers. Lämmerhofer proposed the bonding of thiolated polymers instead of their molecular counterparts to design tentacle-like surface-structured monoliths with the aim to enhance both surface coverage of functional groups and sample loading abilities.¹⁰³ The proof of principle was proposed for polythiol-grafted monoliths following a three-step derivatization protocol. Poly(GMA-co-EDMA) was subjected to (i) amination – *ammonia* – (ii) vinylation – *allyl glycidyl ether* – and (iii) coating – *poly-3-*

mercaptopropyl methylsiloxane (PMPMS)* – in combination with crosslinking by thermally-driven radical addition click reaction. Such an approach allowed more than a 2-fold increase in thiol coverage as compared to a control monolith obtained through direct functionalization by nucleophilic substitution with PMPMS. Thiolated silica monolith was also designed via the polycondensation of TMOS and 3-mercaptopropyltrimethoxysilane (MPTS*). Usual conditions were applied consisting of acetic acid solution of PEG, acting as porogen, and thermal activation at 55°C for 12 h to complete the condensation reaction. Svec et al. illustrated the suitability of the CuAAC for producing brush-type monoliths.¹⁰⁴ Azide functionalities were first introduced on the pore surface of monolithic silica by reaction with 3-(azidopropyl)trimethoxysilane. The Click step was achieved in dimethylformamide (DMF) in the presence of catalytic amounts of copper (I) iodide providing high yield grafting of a proline derivative containing an alkyne moiety. F Tang et al discussed a facile and efficient “single-step” procedure to design azide-functionalized silica monoliths.¹⁰⁵ To a homogeneous precondensation mixture, made of tetramethoxysilane, 3-(chloropropyl)trimethoxysilane, water, methanol and PEG, aqueous solution of sodium azide and potassium iodide was added and the reactive solution was sonicated prior to gelation. Such an approach was compared to the traditional sol–gel process using TMOS and CTMS as precursors, and involving an in-column-functionalization step for the grafting of azide units. The authors notably concluded that their new approach afforded larger amount of accessible azide, prone to further click grafting, on the monolith surface. The presence of azide moieties as surface functionalities was evidenced by the characteristic peak at 2,100 cm^{-1} observed in the FTIR spectroscopic spectra. The average pore diameter of the monolith was calculated as 173 nm by mercury intrusion porosimetry, and the total surface area was 17.69 $\text{m}^2 \cdot \text{g}^{-1}$. Permeability values were calculated to be $6.05 \times 10^{-13} \text{ m}^2$ and $3.72 \times 10^{-13} \text{ m}^2$ for water and methanol, respectively. A one-step approach for the in situ preparation of Click-functionalizable monolithic stationary phase with alkyne surface functionality was presented by the group of Delépée.¹⁰⁶ Poly(propargyl acrylate–pentaerythritol triacrylate–trimethylolpropane trimethacrylate), poly(PA–PETRA–TRIM), monolith was obtained through a photochemically initiated copolymerization process using a mixture of methanol, acetonitrile and sodium phosphate buffer (5 mM, pH 6.8) (2/6/2, v/v/v) as porogen. The authors provided systematic investigation of the effects of molar ratios of both crosslinkers (PETRA vs. TRIM) on the durability and permeability of the resulting polymers. Schachtschneider and his co-workers discussed the design of periodically ordered mesoporous organosilicas and aerogel-like monolithic bodies exhibiting an optimized density of azide as clickable surface groups.¹⁰⁷

The 1,3-dipolar Huisgen cycloaddition was judiciously selected because of its high versatility, enormous tolerance towards a large panel of functional groups and its general feasibility in pores.¹⁰⁸ The use of bridging phenylazide moieties offer a variety of unique possibilities for the grafting of nearly any desired chemical functionality via click chemistry. Surface functionalization was achieved through click grafting of an alkyne-modified fluorescein onto azide-containing aerogel-like monoliths. Fluorescence imaging in combination to spatially resolved IR spectroscopy measurements highlighted undoubtedly the possibility to generate chemical gradient through this elegant approach. Although the authors did not report applications they claimed that materials exhibiting property gradients – chemical, optical and structural – may be potential candidates for uses requiring directionality as it is the case for chromatography. Beside the more conventional methacrylate- and styrenic-based monoliths, polycarbonate monoliths were also considered as functional platforms with click reactivity.¹⁰⁹ Bisphenol A (BPA), 4,4'-(1-methylethylidene)bis(2-allylphenol) (MBP) and 4-nitrophenyl chloroformate (NPC) were initially dissolved in acetonitrile and the polymerization was further conducted under argon at 70°C during 20 h after addition of 4-dimethylaminopyridine (DMAP) and triethylamine. Polycarbonate with allyl side units was thus obtained and further processed in a monolithic structure through a phase separation approach. Cyclohexane was used as precipitation solvent providing 3-D porous network with specific surface area of 145 m²/g as determined by adsorption/desorption measurements. Thiol-sensitive monoliths were also prepared in their hybrid variant through sol-gel process.^{110,80} Inorganic polymerization of tetramethoxysilane (TMOS) and γ -methyl methacrylate trimethoxysilane (γ -MAPS) in presence of PEG (6000, 10000 and 20000 g/mol) urea and acetic acid provided hybrid skeleton with the required flow-through properties and carrying clickable C=C units.¹¹⁰ Other implementation of the “generic monolith” concept with easy surface functionalization features and thus allowing fast preparation of supports with versatile surface properties was proposed by some of us nearly 10 years ago.²⁴ Organic polymer monoliths were prepared in UV-transparent fused-silica capillaries by photo-triggered free radical copolymerization of *N*-acryloxysuccinimide as reactive monomer, ethylene dimethacrylate as crosslinker, azobisisobutyronitrile as initiator and toluene as porogen. Chemical and porous structures of such *N*-hydroxysuccinimide (NHS) decorated monoliths can be simply tuned through judicious choice of synthesis conditions. Addition of a limited amount of polar solvent (DMF or DMSO) to toluene allows controlling the pore size in the range 0.4 – 2.2 μ m, whereas increasing the monomer/crosslinker ratio enables enriching the monolith surface with NHS units.³¹ Activated esters with good leaving group properties have been widely applied to

chemically modify surface of organic or inorganic substrates providing nanostructuration, chemical functionality or biological activity.¹¹¹ Carboxylates ($-\text{COOH}$) can be reacted to NHS or sulfo-NHS in the presence of a carbodiimide such as EDC leading to the formation of a semi-stable NHS or sulfo-NHS ester, which may, in a further step, be reacted with primary amines to form amide anchoring units. Another path to design materials with amine-reactive esters of carboxylate groups relies on the use of polymerizable NHS-derivatives such as N-acryloyloxysuccinimide and N-methacryloxysuccinimide. NHS-ester can be advantageously used through a two-step reactional mechanism path for initial functionalization of NHS-containing materials surface via prompt reaction with functional amines in organic media (providing solubility of the NHS leaving group) and further hydrolysis of the remaining NHS units providing $-\text{COO}^-$ or $-\text{COOH}$ groups depending on the pH of the surrounding medium (Figure 14).

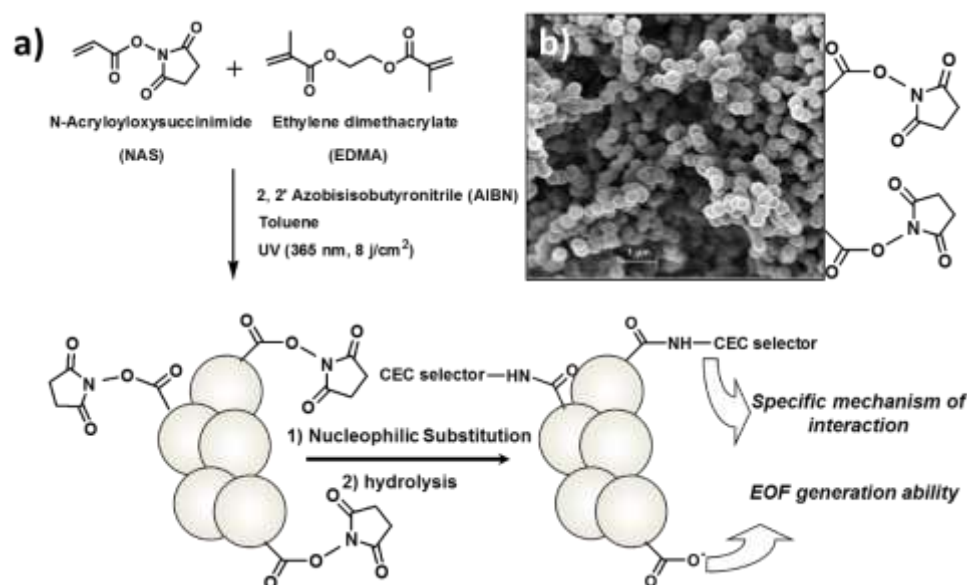


Figure 14. Schematic illustration of the strategy developed by our group to design functional monoliths via the post-functionalization of generic monolithic skeleton with N-hydroxysuccinimide surface functionality.

In the context of separation science, the proof of concept was established through investigation of the electro-osmotic flow generation ability of Poly(NAS-co-EDMA) monoliths initially functionalized with alkylamine in ACN and further hydrolysed at pH.³¹ Indeed, NHS esters are known to exhibit a half-life of 4-5 hours at pH 7, 1 hour at pH 8 and only 10 minutes at pH 8.6.^{112,113,114} We have shown that using background buffer with pH

value of about 6 that is near the pKa of $-\text{COOH}$ groups for polyelectrolyte-like polymeric surfaces, no electrodriven-flow was possible through the monolithic material.

Considering the generic synthetic route presented in Figure.... Clickable monolith with alkene or alkyne surface functionalities were prepared through reaction with allylamine^{10,11} and propargylamine,^{7,8,9,10} respectively. Success of the reactions was ascertained on the basis of in situ micro Raman spectroscopy analysis showing the disappearance of the peaks at about 1730 cm^{-1} (imide asymmetric stretching), 1780 cm^{-1} (imide symmetric stretching) and 1810 cm^{-1} (activated ester stretching) together with clear appearance of Raman signals at 2125 cm^{-1} and 1640 cm^{-1} supporting the presence of $-\text{C}\equiv\text{C}-$ and $-\text{C}=\text{C}-$ units, respectively, on the monolith surface. Thiol groups, known as complementary to enes and ynes for radical addition click reactions, can also be surface-attached onto poly(NAS-co-EDMA).¹¹⁵ The said generic monolith is then reacted with **2-aminoethanethiol**, cysteamine, via nucleophilic substitution of the NHS units. The reaction is conducted in ethanolic solution for 2 hours at room temperature. Through such an approach, free thiols are present on the monolith surface as demonstrated by the appearance of a peak at 2574 cm^{-1} typical for $-\text{SH}$ units. Moreover, the Raman profile did not indicate the presence of a signal in the 700 cm^{-1} Raman shift range that would suggest the formation of a carbon-sulfur bond. All these data confirm the grafting of cysteamine through amide coupling reaction. It is interesting mentioning that thiolated-monoliths can be designed via the grafting of disulphide-intermediate.¹⁰¹ Nucleophilic-sensitive monoliths can be reacted with 2,2'-dithiobis(ethylamine), cystamine, followed by the cleavage of the disulphide links. The approach was implemented for epoxy- and succinimide ester-based generic monolith providing thiol-rich monolith after treatment of their surface with tris(2-carboxylethyl)phosphine and *threo*-1,4-dimercapto-2,3-butanediol, respectively, to reveal thiol functions. In a recent report, the unprecedented use of glycerol carbonate methacrylate as functional monomers was presented for the preparation of generic porous polymer monoliths (**Figure 15**).¹¹⁶ GCMA was copolymerized with EDMA under UV irradiation at 365 nm for 2h. To optimize the porous properties of the resulting monoliths, different porogens combination (toluene/dodecanol or nonane) and monomer/crosslinker ratios were used. Binary porogen mixtures with different solubility parameters enables producing monoliths with bimodal pore size distribution as evidenced by mercury intrusion porosimetry measurements. Micrometer-sized pores provided flow-through properties while mesopores enhanced the surface area of the monolithic structures. Permeability values were calculated to be in the range $0.9 - 4.3 \times 10^{-14}\text{ m}^2$. Cyclic carbonates such as glycerol carbonate methacrylate can undergo ring opening when reacted with primary amines-containing

compounds and this reaction scheme was applied to graft ene-functionalities through reaction with cysteamine.

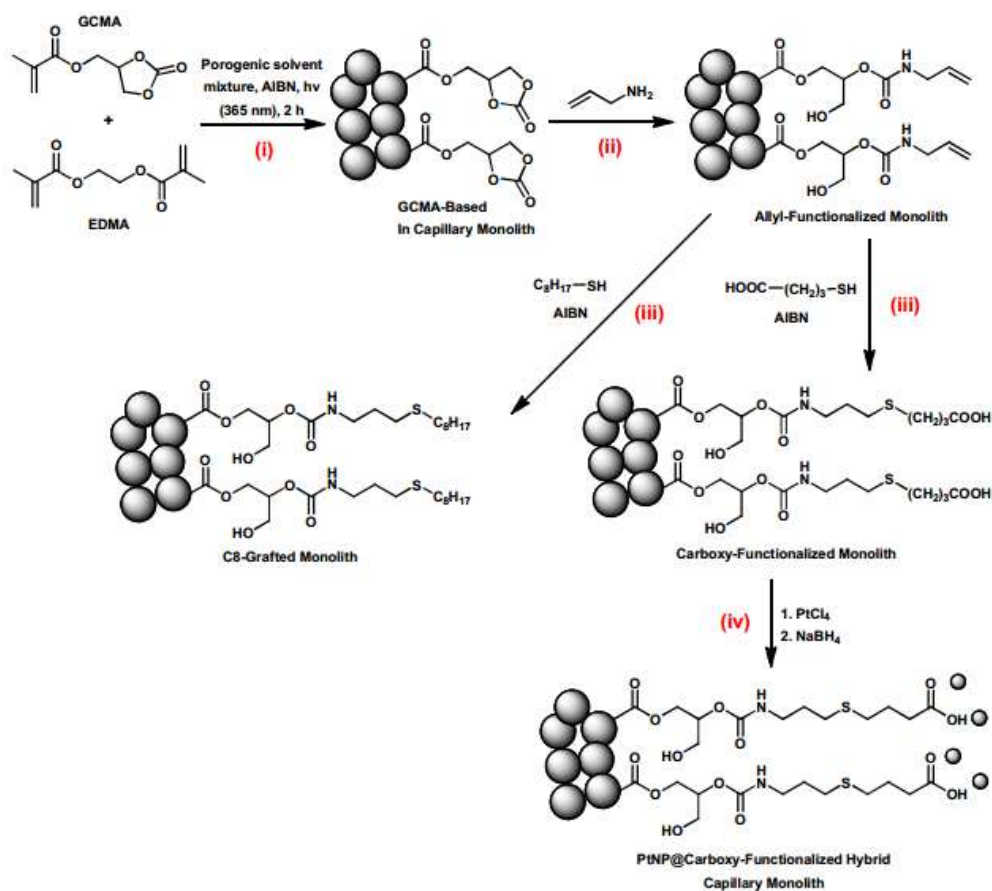


Figure 15. Schematic illustration of the strategy developed by our group to prepare clickable monoliths based on glycerol carbonate methacrylate. Surface functionalization of the monolith through thiol-ene click chemistry is also presented. Reproduced from ref 105 116 by permission of Royal Society of Chemistry.

To best of our knowledge, unique example of surface functionalizable monolith via Diels-Alder click reaction was reported by our group.¹⁰ Monolith with diene surface group was prepared through nucleophilic substitution reaction of the N-hydroxysuccinimide units with *1,3-cyclopentadiene-1-ethanamine* (1M in ACN). The reaction was conducted at room temperature for 2h.

5.3 Click chemistry for the surface functionalization of monoliths

Simplicity, rapidness and high efficiency of “thiol-ene” click reaction account for the broad interest by materials scientist to implement it as unique preparation method, or as a part of a multi-step mechanism process, for designing new monoliths with smart surface properties.

Organic polymer-based monolithic skeletons with surface-grafted alkene groups have proved to be versatile platforms for thiol-ene surface click chemistry as hydrophobic, hydrophilic, oligomeric moieties could be grafted with high yields.^{11,116} Thiol-ene click grafting implies the presence of either alkene or thiol groups onto the pore surface. Post-grafting was developed by Lämmerhofer and co-workers about 10 years ago to design chiral monoliths.^{117,118} After transformation of the epoxide groups of poly(glycidyl methacrylate-co-ethylene glycol dimethacrylate) into 3-mercapto-2-hydroxy-propyl residues, the thiol surface groups were allowed to react with quinone or phosphonic derivatives via thermal radical addition and the columns were used for enantioseparations. As a representative indications of experimental conditions, O-9-tert-butylcarbamoylquinone (6 mg.mL⁻¹ in MeOH) was allowed to react with the mercapto-functionalized monolithic matrix at 60°C, during 24h in the presence of AIBN. Thiol–maleimide Michael addition click reaction was implemented for the first as an efficient and versatile surface modification method of thiol-containing monoliths (**Figure 16**).¹¹⁵ The surface characteristics of clicked monoliths were found to be mainly governed by the chemical nature of the surface-grafted maleimide-ligand providing easily monoliths with very different surface interaction ability. As such hydrophobic and hydrophilic monolith can be obtained from the same generic matrix through Click attachment of aliphatic or carboxylic acid units, respectively.

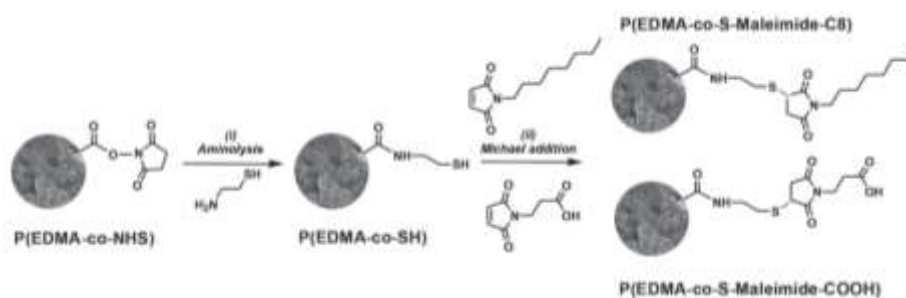


Figure 16. Schematic illustration of the strategy developed by our group to functionalize the surface of monoliths via thiol-maleimide Michael addition click chemistry. Reproduced from ref 103 115 by permission of Elsevier.

Photochemical-initiation process (365 nm) of thiol-ene click grafting from monolith surface was reported for the first in 2012 by Tijnelyte et al. and grafting efficiencies were comparatively studied with the results obtained under thermal (65°C) conditions.¹¹ Pore surface of generic poly(NAS-co-EDMA) with pendant allyl moieties was functionalized *via* a two-step thiol-ene click reaction with thiol-containing oligo(ethylene glycol) and mercaptoethanol, successively. In both cases, the click reaction was carried out in the

presence of AIBN at different molar concentrations (0.1-0.5 M) while the concentration of thiol derivatives was kept at 1M in toluene. Conversion of double bonds was considered as a direct indication for the success of the grafting and was evaluated as a function of reaction time through *in situ* Raman spectroscopy monitoring of the $\nu(\text{C}=\text{C})$ signal at 1647 cm^{-1} . For thermal operating conditions, no noticeable changes were observed in the Raman profile after 3h of reaction whereas decrease in the $\nu(\text{C}=\text{C})$ band intensity became obvious when the reaction time was extended to 24h. Fivefold increase in the initiator concentration (from 0.1 M to 0.5 M) did not improve the grafting yield that remained limited and did not exceed 50%. To provide reliable comparison of the effect of photochemically-driven radical formation, photo-thiol-ene was conducted using AIBN. Interestingly, comparable grafting yields of about 50% were obtained after 3h or UV-irradiation as compared to the 24h or thermal activation. We also mentioned the use of 2,2-dimethoxy-2-phenylacetophenone, a true photoinitiator, however the Raman characterization did not show significant differences within the reaction time range 0-4h. To illustrate the versatility of the approach, the authors synthesized monoliths with surface-grafted octadecyl groups, i.e. hydrophobic monolith, through the grafting of 1-octadecanethiol. The reaction was performed on the same generic poly(NAS-co-EDMA) and did not require any optimization step. Only the reaction solvent was changed to ethanol to fit with solvation properties of 1-octadecanethiol.

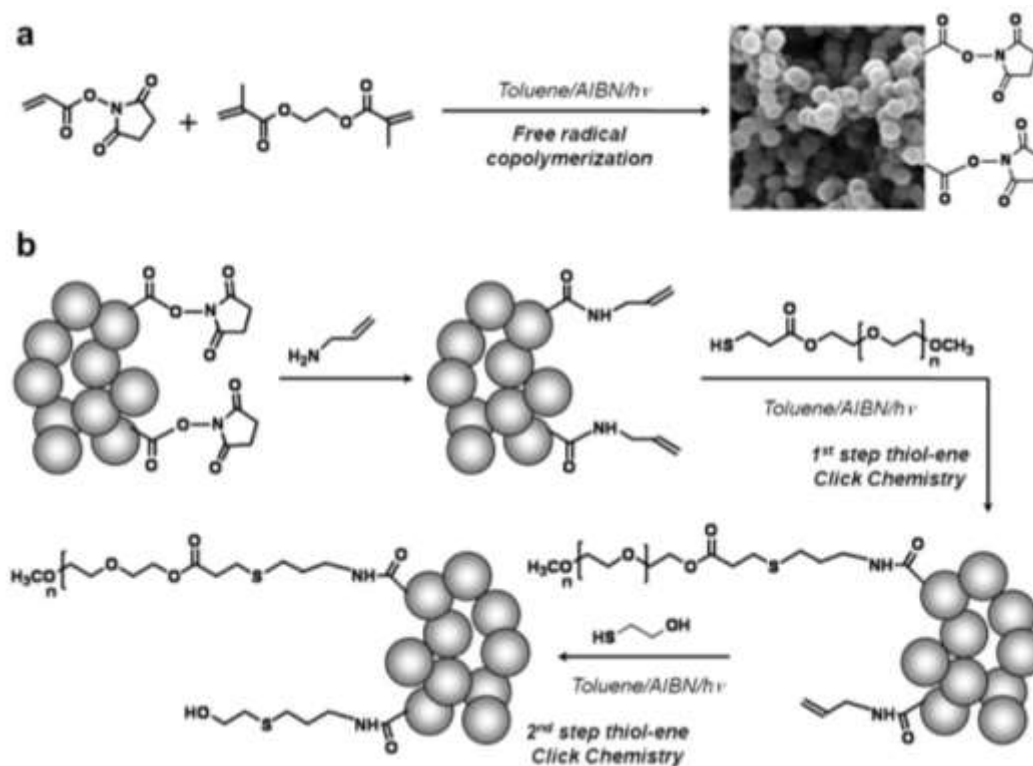


Figure 17. Schematic illustration of the synthetic path developed by our group to functionalize the surface of ene-monolith through thiol-ene click chemistry. Reproduced from ref 11 by permission of Elsevier.

Although less commonly applied, thiol-yne chemistry was also investigated in the context on monolithic materials. Our first report mentioned the hydrophilization of monolith surface through the radical addition of cysteamine onto alkyne containing porous monolith.⁸ The reaction was performed through UV-irradiation at 313 nm for 4 h in the presence of 2-hydroxy-2-methyl-1-phenyl-propanone (20 wt% with respect to cysteamine) as photoinitiator.

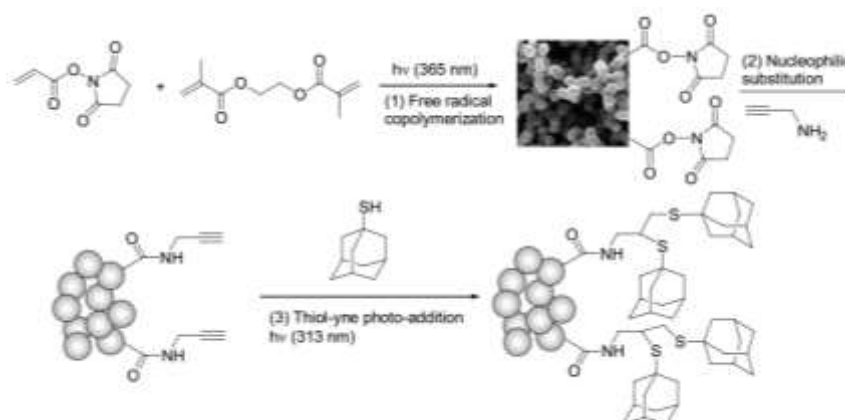


Figure 18. Schematic illustration of the strategy developed by our group to functionalize the surface of yne-monolith through thiol-yne click chemistry. Reproduced from ref 9 by permission of Wiley.

Of particular interest we have shown that the grafting reaction, although initiated through UV-process, occurred homogeneously along the in-capillary monolith section but also over its cross-section. Indeed, Raman mapping with a resolution step of 2 μm afforded 2D-plots indicative for the Raman intensity in the 2125 cm^{-1} region, typical for the $-\text{C}\equiv\text{C}-$ moieties, as a function of the measurement location on the sample. No functionalization gradients were observed after UV-irradiation of the 75 μm thick monolith and photo thiol-yne click reaction was proved to proceed up to completion as ascertained by the disappearance of the alkyne Raman signature. Raman spectroscopy proved also to be a powerful technique to investigate the click reaction mechanism. Although evidence for the radical-mediated mechanism is not accessible through Raman measurements, it was possible to monitor the successive grafting of two equivalent of 1-adamantanethiol per triple bond unit of alkynylated monolith.⁹ Indeed, unique observation of the consumption of the $\text{C}\equiv\text{C}$ is not a proof for a fully thiol-yne addition mechanism as presented in **Figure 6**. Time dependence investigation (over a period of 180 min) of the Raman profiles in the 2100–2160 cm^{-1} and 1500–1800 cm^{-1} regions revealed the

decrease in the signal intensity at 2125cm^{-1} and the appearance within an intermediate reaction time window (30 – 120 min) of a band at 1610 cm^{-1} . The former indicates consumption of the alkyne group that occurs from the early stage of the reaction and is total after 2h of reaction. The latter is considered as indicative of the temporary presence of $-\text{C}=\text{C}-\text{R}$ groups which are produced within the course of the thiol-yne reaction after addition of one equivalent of thiol derivatives per $-\text{C}\equiv\text{C}-$ unit and are further consumed through addition of the second equivalent. These spectroscopic features indicate that the bis addition of 1-adamantanethiol is the major reaction mechanism, in accordance with the thiol-yne mechanism presented in **Figure 6**. Indisputably, alkyne-functionalized monoliths have been mainly meant for the Huisgen 1,3-dipolar cyclo-addition. Here again our group reported the first implementation of the CuAAC of for the covalent attachment of β -cyclodextrin onto organic polymer monolith bearing alkyne units. Mono-(6-azido-6-deoxy)- β -CD was synthesized from β -CD using p-(toluene-sulfonyl)imidazole as tosylation agent as reported elsewhere.¹¹⁹ Azido-reactive monolith surface was further grafted with β -cyclodextrin *via* a triazole ring (**Figure 19**). The reaction was performed in presence of copper iodide and 1,1,4,7,7-pentamethyldiethylenetriamine for 16 h at a temperature of 60°C . Raman spectroscopy confirmed the consumption of the alkyne bond.

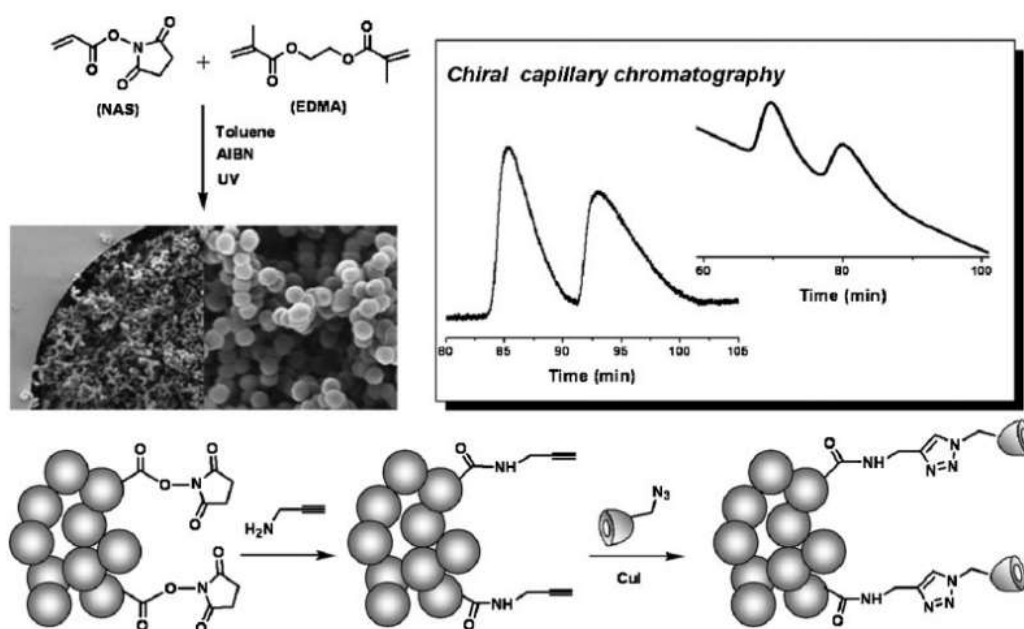


Figure 19. Schematic illustration of the strategy developed by our group to functionalize the surface of yne-monolith through CuAAC click chemistry. Two examples of enantioseparation of flavanone obtained by nan-LC and CEC are also shown. Reproduced from ref 7 by permission of Wiley.

Besides the surface-grafting of molecular segments acting as chromatographic selectors, some researchers have also considered the design of biofunctional monoliths through the well-controlled attachment of biological macromolecules on clickable monoliths. This can be achieved in a straightforward way, while still compatible with biological environment. To this end, thiol groups can be purposely introduced as end-functionality of the considered biomolecule or in situ generated through disruption of the –S–S– bridges. Aptamer with 5'-end modified by a hexyl spacer arm containing end thiol was immobilized on organic-silica hybrid monolith bearing methacrylate surface groups.¹¹⁰ The aptamer was first mixed with 2,2'-azobis (2-methylpropionamide) dihydrochloride as a thermal initiator and reacted with the ene hybrid monolith at 55°C for 5 h. Coverage density of modified aptamer was calculated from sulfur content to reach value of 420 pmol μL^{-1} . This coverage density is about two fold larger than the ones reported for other systems proving the superiority of the click chemistry approach for monolith biofunctionalization purposes.^{120,121}

To date, our group published the unique example in the literature of implementation of Diels-Alder click reaction for the surface functionalization of monolithic stationary phases.¹⁰ Diene-decorated monolithic matrix was allowed to react with N-phenylmaleimide (1M in ACN) for 4h at room temperature. The efficiency of the click grafting was evidenced by Raman spectroscopic investigations with the presence of a signal characteristic for the aromatic ring.

6. Application of “clicked” monoliths to flow chemistry

To date, the panel of applications of polymer monoliths encompasses microreactors for chemical and enzymatic processes,^{122,123} reversed-phase, chiral and affinity chromatographic stationary phases,¹²⁴ solid supports for surface-enhanced laser desorption/ionization time-of-flight mass spectrometry of small molecules¹²⁵ surface-enhanced Raman spectroscopy sensors for detection of proteins¹²⁶ sorbents for preconcentration and solid phase extraction¹²⁷, to mention but a few. Here-after we discuss successively applications of clicked monoliths to liquid phase separation, sample treatment and enzymatic and heterogeneous catalysis.

6.1 Clicked monoliths for (electro) chromatographic separation science

Herein, rather than presenting a long list of applications, we have rationalized our discussion about chromatographic and electrochromatographic applications as a function of the chemical nature of the monolith surface. Indeed, monoliths involving a click step in their preparation process have been designed to fulfill specifications for the different chromatography modes.

Reversed phase capillary (electro)chromatography requires the use of stationary phases with apolar surface features in combination with aqueous-based mobile phase containing usually methanol or acetonitrile as organic modifiers. As such monolith with aliphatic-graft have been prepared as analogous to the famous C4, C8, C18 particulate stationary phases.¹⁰² The said monoliths with dodecyl or octadecyl grafts provided efficient solutions for the separation of low (alkylbenzenes) and large (protein) molar mass analytes. Chromatographic properties of POSS-containing monoliths have been thoroughly investigated under reversed phase separation mode.^{88,89} POSS-epoxy-pentaerythritoltetrakis(3-mercaptopropionate) (PTM) and POSS-epoxy-trimethylolpropanetris (3-mercaptopropionate) (TPTM) provided the baseline separation of five alkylbenzenes according to their hydrophobicity, from low to high (**Figure 20**).⁹⁰ Using ACN/H₂O mixture (50/50, v/v) as mobile phase, the former provided lower retention time and lower plate height (of about 6 μm). Both columns were further applied for the separation of five polycyclic aromatic hydrocarbons (PAHs), six phenols, six anilines, five benzoic acids, five pesticides, three dipeptides and four intact proteins. These results demonstrated the potentiality of this type of monoliths for the analysis of both small molecules and (bio)macromolecules.

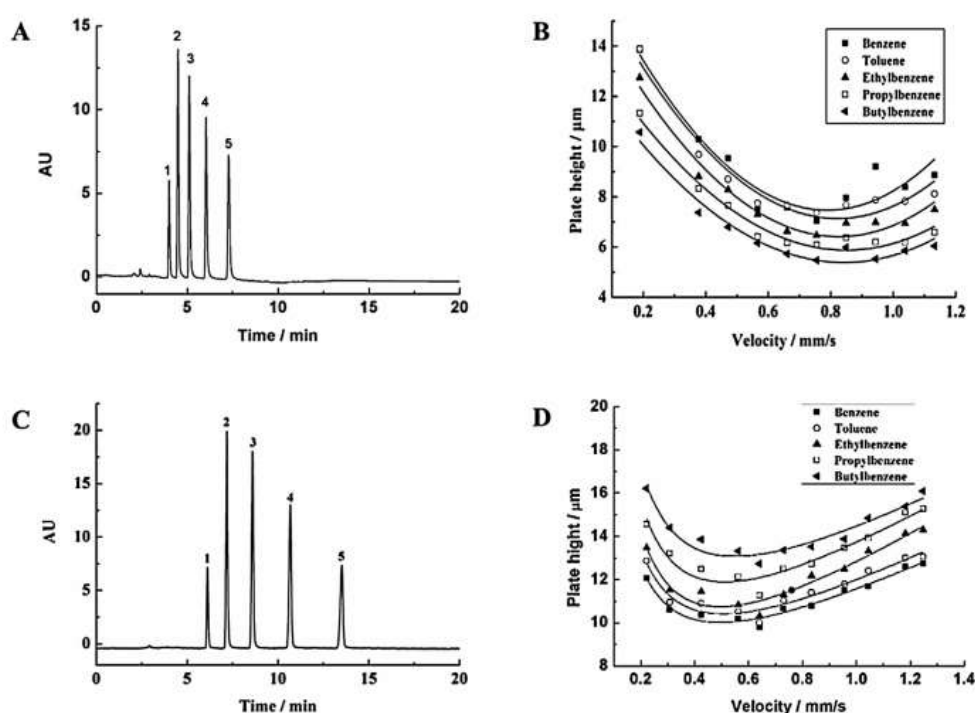


Figure 20. Separation of alkylbenzenes obtained under reversed-phase chromatographic mode using POSS-based hybrid monoliths prepared by thiol-ene click chemistry. Efficiencies are shown vs flow velocity. Reproduced from ref 73 90 by permission of Elsevier.

Additionally, POSS-epoxy-PTM monolith was implemented for cLC-MS/MS analysis of BSA digest. Fifty three unique peptides were positively identified with protein sequence coverage of 58.65%, while C18-particle-packed column, used for comparison purpose, provided lower analytical performances where 51 unique peptides were positively identified with protein sequence coverage of 56.01%. Monolithic matrices, easily prepared through thiol ene, with carbon rich skeleton exhibit hydrophobic surface properties as suggested by contact angle measurements indicating values well above 90°C.⁸² This behavior can be used for the LC separation of apolar solutes such as alkylbenzenes. For such homologous series, selectivity values were extracted from the plots of $\log k = f(n)$ with n being the number of carbon atom in the aliphatic side chain and were found to increase from 1.27 to 1.43 when the ACN content was changed from 80 to 65%. The separation properties were further investigated towards five basic compounds, four pesticides and EPA610, consisting of sixteen priority PAHs pollutants with potential health hazards (**Figure 21**). The authors claimed for very high columns efficiency with values up to 1130,000 plates/meter although phenanthrene and anthracene were not baseline resolved.

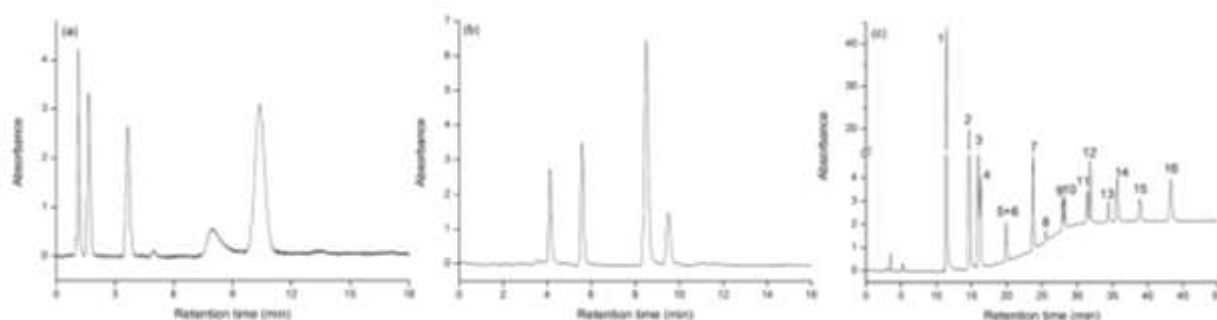


Figure 21. Separation of (A) basic compounds, (B) pesticides (C) EPA610 obtained under reversed phase chromatographic mode using organic monoliths prepared by photolith-ene click chemistry. Reproduced from ref 65 82 by permission of Elsevier.

Incorporation within the polymeric matrix of monomer such as tetraphenylethane glycidyl, i.e. containing phenyl units, provided monoliths with π - π conjugate interaction ability besides the expected RP retention mechanism.⁹¹ This was proved to a large extent for the separation of

analytes with π electron, whose retention was assigned to the large number of benzene rings in their structure. Interestingly enough, the authors showed that for these monoliths obtained through thiol-ene reaction between polyglycidyl and polythiol partners, the monolith may also exhibit some retention mechanism correlated to hydrophilic interaction chromatography (HILIC). Such behavior was assigned to the fact that through ring opening of glycidyl units, hydroxyls are formed and act as hydrophilic interaction sites. Cyclodextrin derivatives became increasingly important as chiral selectors for enantioseparations in capillary electrophoresis,¹²⁸ gas¹²⁹ and liquid¹³⁰ chromatography, capillary electrochromatography¹³¹. Our group reported the first enantioseparation obtained with a monolithic stationary phase with surface-immobilized β -Cyclodextrin via Huisgen click reaction.⁷ The same column was successfully applied to both capillary chromatography and electrochromatography for the separation of flavanone. Other cyclodextrin-functionalized monoliths obtained by alkyne–azide 1,3-dipolar cycloaddition enabled the separation of three flavonols and eleven PAHs.¹⁰⁶ Other type of clickable chiral selector includes a quinine carbamate derivative, namely O-9-tert-butylcarbamoylquinine, allowing the separation of dinitrobenzoyl-(R,S)-leucine in CEC mode.⁷⁹ Organic-silica hybrid monolithic columns incorporating [2-(methacryloyloxy)ethyl]trimethylammonium or acrylamide served for anion-exchange/hydrophilic interaction liquid chromatography.⁸³ Different types of analytes, including benzoic acids, inorganic ions, nucleosides, and nucleotides, were well separated with column efficiency in the range 80,000–130,000 plates/m (**Figure 23**). The columns were found to provide highly reproducible separation properties with batch-to batch, column-to-column and run-to-run relative standard deviation (RSD) of 7.7%, 2.3% and 0.9%, respectively, for the retention time of five nucleosides. Increase in the retention time with the increase in ACN content suggested HILIC retention mechanism. The low RSD values were considered as indicative of both column homogeneity and uniform distribution of functional groups onto the monolith surface.

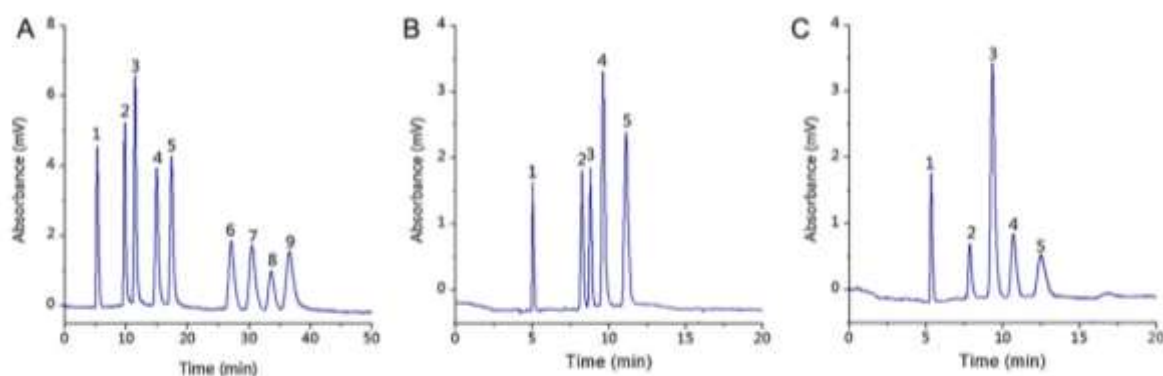


Figure 22. Separation of (A) nucleosides, (B) and (C) nucleotides obtained under hydrophilic interaction chromatographic mode using organic-silica hybrid monoliths prepared by thiolene click chemistry. Reproduced from ref 66 83 by permission of Elsevier.

Monolithic materials with multifunctional surface made of unique – *positive or negative* – or combined – *zwitterionic or amphoteric* – charges, aliphatic segment – *methylene-based spacer arm* – dipolar units – *amide anchoring site* – can provide mixed separation mode allowing, with the use of unique column though simple adjustment of the composition of the mobile phase, the separation of polar and apolar solutes according to their intrinsic hydrophobic/hydrophilic character.³¹ Silica hybrid monoliths with click grafted glutathione were used as chromatographic stationary phases for the separation small molecules and protein tryptic digests.⁸⁶ Separation abilities were tested in terms of hydrophobic, hydrophilic, and cation-exchange interactions using binary mobile phases with varied ratios of ACN/H₂O with or without different pH and concentration of phosphate buffered sodium. The results suggested that hybrid monoliths with grafts of tripeptidic nature may afford hydrophobic interaction, hydrophilic interaction and cation-exchange/hydrophobic interaction modes for the chromatographic separation of alkylbenzene, nucleotides and peptides. Phase mobile-dependent electrochromatographic separation mode was also observed for oligoethylene glycol-clicked poly(acrylate) monolith.¹¹ Polyethylene glycol-containing monoliths are often applied to reversed phase chromatography providing stationary phases with mild hydrophobic character.¹³² Our results showed that the elution order of acrylamide and toluene was reversed when changing the ACN–phosphate buffer (5 mM, pH 8) mobile phase composition from 60/40 (v/v) to 80/20. Toluene was eluted prior to acrylamide for rich ACN content. Phenol-like solutes – *2,3-dimethylphenol*, *p-chlorophenol*, *catechol* and *resorcinol* – were injected on the same column and the separation mechanism was found to governed by hydrophilic interaction as hydroxy-substituted phenols exhibited larger retention (**Figure 24**). All these

results illustrated typical HILIC behaviour for the oligoethylene glycol click grafted monolith.¹³³

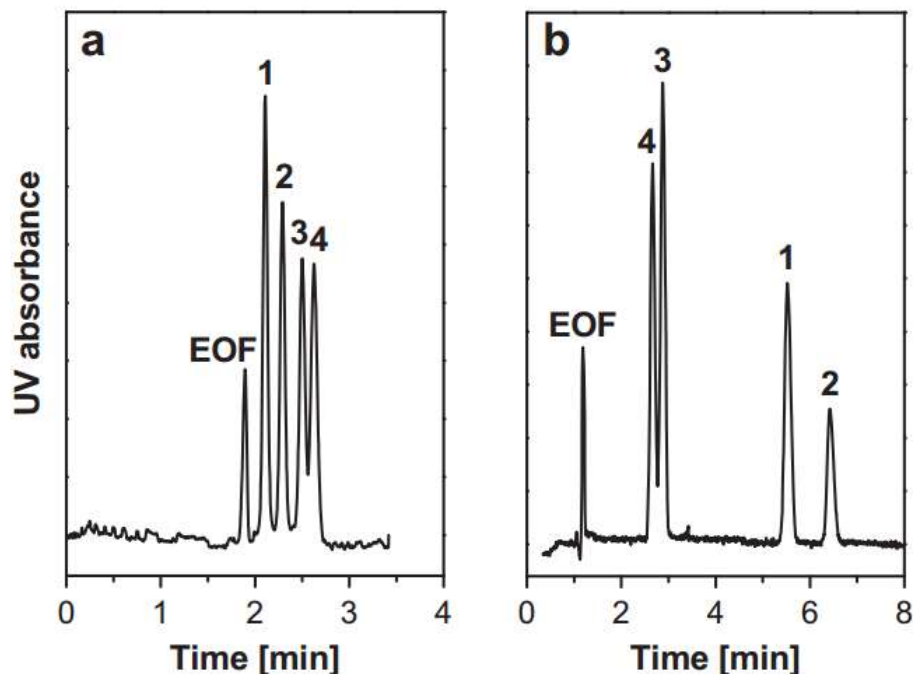


Figure 24. Separation of phenol obtained under (a) hydrophilic interaction and (b) reversed phase electrochromatographic modes using (a) oligoethylene-clicked and (b) C6-grafted monoliths having the same generic skeleton. Reproduced from ref 11 by permission of Elsevier.

Moreover, we showed that opposite separation behaviour was observed when using a C6-monolithic column prepared though functionalization of the same generic monolith. Monoliths with a highly hydrophilic surface chemistry were also obtained following the general scheme of thiol-mediated click chemistry for the surface grafting of amine⁸ or 3-sulfopropyl ammonium betaines¹⁰² moieties. Examples of successfully performed separation concern phenols, peptides and nucleotides. Classical reversed-phase and ion-exchange chromatographic retention mechanism was reported by Huihui Yang et al. using (3-sulfopropyl methacrylate potassium)-silica hybrid monolithic column.⁹² The former was proved from the retention of alkylbenzene, i.e. the retention increased with the number of methyl groups on the benzene ring, while anilines were used to establish the ion-exchange mechanism. Anilines were less retained when the pH rose from 4.0 to 6.0 (**Figure 25**). Anilines exhibited strong retention at low pH, due to their positive charge and the resulting cation-exchange interaction with the sulfonated monolith. Increasing the pH led to anilines

deprotonation and lower retention. Above pH 6.0, the four anilines – aniline, N-methylaniline, p-toluidine, N,N'-dimethylaniline – are neutral and their apolar character accounted for their retention.

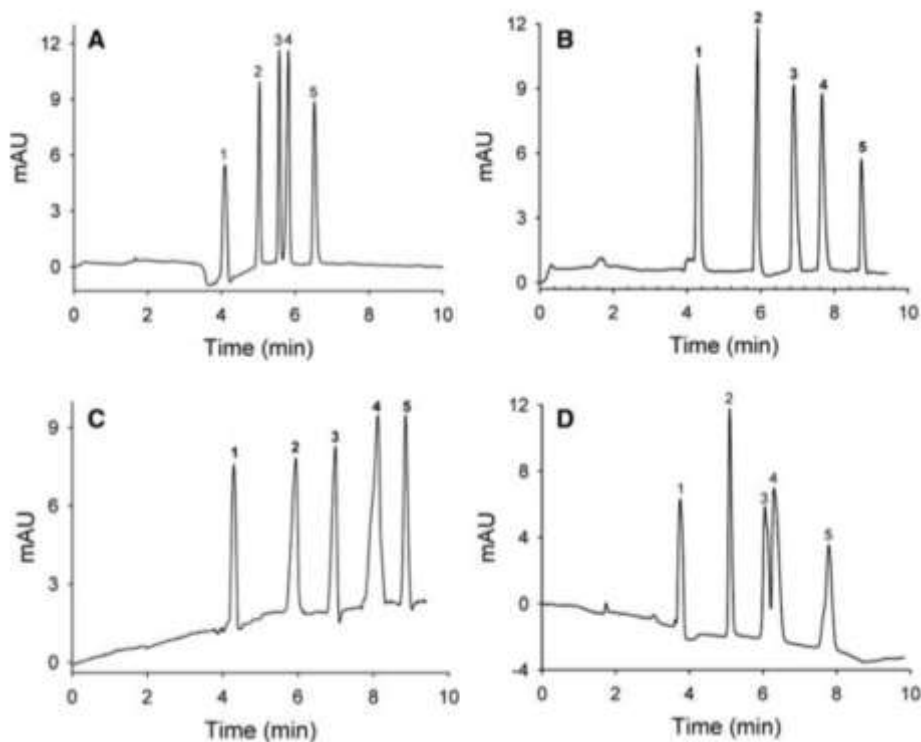


Figure 25. Separation of anilines obtained under ion-exchange electrochromatographic mode using hybrid monoliths with sulfopropyl surface functionality prepared by thiol-ene click chemistry. Reproduced from ref 75 92 by permission of Wiley.

6.2 Clicked monoliths for sample pretreatment technology

Sample treatment is a crucial step in the successful implementation of analytical methods. This is even more challenging when considering the area of bio-related samples analysis as the target (macro)molecules can be present at ultra-trace level and often, if not always, in mixture with interferent of complex chemical nature and topology that may generates false results. As such bioanalysis requires combining advanced technology relevant to microfluidics, surface science, analytical chemistry...

One area of great interest relies on the utilization of monolithic supports, especially the one made of polymers, as building elements of bioanalytical setups.¹³⁴

Recent literature reported about the click chemistry-mediated covalent attachment of bio-recognition elements on monolithic materials. Aptamers which are the artificial single-stranded DNA or RNA sequences have the ability to bind to complementary targets with high selectivity and affinity.¹³⁵ Hence, aptamer technology offers a powerful approach for the one step selective extraction and concentration of a target analyte from liquid matrices as well as sample purification from solid matrices extracts. In a recent study, affinity matrix made of organic-silica hybrid monolithic skeleton surface-decorated with aptamer against human α -thrombin linked through thioether bond was applied to the enrichment of trace proteins. Thrombin was extracted from human serum with recovery of 91.8%. All the results were compared with those obtained with a monolith grafted with a DNA oligo control. Incorporation of nanoparticles with high surface/volume ratios within monolithic materials greatly improved their specific surface area, especially in the case of organic polymer monoliths (**Figure 26**).⁹³ Such effect is beneficial to preconcentration ability even for low abundance peptides. Monoliths incorporating crosslinked and functionalized graphene – through Michael addition between thiolated graphene and EDMA and 4-vinylphenylboronic acid, respectively – exhibited large specific surface area of about 130 m²/g and enhanced binding capacity towards glycoproteins including horseradish peroxidase, ovalbumin, transferrin, alpha fetoprotein and ribonuclease A. The binding values were calculated as 10.16 and 10.47 mg/g (at pH 9.0) for disease markers transferrin and alpha fetoprotein, respectively, and were well-larger than the ones calculated for boronic acid-functionalized monolithic materials.^{105,136,137} Effect of the preconcentration segment length was optimized in a further step. Indeed, short preconcentration monolith led to poor enrichment factor while too-long preconcentration monolith resulted in high back pressure. Reasonable compromise was obtained for 14 cm long monoliths.

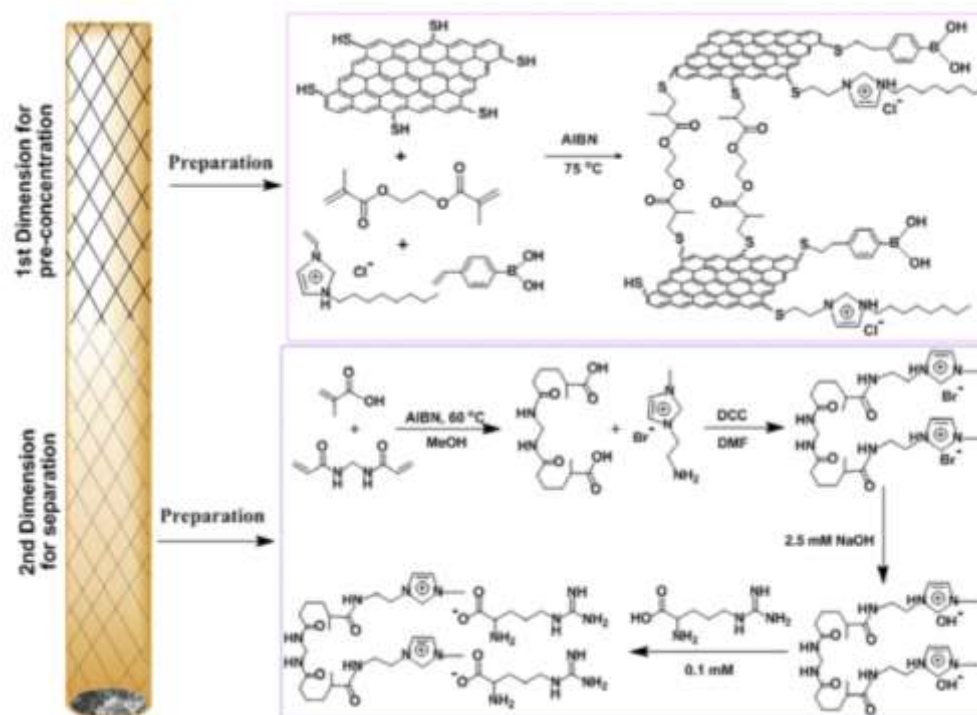


Figure 26. Schematic illustration of the synthetic path developed to prepare 2D monolith with a graphene-contained preconcentration segment incorporated through thiol-ene click chemistry. Reproduced from ref 77 93 by permission of American Chemical Society.

Specificity of boronate affinity hybrid monolith was evaluated toward nucleosides (adenoside) and glycoproteins (horseradish peroxidase, ovalbumin, transferrin), selected as *cis*-diol-containing model compounds under neutral conditions.¹⁰⁵ pH of the phosphate buffer (0.1 M) was set at 7.5 and sodium chloride (0.3 M) was additionally used to prevent non-specific electrostatic interactions. Under these conditions, non-glycoproteins from an egg white sample were eluted at the dead volume while glycoproteins were specifically eluted under acidic (0.2M acetic acid) conditions.

6.3 Clicked monoliths for micro-reactor science and technology.

From the above, it is obvious that the click chemistry and monolith pair has been to date mainly applied to separation science. However, one should mention the utilization of clicked monolith for catalytic reaction both of enzymatic and chemical nature. Some of us have shown that Click chemistry in its thiol-maleimide implementation can afford efficient strategy to graft spacer arms on monolithic surface with enhanced reactivity towards lysine-containing biomacromolecules (**Figure 27**).¹¹⁵

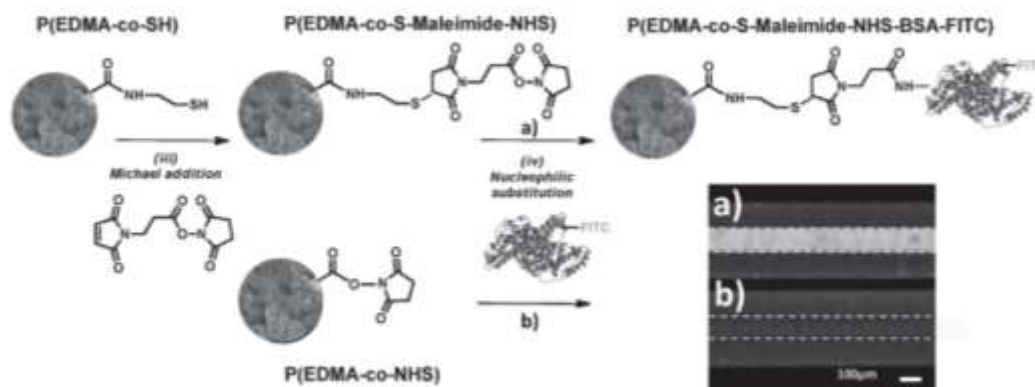


Figure 27. Schematic illustration of the synthetic path developed by our group to functionalize the surface of thiol-monolith through thiol-maleimide click chemistry. Reproduced from ref 103 115 by permission of Wiley.

A pepsin micro-reactor was prepared by conjugating pepsin onto azido-silica monolith via the CuAAC, with the aim to prove the feasibility of clickable monoliths for versatile design enzyme-based micro-reactors.⁹⁸ Efficiency of the as-designed micro-reactor was tested towards the digestion of immunoglobulin G. The monolith digest was analyzed by means of SDS-PAGE gel electrophoresis and the results were compared with immunoglobulin G digest obtained by from in-solution digestion. The authors illustrated that the pepsin micro-reactor efficiency is directly dependent on the flow rate, complete digestion of immunoglobulin G was obtained at $1\mu\text{L}\cdot\text{min}^{-1}$ at room temperature, corresponding to a reaction time of 2.8 min. In contrast, solution digestion required 40 min of incubation at 37°C . Moreover, the alkynyl modification of pepsin, a prerequisite prior to grafting on azido-monolith, did not affect significantly the enzyme activity. Silica hybrid monoliths functionalized with vinyl groups were biofunctionalized with trypsin taking advantage of the reactivity of free thiols produced through reduction of trypsin disulfide bonds (**Figure 28**).¹³⁸ Cysteamine labeled by fluorescein isothiocyanate (FITC) was used as model coupling ligand to evidence the free-radical reaction of ene groups on surface of the vinyl monolith. Then the trypsin containing free thiol groups was attached on the vinyl hybrid monolithic column via thiol-ene click chemistry in mild conditions (25°C , 5 h). Tris(2-carboxyethyl) phosphine hydrochloride was used as reducing agent. BSA and BHb with molecular weight of 67,000 Da and 64,500 Da, respectively were chosen as standard proteins for testing the enzymatic activity of the trypsin-based monolithic microreactor. The results showed that hydrolytic digestion of high molecular weight proteins can be achieved in short time (less than 30 s). Stability of the monolithic microreactors was evaluated over 100 times showing reminiscence of the initial

enzyme activity in the range 45.3 – 85.7%. Finally, lifetime of the enzymatic microreactors was tested by assaying five times per day over 15 days. Although activity of the surface grafted enzyme was found to decrease slowly with time, up to 88.2% of the initial activity could be preserved.

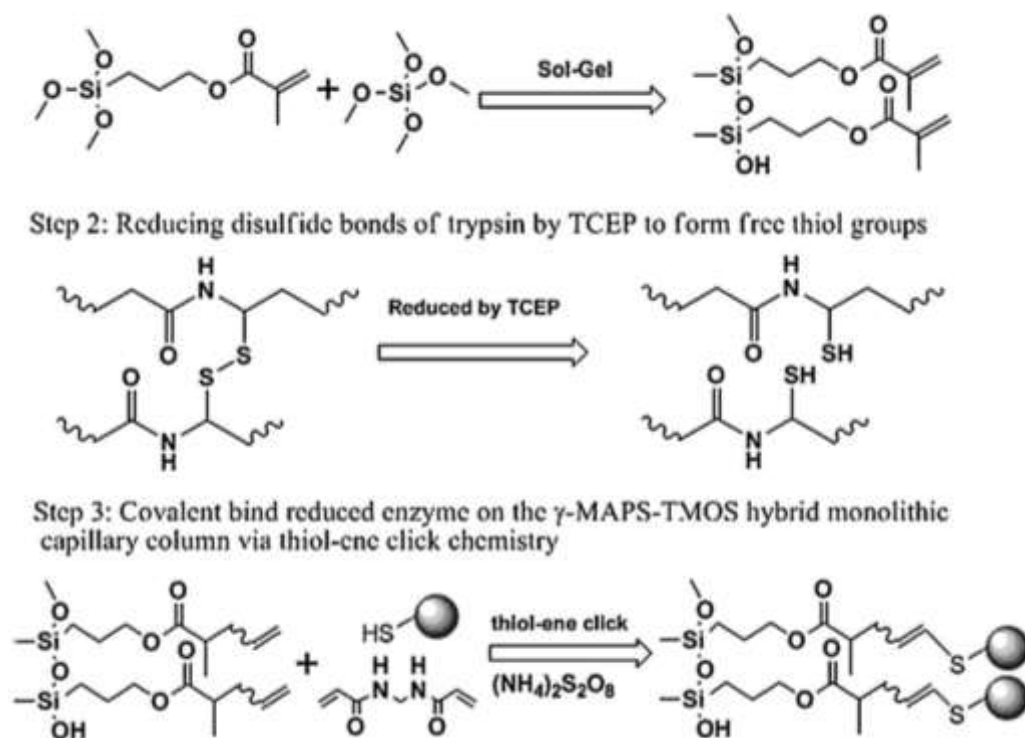


Figure 28. Schematic illustration of the synthetic path developed to synthesize hybrid monolith-based enzymatic microreactors through thiol-ene click chemistry. Reproduced from ref 133 138 by permission of Elsevier.

Our group has reported the use of clicked monoliths for heterogeneous catalysis applications using monolith-immobilized nano-metals as catalysts. The proof of concept was reported in an initial paper published in 2012, describing the versatility of thiol-yne surface click chemistry for the well-controlled functionalization of porous polymer-based monoliths (**Figure 29**).⁸

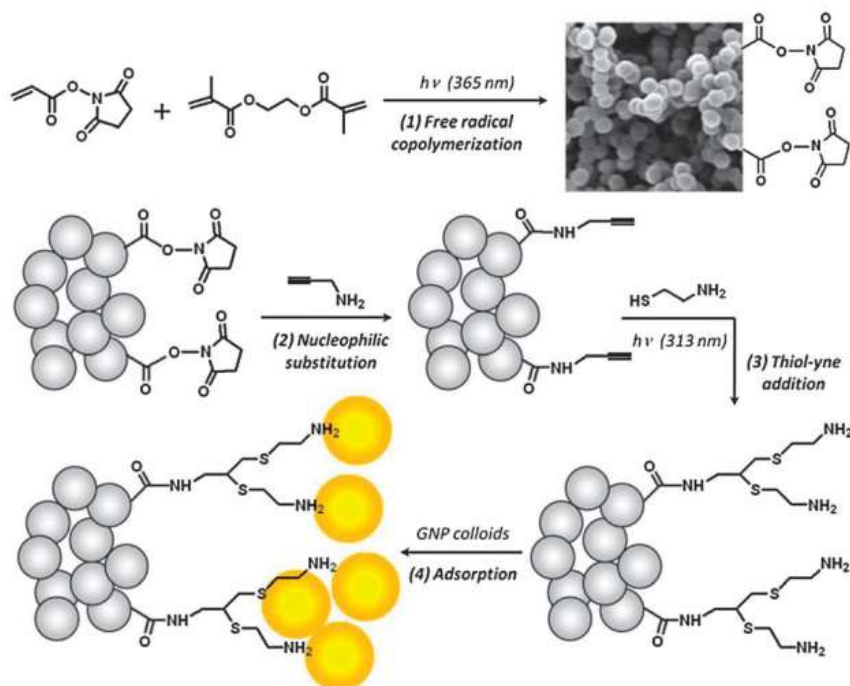


Figure 29. Schematic illustration of the synthetic path developed by our group to functionalize the surface of ene-monolith through thiol-ene click chemistry. Reproduced from ref 8 by permission of Royal Society of Chemistry.

Site specific immobilization of gold nanoparticles was successfully achieved through molecular-scale structuration of the monolithic column with amine groups, acting as gold nanoparticle ligands, using photo-initiated click reactions. The commercial availability of a large panel of functional thiols allows an easy change in the monolith surface functionality so that it can be judiciously adjusted with respect to the nature of the immobilized metal nanoparticles. Using the same generic monolithic matrix bearing N-hydroxysuccinimide surface reactive groups, we developed successively alkenyl- and carboxylated monolith via grafting of allylamine and thiol-ene-assisted addition of 4-mercaptopbutyric acid, respectively (**Figure 30**).¹² The monolith surface with carboxylic acid functionality enabled the robust anchoring of copper nanoparticles. Two pathways were envisioned for the nanoparticles immobilization through either percolation of a suspension of pre-formed copper nanoparticles through the capillary or by in situ reduction with sodium borohydride of Cu(II) Br₂ salt solution preliminary flown through the monolith. The so-called ex-situ and in-situ approaches afforded efficient catalytic microreactors for the reduction of nitroarenes.

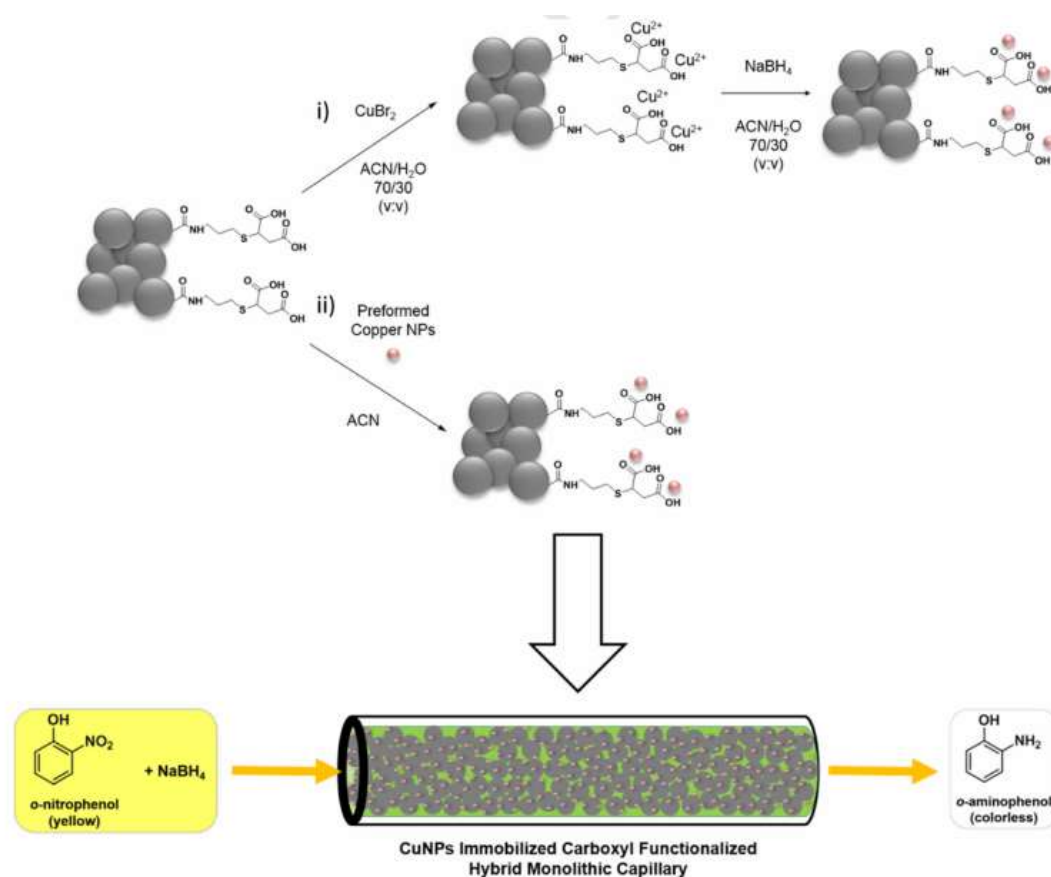


Figure 30. Schematic illustration of the synthetic path developed by our group to apply COOH-monolith obtained thiol-ene click chemistry as catalytic microreactor. Reproduced from ref 26 by permission of Elsevier.

We reported further the design of platinum nanoparticles-decorated monoliths applied as catalytic micro-reactor for the reduction of para-nitrophenol, as a model compound, into the corresponding amino-phenol.¹¹⁶

7. Conclusions

For about 25 years now, monolithic materials have been synthesized using a plethora of synthetic routes enabling the fine control of both skeleton and surface chemistry. The former affords mechanical resistance in combination with transport properties for applications under flow conditions. The latter ensures the functionality of the monolithic surface providing specific interaction with analytes or reactants. Organic (methacrylate, acrylate, carbonate) inorganic (silica, silsesquioxanes) and hybrid monolithic matrices have all been subjects of investigation by the chemists interested in spreading click reactions in all range of materials science. Although thiol-ene radical addition is the prominent click method in the context of monolithic materials, we attempted, in this contribution, to summarize the synthetic strategies, involving a click chemistry step, developed recently for synthesizing or functionalizing monoliths. Undoubtedly, click chemistry has allowed developing fast, one-step, if not one-pot, preparation methods of highly functional monoliths providing advanced solutions in analytical chemistry as exemplified with versatile stationary phases for separation science and smart sorbents for pretreatment of complex sample matrices preparation as well as in micro-reactors technology.

8. References

1. M. S. Silverstein, Special Issue of Polymer on porous polymers. *Polymer* 2014, 55(1), 302
2. F. Svec, T.B. Tennikova, Z. Deyl, *Monolithic materials: preparation, properties and applications*. 2003: Elsevier
3. M. Guerrouache, A.M. Khalil, S. Kebe, B. Le Droumaguet, S. Mahouche-Chergui, B. Carbonnier, *Surface Innovations*, 2015, 3(2), 84.
4. M. R. Buchmeiser, *Polymer* 2007, 48, 2187.
5. F. Svec, *J. Chromatogr. A* 2010, 1217(6), 902.
6. Andreas Brändle, Anzar Khan, *Polym. Chem.*, 2012, 3, 3224-3227
7. M. Guerrouache, M-C. Millot, B. Carbonnier, *Macromol Rapid Commun*, 2009, 30(2), 109
8. M. Guerrouache, S. Mahouche-Chergui, M. M. Chehimi, B. Carbonnier, *Chem. Commun.* 2012, 48(60), 7486
9. T. T. H. Dao, M. Guerrouache, B. Carbonnier, *Chinese J. Chin. Chem.* 2012, 30(10) 2281;
10. M. Guerrouache, S. Mahouche-Chergui, T. Mekhalif, T.T.H. Dao, M.M. Chehimi, B. Carbonnier, *Surf. Interface Anal.* 2014, 46(10-11) 1009-1013.
11. I. Tijunelyte, J. Babinot, M. Guerrouache, G. Valincius, B. Carbonnier, *Polymer* 2012, 53(1), 29;
12. R. Poupard, B. Le Droumaguet, M. Guerrouache, B. Carbonnier, *Mater. Chem. Phys.* 2015, 163, 446
13. Svec F., Frechet J.M.J. *Anal. Chem.* 1992, 64(7), 820.
14. Kubin, M, Spacek P, Chromecek R, *Collect Czech Chem Commun*, 1967, 32, 3881.
15. Hjertén S, Liao JL, Zhang R, *J. Chromatogr.* 1989, 473, 273.
Hjertén S, Nakazato K, Mohammad J, Eaker D, *Chromatographia* 1993, 37(5/6), 287.
16. Hjertén S, Li YM, Liao JL, Mohammad J, Nakazato K, Pettersson G, *Nature* 1992 356(6372): 810-811.
17. Nakazato K, Mohammad J, Hjertén S, *Chromatographia*, 1994, 39(11-12), 655.
18. Svec F., Frechet, JMJ, *Science* 1996, 273, 205.
19. Tennikova T B, Belenkii BG, Svec F, *J. Liq. Chromatogr.* 1990, 13, 63.
20. Tennikova TB, Bleha M, Svec F, Almazova TV, Belenkii BG, *J. Chromatogr. A* 1991, 555(1/2), 97.
21. Minakuchi, H., Nakanishi, K., Soga, N., Ishizuka, N., Tanaka, N., *Anal. Chem.* 1996, 68, 3498 – 3501.
22. Ishizuka, N., Minakuchi, H., Nakanishi, K., Soga, N., Nagayama, H., Hosoya, K., Tanaka, N., *Anal. Chem.* 2000, 72, 1275.
23. Siouffi AM, *J. Chromatogr. A*, 2006, 1126, 86.
24. Guerrouache, M Carbonnier, B Vidal-Madjar, C Millot, MC. *J. Chromatogr. A*, 2007, 1149(2) 368.
25. Guerrouache, Mohamed; Millot, Marie Claude; Carbonnier, Benjamin, *J. Sep. Sci.* 2011, 34(16-17), 2271.
26. Meinus, R Hormann, K Hakim, R Tallarek, U Smarsly, BM, *RSC Advances* 2015, 5(26) 20283-20294.
27. Guerrouache, M; Pantazaki, A; Millot, MC; Carbonnier, *J. Sep. Sci.* 2010, 33 (6-7), 787.
28. Gunasena, Dilani N.; El Rassi, Ziad, *J. Chromatogr. A* 2013, 1317, 77.
29. Lin, XC; Feng, SH; Jia, WC; Ding, K; Xie, ZH, *J. Chromatogr. A* 2013, 1316, 104.
30. Yang, Gengliang, Bai, Ligai, Yan, Cuihong, Gu, Yanzhao, Ma, Junjie, *Talanta*, 2011, 85(5) 2666.
31. Carbonnier, B, Guerrouache, M, Denoyel, R, Millot, MC, *J Sep Sci*, 2007, 30(17), 3000.
32. Dinh, NP Cam, QM Nguyen, AM Shchukarev, A Irgum, K, *J. Sep. Sci.* 2009, 32(15-16), 2556.

33. Araya-Farias, M Taverna, M Woytasik, M Bayle, F Guerrouache, M Ayed, I Cao, HH Carbonnier, B Tran, NT, *Polymer* 2015, 66, 249.
34. Ladner, Y; Bruchet, A; Cretier, G; Dugas, V; Randon, J; Faure, K, *Lab Chip* 2012, 12(9) 1680.
35. Zhu, Tao; Row, Kyung Ho, *J. Sep. Sci.* 2012, 35(10-11) 1294.
36. Lowe, Andrew B, *Polym. Chem.* 2014, 5(17) 4820.
37. Lowe, Andrew B, *Polymer* 2014, 55(22) 5517.
38. Lapwanit, S., Trakulsujaritchok, T., Nongkhai, P.N., *Chem. Eng. J.* 2016, 289, 286
39. Ghaemy, M, Shabzendedar, S, Taghavi, M, *J. Polym. Res.* 2014, 21(6) 464
40. Zhang, ST He, XW Chen, LX Zhang, YK, *N. J. Chem.* 2014, 38(9) 4212.
41. Bayramoglu, G Celikbicak, O Arica, MY Salih, B, *Ind. Eng. Chem. Res.* 2014, 53(12) 4554.
42. Zhang, Q, Su, H, Luo, J, Wei, Y, *Catal. Sci. Technol.* 2013, 3(1), 235.
43. Galan, T, Prieto-Simon, B, Alvira, M, Eritja, R, Gotz, G, Bauerle, P, Samitier, J, *Biosens. Bioelectron.* 2015, 74, 751.
44. Wang, TY, Shannon, C, *Anal. Chim. Acta* 2011, 708(1-2) 37-43.
45. Li, N, Zhao, PX, Liu, N, Echeverria, M, Moya, S, Salmon, L, Ruiz, J, Astruc, D, *Chem. Eur. J.* 2014, 20 (27), 8363-8369.
46. Kolb, H. C.; Finn, Finn, M. G.; Sharpless, K.B.; *Angew. Chem. Int. Ed.* 2001, 40 (11), 2004-2021.
47. Lutz, J.-F.; *Angew. Chem. Int. Ed.* 2007, 46 (7), 1018-1025.
48. Binder, W. H.; Sachsenhofer, R.; *Macromol. Rapid Commun.* 2007, 28 (1), 15-54.
49. Iha, R. K.; Wooley, K. L.; Nystrom, A. M.; Burke, D. J.; Kade, M. J.; Hawker, C. J.; *Chem. Rev.* 2009, 109 (11), 5620-5686.
50. Moses, J. E.; Moorhouse, A. D.; *Chem. Soc. Rev.* 2007, 36 (8), 1249-1262.
51. Binder, W. H.; Sachsenhofer, R.; *Macromol. Rapid Commun.* 2008, 29 (12-13), 952-981.
52. Yu, B.; Chan, J. W.; Hoyle, C. E.; Lowe, A. B.; *J. Polym. Sci. A Polym. Chem.* 2009, 47 (14), 3544-3557.
53. Chan, J. W.; Hoyle, C. E.; Lowe, A. B.; *J. Am. Chem. Soc.* 2009, 131 (16), 5751-5753.
54. Aimetti, A. A.; Feaver, K. R.; Anseth, K. S.; *Chem. Commun.* 2010, 46 (31), 5781-5783.
55. Tunca, U.; *J. Polym. Sci. A Polym. Chem.* 2014, 52 (22), 3147-3165.
56. Peng, H. Y.; Wang, C.; Xi, W. X.; Kowalski, B. A.; Gong, T.; Xie, X. L.; Wang, W. T.; Nair, D. P.; McLeod, R. R.; Bowman, C. N.; *Chem. Mater.* 2014, 26 (23), 6819-6826.
57. Sumerlin, B. S.; Vogt, A. P.; *Macromolecules* 2010, 43 (1), 1-13.
58. Mahouche Chergui, S, Ledebt, A, Mammeri, F, Herbst, F, Carbonnier, B, Ben Romdhane, H, Delamar, M, Chehimi, M. M. *Langmuir* 2010, 26(20) 16115-21.
59. Huisgen, R.; *Angew. Chem.* 1963, 75 (13), 604-37.
60. Jin, L.; Tolentino, D. R.; Melaimi, M.; Bertrand, G.; *Science Advances* 2015, 1(5), e1500304, DOI: 10.1126/sciadv.1500304
61. Makarem, A.; Berg, R.; Rominger, F.; Straub, B. F.; *Angew. Chemie Int. Ed.* 2015, 54 (25), 7431.
62. Becer, C.R.; Hoogenboom, R.; Schubert, U. S.; *Angew. Chemie Int. Ed.* 2009, 48 (27), 4900.
63. Agard, N. J.; Prescher, J. A.; Bertozzi, C. R.; *J. Am. Chem. Soc.* 2004; 126 (46), 15046.
64. Marechal, A.; El-Debs, R.; Dugas, V.; Demesmay, C.; *J. Sep. Science* 2013, 36 (13), 2049.
65. Chu, C.; Liua, R.; *Chem. Soc. Rev.* 2011, 40, 2177.

66. Hoyle, C. E.; Bowman, C. N., *Angew. Chemie Int. Ed.* 2010; 49 (9), 1540.
67. Hoyle, C. E.; Lowe, A. B.; Bowman, C. N.; *Chem. Soc. Rev.* 2010, 39 (4), 1355.
68. Posner, T. *Ber. Dtsch. Chem. Ges.* 1905, 38, 646.
69. Griesbaum, K. *Angew. Chem. Int. Ed.* 1970, 9, 273.
70. Fairbanks, B. D.; Scott, T. F.; Kloxin, C. J. ; Anseth, K. S.; Bowman, C. N.; *Macromolecules* 2009, 42 (1), 211.
71. Hoogenboom, R.; *Angew. Chemie Int. Ed.* 2010; 49 (20), 3415.
72. Grazu, V.; Abian, O.; Mateo, C.; Batista-Viera, F.; Fernandez-Lafuente, R.; Guisan, J. M.; *Biotechnol. Bioeng.* 2005, 90 (5), 597.
73. Carioscia, J. A.; Stansbury, J. W.; Bowman, C. N.; *Polymer* 2007, 48 (6), 1526.
74. Diels, O.; Alder, K.; *Liebigs Ann. Chem.* 1928, 460 (1), 98.
75. Sun, X. L.; Stabler, C. L.; Cazalis, C. S.; Chaikof, E. L.; *Bioconjugate Chem.* 2006, 17 (1), 52.
76. Goodall, G. W.; Hayes, W.; *Chem. Soc. Rev.* 2006, 35 (3), 280.
77. Gacal, B.; Durmaz, H.; Tasdelen, M. A.; Hizal, G.; Tunca, U.; Yagci, Y.; Demirel, A. L.; *Macromolecules* 2006, 39 (16), 5330.
78. Dai, J, Jiang, Y, Liu, X, Wang, J, Zhu, J, *RSC Advances* 2016, 6(22) 17857.
79. Zhang, D, Hu, P, Xu, Z, Chen, S, Zhang, J, Zhang, A, Miao, M, *J. Appl. Polym. Sci.*, 2015, 132(30) 42316
80. El-Debs R, Cadoux F, Bois L, Bonhommé A, Randon J, Dugas V, Demesmay C, *Langmuir* 2015, 31, 11649.
81. R. Goebel, P. Hesemann, A. Friedrich, R. Rothe, H. Schlaad and A. Taubert, *Chem. Eur J.*, 2014, 20(52), 17579.
82. L. Chen, J. Ou, Z. Liu, H. Lin, H. Wang, J. Dong and H. Zou, *J. Chromatogr. A*, 2015, 1394, 103.
83. M-L. Chen, J. Zhang, Z. Zhang, B-F. Yuan, Q.-W. Yu and Y-Q. Feng, *J. Chrom. A*, 1284 (2013) 118.
84. Z. Liu, J. Ou, H. Lin, Z. Liu, H. Wang, J. Dong, H. Zou, *Chem. Commun.*, 2014, 50, 9288
85. Z. Liu, J. Ou, H. Lin, H. Wang, Z. Liu, J. Dong, H. Zou, *Anal. Chem.* 86 (2014) 12334.
86. Zian L, Xiaoqing T, Ruifang Y, Jiashi L, Xiaofei Y, Lan Z, Huanghao Y, *J. Chrom. A*, 2014, 1355, 228.
87. F. Alves, I. Nischang, *Chem.-Eur. J.* 2013, 19, 17310.
88. Lin H, Ou J, Liu Z, Wang H, Dong J, Zou H, *J. Chrom. A*, 2015, 1379, 34.
89. Shen S, Ye F, Zhang C, Xiong Y, Su L, Zhao S, *Analyst* 2015, 140(1), 265
90. Lin H, Chen L, Ou J, Liu Z, Wang H, Dong J, Zou H, *J. Chrom. A*, 2015, 1416, 74.
91. Lin H, Ou J, Liu Z, Wang H, Dong J, Zou H, *Anal. Chem.* 2015, 87 (6), 3476
92. Yang H, Chen Y, Liu Y, Nie L, Yao S, *Electrophoresis* 2013, 34, 510–517.
93. Liu C, Deng Q, Fang G, Huang X, Wang S, He J, *ACS Appl. Mater. Interfaces* 2015, 7(36), 20430.
94. Liu C, Deng, Q, Fang, G, Huang, X, Wang S, *J. Mater. Chem. B* 2014, 2, 5229–5237
95. Currivan S, Jandera P, *Chromatography* 2014, 1(1), 24.
96. Viklund C, Ponten E, Glad B, Irgum K, Horstedt P, Svec F, *Chem Mater* 1997, 9(2) 463.
97. Slater M, Snauko M, Svec F, Fréchet JMJ, *Anal. Chem.* 2006 78(14) 4969.
98. Wu M, Zhang H, Wang Z, Shen S, Le XC, Li XF, *Chem. Commun.* 2013, 49, 1407
99. Cao Q, Xu Y, Liu F, Svec F, Fréchet JMJ, *Anal. Chem.* 2010, 82(17), 7416
100. Xu Y, Cao Q, Svec F, Fréchet JMJ, *Anal. Chem.* 2010, 82(8), 3352.
101. Lv Y, Alejandro FM, Fréchet JMJ, Svec F, *J. Chromatogr. A* 2012, 1261, 121

102. Lv Y, Lin Z, Svec F, *Analyst* 2012, 137, 4114-4118
103. Carrasco-Correa EJ, Ramis-Ramos G, Herrero-Martínez JM, Lämmerhofer M, *J. Chrom. A*, 2014, 1367, 123.
104. Slater MD, Fréchet JMJ, Svec F, *J. Sep. Sci.* 2009, 32, 21.
105. Yang F, Mao J, He XW, Chen LX, Zhang YK, *Anal. Bioanal. Chem.* 2013, 405, 5321.
106. Salwiński A, Roy V, Agrofoglio LA, Delépée R, *Macromol. Chem. Phys.* 2011, 212, 2700.
107. Schachtschneider A, Wessig M, Spitzbarth M, Donner A, Fischer C, Drescher M, Polarz S, *Angew. Chem. Int. Ed.* 2015, 54, 10465.
108. Malvi B, Sarkar BR, Pati D, Mathew R, Ajithkumar TG, Sen Gupta S, *J. Mater. Chem.* 2009, 19, 1409.
109. Xin Y, Sakamoto J, van der Vlies AJ, Hasegawa U, Uyama H, *Polymer* 2015, 66, 52.
110. Wang Z, Zhao JC, Lian HZ, Chen HY, *Talanta* 2015, 138, 52.
111. Maguis S, Laffont G, Ferdinand P, Carbonnier B, Kham K, Mekhalif T, Millot MC, *Opt. Express* 2008, 16(23) 19049.
112. Lomant AJ, Fairbanks G, *J. Mol. Biol.* 1976, 104, 243-61.
113. Cuatrecasas P, Parikh I, *Biochemistry* 1972, 11, 291.
114. Staros JV, Wright RW, Swingle DM, *Anal. Biochem.* 1986, 156, 220.
115. Belbekhouche S, Guerrouache M, Carbonnier B, *Macromol. Chem. Phys.* 2016, 217, 997.
116. Poupert, R; El Houda, DN.; Chellapermal, D; Guerrouache, M; Carbonnier, B; Le Droumaguet, B; *RSC ADVANCES*, 2016 (17) 13614.
117. Preinerstorfer B, Bicker W, Lindner W, Lämmerhofer M. *J. Chromatogr. A* 2004, 1044, 187.
118. Preinerstorfer B, Lindner W, Laemmerhofer M, *Electrophoresis*, 2005, 26, 2005.
119. Tang W, Ng SC, *Nature Protocols* 2008, 3, 691.
120. Zhao Q, Li XF, Shao Y, Le XC, *Anal. Chem.*, 2008, 80, 3915-3920.
121. B. Han, C. Zhao, J. Yin, H. Wang, *J. Chromatogr. B*, 2012, 903, 112-117.
122. Gömann A, Deverell JA, Munting KF, Jones RC, Rodemann T, Cauty AJ, Smith JA, Guijt RM, *Tetrahedron*, 2009, 65(7), 1450.
123. Krenkova J, Lacher NA, Svec F, *Anal. Chem.* 2009, 81(5), 2004.
124. Pfaunmiller EL, Paulemond ML, Dupper CM, Hage DS, *Anal. Bioanal. Chem.* 2013, 405, 2133.
125. Peterson DS, Luo Q, Hilder EF, Svec F, Fréchet JMJ, *Rapid Commun. Mass Spectrom.* 2004, 18(13), 1504.
126. Liu J, White I, DeVoe DL, *Anal. Chem.* 2011, 83, 2119.
127. Wang H, Zhang H, Lv Y, Svec F, Tan T, *J. Chromatogr. A* 2014, 1343, 128.
128. Wang Y, Zhang S, Breitbach ZS, Petersen H, Ellegaard P, Armstrong DW, *Electrophoresis* 2015, 37(5-6) 841.
129. Plotka JM, Simeonov V, Morrison C, Biziuk M, Namiesnik J, *J. Chromatogr. A* 2014, 1347, 146.
130. Janus, L, Carbonnier, B, Deratani, A, Bacquet, M, Crini, G, Laureyns, J, Morcellet, M *New J. Chem.* 2003, 27(2), 307.
131. Pedehontaa-Hiaa G, Guerrouache M, Carbonnier B, Le Derf F, Morin CJ, *Chromatographia* 2015, 78(7-8) 533.
132. Li Y, Tolley HD, Lee ML. *J. Chromatogr. A* 2010;1217:4934-4945.
133. Alpert AJ, *J. Chromatogr.* 1990, 499, 177.

134. Saunders KC, Ghanem A, Hon WB, Hilder EF, Haddad PR. *Anal. Chim. Acta* 2009, 652(1-2), 22.
135. Pichon V, Brothier F, Combes A, *Anal. Bioanal. Chem.* 2015, 407(3) 681.
136. Li Q, Lu C, Li H, Liu Y, Wang H, Wang X, Liu Z, *J. Chromatogr. A* 2012, 1256, 114.
137. Lin, Z.; Wang, J.; Tan, X.; Sun, L.; Yu, R.; Yang, H.; Chen, G. *J. Chromatogr. A* 2013, 1319, 141–147.
138. Chen Y, Wu M, Wang K, Chen B, Yao S, Zou H, Nie L, *J. Chromatogr. A*, 2011, 1218, 7982.

CHAPITRE II

Objectifs

Développer des monolithes à polarité de surface variable et applicable pour la séparation par électrochromatographie de molécules appartenant aux grandes familles de polluants organiques.

Démontrer que les mécanismes mis en jeu pour les séparations sont dictés par la nature des sélecteurs greffés en surface.

Montrer que les phases stationnaires monolithiques ainsi développées sont compatibles avec l'analyse de matrices réelles.

Méthodes

Méthode originale de greffage *via* la photo-addition radicalaire de type thiol-ène.

Greffage de sélecteurs originaux peu ou pas utilisés pour la préparation de phases stationnaires monolithiques.

Electrochromatographie d'interaction hydrophile

Electrochromatographie combinant les modes de phase inversée et de transfert de charge

Limites

Faibles efficacités des monolithes polaires fonctionnalisés par des unités diol et diacide carboxylique (les résultats dans ce dernier cas ne sont pas présentés dans ce manuscrit). A ce titre, la séparation de composés polaires, est considérée encore aujourd'hui par la communauté d'experts en sciences séparatives, comme un défi majeur des sciences analytiques.

Difficulté de greffer des sélecteurs volumineux porteurs de plusieurs phényles.

Faible réactivité des thiols aromatiques (tripénylméthane thiol) vis-à-vis de la chimie thiol-ène notamment du fait de la faible réactivité d'un radical thiyle en position alpha d'un cycle aromatique et stabilisé par mésomérie.

Importance

Premier exemple d'application de phases stationnaires monolithiques pour l'analyse d'analogues d'échantillons extraterrestres.

Premier exemple de préparation et d'application en électrochromatographie de phases stationnaires portant des sélecteurs triphényles ou diphényles.

Thiol-Ene Click Chemistry for the Design of Diol Porous Monolith with Hydrophilic Surface Interaction Ability: A Capillary Electrochromatography Study

Seydina Ibrahima Kebe¹, Meyssoun Ben Boubaker¹, Mohamed Guerrouache¹, Benjamin Carbonnier¹

¹ Université Paris-Est, ICMPE (UMR7182), CNRS, UPEC, F-94320 Thiais, France.

Journal of Chemistry, 2016, DOI: [10.1039/C6NJ00423G](https://doi.org/10.1039/C6NJ00423G)

Keywords: Electrochromatography, Hydrophilic polymer, Monolith, Surface click chemistry, Thiol-ene.

Abstract

Monolithic material with dual functionality was successfully synthesized through the combination of UV-initiated free radical copolymerization, nucleophilic substitution reaction and thiol-ene radical photoaddition. Firstly, poly(N-acryloxysuccinimide-co-ethylene dimethacrylate) was prepared by *non-solvent induced phase separation occurring within the course of the polymerization of the respective monomers*. Toluene was selected as porogen providing percolating pores in the micrometer range. Secondly, N-hydroxysuccinimide units on the monolith surface were converted into ene functionality through covalent immobilization of allylamine. Finally, thioglycerol served as hydrophilizing agent of the pore surface *via* surface confined thiol-ene click grafting. All the preparation steps were performed, *in-situ*, i.e. within the confines of UV-transparent capillary channels, affording micro-column with electro-osmotic flow generation and hydrogen bond forming abilities. Raman microspectroscopy confirmed that all the synthetic steps were accomplished successfully. Investigation of the electrochromatographic retention behavior of hydrophobic and hydrophilic solutes revealed the possibility of tuning the interfacial character of the diol-functionalized monolithic stationary phases with respect to the water content in the surrounding liquid phase. For acetonitrile-rich mobile phase, the diol-monolith interface exhibited highly hydrophilic character allowing fast and efficient separation of phenol and aniline derivatives, as well as methylxantines and pyrimidic bases. Moreover, relative standard deviation of the retention factor values were less than 3.3%.

1. Introduction

Porous polymer monoliths represent a fascinating class of materials discovered in the early 90's that revolutionized liquid chromatography.^{1,2} Pore size and size distribution are controlled by preparation conditions and can be tailored for a specific application.^{3,4} In particular, the porous morphology of monoliths is a key parameter to achieve high throughput analysis. Indeed, channels-like pores along the whole column provide fast mass-transfer kinetics. The ease of their preparation, based on a free radical polymerization process, has been extended to a variety of monomers and geometries.^{5,6,7} An important issue in designing porous polymers with predicted interfacial interaction properties relies on the control of the surface chemistry. Herein, we are discussing mostly post-polymerization functionalization strategies, although a simplest approach can be achieved through single step copolymerization of monomers.^{8,9} Two-step alternatives have been developed to avoid tedious re-optimizations

of the polymerization conditions inherent to any changes in the nature of the functional monomer. To date, epoxy-based monoliths were mainly considered as functionalizable matrix taking advantage of the reactivity of the oxirane groups, usually incorporated through copolymerizing glycidyl methacrylate with ethylene dimethacrylate, towards nucleophilic entities.^{10,11} Other reactive monomers were described in the literature giving a broad range of monoliths with targeted chemical reactivity.^{12,13,14,15} However, it is desirable to continuously develop new grafting method allowing easy and efficient chemical modification to face the growing demand of permeable materials with specific and finely-tuned interfacial properties. In this context, intrinsic properties of the so-called click reactions make them ideal candidates as a versatile platform for surface functionalization of porous materials.¹⁶ Indeed, click reactions are energetically favorable, exhibit insensitivity to solvent, compatibility with a broad range of functional groups and little work-up. Regarding the preparation of chromatographic stationary phases, the copper(I)-catalyzed (3 + 2) azide-alkyne click cycloaddition was first implemented for the chemical modification of silica^{17,18,19,20,21} and polymer²² beads and further extended to monolithic supports for capillary chromatography and electrochromatography applications.^{23,24} Other types of click reaction have also gained interest in separation science over the last years.²⁵ Chemical modification of thiol containing monoliths through reaction with chiral *ene* via thermal-initiated radical addition, in other words thiol-ene click reaction, was reported under conditions nearly 10 years ago.^{26,27} The inverse strategy was applied by the group of Liang to functionalize vinyl silica monolith with cysteine.²⁸

Macroporous hybrid monoliths meant for capillary liquid chromatography LC were successfully synthesized via thiol-ene click polymerization using 2,4,6,8-tetramethyl-2,4,6,8-tetravinylcyclotetrasiloxane, trivinylcyclohexane or tetravinylsilane as vinyl monomers and 1,6-hexanedithiol or pentaerythriol tetra(3-mercaptopropionate) as dithiol and tetrathiol, respectively.^{29,30} The photochemical variant of the thiol-ene³¹ and thiol-yne^{32,33} was recently described for designing electrochromatographic stationary phases through the surface grafting of hydrophilic and/or hydrophobic grafts on organic monoliths with surface-grafted alkene and alkyne groups, respectively. In one of their very recent contribution, the group of Svec focused on chromatographic applications of monoliths with dodecyl and zwitterionic functionalities prepared by thiol-ene surface modification of thiol-containing monoliths with hydrophobic and polar methacrylate ene monomers.³⁴ The thiol-mediated click addition has been applied to other fields of chemistry for designing chemical reactors for noble metal

nanoparticles-catalyzed reactions,^{35,36} affinity reactors for highly selective recognition of trace proteins.³⁷

Herein, a related electrochromatographic support based on hydroxysuccinimide ester-containing monolith was synthesized as reactive platform for the design of capillary column for electrochromatography applications. Hydrophilic functionality of poly(NAS-co-EDMA) was achieved by the subsequent grafting of allylamine and thioglycerol through nucleophilic substitution and thiol-ene photoaddition, respectively. The presented synthesis, characterization and electrochromatographic separation results indicate that interfacial behavior of monolith materials can be easily controlled through engineering the surface chemistry of pore surface.

2 Experimental

2.1 Materials

N-Acryloxysuccinimide (NAS), ethylene dimethacrylate (EDMA), 2,2'-azobisisobutyronitrile (AIBN), allylamine, acrylamide, phenol, resorcinol, pyrogallol, aniline, p-phenylenediamine, N,N-dimethylaniline were obtained from Acros Organics (Geel, Belgium). 3-(Trimethoxysilyl)propyl methacrylate and toluene (extra dry) were purchased from Fluka (Isle-d'Abeau, France). Thioglycerol, caffeine, uracil, thymine, theobromine, thiourea, cytosine, HPLC grade acetonitrile (ACN) and sodium phosphate were obtained from Sigma (Isle-d'Abeau, France). 2-Hydroxy-2-methyl-1-phenyl-propanone (*Darocure-173*) was purchased from BASF (Germany). All the reagents were used without further purification. Buffer was prepared using 18.2 M Ω deionized water filtered through a Milli-Q plus purification pack (Millipore, Bedford, MA, USA). Hydro-organic mobile phases were prepared by mixing the appropriate amount of acetonitrile with the phosphate buffer (5 mM, pH 8). Fused-silica capillaries with a UV-transparent external coating (75 μ m id \times 325 μ m od) were a kind gift from InnovaQuartz (Phoenix, ZA, USA).

2.2 Instrumentation

A Spectrolinker XL-1500 UV crosslinkers (Spectronics, Westbury, NY, USA) equipped with six lamps (6 \times 15 W) was used to photoinitiate the polymerization (365 nm) and to perform the thiol-ene click grafting reaction (313 nm). Chemical composition of the monolithic capillary columns was investigated after the successive preparation steps by Raman microspectroscopy

with the help of a LabRAM HR from Horiba Jobin Yvon (Longjumeau, France) equipped with a laser emitting at 633 nm. Samples were investigated at different places to probe the homogeneity of the surface functionalization. The acquisition time was fixed at 3 min. No specific treatment was applied to the sample prior to analysis. Morphology of the polymeric monoliths was evaluated using scanning electron microscopy with the help of a LEO Gemini 1530 SEM apparatus (Leo Elektronenmikroskopie, Oberkochen, Germany). Microscopic observations were performed for polymer in-capillary samples as obtained after polymerization and functionalization with allylamine and thioglycerol. All samples were rinsed with acetonitrile prior to analysis. Capillaries containing monoliths were cut at different locations and small pieces were deposited onto SEM supports with a silver-containing solution. Samples were dried under reduced pressure and coated with a thin layer of platinum (2 nm) with the help of a sputter coater Cressington 208 HR (Elektronen Optik Service, Dortmund, Germany). Porous characteristics of bulk monoliths were determined by mercury intrusion porosimetry (MIP) using an AutoPore IV 9500 porosimeter from Micromeritics. Determination of pore volume and average pore size was based on the Washburn equation between the applied pressure (from 1.03 to 206.8 MPa). All the electrochromatographic experiments were performed on a P/ACE MDQ (Beckman, Fullerton, CA, USA) equipped with 32 Karat software (version 4.0) for data acquisition. A pressure of 3.5 bar was applied to both ends of the capillary to prevent bubble formation during separation runs. Each analysis was repeated several times to enable statistical evaluation of electro-osmotic flow and retention factor variations.

3 Monolithic capillary column preparation

3.1 Step (i), synthesis of monolith with succinimidyl ester surface groups

Monolith with nucleophile-sensitive reactive groups was synthesized through the *in situ* photo-initiated (365 nm) free radical copolymerization of NAS (200 mg) and EDMA (110 μ L). The polymerization was performed in the presence of toluene (700 μ L) and 2,2'-azobisisobutyronitrile (1wt-% with respect to the total amount of monomers) acting as porogenic solvent and radical initiator, respectively. After brief sonication (5 min), homogeneous polymerization solution was introduced under pressure into fused-silica capillary (i.d. = 75 μ m) with surface-grafted methacrylate units. Experimental details about the activation of the inner wall of the capillary through sialization with 3-(trimethoxysilyl)propyl methacrylate and optimization of the polymerization mixture can be

found in Ref.³⁸ The polymerization process was initiated by placing the filled capillary, sealed at both ends, into the UV reactor. After 12 min of irradiation at 365 nm, the capillary was thoroughly washed with ACN (1h at 2 μ L/min) to remove the porogen and unreacted monomers. The remaining polymerization solution was poured in a sealed glass vial and polymerized under UV-irradiation. The as-obtained polymer was broken in pieces and Soxhlet extracted with ACN overnight. Then, it was dried overnight under vacuum at 60°C prior to bulk characterization.

3.2 Step (ii) synthesis of monolith with alkene surface groups

Succinimidyl groups stemming from the NAS monomer were transformed to ene units through reaction with an ene-containing amine, namely allylamine. Solution of allylamine (1M in ACN) was allowed to react under dynamic flow (2h at 1 μ L/min) at room temperature. Thereafter, the monolithic column was washed with ACN (1h at 2 μ L/min) in order to remove the unreacted allylamine. Hydrolysis of residual succinimide-esters was performed through thorough dynamic washing (4h at 2 μ L/min) of the monolithic capillary column with aqueous basic solution (pH 9). Finally, the column was rinsed successively with pure water and ACN.

3.3 Step (iii), synthesis of monolith with diol surface groups

The ene units present at the pore surface of the monolith provided anchoring sites for the grafting of diol-containing thiol, namely thioglycerol, through radical photoaddition reaction. The thiol-ene click reaction was carried out by filling the alkene-containing monolith with a thioglycerol solution (1M in ACN) containing darocure-173 (30 wt-%) and placing it under UV-irradiation (313 nm for 2 h). The photoinitiator allows hydrogen abstraction from thioglycerol molecules and further grafting of the reactive thiyl on the ene units at the pore surface of the monolith.

4 Results and discussion

4.1 Diol porous monolith: Design via thiol-ene click surface functionalization and characterization

Diol-bonded bead materials have been used since more than two decades as chromatographic packing for normal phase liquid chromatography (NPLC) for the separation of plant extracts³⁹ and steroids,⁴⁰ screening of biological materials, metabolic studies and preparative-scale isolation,⁴¹ steric exclusion chromatography of biological macromolecules,⁴² quantification of

tocopherols in tissues,⁴³ to cite but a few. Similarly to NPLC, polar solutes exhibit enhanced retention under hydrophilic interaction liquid chromatography (HILIC) conditions.⁴⁴ However, unlike NPLC, HILIC mobile phases are mixtures of water and water-miscible organic solvents as in typical reversed phase chromatography. HILIC implies the use of hydrophilic sorbents in conjunction with organic-rich eluent (ACN > 60%) thus creating a water-enriched interfacial layer partially immobilized on the phase stationary phase. Partitioning of the analytes between the organic-rich eluent and the water-rich adsorbed layer is assumed to be the major driving force for the observed separations.⁴⁵ Diol particulate columns have also proved efficient for the HILIC separation and quantification of a large panel of analytes such as vitamins,^{46,47} uric acid and methyl uric acids⁴⁸ while diol-bonded silica monolith served for the electrochromatographic separation of basic compounds.⁴⁹ In the latter case, retention was assumed to arise from reversed-phase, cation-exchange mechanism and electrophoretic effects. Organic monolithic stationary phases with polar surface functionality have also been considered for NPLC, HILIC and hydrophilic interaction capillary electrochromatography (HI-CEC) applications.^{50,51} One-step preparation of neutral diol monoliths through *in situ* polymerization of glyceryl methacrylate has been previously reported by the group of El Rassi, the envisioned applications dealt normal phase nano-LC and CEC,⁵² immuno-sorbents exhibiting reduced nonspecific interactions.⁵³ *In situ* copolymerization of methacrylate monomer and acrylate cross-linker bearing both pendant hydroxyl groups provided neutral monolithic stationary phase enabling HI-CEC separation of neutral and charged analytes.⁵⁴ The most popular monolith surface functionality for HILIC and HI-CEC applications involved amphiphilic and/or zwitterionic types.^{55,56,57} Herein, we suggest an alternative strategy for the preparation of diol monolithic capillary column with cathodic electro-osmotic generation ability following the reaction sequence schematically shown in Figure 1.

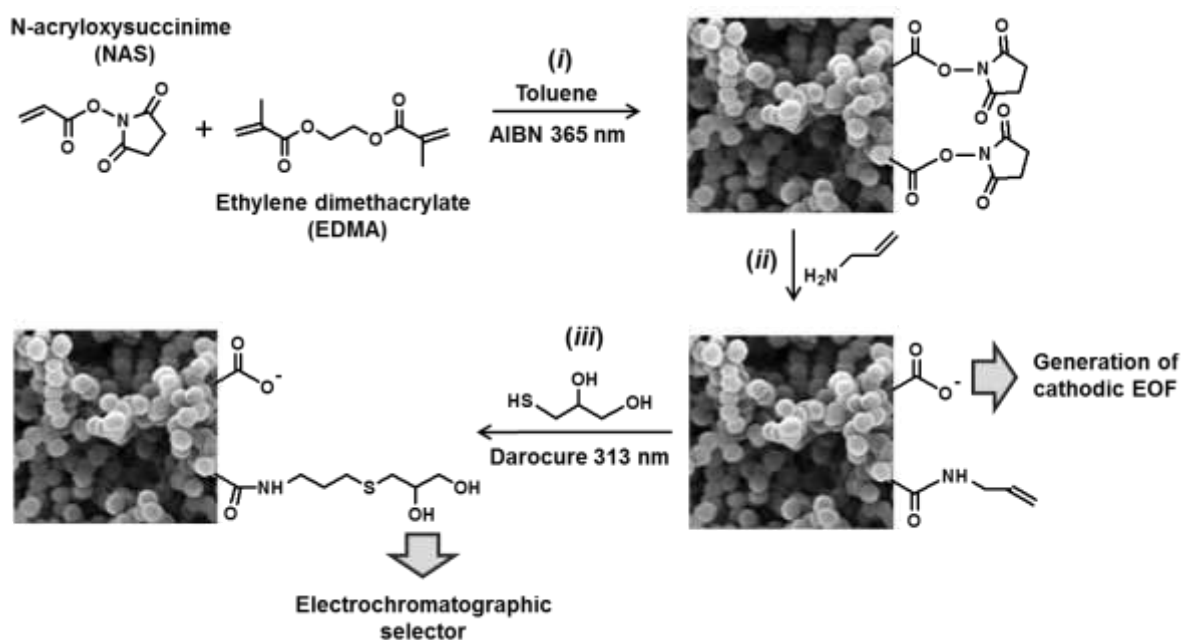


Figure 1: Reaction scheme for the preparation of diol-like monolithic capillary column through a three-step synthetic pathway: (i) copolymerization of NAS and EDMA in the presence of toluene as porogen and AIBN as initiator, via a free radical photo-initiated process (ii) grafting of allylamine via nucleophilic substitution, and (iii) grafting of thioglycerol via thiol-ene photoaddition.

Step (i) Monolith with nucleophile-sensitive surface reactivity and micrometer-sized channel-like pores was obtained through a combination of crosslinking – EDMA – and non-solvent-induced – toluene – phase separation of the growing polymer chains with reactive side groups – NAS – resulting from irradiation at 365 nm. Composition of polymerization mixture as well as UV irradiation time were optimized as previously reported by some of us.³⁵ Monolith with pristine surface was initially characterized by Raman spectroscopy as it is expected that evidence of the chemical derivatization can be ascertained not only by the appearance of new Raman bands characteristic for the grafted molecules, but also by the disappearance, or at least significant intensity decrease, of signals attributed to the hydroxysuccinimide moieties. At first glance, the Raman spectrum for poly(NAS-co-EDMA) displays an intense band centered around 2920 cm^{-1} and a three component signal in the $1770\text{--}1850\text{ cm}^{-1}$ wavenumber range (see the inset in the top spectrum). The latter signal is assigned to succinimidyl esters as the peaks at 1730 cm^{-1} (imide asymmetric stretching), 1785 cm^{-1} (imide symmetric stretching) and 1810 cm^{-1} (activated ester stretching) are typical for carbonyl. The large signal at about 2950 cm^{-1} arises from carbon-hydrogen nature of the polymer skeleton and indicates, for instance, contribution from asymmetric C-H stretching. N-hydroxysuccinimide esters are sensitive to both aminolysis and hydrolysis leading to (bio)molecular grafting *via* amide

bonding and formation of ionizable carboxylic acid groups, respectively.⁵⁸ Both aspects are considered in step (ii) in Figure 1 where the assumed monolithic structure exhibiting carboxylate and alkene groups is well-documented by the middle Raman spectrum in Figure 2.

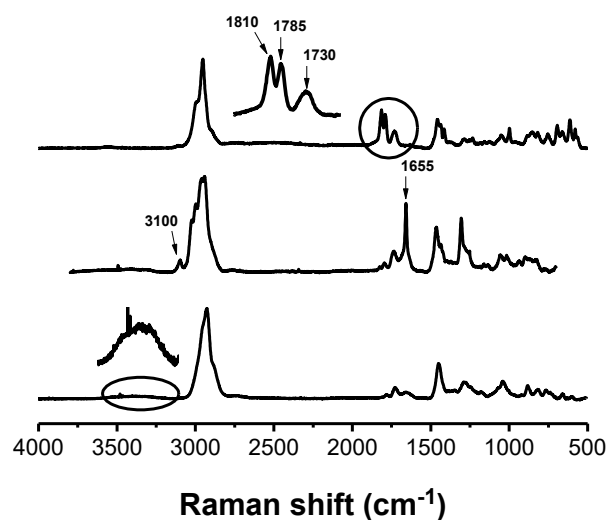


Figure 2: In-situ analysis by microspectrometry Raman of monolithic capillary columns after the different preparation step presented in Figure 1. The Raman spectra correspond to monoliths with pore surface containing (top) succinimidyl, (middle) alkene, and (bottom) diol groups. The insets present magnifications of the circled areas.

Indeed, the Raman intensity profile for the allylamine-grafted monolith shows a strong band at 1655 cm^{-1} , which is due to the presence of the allyl groups, together with a significant decrease in intensity of the carbonyl-related signals. This finding confirms that surface attachment of allylamine occurs *via* formation of amide bond as illustrated in Figure 1. Interestingly, is the presence of a signal, though weak, at a Raman shift of 3100 cm^{-1} corresponding to unsaturated C-H units. Morphology and porous characteristics were analyzed for native and functionalized monoliths synthesized in capillary (scanning electron microscopy) and as bulk samples (mercury intrusion porosimetry). Figure 3 shows SEM images of poly(NAS-co-EDMA) with native (A,B), alkene (C) and diol (D) surface. In all cases, typical monolithic morphology consisting of globuli fused together is observed confirming the porogen role of toluene.

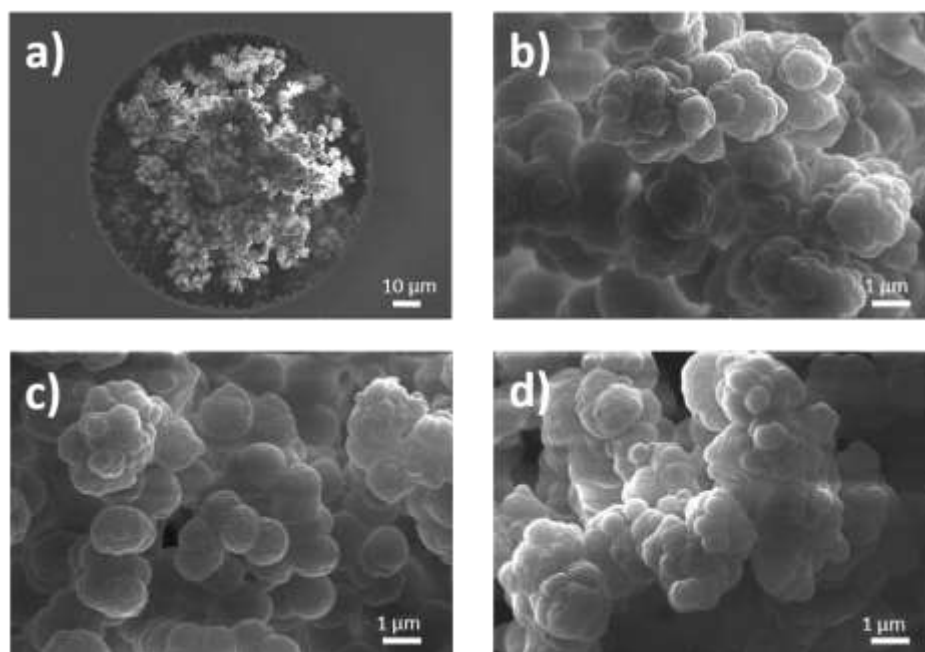


Figure 3: Scanning electron micrographs of poly(NAS-co-EDMA) monoliths synthesized in fused-silica capillary (75 μm id) with (A, B) native, (C) alkene and (D) diol surface. The white bars in the figure represent size of (A) 10 μm and (B-D) 1 μm .

Moreover, Figure 3A fully evidences that using a monomer/porogen ratio of 65.8% (wt/wt) provides complete filling of the cross-section of the capillary. It is also seen that the as-prepared monoliths contains macropores with an average size of 2.2 μm as determined by mercury intrusion porosimetry. The pore size distribution did not reveal the presence of significant mesopores leading to a surface area of 10 m^2/g and pore volume of 1.5 cm^3/g .

The ionized COO^- form is assumed to occur for pH value of the aqueous-based surrounding media above 5. Accordingly to what is observed in capillary electrophoresis, homogeneous distribution of negative charges on the surface of porous monolith may provide cathodic electro-osmotic flow allowing migration of liquid fluid and neutral molecules through the channel network. Electro-osmotic characteristics of the clickable monolith were assessed as a function of voltage and pH of the water-containing mobile phase. The data are summarized in Figure 4 only for the case where the pH value of the aqueous component of the mobile phase was equal to 8. Indeed, no measurable EOF was observed when using acidic PBS (pH < 6).

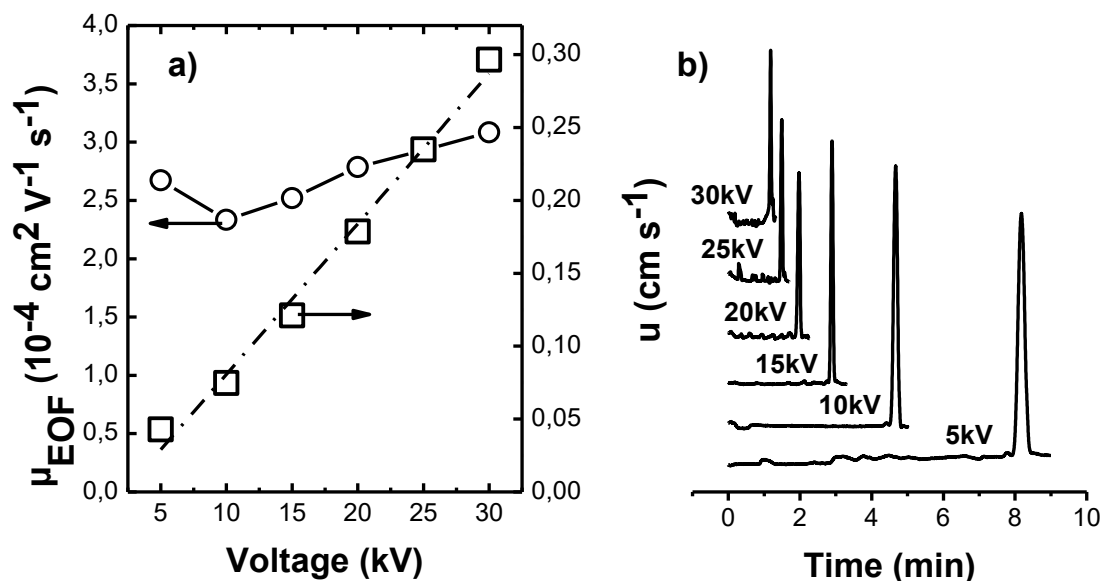


Figure 4: a) Voltage-dependence of EOF (μ_{EOF}) and linear (u) mobilities measured for the alkene-functionalized monolithic capillary column. b) Voltage-dependence of EOF marker elution peak on the alkene-functionalized monolithic capillary column. CEC conditions: Mobile phase: acetonitrile–phosphate buffer (5mM, pH 8) 70/30 (v/v). Column length: 21 cm to detector, 30.2 cm overall. Injections 8 kV for 4 s, running voltage varying from 5 to 30 kV at 25°C, UV detection at 214 nm.

Moreover EOF mobility was found to be pH dependent for pH value in the range 6-8 while remaining constant at pH 8 with a value of $2.7 \pm 0.3 \times 10^{-4} \text{ cm}^2 \text{ V}^{-1} \text{ s}^{-1}$ when changing the applied voltage from 5 to 30 kV. In contrast, linear mobility, calculated as the ratio between the effective length of the monolithic capillary column and the migration time, assumed direct dependence on voltage. An increase of 5 kV in the voltage results in an increase in linear mobility of 0.05 cm s^{-1} and vice versa. The run-to-run and day-to-day relative standard deviation values for EOF determination were 2.2 (n=7) and 6.8 (n=5) respectively. On the basis of the above discussed characteristics, polymer materials as obtained after step (ii) in scheme 1 may provide high permeability and fast mass transfer, stable and adjustable EOF, and easy chemical modification with species reactive towards unsaturated carbon-carbon bond. Free-radical addition reaction on alkenes have been largely applied since the discovery of the anti-markovnikov addition of HBr on $-\text{C}=\text{C}-$ moieties. In 1938, demonstration was made that the thiol-mediated variant proceeds *via* a free-radical chain mechanism.⁵⁹ Today, thiol-ene reaction that is recognized as a part of the so-called “click chemistry” is the focus of many material scientists, for polymer synthesis as well as surface functionalization.^{60,61,62} In step (iii) the surface-grafted ene units were allowed to react with thioglycerol in the presence

of Darocure 1173, acting as a type I photoinitiator. Most of aromatic carbonyl derivatives with appropriate substituents decompose into two distinct radicals under UV-illumination in relevant wavelength region, and one of the radical is efficient enough to initiate radical reaction mechanism.⁶³ In the case of thiol-ene, a thiyl radical react with an electron-rich double bond to form a thioether bridge and a new carbon atom-localized radical. The process goes further through reaction of the secondary resulting radicals with a thiol molecule present in the reactive solution. Hydrogen transfer generates the thioester adduct and a new thiyl radical allowing propagation of the radical cycle. Herein, reaction with the terminal carbon atom of surface-grafted allylamine is assumed to occur preferably. Raman characterization after grafting of thiolglycerol is illustrated by the down Raman spectrum in Figure 2. Accordingly to the assumed reaction mechanism, it clearly demonstrates the absence of C=C and =C-H signals at 1655 and 3100 cm^{-1} , respectively. The broad Raman signal (3200-3600 cm^{-1}) is indicative of the presence of hydroxyl groups on the monolith surface. It is to note that the remaining peak at 1655 cm^{-1} should not be considered as indicative of partial consumption of the C=C bond and thus, non-quantitative thiol-ene surface click functionalization. Indeed, grafting of allylamine is achieved through amide coupling the Raman signature of which is known to occur at about 1660 cm^{-1} . Erreur ! Signet non défini.

2.1 Evaluation of the electrochromatographic interaction ability of diol porous monolith

To evaluate the effect of surface-grafted diol units on the interfacial character of the monolith, capillary electrochromatography experiments were conducted using hydro-organic mobile phase with ACN as organic modifier and phosphate buffer. Obviously, it is expected that diol-containing monolithic interface exhibits hydrophilic character through hydrogen bonding formation with analytes. Depending on the hydrophilic/hydrophobic balance of the local environment, hydration of the interface may be more or less favoured. As described by Alpert in 1990, hydrophilic interaction liquid chromatography mechanism may be obtained for ACN-rich (80% or more) mobile phase. Figure 5 displays the electrochromatograms for the separation of a mixture of toluene, acrylamide and thiourea under typical HILIC (ACN = 80%) and reversed-phase (ACN = 30%) elution conditions.

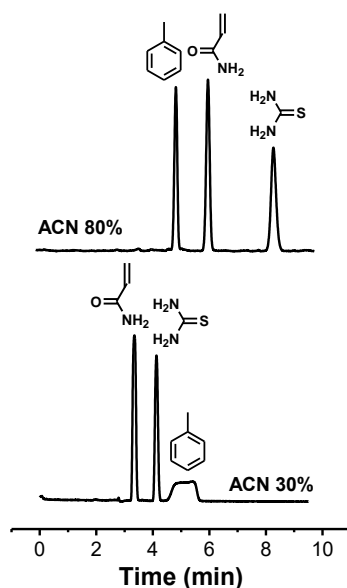


Figure 5: Effect of the ACN content in the aqueous-based mobile phase on the electrochromatographic separation and retention on the diol monolithic capillary column of a mixture consisting of acrylamide, thiourea and toluene. CEC conditions: mobile phase: ACN–phosphate buffer (5 mM, pH 8) the ACN content is indicated in the figure. Running voltage 15 kV. Other conditions as in Figure 4.

The elution profiles indicate a drastic change in the retention behaviour of toluene that is eluted first and last for these two separation modes, respectively. Under HILIC conditions, thiourea that is often selected as EOF marker in RP-CEC is eluted last as reported in previous study on using diol monolith for hydrophilic interaction capillary electrochromatography.⁶⁴ This finding confirms that under organic-rich (-poor) elution conditions, hydrophobic interactions are annihilated (reinforced) so that diol-functionalized monolithic capillary column may be used in HILIC and RP, respectively, in a reversible manner. The square-shaped elution peak indicates the limited solubility of toluene in the water-rich mobile phase.

2.2 Capillary electrochromatographic application of diol porous monolith

To get more insight into the discrimination behavior of the diol monolith, phenol and aniline derivatives were also injected (Figure 6). Hydrogen bonding ability of hydroxyl substituted aromatic rings is directly related to the number of OH groups, and it increases for the studied case from phenol (1 OH) to resorcinol (2 OH) and pyrogallol (3 OH). Correspondingly, pyrogallol exhibits increased retention as compared to phenol and resorcinol as typically observed for other hydroxyl monoliths.⁶⁴

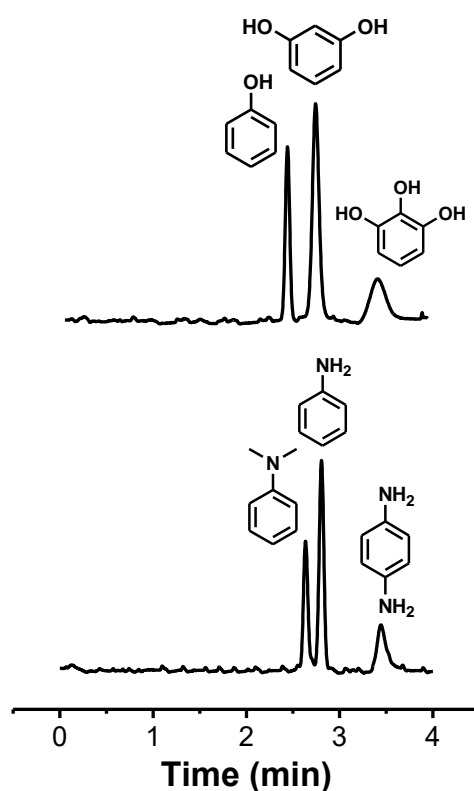


Figure 6: Electrochromatographic separations of (top) phenol and (bottom) aniline derivatives on the diol monolithic capillary column. CEC conditions: mobile phase: acetonitrile–phosphate buffer (5 mmol/L, pH 8) 70:30 (top) and (bottom) 80:20 (v/v). Other conditions as in Figure 4.

The three phenols are eluted with baseline separation within a time window of one minute using a rather low amount of ACN (70%). Indeed, similar separation results were obtained for the same phenols mixture with glyceryl methacrylate-based monoliths, however the ACN content was high as 95%. This finding suggests that the here-designed monolith exhibits highly hydrophilic surface behavior. Concerning aniline derivatives and regarding aniline as the reference compound, the presence of two methyl groups may not only increase the apolar character of N, N-dimethylaniline but also affect the possibility to form hydrogen bonds with the diol-interface. In contrast to that, the second NH₂ group in p-phenylenediamine produces the opposite effect. It is clear that for both phenols and anilines, the retention is primarily governed by the hydrophilic character of the solutes. Finally, we present in Figure 7, examples of separations of bio-related compounds, pyrimidic bases (top) and methylxanthines (bottom), presenting very slight change in their chemical structure.

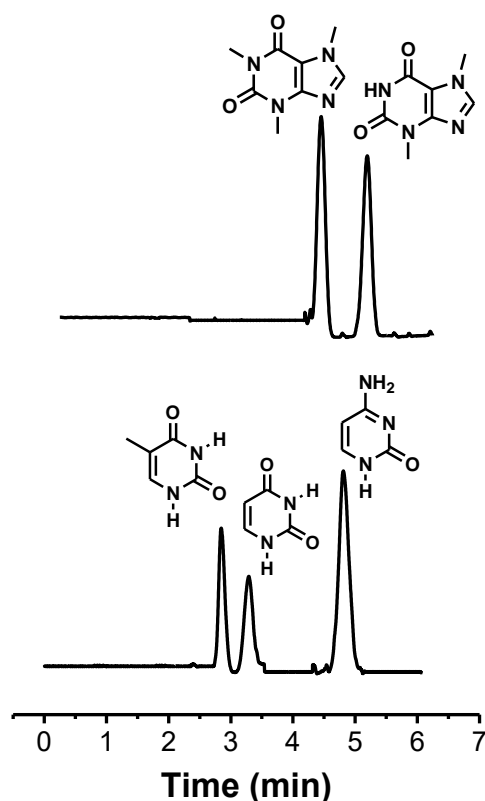


Figure 7: Electrochromatographic separations of (top) methylxanthines and (bottom) pyrimidic bases on the diol monolithic capillary column. CEC conditions: mobile phase: acetonitrile–phosphate buffer (5 mmol/L, pH 8) 80:20. Others conditions as in Figure 4.

For the former case, thymine (the less hydrophilic solute, $\log p = -0.46$) is eluted first and cytosine (the most hydrophilic solute, $\log p = -1.26$) is eluted last. Such an elution profile suggests that the retention is governed by hydrophilic effects.⁶⁴ Caffeine possesses an additional methyl group as compared to theobromine and is eluted first. It should be mentioned that neither poly(NAS-co-EDMA) nor alkene-functionalized poly(NAS-co-EDMA) demonstrated separation ability of phenols and anilines. The solutes were eluted within a broadened peak with retention time slightly larger than the EOF marker. These preliminary electrochromatographic results presented here, fully demonstrate that tailoring surface chemistry of porous monolithic *via* photo-initiated thiol-ene chemistry is an efficient way for designing stationary phases with hydroxylated interface. “For phenols and anilines, efficiencies up to 105 000 plates/m (RSD < 10 for n=5) were obtained while the relative standard deviation values for the retention factor were calculated to be less than 3.3% for phenol, N,N-dimethylaniline and theobromine”.

5 Conclusion

Today progress in separation science is closely related to new developments in the fields of chemistry and materials for designing adsorbents with well-defined interaction properties in constraint geometries. In this paper, thiol-ene click chemistry was envisioned as an original method for the surface functionalization of porous monolith starting with the preparation of reactive monolith inside fused-silica capillary by UV-initiated free radical polymerization of N-acryloxysuccinimide and ethylene dimethacrylate in toluene. Subsequent post-functionalization was performed *in situ* by reaction with allylamine giving rise to monolith surface decorated with alkene moieties. Using thioglycerol as ene sensitive reactant, diol units were covalently bonded through radical photoaddition. *In-situ* Raman microspectroscopy confirmed the success of the successive reaction steps. As interfacial diol functionality is supposed to provide interaction sites through hydrogen bonding, electrochromatographic performances of the monolithic capillary column was essentially tested under organic-rich elution conditions for phenols, anilines, methoxyanilines and pyrimidic bases.

6 References

1. F. Svec and J. M. J. Fréchet, *Anal. Chem.* 1992, **64**, 820.
2. F. Svec, J. M. J. Fréchet, *Science* 1996, **273**, 205.
3. C. Viklund, A. Nordstrom, K. Irgum, F. Svec and J. M. J. Fréchet, *Macromolecules*, 2001, **34**, 4361.
4. M. R. Buchmeiser, *Polymer*, 2007, **48**, 2187.
5. E. C. Peters, M. Petro, F. Svec and J. M. J. Fréchet, *Anal. Chem.*, 1998, **70**, 2288.
6. D. Hoegger and R. Freitag, *Electrophoresis*, 2003, **24**, 2958.
7. B. Xiong, L. Zhang, Y. Zhang, H. Zou and J. Wang, *J. High Resolut. Chromatogr.*, 2000, **23**, 67.
8. X. Jiaoa, S. Shena and T. Shia, *J. Chromatogr. B-Biomedical Applications*, 2015, **1007**, 100.
9. H. Zhang, J. Ou, Y. Wei, H. Wang, Z. Liu, L. Chen and H. Zou, *Anal. Chim. Acta*, 2015, **883**, 90.
10. F. Svec, *Electrophoresis*, 2006, **27**, 947.
11. X. Dong, J. Dong, J. Ou, Y. Zhu and H. Zou, *Electrophoresis*, 2006, **27**, 2518.
12. S. Xie, F. Svec and J. M. J. Fréchet, *Biotechnol. Bioeng.*, 2000, **62**, 30.
13. Q. C. Wang, F. Svec and J. M. J. Fréchet, *Anal. Chem.*, 1995, **67**, 670.
14. A. K. Palm and M. V. Novotny, *Rapid Commun. Mass Spectrom.*, 2004, **18**, 1374.
15. J. Duan, L. Sun, Z. Liang, J. Zhang, H. Wang, L. Zhang, W. Zhang and Y. Zhang, *J. Chromatogr. A*, 2006, **1106**, 165.
16. C. R. Langford, D. W. Johnson and N. R. Cameron, *Polym. Chem.*, 2014, **5(21)**, 6200.
17. Y. Wang, Y. Xiao, T. T. Y. Tan and S.-C. Ng, *Tetrahedron Lett.*, 2008, **49**, 5190.
18. Z. Guo, A. Lei, X. Liang and Q. Xu, *Chem. Commun.*, 2006, 4512.
19. Y. Zhang, Z. Guo, J. Ye, Q. Xu, X. Liang and A. Lei, *J. Chromatogr. A*, 2008, **1191**, 188.
20. K. M. Kacprzak, N. M. Maier and W. Lindner, *Tetrahedron Lett.*, 2006, **47**, 8721.
21. Z. Guo, A. Lei, Y. Zhang, Q. Xu, X. Xue, F. Zhang and X. Liang, *Chem. Commun.*, 2007, 2491.
22. M. Slater, M. Snauko, F. Svec and J. M. J. Fréchet, *Anal. Chem.*, 2006, **78(14)**, 4969.
23. A. Salwiński, V. Roy, L. A. Agrofoglio and R. Delépée, *Macromol. Chem. Phys.*, 2011, **212**, 2700.
24. M. Guerrouache, M.C. Millot and B. Carbonnier, *Macromol. Rapid Commun.*, 2009, **30**, 109.
25. Y. Chen, M. Wu, K. Wang, B. Chen, S. Yao, H. Zou, L. Nie, *J. Chromatogr. A*, 2011, **1218**, 7982.
26. B. Preinerstorfer, W. Bicker, W. Lindner and M. Lämmerhofer, *J. Chromatogr. A*, 2004, **1044**, 187.
27. B. Preinerstorfer, W. Lindner and M. Lämmerhofer, *Electrophoresis*, 2005, **26**, 2005.
28. A. Shen, Z. Guo, L. Yu, L. Cao and X. Liang, *Chem. Commun.*, 2011, **47**, 4550.
29. Z. Liu, J. Ou, H. Lin, Z. Liu, H. Wang, J. Dong and H. Zou, *Chem. Commun.*, 2014, **50**, 9288.
30. L. Chen, J. Ou, Z. Liu, H. Lin, H. Wang, J. Dong and H. Zou, *J. Chromatogr. A*, 2015, **1394**, 103.
31. I. Tijunelyte, J. Babinot, M. Guerrouache, G. Valincius and B. Carbonnier, *Polymer*, 2012, **53**, 29.
32. M. Guerrouache, S. Mahouche-Chergui, M.M. Chehimi and B. Carbonnier, *Chem. Commun.*, 2012, **48**, 7486.
33. T. T. H. Dao, M. Guerrouache and B. Carbonnier, *Chin. J. Chem.*, 2012, **30(10)**, 2281.
34. Y. Lu, Z. Lin and F. Svec, *Analyst*, 2012, **137**, 4114.
35. R. Poupart, B. Le Droumaguet, M. Guerrouache and B. Carbonnier, *Mat. Chem. Phys.*, 2015, **163**, 446.
36. R. Poupart, D. N. El Houda, D. Chellapermal, M. Guerrouache, B. Carbonnier and B. Le Droumaguet, *RSC Adv.*, 2016, **6**, 13614.

37. Z. Wang, J.-C. Zhao, H.Z., Lian and H.-Y., Chen, *Talanta*, 2015, **138**, 52.
38. M. Guerrouache, B. Carbonnier, C. Vidal-Madjar and M.C. Millot, *J. Chromatogr. A*, 2007, **1149**, 368.
39. M. Liibke., J-L. Le Quéré and D. Barron, *J. Chromatogr.*, 1993, *646*, 307.
40. A.W. Salotto, E. L. Weiser, K. P. Caffey, R. L. Carty, S. C. Racine and L. R. Snyder, *J. Chromatogr.*, 1990, **498**, 55.
41. L.R. Treiber, *J. Chromatogr. A*, 1995, **696(2)**, 193.
42. F. E. Regnier, and R. Noel, *J. Chromatogr. Sci.*, 1976, **14**, 316.
43. J. K. G Kramer, L. Blais, R. C. Fouchard, R.A. Melnyk and K. M. R. Kallury, *Lipids*, 1997, **32(3)**, 323.
44. G. Greco and T. Letzel *J. Chromatogr. Sci.*, 2013, 1.
45. A. J. Alpert, *J. Chromatogr.*, 1990, **499**, 177.
46. A. E. Karatapanis, Y. C. Flamegos and C. D. Stalikas, *J. Sep. Sci.*, 2009, **32 (7)**, 909.
47. A.E. Karatapanis, Y. C. Fiamegos and C. D. Stalikas, *Chromatographia* 2010, **71(9-10)**, 751.
48. N. S. Quiming, N. L. Denola, Y. Saito, A. P. Catabay and K. Jinno, *Chromatographia*, 2008, **67(7-8)**, 507.
49. F. Ye, S. Li and S. Zhao, *J. Chromatogr. Sci.*, 2009, **47**, 492.
50. M. Guerrouache, A. M. Khalil, S. I. Kebe, B. Le Droumaguet, S. Mahouche-Chergui, B. Carbonnier, *Surf. Innov.* 2015, 3(2), 84
51. J. Urban, P. Jandera, *Anal. Bioanal. Chem.* 2013, **405(7)**, 2123.
52. H. Zhong and Z. El Rassi. *J. Sep. Sci.*, 2009, **32**, 10.
53. D. N. Gunasena and Z. El Rassi, *J. Sep. Sci.*, 2011, **34**, 2097.
54. X. Wang, X. Lin, Z. Xie and J. P. Giesy, *J. Chromatogr. A*, 2009, **1216**, 4611.
55. Z. Jiang, N. W. Smith, P. D. Ferguson and M. R. Taylor, *Anal. Chem.* 2007, **79**, 1243.
56. Z. Jiang, N. W. Smith, P. D. Ferguson and M. R. Taylor, *Anal. Chem.* 2007, **79**, 1243.
57. M. Guerrouache, A. Pantazaki, M.-C. Millot and B. Carbonnier, *J. Sep. Sci.*, 2010, **33**, 1.
58. B. Carbonnier, M. Guerrouache, R. Denoyel and M-C. Millot, *J. Sep. Sci.*, 2007, **30**, 3000.
59. M.S. Kharasch, A.T. Read and F.R. Mayo, *Chem. and Ind.* 1938, **57**, 752.
60. C. E. Hoyle and C. N. Bowman, *Angew. Chem. Int. Edit.*, 2010, **49(9)**, 1540.
61. A. B. Lowe, *Polym. Chem.*, 2014, **5**, 4820.
62. S. Zhang, X. He, L. Chen, Y. Zhang, Yukui, *New J. Chem.*, 2014, 38 (9) 4212.
63. Y. Yagci, S. Jockusch and N. J., Turro, *Macromolecules*, 2010, **43**, 6245.
64. D. N. Gunasena and Z. El Rassi, *J. Chromatogr. A*, 2013, **1317**, 77.

Novel monolithic stationary phase with surface-grafted triphenyl selector for reversed-phase capillary electrochromatography

Tahar Mekahlif^{1,2}, Seydina Ibrahima Kebe¹, Mohamed Guerrouache¹, Noureddine Belattar², Marie Claude Millot¹, Benjamin Carbonnier¹

¹ Université Paris-Est, ICMPE (UMR7182), CNRS, UPEC, F-94320 Thiais, France.

² Département de Biologie, Laboratoire de Biochimie Appliquée, Faculté des Sciences, Université Ferhat Abbas, 19000 Sétif, Algeria.

Chromatographia, 2016, DOI [10.1007/s10337-016-3156-3](https://doi.org/10.1007/s10337-016-3156-3)

Keywords: Capillary electrochromatography; Phenyl-like monolith; Reversed-phase; Trityl

Abstract

A triphenylmethylamine-functionalized monolithic capillary column was newly designed for reversed-phase capillary electrochromatographic applications. Incorporation of the three phenyl rings-containing selector (also referred to as trityl selector) was achieved through post-polymerization functionalization of a generic monolithic matrix bearing nucleophilic-sensitive hydroxysuccinimide moieties. Such a 3D polymer matrix was obtained through UV-induced *in-situ* free radical copolymerization of N-acryloxysuccinimide and ethylene dimethacrylate. The separation properties of the trityl monolithic capillary column were initially evaluated *vis-à-vis* polycyclic aromatic hydrocarbons, as model hydrophobic compounds, and compared to the separation ability of a benzylamine-functionalized monolithic capillary column prepared using the same generic monolithic matrix. Electrochromatographic separation of phenols and anilines was also considered, and our preliminary results suggest the occurrence of hydrophobic interactions due to the aromatic and non-polar nature of the surface-grafted trityl selector. The triphenyl monolithic capillary column exhibited percent relative standard deviation values (%RSD) below 4.1% for the here-studied chromatographic parameters, namely retention factor, selectivity, resolution and efficiency.

1. Introduction

It is well-accepted that one of the major advantages of polymer-based monolithic stationary is the ease and flexibility of their synthesis owing to the wide range of available monomers incorporating side chains of interest as chromatographic selectors [1-4]. This is particularly true regarding the development of miniaturized chromatographic columns, where the polymeric monolith approach allows avoiding drawbacks inherent to the packing of small diameter particles into narrow-bore tubes as-well as the tedious fabrication of retaining frits. Inspired by the suspension polymerization protocols applied to the synthesis of porous polymer beads, free radical polymerization remains the most widely used method for the design of such monolithic columns. Thermal initiation was firstly implemented for the free radical copolymerization of functional monomers and crosslinkers in the presence of porogenic solvents [5, 6]. Photochemically-driven conditions were considered for the first time in 1997 and proved well-suited to the spatially controlled incorporation of monolithic materials within the confines of microchannels [7]. These two initiation methods are compatible with (meth)acrylate and styrenic monomers offering the possibility for a vast range of separation applications. Zwitterionic/betaine, hydroxyl- and amine-containing monomers have been used to prepare monoliths for the separation of hydrophilic solutes under normal phase [8], and hydrophilic interaction [9, 10] liquid (electro)chromatography conditions. Similarly to the case of particulate stationary phases, a large number studies aimed at applying monolithic stationary phases to separating hydrophobic solutes under reversed-phase analysis conditions [11-13]. In this respect, much experimental effort to date has been directed towards polymerizing phenyl-containing monomers – *styrene*, *phenylacrylate* – and crosslinkers – *divinylbenzene*, *1,4-phenylene diacrylate* – to design non-polar monoliths [14-19]. Benzyl methacrylate was also considered and free radical copolymerization with either bisphenol A dimethacrylate [20] or ethylene dimethacrylate [20, 21] provided well-defined monolithic stationary phases successfully applied to the separation of aromatic hydrocarbons and phenolic solutes. To date, reported applications of phenyl-type monoliths encompassed both chromatographic [14, 15, 20, 22] and electrochromatographic [16, 18, 19, 21, 23, 24] separations. An original synthesis approach involving alkylation of poly(styrene-divinylbenzene) monolith through Friedel-Crafts reaction was reported by the group of Buszewski and the separation properties were further evaluated under both μ -HPLC and CEC [17]. The post-functionalization strategy for designing phenyl-like monoliths is appealing as it allows avoiding problems inherent to the limited solubility and low reactivity

of monomers bearing bulky aromatic side chains [25]. Herein, we described the preparation of phenyl-like monolithic stationary phase through the post-polymerization grafting of aromatic amines onto N-acryloxysuccinimide-containing monolith. Triethylamine, also referred to as triphenylmethanimine according to the IUPAC nomenclature, is a well-known reactant in organic chemistry [26]. It was selected to surface-functionalize poly(NAS-co-EDMA) to provide monolithic stationary phase with local high electron-density with the aim to enhance pi electrons-mediated interactions between analytes and the stationary phase surface. The separation properties of the said monolith are discussed and compared with respect to the ones obtained for a benzyl-functionalized monolithic column. With such an approach, negative charges are generated *in situ* through hydrolysis of hydroxysuccinimide units on the monolith surface allowing generation of stable cathodic electro-osmotic flow at pH above 6.5 [27]. To the best of our knowledge, only one report discussed the use of a triphenyl selector in chromatography [28]. In 1994, Saito et al. applied triphenyl-bonded silica stationary phase for microcolumn liquid chromatography. Of particular interest, the triphenyl bonded phase was proved to exhibit larger retention ability towards C-60 and C-70 fullerenes than that observed for typical octadecyl silica phases. Hence the motivation for this work to further extend to use of triphenyl selector to both monolithic column and capillary electrochromatography.

2. Materials and method

2.1 Chemicals and materials

N-acryloxysuccinimide (NAS), ethylene dimethacrylate (EDMA), 2,2'-azobisisobutyronitrile (AIBN), aniline (99+%), *p*-phenylenediamine (99+%), 3,4-dimethylaniline (99.5%), 2-nitroaniline (98%), 4-nitroaniline (98%), 2,4-dinitroaniline (99%), 2,6-dichloro-4-nitroaniline (95%), resorcinol (98%), catechol (99+%), *m*-cresol (99%), *p*-chlorophenol (99%), 2,3-dimethylphenol (99%), benzylamine (99.5%) and triethylamine (99%) were obtained from Acros Organics (Geel, Belgium). 3-(trimethoxysilyl)propyl methacrylate, sodium hydroxide (NaOH), hydrochloric acid (HCl), toluene (extra dry), benzene (99+%), naphthalene (99+%), fluorene (98%), anthracene (99+) and pyrene (98%) were purchased from Fluka (Isle-d'Abeau, France). 3,3-Diphenylpropylamine (97%), HPLC grade acetonitrile (ACN), N,N-dimethylformamide (DMF) and sodium phosphate were from Sigma (Isle-d'Abeau, France). All the reagents were used without further purification. Buffers were prepared using 18.2 MΩ deionized water filtered through a Milli-Q plus purification pack (Millipore, Bedford, MA, USA). Hydro-organic mobile phases were prepared by mixing the appropriate amount of

acetonitrile with the phosphate buffer of desired pH value. Fused silica capillaries with a UV-transparent external coating (75 μ m ID \times 325 μ m OD) were a kind gift from InnovaQuartz (Phoenix, ZA, USA).

2.2 Instrumentation and methods

Functionalization and conditioning steps of the monolithic columns were achieved with an HPLC pump (Shimadzu LC-10ATVP, Champs sur Marne, France). Spectrolinker XL-1500 UV crosslinker (Spectronics, Westbury, NY, USA) equipped with six lamps (6 \times 15W, 365nm) was used to photo-initiate the polymerization. Monolithic capillaries were cut at different locations and small pieces were deposited onto the SEM supports with a silver-containing solution. Then, samples were dried under reduced pressure and coated with a thin platinum layer (2 nm) using a sputter coater Cressington 208 HR (Elektronen Optik Service, Dortmund, Germany). Porous characteristics of bulk monoliths were analyzed by mercury intrusion porosimetry (MIP) using an AutoPore IV 9500 porosimeter from Micromeritics. Determination of pore volume and average pore size was based on the Washburn equation between the applied pressure (from 1.03 to 206.8 MPa). All the electrochromatographic experiments were performed on a P/ACE MDQ (Beckman, Fullerton, CA, USA) equipped with 32 Karat software (version 4.0) for data acquisition. The analyte solutions (0.2 mg/mL) were injected using a voltage of 10 kV for 10 s. The separation runs were carried out at a voltage of 20 or 30 kV while the detection wavelength was set at 214 nm and temperature was kept at 25°C. A pressure of 3.5 bar was applied to both ends of the capillary to prevent bubble formation during separation runs. DMF was selected as unretained compound for EOF determination. Specific separation conditions are mentioned in the legend captions of the corresponding figures. Each analysis was repeated several times to enable statistical evaluation.

2.3 Synthesis of monolithic CEC columns

The synthetic pathway can be divided into three major steps as follows: (i) To ensure covalent attachment of the trityl-functionalized monolith within the capillary channel, inner wall was submitted to a vinylization step using 3-(trimethoxysilyl)propyl methacrylate [27]; (ii) monolith with flow-through pores was prepared by a free radical polymerization of NAS (200 mg) and EDMA (110 μ L) in toluene (700 μ L) solution. Initiation was achieved through UV-irradiation at 365 nm in the presence of AIBN (1% in mass with respect to the total amount of

monomers). UV-polymerization was performed on the whole length (50 cm) of the capillary column so that subsequent UV-degradation of a short section of the in-capillary monolith was necessary to design the detection window. After 12 min of irradiation, the capillary column was washed with ACN (1 h at a flow velocity of 2.5 $\mu\text{L}/\text{min}$) to remove the porogen and other remaining soluble compounds. The remaining polymerization solution was poured in a sealed glass vial and photopolymerized. The resulting polymeric monolith was broken into small pieces and Soxhlet extracted with ACN for 16h. Then, it was dried overnight under vacuum at 60°C prior to mercury intrusion porosimetry characterization. (iii) Chemical modification of the monolith surface was performed at room temperature under dynamic flow (2h at a flow rate of 1 $\mu\text{L}/\text{min}$) with a solution of tritylamine, 3,3-diphenylpropylamine or benzylamine (0.5 M in ACN). The 0.5 M concentration was dictated by the solubility of tritylamine. It was observed that using longer functionalization time did not lead to significant improvement of the separation properties of both monolithic columns. Thereafter, the monolithic column was washed successively with ACN (1 h) and a 70/30 (v/v) mixture of ACN and phosphate buffer (5 mM, pH 8) for 30 min. Such last step induces complete hydrolysis of remaining N-hydroxysuccinimide esters and the concomitant formation of carboxylic acid units allowing generation of cathodic electro-osmotic flow [26]. Overnight equilibration of the capillary was performed in the CE apparatus at a potential of +15 kV using similar hydro-organic mobile phase. Detection window was created by overnight irradiation of a small part of the monolith-filled capillary (0.8 mm, at a distance of ~ 10 cm from the outlet end) with the deuterium light of the detector [28]. Thus, total and effective lengths of the capillary columns for CEC applications are 30 and 20 cm, respectively.

3. Results and discussion

3.1 Preparation of triphenyl monolithic stationary phase

To date, glycidyl methacrylate was mainly used as reactive monomer for post-polymerization modification purposes allowing designing a nearly limitless range of smart monolithic supports [1]. In this study, we prepared hydroxysuccinimide-containing porous scaffold *via* the UV-driven copolymerization of N-acryloxysuccinimide and ethylene dimethacrylate (Fig. 1).

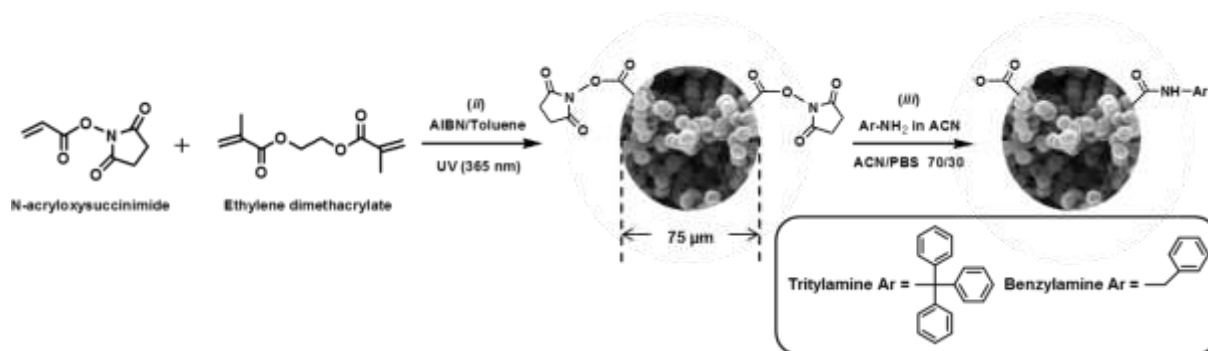


Fig. 1 Schematic representation of two of the synthetic steps (steps ii and iii described in the experimental section) applied to prepare poly(NAS-co-EDMA) monolith functionalized with tritylamine or benzylamine; (ii) NAS and EDMA are photopolymerized in the presence of toluene as porogen and AIBN as initiator, (iii) aromatic amine is grafted on the surface of the macroporous monolith via nucleophilic substitution of N-hydroxysuccinimide esters. Residual activated esters lead, under well-defined conditions, to carboxylic groups enabling generation of cathodic EOF.

As a result of the large amount of porogen added to the reactive mixture, 3-D structured polymeric skeleton with micrometer-sized tortuous porous channel network was obtained as shown in the SEM images in Fig. 2. size distribution centred around 2.2 μm was obtained by mercury intrusion porosimetry. Moreover, no significant mesopore (diameter in the range of 2–50 nm) fraction could be seen leading to a surface area of 10 $\text{m}^2\cdot\text{g}^{-1}$ and volume of $\sim 1.5 \text{ cm}^3\cdot\text{g}^{-1}$. The NAS monomer is expected to play a dual role in the functionality of the polymeric matrix that is to afford on the monolith surface (i) reactive sites for the grafting of hydrophobic and electron-rich selectors and (ii) negative charges upon hydrolysis for the generation of a cathodic EOF.

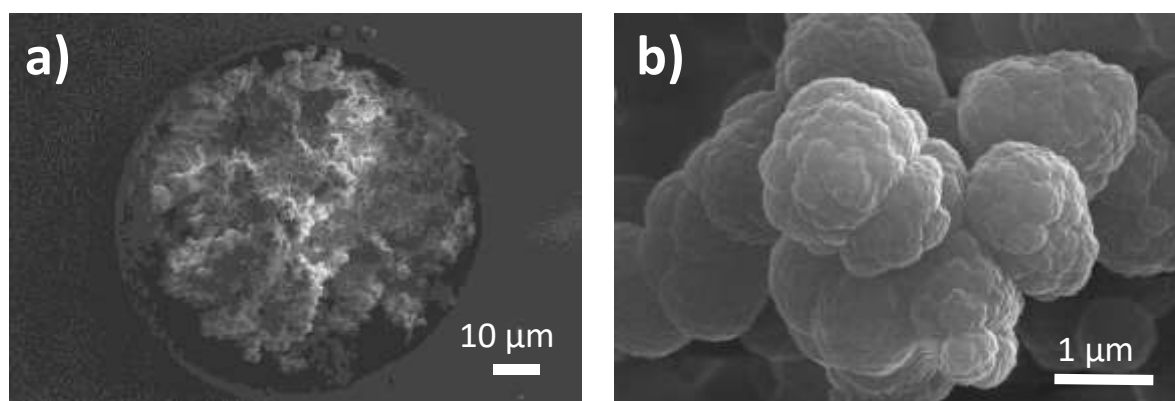


Fig. 2 Scanning electron micrographs of poly(NAS-co-EDMA) monoliths synthesized in fused-silica capillary (75 μm id) via photo-initiated polymerization. The white bars in parts a) and b) of the figure represent size 10 μm and 1 μm , respectively.

3.2 Evaluation of EOF generation ability

Separation performances of the tritylamine-functionalized monolithic capillary column was evaluated in CEC mode and comparatively studied with the performances of a benzylamine-grafted monolith. The latter was prepared *via* the grafting of benzylamine at the step (ii) of the synthetic pathway shown in Fig. 1. After the functionalization and hydrolysis/conditioning steps described in the experimental part, the direction of the EOF was detected from anode to cathode suggesting a negative value of the zeta potential in agreement with the scheme in Fig. 1. EOF generation ability for the tritylamine-functionalized was observed to be dependent on the electrolyte pH monolith in correspondence with the protonation/deprotonation behaviour of carboxylic acid groups as previously reported for related monolithic columns [26]. In other words, EOF could not be measured at pH below 5.5 while stable cathodic EOF assuming value of about $2.1 \times 10^4 \text{ cm}^2 \cdot \text{s}^{-1} \cdot \text{V}^{-1}$ was observed in the pH range 7.5-9.

3.3 Evaluation of retention mechanism

Based on the EOF-generation ability of the trityl-bonded monolith stationary phase, further CEC experiments were performed with mobile phase containing various amount of PBS at pH= 8. For initial evaluation of the separation behaviour of the tritylamine-functionalized monolithic capillary column, a mixture of five polycyclic aromatic hydrocarbons (PAH) was injected and the separation was compared to the one obtained on benzylamine-functionalized monolith (Fig. 3).

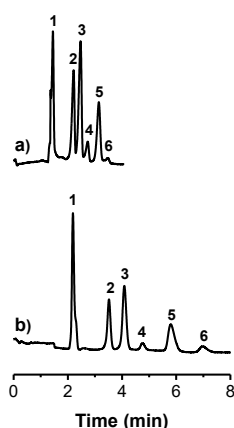


Fig 3 Electrochromatograms showing the separation of a mixture of (1) DMF, (2) benzene, (3) naphthalene, (4) fluorene, (5) anthracene and (6) pyrene on (a) tritylamine- and (b) benzylamine-functionalized monolithic capillary columns. CEC conditions; mobile phase acetonitrile-phosphate buffer (5 mM) pH 8 (70/30, v/v), running voltage 30kV at 25°C.

For neutral solutes such as PAH that do not exhibit electrophoretic mobility, the separation is strongly related to the interaction with the stationary phase that can be modulated through change in the elution power of the mobile phase. Thus, composition of the mobile phase was varied to reveal the nature of the separation mechanism (Fig. 4).

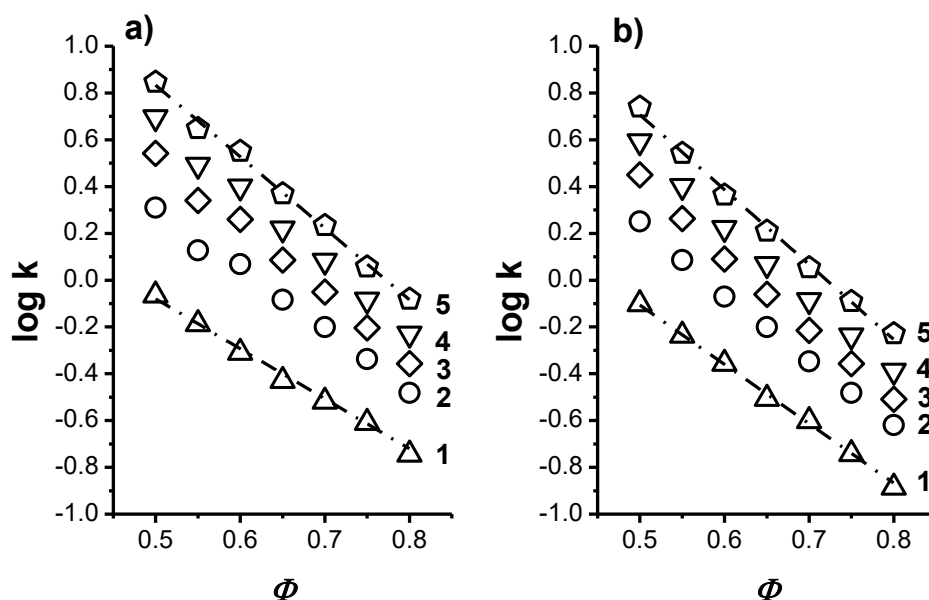


Fig. 4 Plots of logarithmic retention factor ($\log k$) on (a) tritylamine- and (b) benzylamine-functionalized monolithic capillary columns vs content of acetonitrile in the mobile phase (Φ) for (1) benzene, (2) naphthalene, (3) fluorene, (4) anthracene and (5) pyrene. CEC conditions; mobile phase acetonitrile-phosphate buffer (5 mM) pH 8, running voltage 30kV at 25°C.

The results as exemplified in both Fig. 3 and 4 demonstrate that the elution order of the monolithic capillary columns is similar to that of reversed-phase electrochromatography as the following comments can be formulated for both cases; (i) analytes with larger size (or more hydrophobic analytes) were eluted later than the analytes with smaller size (or less hydrophobic analytes), (ii) the retention decreases with increasing ACN content in the mobile phase and (iii) the elution order of the PAH is not changed for the tested mobile phase compositions.

It is also seen that retention and selectivity are larger on the tritylamine-functionalized monolithic capillary column. Baseline resolution is obtained for the five PAH on this column while it was not the case on the benzylamine-functionalized monolithic capillary column (Table 1).

Nature of the selector	Resolution for PAH			
	2,3	3,4	4,5	5,6
Benzylamine	1.21	1.17	1.61	1.26
Tritylamine	2.24	2.23	2.71	2.19

Table 1: Resolution values for the electrochromatographic separations of PAH, namely (2) benzene, (3) naphthalene, (4) fluorene, (5) anthracene and (6) pyrene on benzylamine- and tritylamine-functionalized monolithic capillary columns. CEC conditions; mobile phase acetonitrile-phosphate buffer (5 mM) pH 8 (70/30, v/v), running voltage 30kV at 25°C.

Fig. 5 displays the effects of varying molecular size and topology of PAHs on two chromatographic parameters, namely k and S . The latter parameter represents the slope of the linear variation of $\log k$ versus the ACN content in the mobile phase as illustrated in Fig. 3 for the two types of monolithic capillary columns.

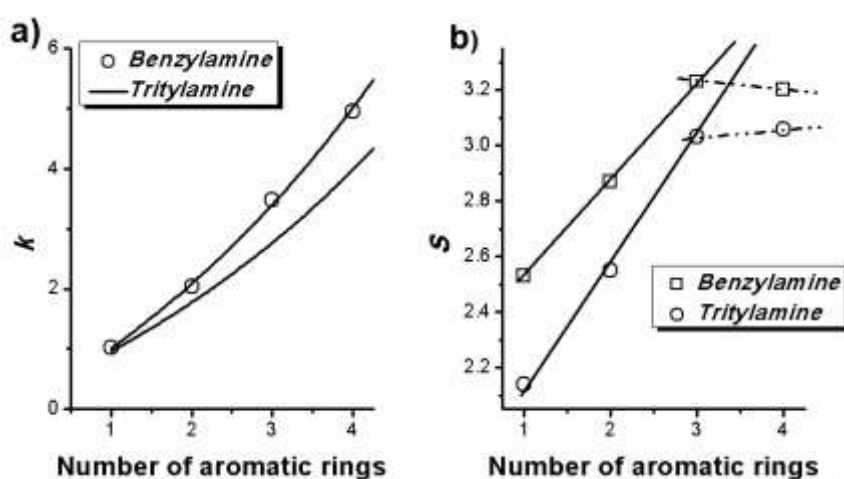


Fig. 5 Plots of (square) retention factor (k) and (circle) slope (S) of the linear dependence of ($\log k$) versus \square (%ACN in the mobile phase) presented in Figure 3a as a function of number of aromatic rings of PAHs, namely benzene (1 ring), naphthalene (2 rings), anthracene (3 rings) and pyrene (4 rings). CEC conditions for k values determination; mobile phase acetonitrile-phosphate buffer (5 mM) pH 8 (50/50, v/v), running voltage 30kV at 25°C.

As can be seen in Fig. 5a, the k values increase with the number of aromatic ring in the solutes, in other words with the number of π -electrons in the molecular structure. Such behavior supports π - π interactions between PAH and the aromatic amine-functionalized monolithic stationary phases in addition to typical nonpolar character [23]. The growth gets faster on the tritylamine-functionalized monolithic capillary column as compared to the

benzylamine-functionalized column suggesting a more pronounced contribution of the electron-mediated interaction to the overall separation mechanism. For RPLC applications, the direct dependence of $\log k$ versus the composition of the mobile phase has been expressed as follows [30, 31]:

$$\log k = \log k_w - S\phi \quad (eq.1)$$

where k_w is the hypothetical retention factor in the absence of organic modifier, i.e. in a poor solvent, S quantifies the changes in retention with the mobile phase composition and ϕ is the ACN content in the mobile phase. For linear PAHs, namely benzene, naphthalene and anthracene, S increases linearly with the number of aromatic rings (Fig. 5b). Discontinuity in the variation of S is observed for pyrene on the two monolithic capillary columns suggesting a change in selectivity. In our case such behavior can be assigned to the non-linear topology of pyrene although similar effect was also reported by Kayillo et al. for the retention of the fourth ring member of a PAHs series comprising benzene, naphthalene, anthracene, 2,3-benzanthracene and pentacene on phenyl-containing columns [31]. In the linear variation range, the retention is assumed to result from the occurrence of solute-stationary phase interaction with a direct dependence of the number of interaction sites on the number of aromatic rings in the PAH. Extrapolations of the linear fits for the two monolithic columns suggest that crossover would occur for larger linear PAHs. Indeed, the tritylamine-functionalized monolithic capillary column exhibits a larger rate of change in S as a function of the molecular weight in the PAH (0.45 to be compared with a value of 0.35 for the benzylamine-functionalized monolith) suggesting highest molecular-stationary phase interactions.

3.4 CEC applications

To gain further insight into the separation potential of tritylamine-functionalized monolithic capillary column, aromatic solutes with polar side groups were also tested. Electrochromatograms in Fig. 6a show the effect of the salt concentration on the separation of phenol derivatives. Increasing the buffer concentration from 5 mM to 20 mM leads to an increase in the retention factor while the resolution is not globally improved. As evidenced by peaks (1) in both electrochromatograms, the change in retention results from an increase in the electro-osmotic mobility at lower buffer concentration [27]. In these conditions, (2) resorcinol, (3) catechol, and (4) m-cresol are well-separated while (5) 2,3-dimethylphenol and (6) 4-chlorophenol are co-eluted last. The trityl-grafted monolithic stationary phase exhibited

an efficiency of 38 500 and 38 300 plates/m for the first eluted phenol 20 and 5 mM, respectively.

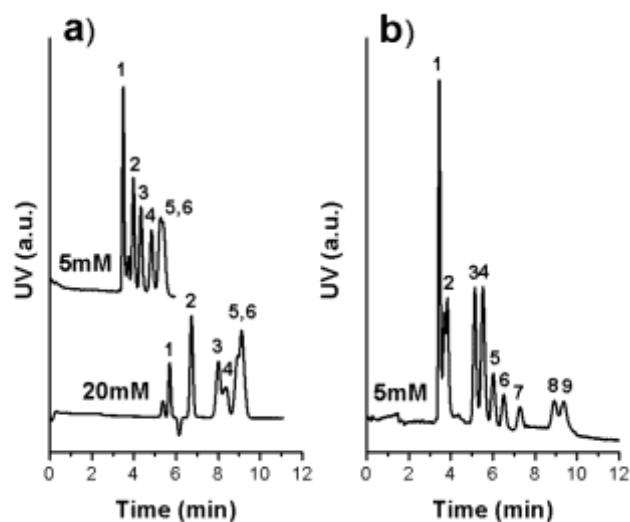


Fig. 6 Electrochromatograms showing the separation of a mixture of a) (1) DMF, (2) resorcinol, (3) catechol, (4) *m*-cresol, (5) 2,3-dimethylphenol and (6) 4-chlorophenol and b) (1) DMF, (2) *p*-phenylenediamine, (3) aniline, (4) 3,4-dimethylaniline, (5) 4-nitroaniline, (6) 2-nitroaniline, (7) 2,6-dinitroaniline, (8) 2,4-dinitroaniline and (9) 2,6-dichloro-4-nitroaniline on trytilamine-functionalized monolithic capillary column. CEC conditions; running voltage 30kV at 25°C, mobile phase acetonitrile-phosphate buffer pH 8 (55/45, v/v). The phosphate buffer concentration is given in the figure for each electrochromatogram (a top, b) 5 mM and (a, bottom) 20 mM.

Eight basic aromatic compounds, including (2) *p*-phenylenediamine, (3) aniline, (4) 3,4-dimethylaniline, (5) 4-nitroaniline, (6) 2-nitroaniline, (7) 2,6-dinitroaniline, (8) 2,4-dinitroaniline and (9) 2,6-dichloro-4-nitroaniline were tested (Fig. 6b). At pH 8, the aniline derivatives are not charged and their separation/retention should result from their difference in chromatographic partitioning. For typical RP-CEC, the retention is strictly governed by the hydrophobic character of the solutes. Thus considering the nature of the aniline substituents, non-polar groups, such as methyl, should lead to a larger retention. Such behaviour was not observed on the tritylamine-functionalized monolithic capillary column. Indeed, 3,4-dimethylaniline is eluted after aniline and before the aniline derivatives bearing polar nitro groups. This finding can be rationalized by the effect of electron-drawing nitro groups. Solutes with lowered π -electron density can interact more strongly with π -electron-containing selectors acting as weak electron donor systems. Consequently, electron density of the

anilines decreases with increasing the number of nitro groups so that 4-nitroaniline and 2-nitroaniline are eluted before 2,6-dinitroaniline and 2,4-dinitroaniline.

	EOF	k	α^a	Column efficiency
Run to run ($n=10$)	2.1	1.9	2.4	2.5
Day to day ^b ($n=5$)	2.8	3.3	2.9	3.8
Column to column ^c ($n=4$)	3.1	2.9	4.1	3.7

With n the number of injections

^a calculated for benzene and naphthalene

^b day, day + 3, day + 5, day + 9, day + 11

^c including batch to batch

Table 2: Relative standard deviation (RSD) values (%) for tritylamine-functionalized monolithic capillary columns

Electrochromatographic parameters were calculated as average values relative to the injection of a mixture of DMF, toluene and naphthalene. The run-to-run ($n=10$) %RSD values were 2.1, 1.9, 2.4 and 2.5 for EOF, retention factor, selectivity and column efficiency, respectively. Complementary information are provided in Table 2. These values are consistent with other studies on monolithic stationary phases for electrochromatography applications [32, 33].

4. Conclusion

In this contribution, the preparation and electrochromatographic applications of monolithic stationary phase with triphenyl selector are presented for the first time. The synthesis strategy relied on the post-polymerization functionalization of a monolithic support incorporating N-acryloxysuccinimide as reactive monomer. The hydroxysuccinimide units enabled the covalent bonding of tritylamine together with the generation of ionisable carboxylic groups acting as chromatographic selector and cathodic electro-osmotic flow provider, respectively. Reversed-phase electrochromatographic separation mode was found to account for the observed separations in agreement with the chemical nature of solutes and selector. Enhanced

separation ability was observed for the tritylamine-functionalized monolithic capillary column as compared to monolithic capillary column with surface-grafted benzylamine selectors. This study shows the feasibility of the grafting of bulky aromatic selector on generic monolith providing electrochromatographic separation ability in concordance with the chemical nature of the surface-grafted selector. With the aim to improve the separation selectivity and efficiency, we have developed a monolithic column bearing diphenyl selector using the same poly(NAS-co-EDMA) generic monolith (part a in Fig. 7). As preliminary result, we present in Fig 7b the separation of five PAH with the said column. Efficiency up to 90,000 plates/m were calculated for toluene. Thorough discussion about optimization of the grafting conditions, chemical characterization, and separation properties will be discussed in a forthcoming paper.

5. References

1. Svec F (2010) Porous polymer monoliths: Amazingly wide variety of techniques enabling their preparation. *Journal of Chromatography A* 1217:902-924
2. Buchmeiser M (2007) Polymeric monolithic materials: Syntheses, properties, functionalization and applications. *Polymer* 48:2187-2198
3. Guiochon G (2007) Monolithic columns in high-performance liquid chromatography. *Journal of Chromatography A*. 1168(1-2):101-168
4. Alothman ZA, Aqel A, Al Abdelmoneim HA, Badjah-Hadj-Ahmed AY, Al-Warthan AA (2011) Preparation and evaluation of long chain alkyl methacrylate monoliths for capillary chromatography. *Chromatographia* 74(1-2):1-8
5. Hjerten S, Liao JL, Zhang R (1989) High-performance liquid chromatography on continuous polymer beds. *Journal of Chromatography A* 473:273-275
6. Tennikova TB, Svec F. and Belenkii, BG (1990) High-Performance Membrane Chromatography. A Novel Method of Protein Separation. *Journal of Liquid Chromatography* 13:63-70
7. Viklund C, Ponten E, Glad B, Irgum K., Horsted P and Svec F (1997) "Molded" Macroporous Poly(glycidyl methacrylate-co-trimethylolpropane trimethacrylate) Materials with Fine Controlled Porous Properties: Preparation of Monoliths Using Photoinitiated Polymerization. *Chemistry of Materials* 9:463-471
8. Lammerhofer M, Svec F, Frechet, JMJ and Lindner W (2001) Capillary electrochromatography in anion exchange and normal-phase mode using monolithic stationary phases. *Journal of Chromatography A* 925:265-277
9. Jiang Z, Smith NW, Ferguson PD and Taylor MR (2007) Hydrophilic interaction chromatography using methacrylate-based monolithic capillary column for the separation of polar analytes. *Analytical Chemistry* 79:1243-1250
10. Jandera P and Stankova M (2015) The Effects of the Column Length on the Efficiency of Capillary Zwitterionic Organic Polymer Monolithic Columns in HILIC Chromatography. *Chromatographia* 79(13-14): 853-859
11. Karenga S and El Rassi Z (2011) Trends in nonpolar polymer-based monolithic columns for reversed-phase capillary electrochromatography. *Electrophoresis* 32:90-104
12. Liu K., Aggarwal P, Lawson JS, Tolley HD and Lee ML (2013) Organic monoliths for high-performance reversed-phase liquid chromatography. *Journal of Separation Science* 36(17):2767-2781
13. Urban J and Jandera P (2013) Recent advances in the design of organic polymer monoliths for reversed-phase and hydrophilic interaction chromatography separations of small molecules. *Analytical and Bioanalytical Chemistry* 405(7): 2123-2131
14. Bisjak CP, Lubbad SH, Trojer L and Bonn GK (2007) Novel monolithic poly(phenyl acrylate-co-1,4-phenylene diacrylate) capillary columns for biopolymer chromatography. *Journal of Chromatography A* 1147:46-52
15. Bisjak CP, Trojer L, Lubbad SH, Wieder W. and Bonn GK.(2007) Influence of different polymerisation parameters on the separation efficiency of monolithic poly(phenyl acrylate-co-1,4-phenylene diacrylate) capillary columns. *Journal of Chromatography A* 1154:269-276

16. Lav TX, Carbonnier B, Guerrouache M. and Grande D (2010) Porous polystyrene-based monolithic materials templated by semi-interpenetrating polymer networks for capillary electrochromatography. *Polymer* 51:5890-5894
17. Kucerova Z, Szumski M, Buszewski B and Jandera P (2007) Alkylated poly(styrene-divinylbenzene) monolithic columns for μ -HPLC and CEC separation of phenolic acids; *Journal of Separation Science* 30:3018-3026
18. Lav TX, Grande D, Gaillet C, Guerrouache M and Carbonnier B (2012) Porous Poly(styrene-co-divinylbenzene) Neutral Monolith: From Design and Characterization to Reversed-Phase Capillary Electrochromatography Applications. *Macromolecular Chemistry and Physics* 213: 64-71
19. Szumski M, Kučerova Z, Jandera P and Buszewski B (2009) EOF in monolithic poly(styrene-co-divinylbenzene) capillary columns. *Electrophoresis* 30:583-588
20. Aqel A, Alothman ZA, Yusuf K, Badjah-Hadj-Ahmed AY and Alwarthan, AA (2014) Preparation and evaluation of benzyl methacrylate monoliths for capillary chromatography *Journal of Chromatographic Science* 52(3):201-210
21. Ou J, Gibson GTT and Oleschuk, RD (2010) Fast preparation of photopolymerized poly(benzyl methacrylate-co-bisphenol A dimethacrylate) monoliths for capillary electrochromatography. *Journal of Chromatography A* 1217:3628-3634
22. Trojer L, Lubbad SH, Bisjak CP and Bonn GK (2006) Monolithic poly(p-methylstyrene-co-1,2-bis(p-vinylphenyl)ethane) capillary columns as novel styrene stationary phases for biopolymer separation. *Journal of Chromatography A* 1117:56-66
23. Karenga S. and El Rassi, Z (2010) Naphthyl methacrylate-based monolithic column for RP-CEC via hydrophobic and pi interactions. *Electrophoresis* 31:991-1002
24. Karenga S and El Rassi Z (2010) Naphthyl methacrylate-phenylene diacrylate-based monolithic column for reversed-phase capillary electrochromatography via hydrophobic and pi interactions. *Electrophoresis* 31:3200-3206
25. Guerrouache M, Millot MC and Carbonnier B (2011) Capillary columns for reversed-phase CEC prepared via surface functionalization of polymer monolith with aromatic selectors. *Journal of Separation Science* 34(16-17):2271-2278
26. Theodorou V, Ragoussis V, Strongilos A, Zelepos E, Eleftheriou A and Dimitriou M (2005) A convenient method for the preparation of primary amines using tritylamine. *Tetrahedron Letters* 46(8):1357-1360
27. Carbonnier B, Guerrouache M, Denoyel R and Millot MC (2007) CEC separation of aromatic compounds and proteins on hexylamine-functionalized N-acryloxysuccinimide monoliths. *Journal of Separation Science* 30:3000-3010
28. Saito Y, Ohta H, Nagashima H, Itoh K, Jinno K, Okamoto M, Chen YL, Luehr G. and Archer J (1994) Separation of C-60 and C-70 fullerenes with a triphenyl bonded silica phase in microcolumn liquid-chromatography. *Journal of Liquid Chromatography* 17(11):2359-2372
29. Guerrouache M, Carbonnier B, Vidal-Madjar C and Millot MC (2007) In situ functionalization of N-acryloxysuccinimide-based monolith for reversed-phase electrochromatography. *Journal of Chromatography A* 1149:368-376

30. Valko K, Snyder LR. and Glajch, JL (1993) Retention in reversed-phase liquid chromatography as a function of mobile-phase composition. *Journal of Chromatography A* 656:501-520
31. Kayillo S, Dennis G R and Shalliker R A (2006) An assessment of the retention behaviour of polycyclic aromatic hydrocarbons on reversed phase stationary phases: Selectivity and retention on C18 and phenyl-type surfaces. *Journal of Chromatography A* 1126:283-297
32. Gunasena DN, El Rassi Z (2013) Neutral, charged and stratified polar monoliths for hydrophilic interaction capillary electrochromatography. *Journal of Chromatography A* 1317:77-84.
33. Chen Y, Wang K, Liu Y, Yang H, Yao S, Chen B, Nie L, Xu G (2013) Improved sulfoalkylbetaine-based organic-silica hybrid monolith for high efficient hydrophilic interaction liquid chromatography of polar compounds. *Electrophoresis* 34:1877-1885.

Using capillary electrophoresis and electrochromatography for *in situ* detection of diverse organic molecules in space

Keywords: Analysis of flyby sample, Biomarkers, Electrochromatography, Monolith, Capillary electrophoresis, Versatile monolith

Abstract

In situ detection of organic molecules in space is a key step towards understanding the variety and the distribution of the building blocks of life, and contributes to searching for extraterrestrial life in our solar system. While gas chromatography/mass spectrometry (GC/MS) has proven to be a successful and robust analytical instrument in space, it is not suited for the separation and detection of non-volatile and heat-degradable complex organic molecules that life creates, and indeed may themselves be biosignatures. In this study we show that a capillary electrochromatography (CEC) approach can separate and identify various polycyclic aromatic hydrocarbons (PAHs) and pyrimidines that are potentially formed under astrophysically relevant conditions. Further, by using 16 stereoisomeric tripeptides as a candidate biosignature, we performed a simulated Enceladus flyby sample return by accelerating peptide-rock particles to a speed of 5.7 km/s and capturing them using aerogel. Direct peptide extraction and capillary electrophoresis led to the detection of two stereoisomeric peptides peaks, thus providing initial proof of the utility of this approach for detecting candidate biomolecules during flight missions that would be missed by GC/MS alone.

1. Introduction

Earth was once home to a period of chemical evolution. These organic materials were synthesized on the earth as well as likely delivered by extraterrestrial objects including carbonaceous meteorites, comets and interplanetary dust particles ¹. Diverse organic molecules such as amino acids, alcohols, sugar, ketones, lipids, various hydrocarbons have been discovered from direct analysis of carbonaceous meteorites ^{2,3}, and through the observation of interstellar clouds using near infrared spectroscopy ⁴. These findings suggest that extraterrestrial environments can produce complex molecules abiotically. Among these extraterrestrial organics, family of hydrocarbon molecules known as polycyclic aromatic hydrocarbons (PAH) were found to be dominant and ubiquitous in the interstellar medium (ISM), contributing to the formation of small hydrocarbon radicals ⁵. Thus PAHs are considered as the major carbon supplier for Earth and other planetary bodies, although direct contribution of aromatic structure to the origin of life is still under debate. Purines and pyrimidine bases are the essential units of nucleotides, molecules that form base pairs to store and copy genetic information to pass on to the next generation. Although a complete nucleotide molecule has not yet been found in any prebiotic context, several possible chemical pathways that lead to nucleotide formation have been presented ^{6,7}. Biologically common purines such as adenine, guanine, hypoxanthine, and xanthine have been reported from various carbonaceous meteorites along with nucleobase analogs ⁸. However, conclusive evidence for the existence of nitrogenous bases remains elusive due to the poor electrospray ionization efficiency. Formation of purines is predicted as oligomerization of HCN or from other observed interstellar precursor molecules such as C₃NH and HNCNH ⁹. One of the major classes of organic compounds associated with life is the amino acids and their precursors. It has been proposed that the Strecker reaction can occur in the interstellar medium forming amino acid during aqueous alteration of the parent body ¹⁰, suggesting that amino acids, an essential building blocks of biological enzyme are found in space. By far over 80 different amino acids have been detected from various carbonaceous meteorites ¹¹. Similarly, outer planet icy moons such as Europa and Enceladus are made of icy planetesimals initially produced in the solar nebula, and now likely harbor amino acids and their precursors in the subsurface ocean ¹². Amino acids have been long considered as a potential biomarker for extraterrestrial life detection on Mars and other planetary bodies, however chemical studies of extraterrestrial matter have often been challenged due to the risk of terrestrial contamination. For example, several criteria including amino acid distribution,

enantiomeric ratio and stable isotopic analysis have been suggested to assess the true origins of amino acids from a Murchison meteorite¹³. The attempt to capture and return extraterrestrial organic materials to earth was first achieved by the NASA Stardust spacecraft targeting the comet 81P/Wild 2¹⁴. The analysis of the small cometary dust particle by Stardust revealed the structurally simplest amino acids known, glycine¹⁵. While the monomers of amino acids are likely to be abundant in the universe, chain of amino acids known as peptides or proteins are less common in the prebiotic context due to thermodynamic instability. Therefore, detection and characterization of high energy organic polymers could serve as the next generation biomarker. Gas chromatography - mass spectrometry (GC-MS) has a long and distinguished heritage as a flight instrument, and is still one of the most sensitive bioanalytical instruments. GC-MS has played a major analytical role in space missions from NASA's Viking, Phoenix, Curiosity missions to ESA's Rosetta space probe. However, the pyrolytic procedure required in gas chromatography destroys thermally labile molecules including biologically significant polymers such as polypeptides, oligonucleotides and polysaccharides. Recently this became the major issue for detecting organics from the Martian soil, since chlorinated organics were detected through Curiosity's SAM instrument which are likely to be a derivative of organic molecules reacting with perchlorate inside the oven. *Thus, the very polymers that are indicative of life are rendered undetectable with GC-MS*¹⁶. Other analytical strategies proposed for space missions include biosensors.¹⁷ However, this approach lacks of flexibility as only initially targeted substances can be detected. Thus far, liquid-based separation techniques are the only alternative to GC. Electro-migration techniques are especially advantageous due to their unquestionable separation power, low consumption of solvents and ease of miniaturization. The Urey instrument, known as Mars Organic Analyzer (MOA), was the first microfabricated capillary electrophoresis (CE) system proposed for the first liquid based organic detection on Mars¹⁸. The laser-induced fluorescence (LIF) with fluorescent amine reactive probe has detected amino acids with significantly low concentration of sub-parts-per-trillion.^{19,20} Further work enabled to broaden the panel of investigated substances including aldehydes, ketones, organic acids and thiols^{21,22}. This system has now been adopted to explore potential life on icy moons (ref). The only drawback is it lacks the possibility to prove the structure and mass of detected peaks. As a result, samples containing complex organics such as peptides can be challenging. Application of MS detection is the most convenient solution of this problem. However, the MS approach exclude the usage of surfactants like in the Urey prototype¹⁸ thus while simple CZE mode faces difficulty to separate neutral species and stereoisomers within the scope of

space science²³. All these advantages are found in capillary electrochromatography (CEC), a hybrid technique that couple speed and separation efficiency of CE as well as versatility and robustness of chromatography. In order to validate the applicability evaluate diastereomeric separation of variety of tripeptides under CE and apply the same condition to peptides that undergone hypervelocity impact experiment simulating *in situ* analysis of peptides from Enceladus plume. In this study, we first conduct CEC to and to

2. Experimental section

2.1 Chemicals

Milli-Q water was used in all experiments (Millipore Corporation, Billerica, Massachusetts, USA). N-acryloxysuccinimide (NAS, Alfa Aeser, 98%), ethylene glycoldimethacrylate (EDMA, Sigma-Aldrich, 98%), 2,2'-azobis (2-methylpropionitrile) (AIBN, Sigma-Aldrich, 98%), ethylenediamine (EDA, Sigma-Aldrich, >99%) 3,3-diphenylpropylamine (Sigma-Aldrich, 97%), toluene (Alfa Aeser, extra dry 98%), acetonitrile (ACN, Carlo Erba, > 96%), thymine, uracil, cytosine, adenine, indene, naphthalene, fluorene, anthracene, pyrene, chrysene, 7,12-dimethylbenz[α]anthracene, benzo[α]pyrene were obtained from Sigma Aldrich and were of the highest purity available. Hydro-organic mobiles phases were prepared by mixing the appropriated amount of acetonitrile with phosphate buffer (5 mM, pH 8). Fused silica capillaries with a UV-transparent external coating (75 μ m id x 325 μ m od) were purchased from InnovaQuartz (Phoenix, ZA, USA).

2.2 Peptide rock sample preparation

A total 17 tripeptides L-Tyr-(each of the following: Gly, D-Ala, L-Ala, D-Asp, L-Asp, D-Glu, L-Glu, D-Ser, L-Ser, D-Val, L-Val, AIB, ABA, IsoV, Bala, norV, gABA)-L-Tyr with >90% purity were purchased from Elim Biopharmaceuticals, Inc (Hayward, CA). Lyophilized peptide samples were dissolved in 1:1 water/acetonitrile solution at a stock concentration of 1 mg/ml. Montmorillonite rock (Tantora) was crushed by a hammer into small particles. Sizes between 100 to 200 μ m in diameter were collected using a mesh filter. Particles were rinsed with MiliQ water and dry-heat sterilized at 150 °C for 2 hrs. A total 10 mg of particles were soaked with 100 μ l of the 50% acetonitrile peptide solution containing 10 μ g of L+D peptides (Gly, D-Ala, L-Ala, D-Asp, L-Asp, D-Glu, L-Glu, D-Ser, L-Ser, D-Val, L-Val,) in a test tube and dried.

2.3 Hypervelocity Impact Experiment

Hypervelocity impact experiments were performed using a two-stage light-gas gun (LGG) at the Institute of Space and Astronautical Science, Japan Aerospace Exploration Agency (ISAS/JAXA). Particles were placed into a spherical cavity formed by the inner surfaces of a cylindrical bullet called a “sabot” and shot at speeds ranging between 5.53-5.81 km/s. Hypervelocity particles were captured using a methylated hydrophobic silica aerogel developed by Tabata *et al*²⁴.

2.4 Extraction of peptides from rock and aerogel

Rock particles with dried peptides were soaked in 50 μ L of 40% acetonitrile water in standard Eppendorf tubes. The extraction was conducted using the ultrasonic bath to enhance the speed and efficiency of the process. After 10 min of sonication, the tube was centrifuged and supernatant was directly analyzed with CE. Aerogels with entrapped particles (see the Section ‘Hypervelocity Impact Experiment’) were carefully excised into small pieces and placed inside a glass 10 mL Hamilton syringe (Hamilton, Reno, NV, USA) and soaked with 2 mL of 40% acetonitrile solution. The solution was pushed out and subsequently back-aspirated to the Eppendorf tube to perfuse the rock sample. The action was performed manually for 5 min and piston was pushed fully to crush the aerogel to recover whole liquid retained in aerogel. The extract was centrifuged, the supernatant removed to new tube, and evaporated at 50 °C. The evaporation resulted in about 10-fold volume reduction and removal of volatile acetonitrile which presence in sample analytical matrix was found to deteriorate sensitivity enhancement in developed field-amplified sample injection technique. Twenty μ L of pre-concentrated extract was mixed with 5 μ L of 5-fold diluted separation buffer (pH 2.5) and analyzed with CE.

2.5 Peptide separation using capillary electrophoresis

All free-flow electrophoresis experiments were conducted using Agilent 7100 CE System (Agilent Technologies, Santa Clara, CA, USA) equipped with UV diode-array detector. The analysis was monitored at 214 and 280 nm corresponding to the absorbance of the tyrosine aromatic ring. The separation process was performed using bare fused silica capillaries 60 cm long with 50 μ m i.d. purchased from Polymicro Technologies (Phoenix, AZ, USA). The separation buffers used were composed of 40 mM ammonium acetate (pH 3.65) or 100 mM Tris, 95 mM citric acid (pH 3.65). The pH of the buffer was adjusted to the desired value

using 0.1 M HCl. Samples were introduced into the capillary using the hydrodynamic or electrokinetic mode. Pressure injection of a pure aqueous sample was performed for 8 s at 50 mbar. Electrokinetic injection (20 or 50 s at 10 kV) was preceded by a short plug of sample introduction (3 s, 50 mbar). In the electrodriven injection sample, the analytical matrix was composed of 20-fold diluted separation buffer adjusted to pH 2.5. At the beginning and at the end of each day the capillaries were sequentially flushed with 0.1 M NaOH and water (2 bars, 10 min). Additionally, before the first run, the capillary was conditioned with a separation buffer for 10 min at 2 bars. Between each analysis, there was a 2 min rinse with 0.1 M NaOH, water and separation buffer. All the electrochromatographic experiments were carried out on a P/ACE MDQ (Beckman, Fullerton, CA, USA) equipped with 32-Karat software (version 4.0) for data acquisition. The detection window was created by the exposure of a short section (0.8 mm, located at 10 cm from the outlet end) of the monolithic capillary column to the light of the detector without any filter. The total and effective lengths of the capillary columns were 31 and 10 cm, respectively. Analytes were dissolved in the mobile phase at a concentration of $5 \cdot 10^{-3}$ mM. The detection wavelength was set at 214 nm and the temperature was kept at 25 °C. A pressure of 3.5 bar was applied to both ends of the capillary to prevent bubble formation during separation runs. Specific separation conditions are mentioned in the captions of the corresponding figures.

2.6 Synthesis of generic monolith P(EDMA-co-NHS)

The *in situ* synthesis of a generic monolith was achieved via photo-triggered free radical polymerization of NAS (200 mg) and EDMA (110 μ L) using dry toluene (700 μ L) as porogen. AIBN (1% in mass with respect to the total amount of monomers) was added to the monomer solution as initiator. The polymerization mixture was sonicated for about 5 min to obtain a homogeneous solution and filtrated (**polytetrafluoroethylene membrane, pore size: 0.45 μ m**). The sonicated mixture was pushed through the capillary under nitrogen pressure (3 bar) and both ends of the capillary were sealed with rubber septa. The as-filled capillary was submitted to short time (800s) UV (365 nm, 6 \times 15W) irradiation to initiate the polymerization step. The monolith-containing capillary then was extensively flushed with ACN (2 μ L \cdot min⁻¹, 1h) for removal of porogenic solvent and unreacted monomers.

2.7 Synthesis of phenyl-like monolithic stationary phase for reversed phase charge transfer²⁵

A solution of 3,3diphenylpropylamine (1M in CH₃OH) was continuously (2μL/min) pumped through the generic monolith column for 1 h at room temperature. Thereafter, the monolithic column was washed with ACN (1 h, 2μL/min) and kept at room temperature with sealed ends till CEC use.

2.8 Synthesis of amino-like monolithic stationary phase for hydrophilic interaction CEC

A solution of ethylenediamine (1 M in ACN) was pumped continuously (2 μL/min) through the generic monolith column for 1 h at room temperature. Thereafter, the monolithic column was washed with ACN (1 h, 2 μL/min) and kept at room temperature with sealed ends until use in the CEC.

3. Resultats and discussion

Separation of structurally similar peptides is challenging. For this purpose, CE was chosen as a technique that features extremely high separation efficiency and whose usefulness in chiral and stereoisomeric peptides has been proved in a number of studies²⁶⁻³⁰. Herein, we analyzed seventeen tripeptides including five pairs of diastereoisomers. Separation of the compounds in capillary zone electrophoresis (CZE) is possible because of the difference in the migration velocities of the ions. In case of a large number of very similar molecules, pK_a values of each species are expected to be substantially similar. Only peptides containing glutamic and aspartic acid in their structure are predicted to feature lower pK_a values compare to other analytes. Initially, the influence of separation buffer pH value on selected peptides resolution was investigated in the range from 2.50 to 7.00. The baseline separation of most compounds was achieved with 50 mM ammonium acetate buffer (pH 3.65). Under this condition most compounds migrate in cationic form while TET diastereoisomers were resolved as anions. Significant asymmetry of early detected peaks was due to the high electrophoretic mobility of co-migrating ammonium ions ($\mu_{\text{ammonia}} = 76.2 \cdot 10^{-9} \text{m}^2 \text{V}^{-1} \text{s}^{-1}$). Peak asymmetry is inconvenient as it deteriorates separation efficiency and resolution. Moreover, the ammonium and acetate constituents of used buffer are volatile. In contrast, this feature is highly desirable in case of mass spectrometry detection with electrospray ionization³¹. In our case, aside to the above-mentioned difficulties, buffer volatility resulted in poor migration times repeatability due to

evaporation additionally enhanced by ongoing electrolysis process. Taking into consideration all these factors, the buffer composition was modified. Tris was used instead of ammonium as the former ions feature lower electrophoretic mobility ($\mu_{\text{Tris}} = 29.5 \cdot 10^{-9} \text{ m}^2 \text{ V}^{-1} \text{ s}^{-1}$) and can be considered as nonvolatile in comparison to the latter. Moreover, Tris ions were reported to dynamically coat the capillary wall and protect peptides and proteins from adsorption to silica in CE ²⁷. To obtain proper buffering effect in the desired pH range, citric acid was used instead of volatile acetate.

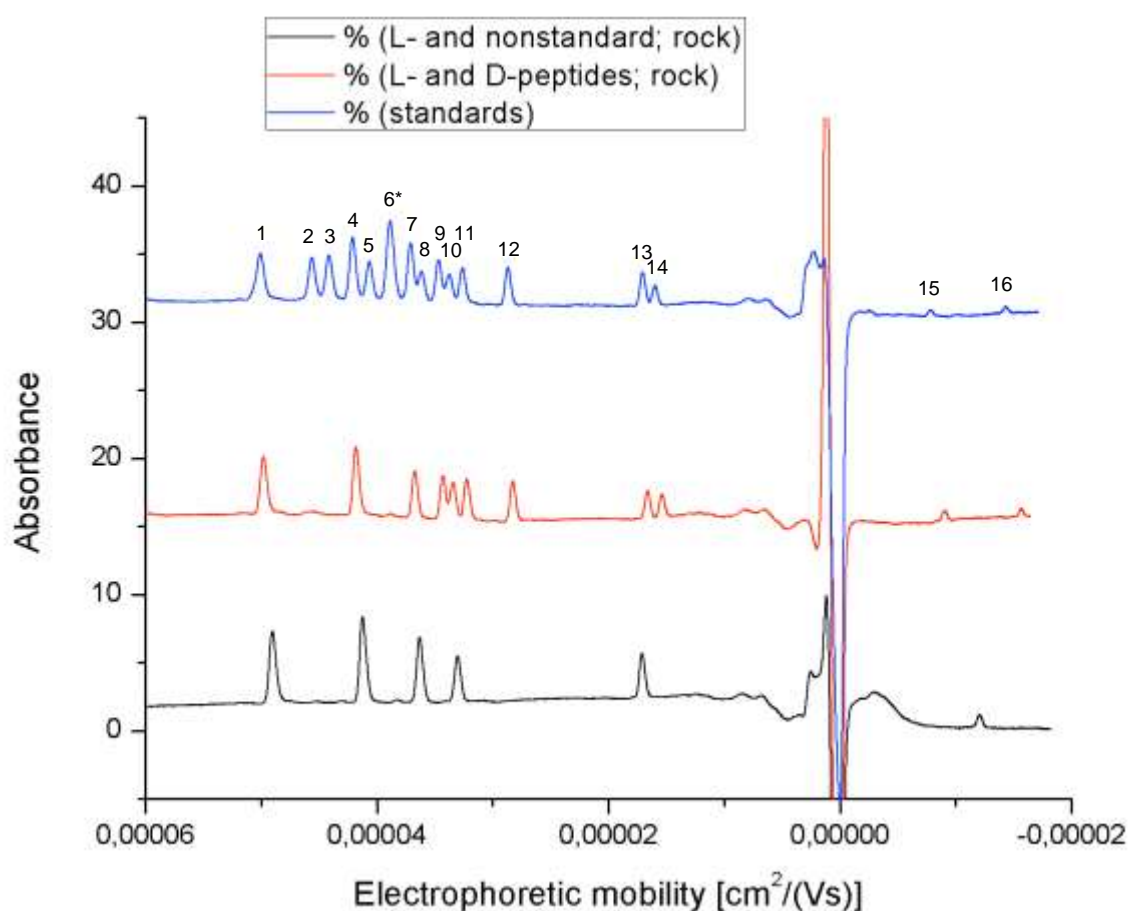


Figure 1. Capillary electrophoresis separation of YNY-tripeptides. (1)*L*-Tyr-*L*-Val-*L*-Tyr, (2)*L*-Tyr-ABA-*L*-Tyr, (3)*L*-Tyr-NorV-*L*-Tyr, (4)*L*-Tyr-*L*-Ala-*L*-Tyr, (5)*L*-Tyr-IsoV-*L*-Tyr, (6)*L*-Tyr-GABA-*L*-Tyr and *L*-Tyr- β Ala-*L*-Tyr, (7)*L*-Tyr-*L*-Ser-*L*-Tyr, (8)*L*-Tyr-AIB-*L*-Tyr, (9)*L*-Tyr-*D*-Val-*L*-Tyr, (10)*L*-Tyr-Gly-*L*-Tyr, (11)*L*-Tyr-*D*-Ala-*L*-Tyr, (12)*L*-Tyr-*D*-Ser-*L*-Tyr, (13)*L*-Tyr-*L*-Glu-*L*-Tyr, (14)*L*-Tyr-*D*-Glu-*L*-Tyr, (15)*L*-Tyr-*L*-Asp-*L*-Tyr, (16)*L*-Tyr-*D*-Asp-*L*-Tyr. Mobile phase: 100 mMTris, 95 mM citric acid (pH 3.65 adjusted with 0.1M HCl).

An increase of buffer concentration was tested to enhance separation efficiency and detection sensitivity due to the stacking effect ³². Modification of this parameter had also impact on peak resolution. Dynamic coating of capillary by Tris ions decrease electroosmotic flow in

capillary simultaneously extending the separation time. Under the optimized conditions it was possible to distinguish 16 signals originating from 17 compounds (Figure 1). Co-migration was observed in case of GABA and β -alanine moiety containing peptides. However, the separation was considered to be satisfactory for the project needs and sufficient to assess the analyzed samples. Due to the fact that the concentration of peptides in samples was expected to be in nanogram per milliliter range, head-column injection field-amplified sample injection technique was added to the developed method^{33,34}. Sample analytical matrix was composed of 20-fold diluted separation buffer adjusted to pH 2.5 to provide positive ionization of analytes and facilitate the stacking effect³⁵. A short plug of sample was introduced hydrodynamically followed by electrokinetic sample injection. An injection for as long as 50 s could have been performed without any significant band broadening effect. Further extension of injection time resulted in loss of separation efficiency and resolution. Aerogel is a micro-porous network of silicates featuring extremely low density and thermal conductivity. The hypervelocity impact experiment was conducted to simulate solid particle collection during an Enceladus flyby. Entrapped aerogel montmorillonite debris was perfused with 40% acetonitrile to extract the peptides according to the procedure described in experimental section. Methylated silica aerogel used in this experiment do not allow pure water to permeate. Because of hydrophilic character of targeted compounds, 40% acetonitrile solution in water was selected to provide good solubility of peptides and sufficient permeability to aerogel. Performed test have proved the efficiency of the applied solvent for peptides desorption from rock surface (Figure 1). Indeed, peptides were detected in analyzed rock samples and the intensity of obtained signals was clearly seen. Next, the extraction of peptides from enriched rock particles in a presence of blank aerogel was tested to assess if the silica aerogel binds analytes released from montmorillonite surface. Again all expected signals were detected which exclude any significant interaction between targets and used materials. Finally, samples of aerogel with entrapped rock particles obtained in hypervelocity impact test were examined. Surprisingly only two peaks were detected in preliminary tests using hydrodynamic injection (Figure 2). The signals were identified as TAT diastereoisomers which could have suggested easier release of acidic peptides from negatively charged rock surface. However, the tests later done with bare rock samples have not proved this hypothesis and insufficient sensitivity was concluded to be the major problem.

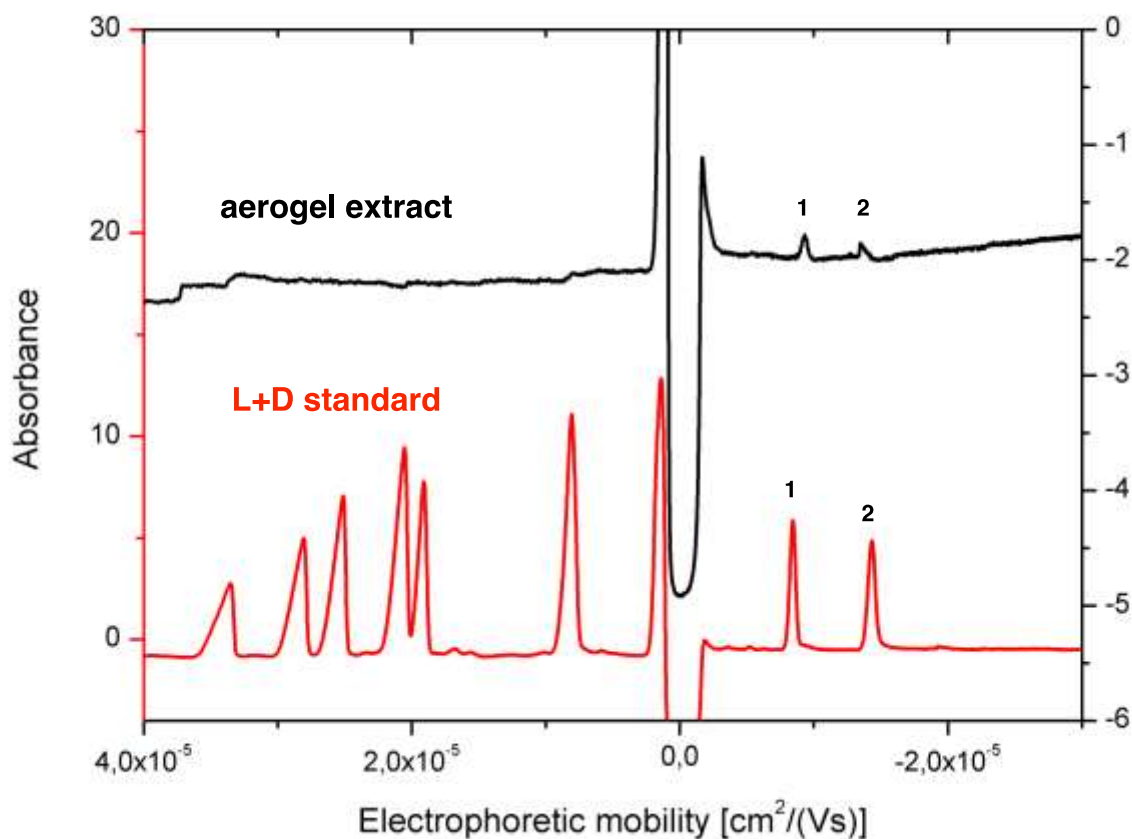


Figure 2. Capillary electrophoresis separation of tripeptides extracted from aerogel. (1) *L-Tyr-L-Asp-L-Tyr*, (2) *L-Tyr-D-Asp-L-Tyr*. Mobile phase: 100 mM Tris, 95 mM citric acid (pH 3.65 adjusted with 0.1M HCl).

To further demonstrate the potential of electrodriven separation methods for the detection of molecular targets of exobiological interest we have performed electrochromatographic analysis of PAHs and nucleobases using monolith-filled capillary columns. Although CE provides highly efficient separation it is restricted to the separation and detection of relatively small metabolites bearing charges – *either negative or positive* – at the running pH of the analysis. Direct separation of neutral solutes is indeed not possible and requires implementing micellar electrokinetic chromatography where neutral solutes can be separated based on their differential partitioning between a pseudo-stationary phase (micelles) and the background electrolyte. A related strategy has been suggested by the group of Mathies RA, from the University of California Berkeley, who applied a portable microchip capillary electrophoresis (CE) instrument, named the Mars Organic Analyzer (MOA), initially developed to the sensitive electrophoretic analysis of biomarkers on Mars,³⁶ to the separation of Polycyclic Aromatic Hydrocarbon³⁷. A PAH standard consisting of two terrestrial PAHs and seven PAHs found in extraterrestrial matter was baseline separated through addition of sulfobutylether-

beta-cyclodextrin in the separation buffer. The strategy was extended to the analysis of amines, amino acids, aldehydes, ketones and carboxylic acids.³⁸

Herein, we propose another approach based on the use of monolithic stationary phases with molecular target-oriented interfacial interaction ability to perform the separation of neutral exobiological solutes under electroosmotic flow. Regarding the chemical structure of PAHs, aromatic acids, and pyrimidines, it is expected that these solutes can be separated through specific interaction mechanisms with the stationary phase based on a combination of hydrophobic interaction, and charge-transfer mechanisms (PAHs) and hydrogen bonds formation (aromatic acids, and pyrimidines). As such, monolithic stationary phases with either phenyl or primary amines were prepared *via* the synthetic pathways presented in Figure 3 using Poly(NAS-co-EDMA) monolith serving as generic stationary phase for the design of monolith with molecular-level controlled surface properties

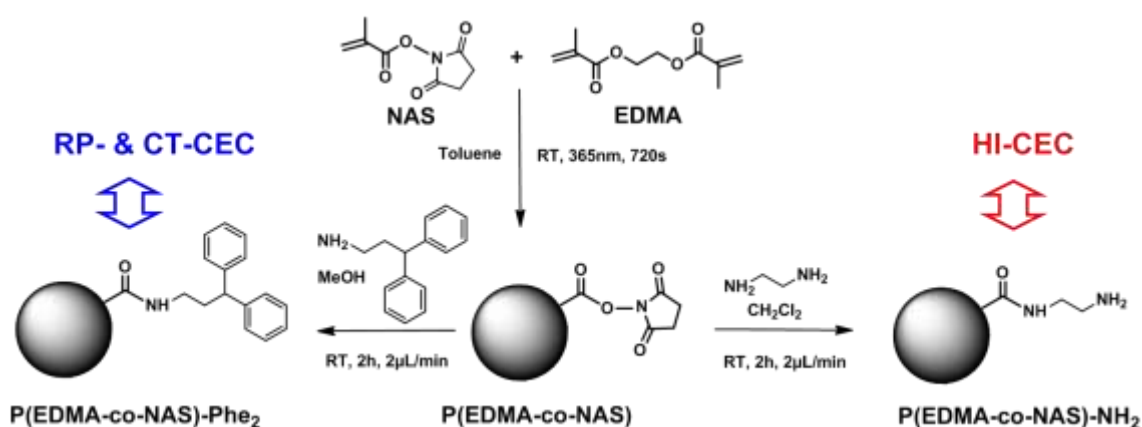


Figure 3. Schematic illustration of the synthetic path applied to the synthesis of monolithic stationary phases for reversed phase-charge transfer (RP-&CT-CEC) and hydrophilic interaction (HI-CEC) capillary electrochromatography.

The left hand side of Figure 3 illustrates the preparation of phenyl-like monolithic column *via* grafting of the 3,3-diphenylpropylamine on the surface of Poly(NAS-co-EDMA). The selector has been purposely selected for the separation of PAHs because it allows combining hydrophobic interaction together with charge transfer owing to the presence of aliphatic spacer arm and electron-rich phenyl rings, respectively. The separation ability of the diphenyl-grafted Poly(NAS-co-EDMA) was initially evaluated towards alkybenzenes selected as model solutes (Fig SII). The alkybenzenes were eluted in the order methylbenzene, ethylbenzene, propylbenzene, butylbenzene, pentylbenzene, phenylhexane, phenylheptane,

phenyloctane and phenylnonane that is according to their hydrophobic character that is dictated by the number of carbon atoms in the aliphatic side chain. This elution feature evidences the reversed phase behavior of the diphenyl-grafted monolith. Other examples of separation can be seen in fig SI2, SI3 and SI4 illustrating the separation of seven parabens, thirteen nitroarens and fourteen phenols, respectively (page 111-114).

A mixture of 9 PAHs composed of toluene, indene, naphthalene, fluorene, anthracene, pyrene, chrysene, 7,12-dimethylbenz[α]anthracene and benzo[α]pyrene was baseline separated within a less than four minutes time window on the phenyl-bearing monolithic column. The retention of PAHs increases with the size of – *the number of aromatic rings in* – the molecules confirming the separation mechanism. Large planar aromatic structures favor interaction with the phenyl ring grafted on the monolith surface via a flexible aliphatic spacer arm. Of utmost importance, our preliminary results presented in FigSI5 (page 114) show that the diphenyl-grafted monolith can be applied to the analysis of real matrices. Indeed, four polycyclic aromatic hydrocarbons could be analyzed in environmental solid samples by the combination of *ultrasonic-assisted extraction* and capillary electrochromatography using the diphenyl monolithic stationary phase.

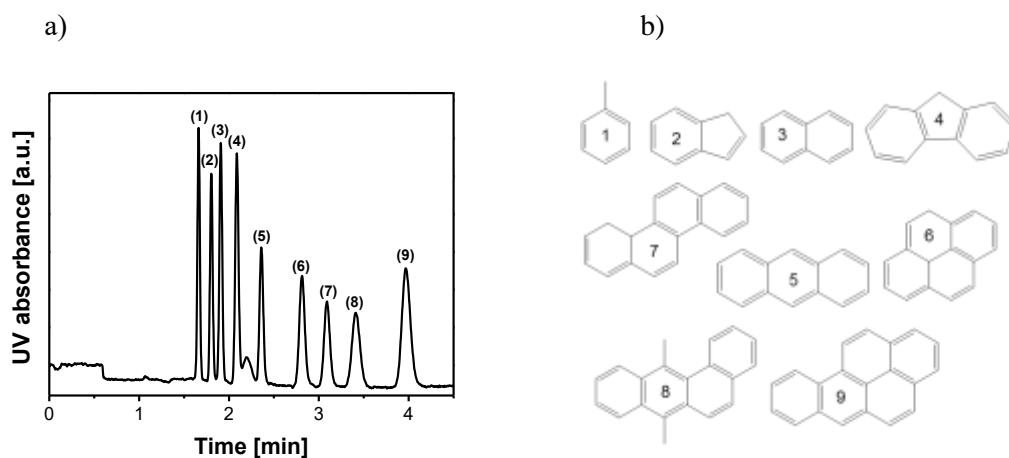


Figure 4. a) Electrochromatographic separation of a mixture of nine PAHs, namely (1) toluene, (2) indene, (3) naphthalene, (4) fluorene, (5) anthracene, (6) pyrene, (7) chrysene, (8) 7,12-dimethylbenz[α]anthracene and (9) benzo[α]pyrene on phenyl-like monolithic column. b) Chemical structures of the PAHs respectively. CEC conditions: effective column length = 20 cm; mobile phase 60/40 ACN/PBS (2.5mM pH 8); injection 5 kV/5s, voltage 30 kV, detection 214 nm

NHS-based generic monoliths allow an easy preparation of stationary phases with different wettability properties. Grafting of ethylene diamine provides amino-like stationary phases. Such monolith exhibits pH-dependent electro-osmotic generation ability depending on the

charge state of the primary amine. At pH 8, cathodic EOF is obtained similarly to what was obtained in the case of the phenyl-like monolith. However, the separation mechanism of amino-like monolith is dictated by the hydrated nature of the stationary phase and can be rationalized in terms of hydrophilic interaction as described for HILIC³⁹. Such a separation mechanism is well-suited to the separation of polar and hydrophilic solutes such as pyrimidines, carbohydrates^{40,41}. Figure 5 shows the electrochromatographic separation of thymine, uracil, adenine and cytosine where the methyl-substituted base is eluted first.

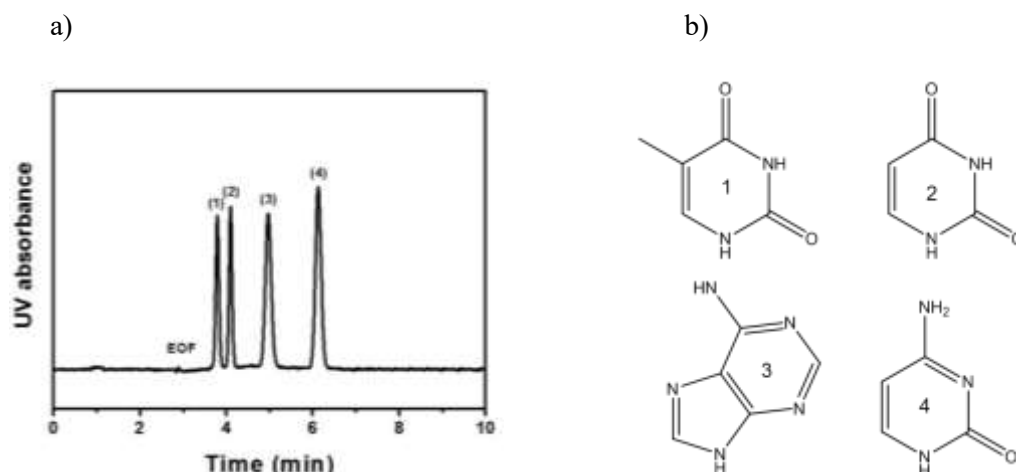


Figure 5. a) Electrochromatographic separation of a mixture of four pyrimidines, namely (1) thymine, (2) uracil, (3) adenine and (4) cytosine on amino-like monolithic column. b) Chemical structures of the pyrimidines respectively. CEC conditions: effective column length = 20 cm; mobile phase 85/15 ACN/PBS (5mM pH 8); injection 5 kV/5s, voltage 20 kV, detection 214 nm

It was observed that the electrochromatographic resolution of thymine and uracil increased with the ACN content in the mobile phase confirming the proposed separation mechanism. It is noteworthy that pyrimidines possess acido-basic properties (thymine pKa = 9.7, adenine pKa₁ = 4.2 pKa₂ = 4.8, uracil pKa = 9.5, cytosine pKa₁ = 4.6 pKa₂ = 12.2) and can thus be separated by conventional CE. However, it requires generally highly basic elutions conditions (pH = 10)⁴² or the use of additives such as cyclodextrins⁴³ or carboxylic multiwalled carbon nanotubes⁴⁴. However, herein pyrimidines are separated at the same pH value (pH = 8) as the one used for PHAs.

4. Conclusion

We have shown the great potential of electromigration techniques in the search for extraterrestrial biosignatures. These CE and CEC approaches have the benefits of miniaturization and versatility. The application of CE allowed us to separate short, highly similar peptides in a relatively short time with a high separation efficiency. The monolithic technology when applied to the field of analytical science provides efficient and complementary solutions to classical CE for the separation of neutral biomarkers with varied polarity under electrochromatographic mode. We have also detected for the first time peptides from the particles entrapped in hydrophobic aerogel after hypervelocity impact speed of 5.7 km/s. The given data will help us solve the physicochemical process of peptide during the impact and after the aerogel capture to improve the extraction procedure in the future. The importance of detecting polypeptides in their native form lies in its predominant roles in maintaining biochemical reactions for terrestrial life. While it is still an open debate whether homochirality and specific set of amino acids could serve as an universal biosignature, it can rule out terrestrial contamination and provide insights into the environmental conditions of where, when and how these peptides originated.

5. REFERENCES

1. Sephton, M. A.; Botta, O. *Space Sci Rev* **2008**, *135*, 25-35.
2. Schmitt-Kopplin, P.; Gabelica, Z.; Gougeon, R. D.; Fekete, A.; Kanawati, B.; Harir, M.; Gebefuegi, I.; Eckel, G.Hertkorn, N. *P Natl Acad Sci USA* **2010**, *107*, 2763-2768.
3. Yabuta, H.; Williams, L. B.; Cody, G. D.; Alexander, C. M. O.; Pizzarello, S. *Meteoritics & Planetary Science* **2007**, *42*, 37-48.
4. Belloche, A.; Muller, H. S. P.; Menten, K. M.; Schilke, P.; Comito, C. *Astron Astrophys* **2014**, *561*.
5. Tielens, A. G. G. M. *Annu Rev Astron Astr* **2008**, *46*, 289-337.
6. Patel, B. H.; Percivalle, C.; Ritson, D. J.; Duffy, C. D.; Sutherland, J. D. *Nat Chem* **2015**, *7*, 301-307.
7. Powner, M. W.; Gerland, B.; Sutherland, J. D. *Nature* **2009**, *459*, 239-242.
8. Callahan, M. P.; Smith, K. E.; Cleaves, H. J.; Ruzicka, J.; Stern, J. C.; Glavin, D. P.; House, C. H.; Dworkin, J. P. *P Natl Acad Sci USA* **2011**, *108*, 13995-13998.
9. Jung, S. H.; Choe, J. C. *Astrobiology* **2013**, *13*, 465-475.
10. Lerner, N. R.; Peterson, E.; Chang, S. *Geochim Cosmochim Acta* **1993**, *57*, 4713-4723.
11. Glavin, D. P.; Callahan, M. P.; Dworkin, J. P.; Elsila, J. E. *Meteoritics & Planetary Science* **2010**, *45*, 1948-1972.
12. Mousis, O.; Lunine, J. I.; Waite, J. H.; Magee, B.; Lewis, W. S.; Mandt, K. E.; Marquer, D.; Cordier, D. *Astrophys J Lett* **2009**, *701*, L39-L42.
13. Engel, M. H.; Macko, S. A. *Nature* **1997**, *389*, 265-268.
14. Brownlee, D.; Tsou, P.; Aleon, J.; Alexander, C. M.; Araki, T.; Bajt, S.; Baratta, G. A.; Bastien, R.; Bland, P.; Bleuet, P.; Borg, J.; Bradley, J. P.; Brearley, A.; Brenker, F.; Brennan, S.; Bridges, J. C.; Browning, N. D.; Brucato, J. R.; Bullock, E.; Burchell, M. J.; Busemann, H.; Butterworth, A.; Chaussidon, M.; Chevront, A.; Chi, M.; Cintala, M. J.; Clark, B. C.; Clemett, S. J.; Cody, G.; Colangeli, L.; Cooper, G.; Cordier, P.; Daghlian, C.; Dai, Z.; D'Hendecourt, L.; Djouadi, Z.; Dominguez, G.; Duxbury, T.; Dworkin, J. P.; Ebel, D. S.; Economou, T. E.; Fakra, S.; Fairey, S. A.; Fallon, S.; Ferrini, G.; Ferroir, T.; Fleckenstein, H.; Floss, C.; Flynn, G.; Franchi, I. A.; Fries, M.; Gainsforth, Z.; Gallien, J. P.; Genge, M.; Gilles, M. K.; Gillet, P.; Gilmour, J.; Glavin, D. P.; Gounelle, M.; Grady, M. M.; Graham, G. A.; Grant, P. G.; Green, S. F.; Grossemy, F.; Grossman, L.; Grossman, J. N.; Guan, Y.; Hagiya, K.; Harvey, R.; Heck, P.; Herzog, G. F.; Hoppe, P.; Horz, F.; Huth, J.; Hutcheon, I. D.; Ignatyev, K.; Ishii, H.; Ito, M.; Jacob, D.; Jacobsen, C.; Jacobsen, S.; Jones, S.; Joswiak, D.; Jurewicz, A.; Kearsley, A. T.; Keller, L. P.; Khodja, H.; Kilcoyne, A. L.; Kissel, J.; Krot, A.; Langenhorst, F.; Lanzirrotti, A.; Le, L.; Leshin, L. A.; Leitner, J.; Lemelle, L.; Leroux, H.; Liu, M. C.; Luening, K.; Lyon, I.; Macpherson, G.; Marcus, M. A.; Marhas, K.; Marty, B.; Matrajt, G.; McKeegan, K.; Meibom, A.; Mennella, V.; Messenger, K.; Messenger, S.; Mikouchi, T.; Mostefaoui, S.; Nakamura, T.; Nakano, T.; Newville, M.; Nittler, L. R.; Ohnishi, I.; Ohsumi, K.; Okudaira, K.; Papanastassiou, D. A.; Palma, R.; Palumbo, M. E.; Pepin, R. O.; Perkins, D.; Perronnet, M.; Pianetta, P.; Rao, W.; Rietmeijer, F. J.; Robert, F.; Rost, D.; Rotundi, A.; Ryan, R.; Sandford, S. A.; Schwandt, C. S.; See, T. H.; Schlutter, D.; Sheffield-Parker, J.; Simionovici, A.; Simon, S.; Sitnitsky, I.; Snead, C. J.; Spencer, M. K.; Stadermann, F. J.; Steele, A.; Stephan, T.; Stroud, R.; Susini, J.; Sutton, S. R.; Suzuki, Y.; Taheri, M.; Taylor, S.; Teslich, N.; Tomeoka, K.; Tomioka, N.; Toppani, A.; Trigo-Rodriguez, J. M.; Troadec, D.; Tsuchiyama, A.; Tuzzolino, A. J.; Tyliszczak, T.; Uesugi, K.; Velbel, M.; Vellenga, J.; Vicenzi, E.; Vincze, L.; Warren, J.; Weber, I.; Weisberg, M.; Westphal, A. J.; Wirick, S.; Wooden, D.; Wopenka, B.;

- Wozniakiewicz, P.; Wright, I.; Yabuta, H.; Yano, H.; Young, E. D.; Zare, R. N.; Zega, T.; Ziegler, K.; Zimmerman, L.; Zinner, E.; Zolensky, M. *Science* **2006**, *314*, 1711-1716.
15. Elsila, J. E.; Glavin, D. P.; Dworkin, J. P. *Meteoritics & Planetary Science* **2009**, *44*, 1323-1330.
16. Poinot, P.; Geffroy-Rodier, C. *Trac-Trend Anal Chem* **2015**, *65*, 1-12.
17. Vigier, F.; Le Postollec, A.; Coussot, G.; Chaput, D.; Cottin, H.; Berger, T.; Incerti, S.; Triqueneaux, S.; Dobrijevic, M.; Vandenabeele-Trambouze, O. *Advances in Space Research* **2013**, *52*, 2168-2179.
18. Aubrey, A. D.; Chalmers, J. H.; Bada, J. L.; Grunthaner, F. J.; Amashukeli, X.; Willis, P.; Skelley, A. M.; Mathies, R. A.; Quinn, R. C.; Zent, A. P.; Ehrenfreund, P.; Amundson, R.; Glavin, D. P.; Botta, O.; Barron, L.; Blaney, D. L.; Clark, B. C.; Coleman, M.; Hofmann, B. A.; Josset, J. L.; Rettberg, P.; Ride, S.; Robert, F.; Sephton, M. A.; Yen, A. *Astrobiology* **2008**, *8*, 583-595.
19. Takizawa, K.; Nakamura, H. *Analytical sciences* **1998**, *14*, 925-928.
20. Warren, C. R. *Soil Biology and Biochemistry* **2008**, *40*, 916-923.
21. Bachmann, K.; Bazzanella, A.; Kibler, M.; Lochmann, H.; Mainka, A. *NACHRICHTEN AUS CHEMIE TECHNIK UND LABORATORIUM* **1997**, *45*, A4-A5.
22. Hart, J. J.; Welch, R. M.; Norvell, W. A.; Kochian, L. V. *Electrophoresis* **2002**, *23*, 81.
23. Kim, J.; Jensen, E. C.; Stockton, A. M.; Mathies, R. A. *Anal Chem* **2013**, *85*, 7682-7688.
24. Tabata, M.; Yano, H.; Kawai, H.; Imai, E.; Kawaguchi, Y.; Hashimoto, H.; Yamagishi, A. *Origins Life Evol B* **2015**, *45*, 225-229.
25. Mekhalif, T.; Kebe, S. I.; Guerrouache, M.; Belattar, N.; Millot, M. C.; Carbonnier, B. *Chromatographia* **2016**, *79*, 1333-1341.
26. Ali, I.; Al-Othman, Z. A.; Al-Warthan, A.; Asnin, L.; Chudinov, A. *Journal of Separation Science* **2014**, *37*, 2447-2466.
27. Kasicka, V. *Electrophoresis* **1999**, *20*, 3084-3105.
28. Kasicka, V. *Electrophoresis* **2006**, *27*, 142-175.
29. Scriba, G. K. E. *Electrophoresis* **2006**, *27*, 222-230.
30. Scriba, G. K. E. *Electrophoresis* **2009**, *30*, S222-S228.
31. Schmitt-Kopplin, P.; Frommberger, M. *Electrophoresis* **2003**, *24*, 3837-3867.
32. Burgi, D. S.; Chien, R. L. *Anal Chem* **1991**, *63*, 2042-2047.
33. Dziomba, S.; Kowalski, P.; Slominska, A.; Baczek, T. *Anal Chim Acta* **2014**, *811*, 88-93.
34. Zhang, C. X.; Thormann, W. *Anal Chem* **1996**, *68*, 2523-2532.
35. Quirino, J. P.; Terabe, S. *J Chromatogr A* **2000**, *902*, 119-135.
36. Hutt, L.; Mathies, R.; Grunthaner, F.; Bada, J. In *ABSTRACTS OF PAPERS OF THE AMERICAN CHEMICAL SOCIETY; AMER CHEMICAL SOC 1155 16TH ST, NW, WASHINGTON, DC 20036 USA, 1999*, pp U845-U845.
37. Stockton, A. M.; Chiesl, T. N.; Scherer, J. R.; Mathies, R. A. *Analytical chemistry* **2008**, *81*, 790-796.
38. Mathies, R. A.; Stockton, A. M.; Jensen, E. C.; Benhabib, M.; Chiesl, T. N. *Abstracts of Papers of the American Chemical Society* **2011**, 242.
39. Alpert, A. J. *Journal of chromatography A* **1990**, *499*, 177-196.
40. Alpert, A. J.; Shukla, M.; Shukla, A. K.; Zieske, L. R.; Yuen, S. W.; Ferguson, M. A.; Mehlert, A.; Pauly, M.; Orlando, R. *Journal of Chromatography A* **1994**, *676*, 191-202.

41. Guerrouache, M.; Pantazaki, A.; Millot, M. C.; Carbonnier, B. *Journal of separation science* **2010**, *33*, 787-792.
42. Geldart, S. E.; Brown, P. R. *Journal of Chromatography A* **1999**, *831*, 123-129.
43. Wang, P.; Ren, J. *Journal of pharmaceutical and biomedical analysis* **2004**, *34*, 277-283.
44. Xiong, X.; Ouyang, J.; Baeyens, W. R.; Delanghe, J. R.; Shen, X.; Yang, Y. *Electrophoresis* **2006**, *27*, 3243-3253.

Electronic Supporting Information

Using capillary electrophoresis and electrochromatography for *in situ* detection of diverse organic molecules in space

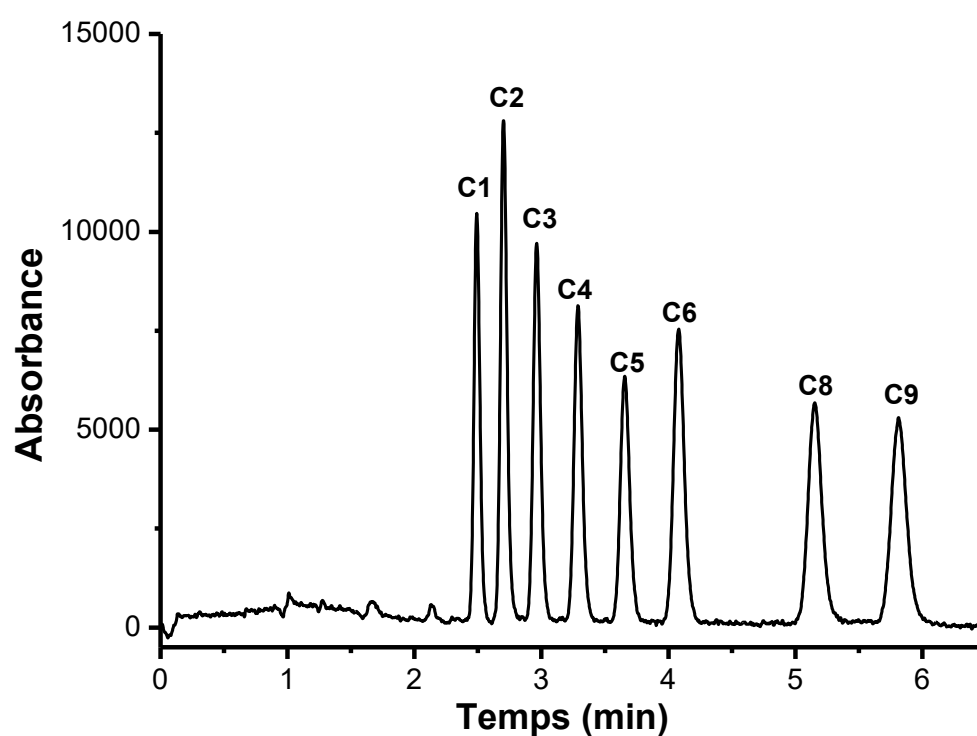


Fig S11: Electrochromatographic separation of a mixture of nine alkylbenzenes, namely (C1) methylbenzene, (C2) ethylbenzene, (C3) propylbenzene, (C4) butylbenzene, (C5) pentylbenzene, (C6) phenylhexane, (C7) phenylheptane, (C8) phenyloctane and (C9) phenylnonane on phenyl-like monolithic column. CEC conditions: effective column length = 20 cm, respectively; mobile phase 60/40 ACN/PBS (2.5mM pH 8); injection 5 kV/5s, voltage 30 kV, detection 214 nm

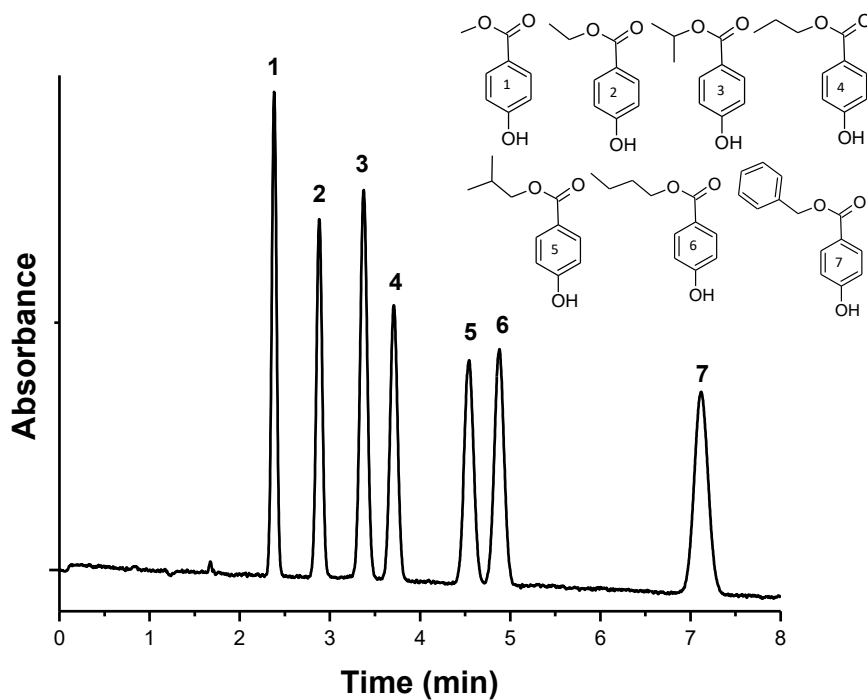


Fig SI2: Electrochromatographic separation of a mixture of seven parabens, namely (1) methylparaben, (2) ethylparaben, (3) isopropylparaben, (4) propylparaben, (5) isobutylparaben, (6) butylparaben and (7) benzylparaben on phenyl-like monolithic column. CEC conditions : effective column length = 20 cm, respectively; mobile phase 45/55 ACN/PBS (2.5mM pH 8); injection 5 kV/5s, voltage 15 kV, detection 214 nm

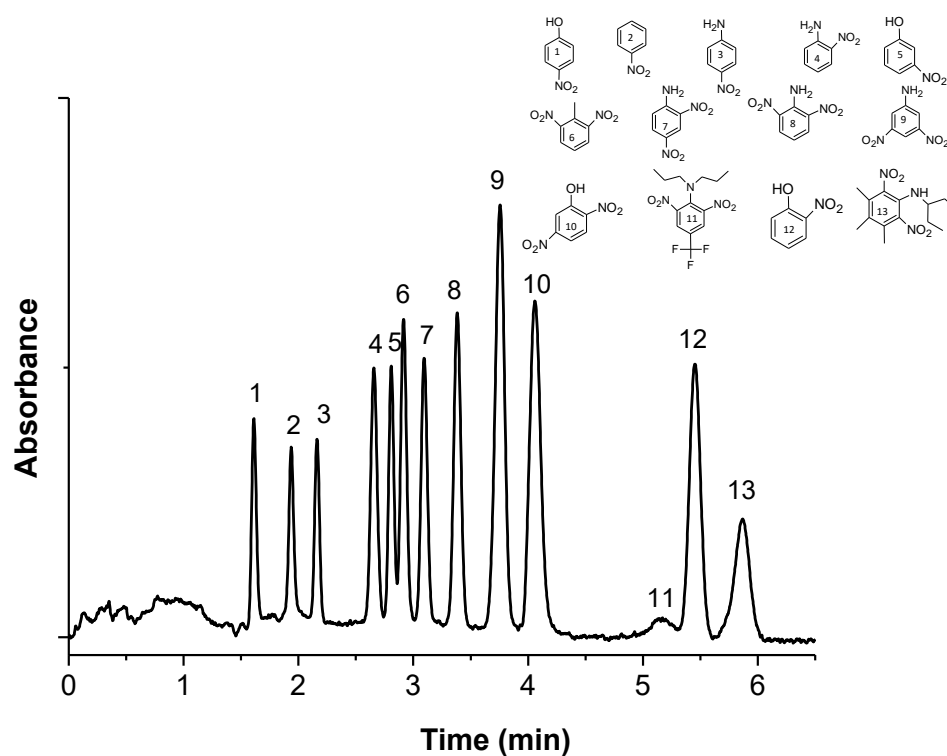


Fig SI3: Electrochromatographic separation of a mixture of thirteen nitroarenes on phenyl-like monolithic column. The chemical structure of the phenols is shown as inset. CEC conditions: effective column length = 20 cm, respectively; mobile phase 10/45/45 isoPropanol/ACN/PBS (2.5mM pH 8); injection 5 kV/5s, voltage 15 kV, detection 214 nm

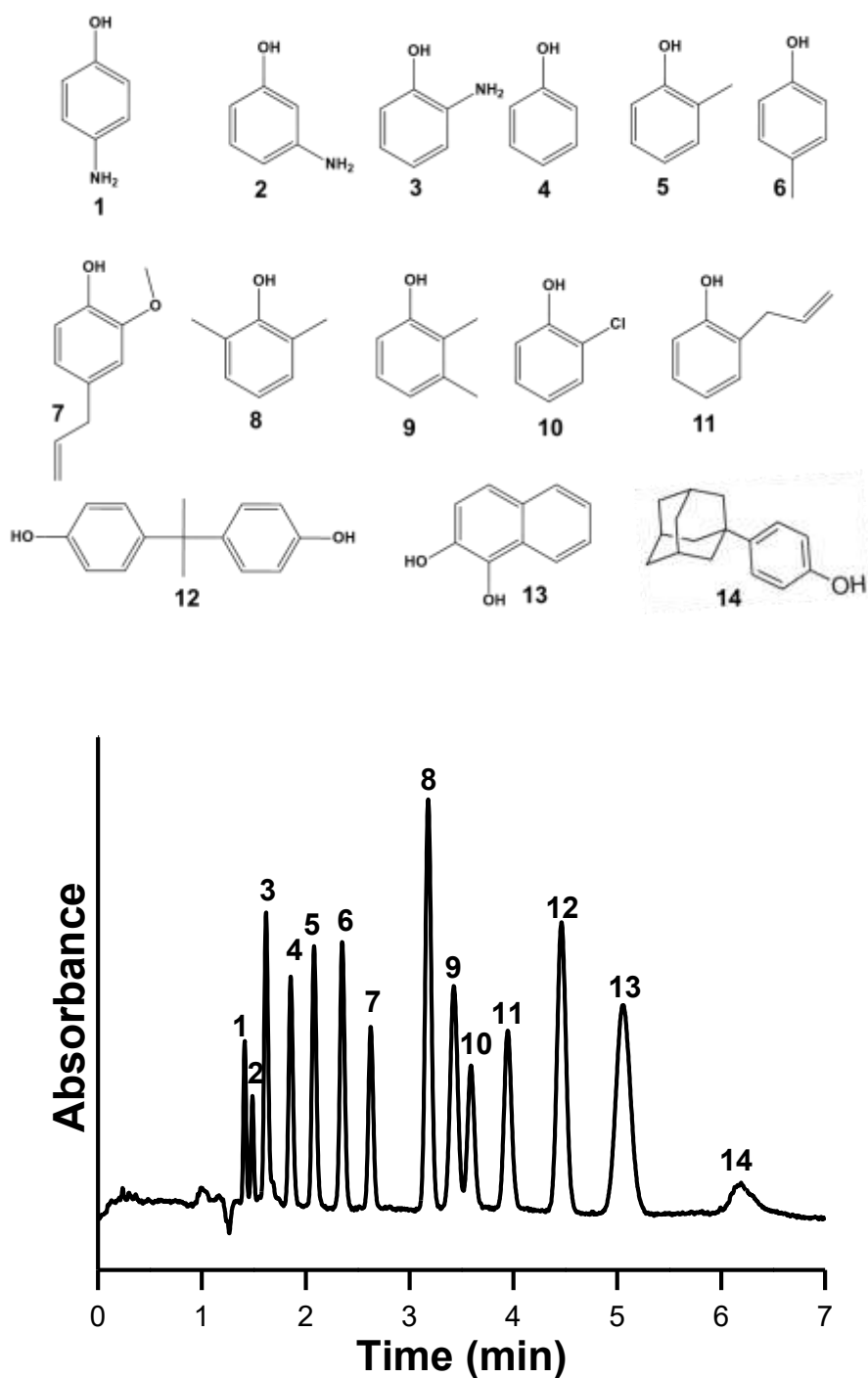


Fig SI4: Electrochromatographic separation of a mixture of fourteen phenols on phenyl-like monolithic column. The chemical structure of the phenols is shown as inset. CEC conditions : effective column length = 20 cm, respectively; mobile phase (2.5mM pH 8); injection 5 kV/5s, voltage 15 kV, detection 214 nm.

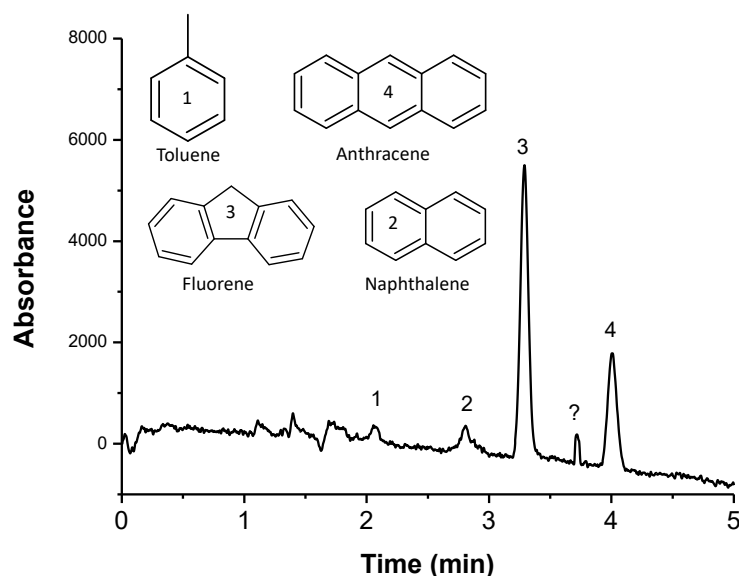


Fig SI5: Electrochromatographic separation of a mixture of four parabens, namely (1) toluene, (2) naphthalene, (3) fluorine and (4) anthracene on phenyl-like monolithic column. The parabens solution was extracted from spiked sand samples. The chemical structure of the phenols is shown as inset. CEC conditions: effective column length = 20 cm, respectively; mobile phase ACN/PBS 70/30 (2.5mM pH 8); injection 5 kV/5s, voltage 15 kV, detection 214 nm. The sample was prepared as follows. Fontaineblau sand was thoroughly washed with sulfuric acid (2 M) under magnetic stirring for 30 min. Then the sand was recovered by filtration and further washed with deionized water until the aqueous filtrate exhibits neutral pH. Then the sand was dried under vacuum at 80°C during 24h. Stock solution of each paraben were prepared in ACN at a concentration of 5mM. A mixture solution containing the four parabens with a concentration of 0.5 mM each was prepared by mixing 1mL of each stock solution and completing the volume to 10 mL with 6 mL of ACN. The as-treated sand was then mixed with 4mL of the parabens mixture solution under magnetic stirring during 24h. The solvent was then evaporated under vacuum and the as-obtained sand was dispersed in 2 mL of a hydro-organic (H₂O/ACN 10/90) solution. After 15 min of ultrasonic-assisted extraction at room temperature during, the solution was filtrated and the filtrate was injected on the diphenyl-grafted monolith for electrochromatographic analysis.

Chapitre III

Objectifs

Appliquer la chimie interfaciale des sels de diazonium pour l'ancrage robuste de nanoparticules d'or à la surface des pores de matériaux monolithiques.

Tester les potentialités d'un intermédiaire monolithique de synthèse portant des unités aniline en surface en électrochromatographie.

Mettre en évidence le rôle du sélecteur aniline sur le mécanisme de séparation.

Méthodes

Génération *in situ* de sels de diazonium à partir d'une amine aromatique greffée en surface par traitement à l'acide nitreux.

Proposer une nouvelle voie d'immobilisation de nanoparticules d'or à la surface des pores de monolithes

Electrochromatographie utilisant des phases stationnaires monolithiques portant des sélecteurs riches en électrons.

Limites

Difficulté de caractériser la formation *in situ* de sels de diazonium notamment du fait de leur forte réactivité.

Estimer l'efficacité de la transformation des amines aromatiques en sels de diazonium.

Importance

Premier exemple d'application de la chimie interfaciale des sels de diazonium à la technologie des monolithes.

Premier exemple de phase stationnaire monolithique modifiée par des sélecteurs de type aniline et appliquée à l'électrochromatographie.

Aniline-grafted monolith as electrochromatographic and nano-gold catalyst supports: New implementation of diazonium salt chemistry

Keywords: Diazonium chemistry, Electrochromatography, Flow through catalysis, Nanostructured monolith, Porous polymer

Abstract:

Herein, we report for the first time the preparation of aniline-grafted monolith serving on the one hand as precursor support for gold metal nanoparticles and, on the other hand, as stationary phase for capillary electrochromatography. To do so, 4-aminophenyl ethylene amine was grafted on the monolith's surface obtained *via* the photopolymerization of N-acryloxysuccinimide and ethylene glycol dimethacrylate. The aniline-grafted monolith proved efficient for the separation of six anilines and six polycyclic aromatic hydrocarbons. The results suggest the major contribution of the surface-grafted aniline selector on the separation governed through an electron-releasing effect induced by the primary amine. The well-known diazonium salts chemistry was then considered applying the Mirkhalaf's strategy taking advantage of the N^{2+} cation ability of diazonium to complex MX^{n-} metal salts.¹ The treatment of aniline surface-grafted monolith with nitrous acid produces a diazonium salt on the monolith surface *via* diazotization. Upon hydride-mediated chemical reduction of the surface immobilized metal salt, the release of the diazo moiety and the corresponding formation of free radical occur concomitantly yielding to the grafting of the metal nanoparticles on the monolith surface. Success of each synthetic step, from photodriven free radical polymerization, through nucleophilic substitution, to radical grafting surface modification was evidenced by Raman spectroscopy measurements, scanning electron microscopy observations and energy dispersive X-ray analysis. Finally, the gold nanoparticles-grafted monolith was used as flow through catalytic support meant for the reduction of 4-nitrophenol into 4-aminophenol. Besides the presentation of a new type of monolith bearing aniline selector, this study constitutes, to the best of our knowledge, a unique example in the literature describing the use of diazonium salt chemistry strategy for the nanostructuration, and more generally the functionalization of the pore surface of polymeric monolithic materials.

1. Introduction

Porous polymers belong to the class of interface-dominated materials, *i.e.* materials whose macroscopic properties are mainly governed by interfacial phenomena.² Correspondingly, numerous efforts have been devoted to adjust, through a judicious choice of synthesis conditions, the surface chemistry of such polymers.³⁻⁵ This is particularly true for monoliths having a channel-like macroporous structure well-suited for flow-through applications such as separation, pre-concentration, catalysis...⁶⁻¹⁰ Monoliths exhibit high permeability associated with efficient transport properties, notably in terms of fast mass transfer and low back pressure even at high throughput, as compared to particulate filled systems.¹¹ These intrinsic properties are to be related to the absence of interparticular voids so that the fluid (mobile phase, reactive solution...) is forced to circulate through the entire monolithic sorbent by convective flow instead of diffusion. Other advantages of polymer-based monoliths are the ease and versatility of their preparation methods allowing *in situ* synthesis, *i.e.* directly within the confines of glass or polymer microchannel devices,^{12, 13} in combination with a possible control over porosity, surface area and surface chemical nature.¹⁴⁻¹⁷ For instances, by (i) changing the monomer(s)/porogen(s) ratio in the polymerization mixture, one can tune the pores size in the 0.7-2 μm range, (ii) choosing a judicious monomer one may provide specific surface properties. Although such monolithic structures can be obtained *via* one-step polymerization, post-functionalization strategies afford better control and unique way towards further surface chemical derivatization. To date, nucleophile-sensitive monomers such as glycidyl methacrylate (GMA) or N-acryloxysuccinimide (NAS) have been mainly applied to synthesizing functionalizable monoliths allowing the surface-grafting of chromatographic-active sites bearing diol,¹⁸ zwitterion,^{19, 20} aromatic,^{21, 22} carboxyl,²³ amino²⁴ and thiol^{25, 26} end functionalities. The latter two approaches proved also particularly suitable for the attachment of colloidal gold.²⁷⁻²⁹ Since the demonstration that dense, homogeneous, finely dispersed and patterned deposition of gold colloids can be achieved onto on-purpose chemically modified monolith surface, the success of gold nanoparticles@monolith, and more generally other related nanostructured monolithic materials, has continued unabated.^{30, 31} Such hybrid monolithic materials have been cleverly used in various fields of flow chemistry including analytical chemistry and catalysis. Microfluidic device meant for on-column SERS detection of pesticides, dyes and biomolecules was prepared through the surface immobilization of gold nanoparticles on thiolated monolith.³² On-site Turkevich synthesis method was implemented through injection of a mixture of sodium citrate and chloroauric acid tetrahydrate in aqueous

solution on thiol-modified monolith obtained from the reaction of Poly(GMA-co-EDMA) and sodium-hydrogen sulfide. The group of F. Svec fabricated miniaturized solid phase microextraction and separation supports using thiol-modified monoliths for the surface-stabilization of GNP.³³ The gold monolithic support was obtained by reacting Poly(GMA-co-EDMA) with cysteamine. The results clearly indicated that the preconcentration process was based on the high affinity of cysteine-containing peptides for gold. In other implementations, reversibility of the thiol–gold bonding was exploited to use gold nanoparticles as intermediate ligands providing chromatographic and extraction supports with versatile surface interaction ability.^{34, 35} Monolithic microreactors are also very appealing for heterogeneous catalysis purposes.^{36, 37} Surface attachment of nanometals allows preventing not only nanoparticles aggregation but also their release in the end product-containing solution so that laborious and time consuming metal recovery step is not required. Obviously, robust anchoring of the gold nanoparticles is mandatory to provide recyclable systems and to avoid any decrease of activity upon successive catalytic cycles.³⁸ Gold nanoparticle-modified monoliths have been considered for various reactions such as the reduction of. The catalytic supports proved stable under flow through operating conditions at room temperature and no leaching effect was reported. Formation of multiple bonds between the monolith surface functional groups and the nanoparticle is the key towards strong interfacial adhesion. Indeed, although gold-thiol links exhibit lower stability at elevated temperatures, multiplicity of bonds between thiol monolithic support and the gold nanoparticles prevents their detachment even under treatment with pure thiol-containing molecular competitor, namely 2-mercaptoethanol, or boiling water for 5 h.³³ To the best of our knowledge, no such a study was reported for the case where gold nanoparticles were deposited on amino-modified monolith.

In this framework, this study is intended to explore new route to immobilize covalently gold nanoparticles on monolith's pore surface beyond the up-to-date widely applied methods using gold-amine or gold-thiol bonds. Rapid survey of the literature reveals that diazonium salts have been used in all sorts of research area ranging from composites (nano)materials^{39, 40} to bioactive surfaces^{41, 42} and sensors^{43, 44} that are applications for which a fine tuning at either molecular- or nano-scales is required. Due to its versatility and high reaction yield, diazonium-based chemistry has become one of the finest functionalization techniques to modify in a controlled way all types of surfaces based on polymer, noble metal, metal oxide, sp²- and sp³- hybridized carbon with varied (flat vs spherical or rod-shape) geometries. The reader is kindly invited to refer to recently published review for thorough discussion.⁴⁵⁻⁵⁰

However it appears that no published studies reported on the chemical modification of organic monolith's surface *via* diazonium salt.

To expand further the use of diazonium salt chemistry to the generic domain of porous polymer surface modification, we envisioned the grafting of aromatic amine on the surface of Poly(NAS-co-EDMA) with the aim to generate *in situ* diazonium units $-N^{2+}$ upon treatment with an equimolar solution of tetrafluoroboric acid and sodium nitrite. Through our strategy, we took advantage of the high reactivity of diazonium to graft gold nanoparticles on monolith.¹ This contribution conjoins the surface chemistry of diazonium and technology of porous polymer monolith to strongly anchor gold nanoparticles on solid and permeable support. As a proof of concept, the so-designed hybrid monolith was applied to the flow through hydride-mediated reduction of 4-nitrophenol into the corresponding amine, selected as a model catalytic reaction.

In the course of our investigation, we also considered the use of aniline-grafted poly(NAS-co-EDMA) as monolithic stationary phase meant for capillary electrochromatography. Indeed, the chemical nature of the said monolith resembles the one reported previously by some us, based on phenylbutylamine, benzylamine or naphthylamine grafted on monolithic skeleton through their primary amine functionality.²¹ Analytes as diverse as phenol naphthalene, fluorene, anthracene, pyrene, chrysene, p-phenylenediamine, aniline, 3,4-dimethylaniline, 4-nitroaniline, 2-nitroaniline, 2,6-dinitroaniline, 2,4-dinitroaniline, 2,6-dichloro-4-nitroaniline, resorcinol, catechol, m-cresol, 2,3-dimethylphenol 4-chlorophenol were separated based on a combination of reversed-phase and charge transfer mechanisms. NAS is a smart alternative to GMA for preparing monolith meant for electro-driven process. Indeed, NHS moieties are more reactive towards nucleophile molecules than three membered-ring oxirane and allow the concomitant generation of carboxylic acid surface groups enabling the generation of cathodal electro-osmotic flow.^{51, 52} These beneficial features have been exploited herein, and only preliminary results on the electrochromatographic properties of newly prepared aniline-grafted monolith are presented.

2. Experimental Part

2.1 Materials

Fused silica capillaries with a UV-transparent external coating (75 μm I.D. \times 325 μm O.D.) were purchased from InnovaQuartz (Phoenix, ZA, USA). Spectrolinker XL-1500 UV

crosslinker (Spectronics, Westbury, NY, USA) equipped with eight lamps (8×15 W, 365 nm) was used to photoinitiate the polymerization. Morphology of the polymeric monoliths was evaluated using scanning electron microscopy with the help of a LEO Gemini 1530 SEM apparatus (Leo Elektronenmikroskopie, Oberkochen, Germany). Capillaries were cut at different places and small pieces were deposited on a SEM support with a silver-containing solution. The samples were dried under reduced pressure and coated with a thin layer of palladium (2 nm) with the help of a sputter coater Cressington 208 HR (Elektronen Optik Service, Dortmund, Germany). Chemical structure of the monoliths was investigated using a Raman apparatus Xplora from Horiba Jobin Yvon (Longjumeau, France) equipped with a laser emitting at 638 or 785 nm. Samples were investigated in different places to control the homogeneity. The acquisition time was fixed at 1 min. An HPLC pump (Shimadzu LC-10ATVP, Champs sur Marne, France) was used to flush monolithic columns for the chemical functionalization and rinsing steps. A UltiMate 3000 *pump* (Dionex) was used for the flow-through catalytic experiments. N-acryloxysuccinimide (NAS), ethylene dimethacrylate (EDMA), methacrylo-propyltrimethoxisilane, 2,2-azobisisobutyronitrile (AIBN), aminophenyl ethylamine, tetrafluoroboric acid (HBF_4 , 54% aq) and sodium nitrite (NaNO_2) were purchased from ACROS. The aromatic derivatives used for capillary electrochromatographic applications were of the highest quality available and all chemicals were used without further purification.

2.2 Synthesis of aniline-grafted monolith

A three step reaction pathway was used to prepare the porous monolith with surface grafted aromatic amines within a fused silica capillary (75 μm I.D.) as depicted in Fig. 1. Prior to polymerization, the inner wall of the capillary was silanised with methacryloxypropyltrimethoxisilane (400 μL in 1 mL of toluene during 12h at 100°C). After rinsing with toluene and acetone and after drying at 100°C under a stream of N_2 , the reactive monomer N-acryloxysuccinimide (NAS, 200 mg) was copolymerised with the crosslinker ethylene glycol dimethacrylate (EGDMA, 110 μL) in the presence of toluene (700 μL) and 2,2-azobisisobutyronitrile (1% w/w, with respect to the total amount of monomers) as a porogenic solvent and as an initiator, respectively. The porous monolith, hereafter poly(NAS-co-EDMA), with well-defined interconnected pores in the micrometer-size range and nucleophilic-sensitive N-hydroxysuccinimide functionalities is obtained through UV-irradiation at 365 nm in a Spectrolinker XL-1500 UV (about 8 $\text{J}\cdot\text{cm}^{-2}$). The obtained monolith

was rinsed (2 $\mu\text{L}/\text{min}$) with ACN for 1 h. The final step consisted in flushing a solution of 4-aminophenyl ethylene amine (0.5M in ACN) through the as-prepared monolith. The diazonium was generated *in situ* by passing (2 $\mu\text{L}/\text{min}$) a solution made of HBF_4 (0.5M) and NaNO_2 (0.5M) in water cooled at 0°C , for one hour.

2.3 On-site synthesis of gold nanoparticles

Aqueous solution of HAuCl_4 (0.5M) was passed (2 $\mu\text{L}/\text{min}$) through the diazonium modified monolith column for 1 hour followed with a rinsing step with water (2 $\mu\text{L}/\text{min}$, 20 min). *In situ* reduction of the gold salt was then reduced by passing (2 $\mu\text{L}/\text{min}$, 30 min) a solution of NaBH_4 in water (5 mg in 1 mL). The monolithic support was finally rinsed with water (2 $\mu\text{L}/\text{min}$, 30 min) and kept at room temperature for further catalysis test and analysis.

2.4 Catalysis reduction of 4-nitrophenol

Catalytic activity of the gold modified monolith was evaluated towards the well-known reduction of nitrophenol. To do so, a mixed solution of NaBH_4 and 4-nitrophenol was injected through the monolith using water as elution fluid (1-4 $\mu\text{L}/\text{min}$). The product-containing solution was collected at the outlet of the column and analysed by UV-Visible spectroscopy to monitor the disappearance of the spectral signature of nitro groups as a function of the flow rate. The reaction yield was estimated as follows:

$$\text{Reaction yield} = \frac{A_{400\text{nm}}^{\text{Gold-free monolith}} - A_{400\text{nm}}^{\text{Gold-coated monolith}}}{A_{400\text{nm}}^{\text{Gold-free monolith}}} \quad (1)$$

Reactant solutions were prepared by dissolving both 4-nitrophenol (5mg) and NaBH_4 (114 mg) in 10 mL of water. 200 μL of the NaBH_4 solution was taken out and further diluted in 4 mL of water. Freshly prepared solutions of the two reactants were mixed 1/1 (v/v) and the mixture was introduced in a 20 μL loop connected to a six-port injection valve. After switching the valve, the reactive solutions were passed through the gold-modified and gold-free monoliths using an HPLC pump at a controlled flow rate (0.5-4 $\mu\text{L}/\text{min}$) using H_2O as running solution. To evidence the catalytic role of the surface immobilized gold nanoparticles, the procedure was initially performed on nanoparticle-free monolith as obtained after step (ii) of the overall preparation process (Fig. 1).

3. Result and discussion:

3.1 Synthesis of aniline-grafted monolith

With the aim to prepare reactive monoliths for supporting gold nanoparticles *via* diazonium salt-related linker, poly(NAS-co-EDMA) with monodisperse flow-through pore channels was synthesized following a protocol previously reported by Guerrouache *et al.*⁵¹ In this protocol, polymerization of the corresponding monomers was carried out through conventional free radical polymerization under photochemical irradiation at 365 nm. The robust anchoring of the monolithic support onto the capillary was ensured within the course of the polymerization process through covalent grafting of the growing polymer chains onto vinylized inner channel wall. In this way, monolith with pore channel of about $2.0 \pm 0.2 \mu\text{m}$, high permeability and nucleophile-sensitive surface groups – *N*-hydroxysuccinimide – can be obtained.

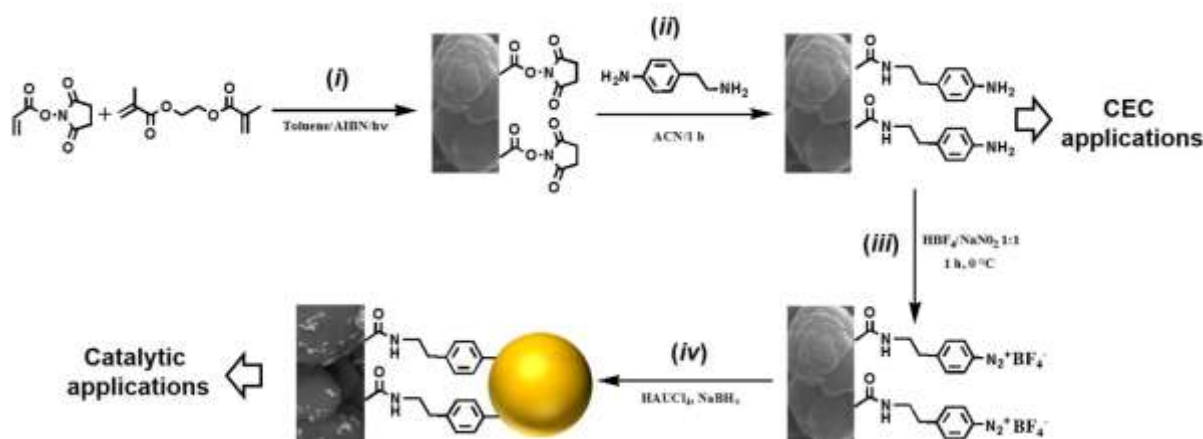


Figure 1: Schematic representation of the synthetic path applied to the surface immobilisation of gold nanoparticles on aniline-grafted monolith via in-situ generation of diazonium salt and chemical reduction. The whole reaction path involves (i) free radical UV-initiated copolymerisation, (ii) surface grafting of 4-aminophenyl ethylene amine, (iii) nitrous acid and (iv) hydride treatment. The aniline-grafted and gold-decorated monoliths were applied as capillary electrochromatography (CEC) stationary phase and flow-through catalytic microreactor, respectively.

As shown in Fig 1, aniline-grafted monolith can be easily obtained in 2 steps (i) and (ii). Raman spectroscopy was used to evidence the chemical structure of the Poly(NAS-co-EDMA) monolith as well as the success of the grafting step of 4-aminophenyl ethylene amine. The latter is achieved *via* nucleophilic substitution of the N-hydroxysuccinimide esters taking advantage of the nucleophilic character of the ethylene amine end. Indeed, the ethylene group prevents mesomeric effect with the phenyl ring providing true primary amine nature. Thus, it is expected that 4-aminophenyl ethylene amine is grafted only by the ethylene amine end

providing aniline-decorated monolith as depicted in Fig 1. Efficiency of the grafting can be easily concluded from the spectra a) and b) shown in Fig 2.

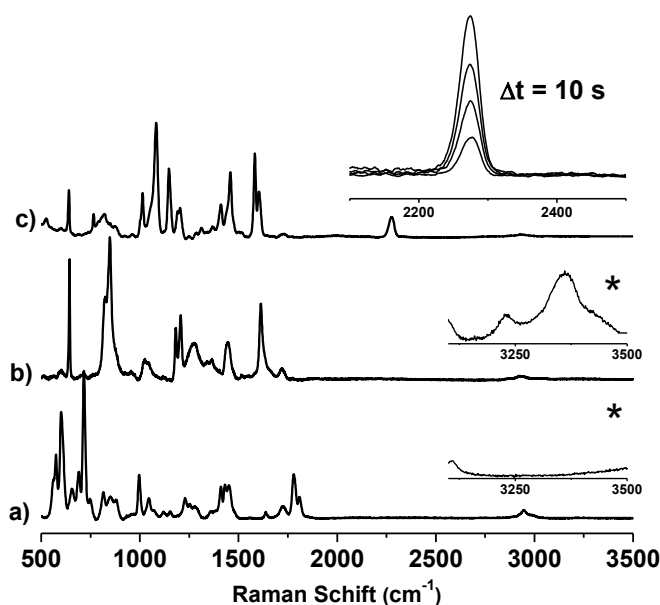


Figure 2: Raman spectra of a) pristine, b) aniline-grafted and c) diazotized monoliths recorded at 638 nm. The insets in a) and b) show expanded regions of the corresponding monoliths in the Raman shift range between 3100 and 3500 cm^{-1} as recorded at 785 nm. The inset in c) shows expanded region of the corresponding spectrum in the Raman shift range between 2100 and 2500 cm^{-1} at 638 nm.

Indeed, after reaction with 4-aminophenyl ethylene amine, we clearly see the appearance of two bands characteristics of aniline moieties at 3000 cm^{-1} and 3300 cm^{-1} corresponding to the aromatic ring and the amine, respectively (see insets in parts a) and b) of Fig 2). Moreover, intensity of the peaks indicative of N-hydroxysuccinimide esters decreases significantly (see peaks in the wavenumber range between 1730 and 1820 cm^{-1}). Such changes in the Raman profile can, to our point of view, be considered as valuable evidences for the substitution of NHS units with aniline groups.

3.2 Aniline-grafted monolith as CEC stationary phase

The development of phenyl-containing monolithic stationary phases has been the subject of intense interest in analytical chemistry providing efficient solutions for the separation of a plethora of solutes in both chromatographic and electrochromatographic modes.⁵³⁻⁶⁰ A general obstacle that has to be overcome in the synthesis of such monoliths, is the inherent limited solubility and low reactivity of monomers bearing bulky aromatic side chains. In previous papers, monoliths decorated with butylphenyl, naphthyl, benzyl and terphenyl selectors were

described.^{21, 22} It was shown that bulky selectors could not be grafted quantitatively affording monolithic columns with limited selectivity. In contrast, the grafting of selector sur as phenyl butyl combining hydrophobic and electron-rich fragments, in other words, aliphatic spacer arm and aromatic rings, respectively, provides mixed selectivity enabling the successful separation of analytes differing in their hydrophobic nature and/or number of pi-electrons in their conjugated structure. In this framework, the aniline-grafted monolith appears as a good candidate as monolithic stationary phases for the separation of aromatic derivatives. Indeed, regarding the chemical structure of the polymeric material obtained after step (ii) in Fig 1, one can see a spacer arm made of an ethylene unit between the amide anchorage and the aminophenyl end. The former may provide interaction sites involving dipole-dipole while the aniline moiety may induce charge transfer interactions. Of utmost importance, the primary amine is expected to induce a donating effect on the phenyl ring *via* mesomery. Prior to performing separation tests, the ability of aniline-grafted monolith to generate stable and high enough electro-osmotic flow for enabling fast migration of neutral solutes under typical voltage was evaluated using various buffer. For pH values in the range between 6.8 and 8.5, phosphate and/or TRIS buffers used in mixture with ACN (30 wt.-%) produced EOF directed toward the negatively charged cathode as high as $2.1 \pm 0.3 \times 10^4 \text{ cm}^2 \cdot \text{s}^{-1} \cdot \text{V}^{-1}$. This corresponds typically to a linear velocity of $0.15 \text{ cm} \cdot \text{s}^{-1}$ that is a migration time of 1.25 min for an EOF marker travelling through a capillary of 10 cm. The cathodal EOF is assumed to arise from a superimposition of complex phenomena consisting in adsorption of buffer ion pairs and formation of carboxyl groups upon hydrolysis of N-hydroxysuccinimide units. Ester groups contained in the skeleton-forming (meth)acrylate monomers, amide bonds or phenyl rings are known to favor ions adsorption allowing the occurrence of electrophoretic processes even for monoliths with neutral surface.^{59, 61-64} The dual role of the NAS monomer affording reactive-sensitive sites for the grafting of hydrophobic, hydrophilic, chiral or zwitterionic selectors and negative charges for the generation of a cathodic EOF has been evidenced elsewhere.^{52, 65} Accordingly, no noticeable EOF was obtained for the aniline-grafted monolith using buffer pH lower than 6. Phosphate buffer (pH 8, 5 mmol) was selected as separation buffer. Alkylbenzenes are commonly used as model solutes to evaluate the hydrophobicity of monolithic stationary phased providing evidence for the occurrence of reversed phase separation mode.⁶⁶ Indeed, upon increasing the length of the aliphatic side chain, the overall hydrophobicity of the molecules increases. As such, for a given composition of mobile phase, the retention time of alkylbenzenes increases with the number of carbon atoms in the alkyl chain while increasing the aqueous phase in the eluent leads to an increase of the alkylbenzenes' retention.⁵² Such

behaviour was not observed for the aniline-grafted monolith. In this case, a mixture on benzene, toluene, ethylbenzene, propylbenzene, butylbenzene, pentylbenzene and phenylhexane was co-eluted independently of the mobile phase composition (Fig. 3). Although the alkylbenzenes were not separated they were more retained than DMF used as EOF marker. Similarly, phenol mixture including *o*-cresol, *m*-cresol, *p*-cresol, dimethylphenol, phenol and 4-chlorophenol was not separated. This finding suggests that the aniline-grafted monolith although exhibiting a slight hydrophobic character does not provide selectivity, i.e. methylene selectivity, towards solutes with small hydrophobicity change. This is in agreement with the use of aniline-modified porous supports for hydrophilic interaction liquid or attenuated reversed-phase chromatographies.⁶⁷

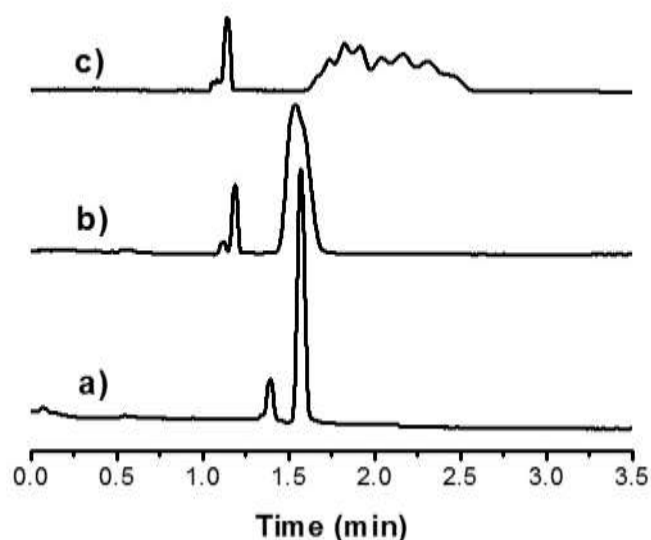


Figure 3: Electrochromatograms corresponding to the injection of 6 alkylbenzenes, namely toluene, ethylbenzene, propylbenzene, butylbenzene, pentylbenzene and phenylhexane on aniline-grafted monolith. The first peak corresponds to the electro-osmotic flow marker, namely dimethylformamide. CEC conditions: mobile phase: acetonitrile–phosphate buffer (5 mmol/L, pH 8) a) 70:30, b) 60:40 and c) 50/50 (v/v). Column length: 10 cm to detector, 31.2 cm overall. Injections -10 kV for 10 s, running voltage -15 kV at 25°C, detection at 214 nm.

Such behaviour can be rationalized on the basis of the chemical nature of the surface grafted selector as discussed here-above in terms of electron relasing effect of the NH₂ group on the phenyl ring. This result motivated us to further evaluate the aniline-grafted monolith for the separation of electron deficient aromatics with antagonist behaviour as compared to the surface-grafted aniline moieties. Nitro groups are well-known to enhance acidity of phenol due to stabilization effect of the phenolate form through impoverishing the aromatic cycle

electron density. Nitroanilines were selected as reference compounds to assess the separation mechanism of aniline-grafted monolith and the retention profile was discussed versus the one observed for amino-, methyl- and chloro-substituted anilines. The pH 8 the mobile phase is well above the typical pKa of anilines (~ 5).⁶⁸ Hence aniline derivatives are expected to be deprotonated in the separation conditions so that their retention behaviour should result from their difference in chromatographic partitioning. Fig 4 shows that on the one hand the retention increases with the number of nitro groups, and on the other hand changing a nitro group with a methyl one induces an decrease in retention. It is however that dimethylanilines have larger Log P values (2.34 for 2,5-dimethylaniline) in comparison to mononitro substituted anilines (1.34 for 4-nitroaniline).⁶⁹ Efficiency values up to 52,000 plates/meter were calculated.

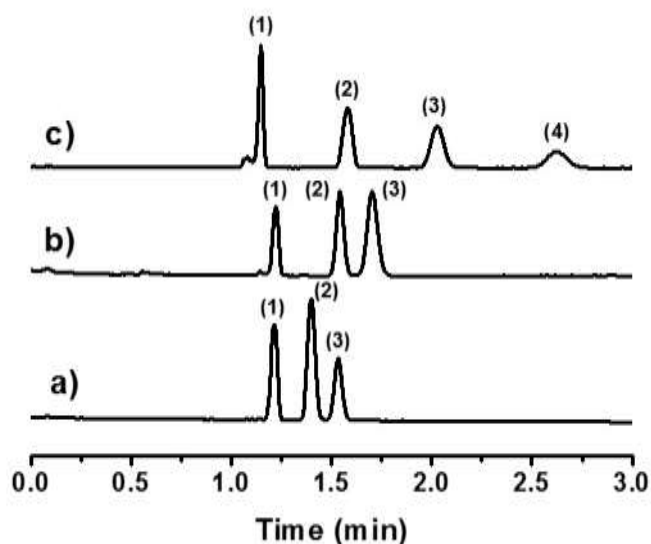


Figure 4: Electrochromatograms corresponding to the injection of a) (1) dimethylformamide (2) 3,4-dimethylaniline and (3) 4-nitroaniline, b) (1) dimethylformamide (2) 4-nitroaniline and (3) 2,4-dinitroaniline and c) (1) dimethylformamide (2) aniline (3) 4-nitroaniline and (4) 2,4-dinitroaniline on aniline-grafted monolith. CEC conditions: mobile phase: acetonitrile–phosphate buffer (5 mmol/L, pH 8) a) and b) 70:30 and c) 50:50. Column length: 10 cm to detector, 31.2 cm overall. Injections -10 kV for 10 s, running voltage a) and b) -30 kV and c) -15kV at 25°C, detection at 214 nm.

In figure 5 it is seen that six anilines were separated with baseline resolution, good peak symmetry and reasonable efficiency. Moreover, no serious peak tailing was observed as it is often the case for the separation of anilines. Similar elution order was obtained using zwitterionic monolithic stationary phase based on lysine-bonded poly(glycidyl methacrylate-

co-ethylene dimethacrylate).⁷⁰ However, the said column exhibited true reversed phase separation mechanism allowing the separation of alkylbenzenes and phenol compounds according to their hydrophobicity. It is noteworthy that the retention of phenylenediamine and 3,4-dimethylaniline was not significantly affected by the change in the mobile phase composition while increasing the buffer content from 50 wt-% to 60 wt-% yielded significant increase in the retention of nitro- and chloro-substituted anilines.

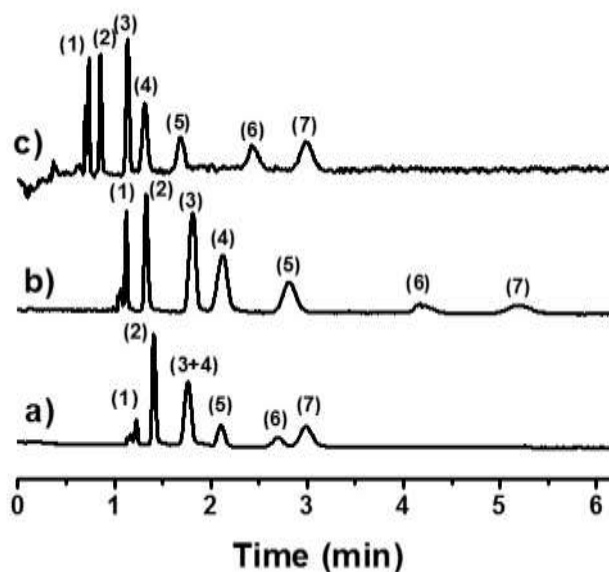


Figure 5: Electrochromatograms corresponding to the injection of (1) dimethylformamide (2) phenylenediamine, (3) 3,4-dimethylaniline, (4) aniline, (5) 4-nitroaniline, (6) 2,4-dinitroaniline and (7) 2,4-dichloroaniline on aniline-grafted monolith. CEC conditions: mobile phase: acetonitrile–phosphate buffer (5 mmol/L, pH 8) a) 50:50, b) and c) 40:60. Column length: 10 cm to detector, 31.2 cm overall. Injection -10 kV for 10 s, running voltage a) and b) -15 kV and c) -30 kV at 25°C, detection at 214 nm.

In a further step we investigated the separation of polycyclic aromatic hydrocarbons (Fig 6). The selected analytes were separated in the order toluene, naphthalene, fluorene, anthracene, pyrene and chrysene and their elution was achieved in a separation window of less than 3 min.

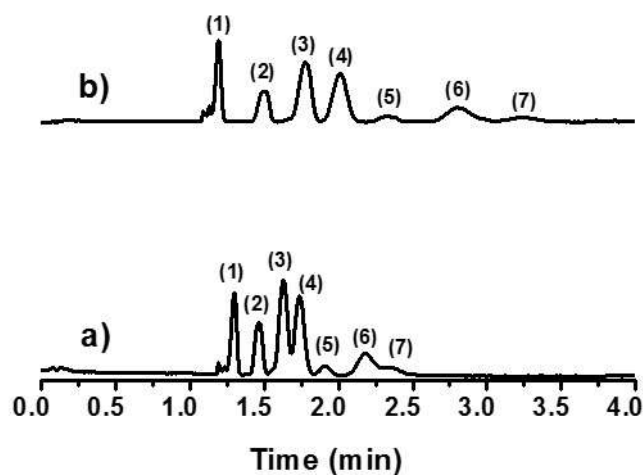


Figure 6: Electrochromatograms corresponding to the injection of (1) dimethylformamide (2) toluene, (3) naphthalene, (4) fluorene, (5) anthracene, (6) pyrene and (7) chrysene on aniline-grafted monolith. CEC conditions: mobile phase: acetonitrile–phosphate buffer (5 mmol/L, pH 8) a) 50:50, b) 40:60. Column length: 10 cm to detector, 31.2 cm overall. Injections -10 kV for 10 s, running voltage a) and b) -15 kV and c) -30 kV at 25°C, detection at 214 nm.

Such elution is in good agreement with previous investigation using monolithic column surface-grafted with aromatic selector.²¹ As expected, the retention increases with decreasing the ACN content while the elution order was preserved providing baseline resolution of the pyrene-chrysene pair with the latter one being the most retained. Decreasing the applied voltage was used as a second way to improve the quality of the separation (Fig 6b). By decreasing twice the voltage value, the pyrene – chrysene pair (indicated by (6) and (7) in the Figure 6) was baseline separated.

3.3 Aniline-grafted monolith as gold nanoparticle support

Starting from aniline-grafted monolith, the envisioned strategy for the *in situ* and on-monolith surface production of diazonium salt relied on the combined use of tetrafluoroboric acid and sodium nitrite at equimolar concentration. To ensure that such a reactive mixture does not induce chemical degradation or side reactions of/with the monolithic skeleton, native poly(NAS-co-EDMA) was analyzed by Raman spectroscopy after treatment with $\text{HBF}_4/\text{NaNO}_2$ under dynamic conditions. Figure 7 shows that the spectra exhibit similar

features and can be perfectly superimposed suggesting chemical stability of the monolith under such rather harsh conditions.

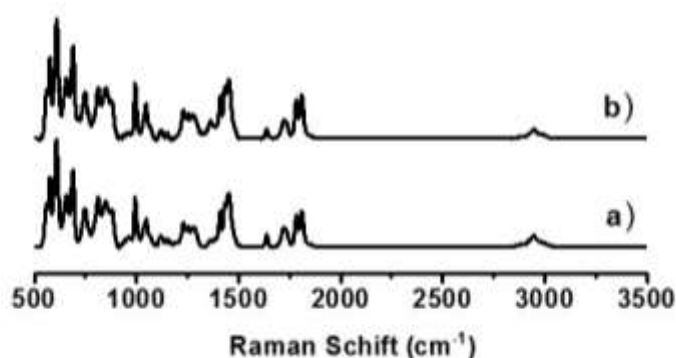


Figure 7: Raman spectra for pristine monoliths as-obtained a) directly after step (i) of the synthesis path shown in Figure 1 and b) after treatment with nitrous acid as recorded at 785 nm.

After having confirmed the chemical integrity of the polymeric skeleton, we evaluated in the next step the possibility to generate diazonium species on monolith surface for the first time by subjecting aniline-modified monolith to a diazotation mixture. The diazonium modification is clearly evidenced by the appearance of a peak at about at 2250 cm^{-1} typical for diazonium units (inset in Fig 2 c). Interestingly, we noticed a fast decrease (within 30 s) of the intensity of the diazonium-related peak while the monolith was continuously exposed to the excitation irradiation of the 785 nm laser. Such decrease was even enhanced using higher power excitation source so that the presence of the diazonium was hardly evidenced when an excitation wavelength of 638 nm was applied. These findings suggest a high sensitivity of on-monolith grafted diazonium salt to visible light. Herein, we did not consider a photodriven approach for the functionalization of the diazotized monolith, but rather we exploited the concomitant reduction of gold ions and the diazonium compound by flowing an aqueous solution of NaBH_4 . Prior to the reduction step, diazotized monolith was loaded with an aqueous solution of hydrogen tetrachloroaurate and further rinsed with water. The ability of diazonium salt cation to complex metal salt anion provides monolith with surface pre-concentrated gold metal precursor.¹ Effective reduction of Au^{3+} into Au^0 was initialled assumed from the change in the color of the in-capillary monolith which turned to dark purple upon flowing the hydride-containing solution. Such a coloration remained after thorough washing of the monolith as expected for robust anchoring of metal nanoparticle on surface. It is assumed that the surface-attachment of gold nanoparticles proceeds according to the mechanistic path described by Mirkhalaf et al. where the individual reduction of both surface

coupling agent and metal precursor occurs initially. The latter results in the formation on the monolith pore surface of aryl radicals which are prone to hinder the hydride-mediated growth of gold structures through the formation carbon-metal bond. As such, it is expected that the monolith surface would be loaded with gold nanoparticle with nanometric size, i.e. exhibiting interesting catalytic activity. These features were confirmed to a large extent by scanning electron microscopy and energy dispersive X-ray Analysis (Fig 8).

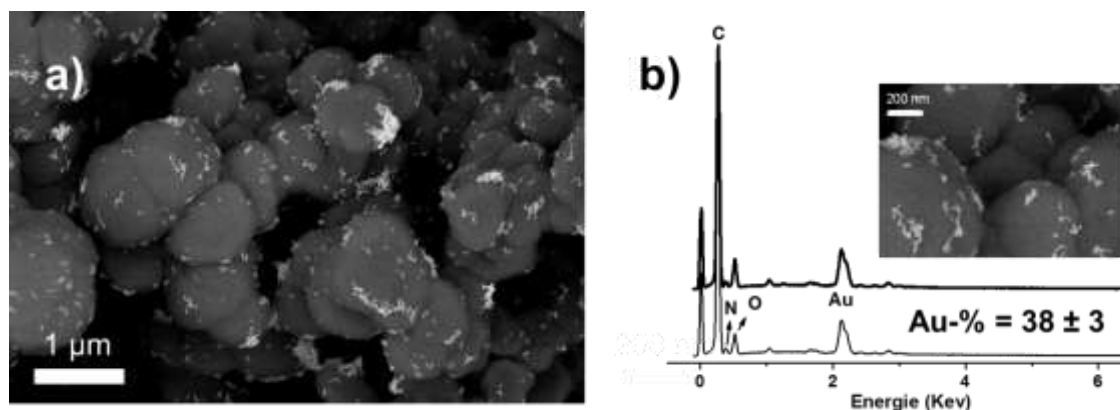


Figure 8: a) Scanning electron microscopy image and b) energy dispersive X-ray analyses recorded for gold nanoparticle-decorated monolith prepared via the diazonium route. The inset in b) presents a SEM image with higher magnification. The energy dispersive X-ray profiles correspond to measurement performed on gold-grafted monolith as obtained after (thick plot) step (iv) in Figure 1 and (thin plot) after thorough washing of gold-grafted monolith with hot water (80°C, 30 min at 2μL/min) and ACN (RT, 15 min at 2μL/min).

The SEM investigations revealed typical monolithic morphology, made of all-fused together globuli, for the hybrid material. This confirms further that the $\text{HBF}_4/\text{NaNO}_2$ treatment did not affect the integrity of the polymer. Presence of nanometer-sized structures covering homogeneously the monolith surface is also clearly seen. Such morphological details evidences the stabilizing ligand effect of the surface diazotized monolith. The gold content was estimated to be in the range 35-41 % comparable reported values for high capacity gold nanoparticles modified monoliths prepared using the more conventional thiol-gold pair.²⁷ It is assumed that besides the as-observed in Fig 8a nanogold-pearl-necklace appearance, the diazonium strategy produces gold nanoparticles with lower size which are undistinguishable by SEM explaining the high gold loading. On the basis of these preliminary results discussing the first implementation of diazonium salt for the covalent attachment of nanogold on monolith pore surface, the so-designed hybrid monolith was applied to flow catalysis application. We focused on a model catalytic reaction, namely the reduction of 4-nitrophenol

into 4-aminophenol. Monitoring of the reaction was achieved by collecting the product-containing solution at the outlet of the monolithic material and measuring its UV-visible absorption spectrum in the wavelength range between 200 nm and 600 nm. Progress of the reaction was estimated by comparing the UV-visible absorbance signals as a function of the flow rate. Indeed, it is expected that the reaction time exhibits a direct dependence on the flow rate so that decreasing the flow rate would lead to an increase in the yield of the reaction in agreement with the early reported pseudo-first-order or first-order (depending on the 4-NP concentration) kinetics for the solution reduction of *p*-nitrophenol in presence of an excess of borohydride. Measurements were performed at 400 nm, because phenol derivatives are spontaneously transformed into the corresponding phenolate ions upon reaction with hydride. The deprotonation is accompanied by a shift of the maximum of absorption to 400 nm. The value of the UV absorbance measured using a gold-free nanogold was used as blank to calculate the reaction yields. The results as displayed in Figure 9 illustrate unambiguously the here-above discussion. All measurements were performed using freshly prepared reactant solutions to avoid any decomposition of NaBH_4 . For clarity purposes, only the UV-visible spectra recorded for two flow rates using the gold-containing monolith are presented while the dependence of reaction yield *vs* the tested flow rate value is shown as inset. The blank UV signal was found to be independent on the flow rate and a variation of less than 4% was obtained when the flow rate was changed from $4\mu\text{L}/\text{min}$ to $1\mu\text{L}/\text{min}$. In contrast, the profile as-obtained after elution through the monolith bearing gold nanoparticles are significantly dependent on the flow rate, in other words the linear velocity of displacement of reactants along the catalytic support. The intensity measured at 300 nm increases accordingly to the decrease of the peak intensity measured at 400 nm. By decreasing the flow rate from $4\mu\text{L}/\text{min}$ to $2\mu\text{L}/\text{min}$, the reaction yield increases from 82% to 94.4% and a linear variation was obtained in the studied flow rate range (from $1\mu\text{L}/\text{min}$ to $4\mu\text{L}/\text{min}$). From this linear variation it is assumed that the quantitative transformation (yield > 99.9%) of 4-nitrophenol into 4-aminophenol can be achieved using a flow rate of $1.3\mu\text{L}/\text{min}$ providing the shortest reaction time.

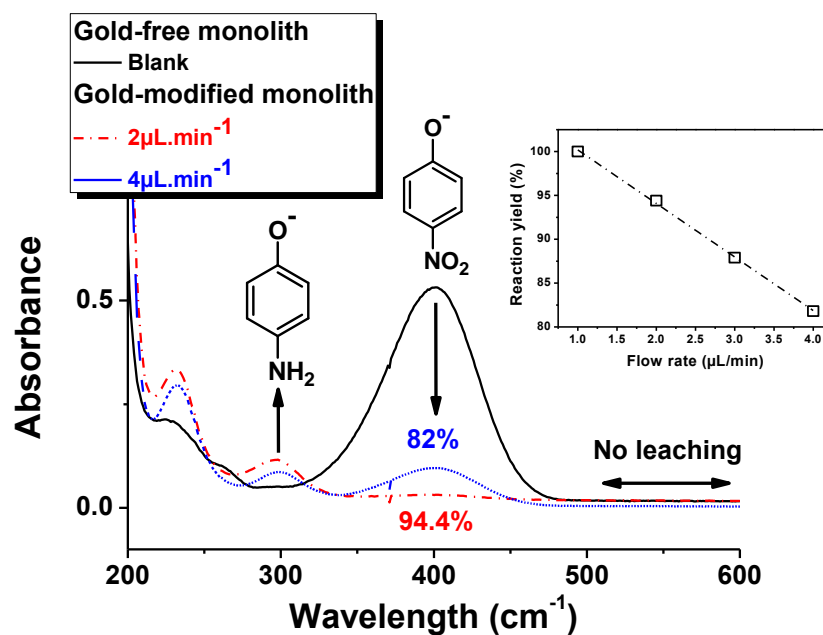


Figure 9: UV-visible spectra recorded for product-containing solutions collected at the outlet of the catalytic microreactors containing (thick plot) nanogold-free aniline-grafted and (thin plots) gold-immobilized monoliths. The latter measurements were performed at two different flow rates as indicated in the figure. The inset shows the variation of the reaction yield as a function of the flow rate. The UV-Vis measurements were extended up to 600 nm to show that no gold nanoparticles were released in the course of the catalytic process as it would be expected, in this case, that UV surface plasmon signature shows up in the range 500-600 nm.

Although we discuss herein only preliminary results in the form of a proof of concept for the possibility to apply the surface science of diazonium salt to the grafting of gold nanoparticles on the wall of porous polymeric monoliths, we anticipate that this approach can be extended to other noble metal. Moreover, the nature of the monolith-metal nanoparticle bond ensures robust interfacial tethering of nanometal so that the catalytic reactor can be extended to the use at moderately high temperature (below 120°C in accordance with the thermal stability of the crosslinked monolithic skeleton) process.

To consolidate this assumption, we have recorded the energy dispersive X-ray profile after dynamic washing of the gold-modified monolith with hot (80°C) water during 30 min. As shown in Fig 8, the results show that the gold loading remains constant suggesting enhanced stability of the carbon-gold bond arising from the diazonium chemistry. In addition, the UV-Visible plots in Figure 9 do not reveal any surface plasmonic spectral signature typically observed in the wavelength range from 470 to 650 nm. Finally, the reaction yield was calculated for successive catalytic cycles (Fig 10). No noticeable changes were observed up to six successive cycles. To our point of view, these results evidence of the absence of gold

nanoparticles leaching even upon continuous flow in aqueous basic conditions can be considered as a reliable proof that the diazonium route provides robust anchoring of gold nanoparticles on monolith surface.

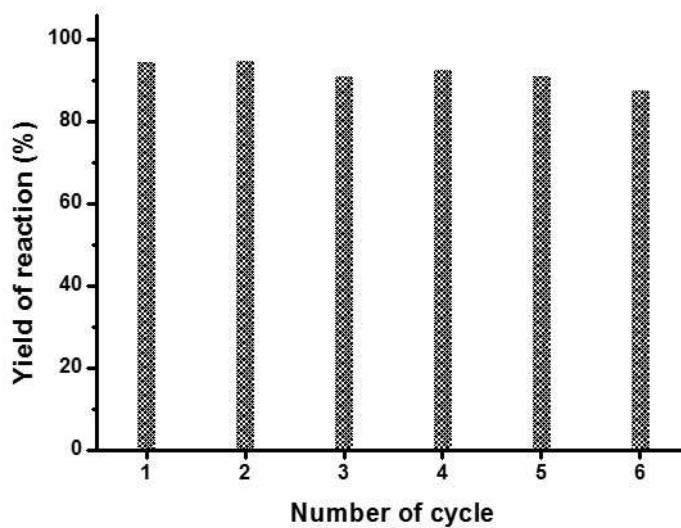


Figure 10: Reaction yields calculated for successive hydride-mediated catalytic reductions of 4-nitrophenol into 4-aminophenol using the gold-modified monolithic microreactors. The reaction was performed under flow conditions at 2 $\mu\text{L}/\text{min}$.

4. Conclusion:

Polymer monolith bearing aniline surface-grafted moieties has been successfully synthesized for the first time in the capillary format following a two-step approach. Reactive monolith was initially prepared through the UV-driven copolymerization of N-acryloxysuccinimide and ethylene glycol dimethacrylate. Then, 4-aminophenyl ethylene amine was grafted quantitatively *via* nucleophile substitution. Electrochromatographic performances of the so-designed monolith was evaluated towards the separation of alkylbenzenes, phenols, anilines and polycyclic aromatic hydrocarbons. Interestingly, only the last two series of solutes could be separated with baseline separation and efficiency up to 52,000. This separation feature suggests specific separation ability for the aniline-grafted monolith. Indeed, the naphthalene-anthracene pair, having polarity of 3.30 and 4.45, respectively, was successfully separated while no separation was observed for a mixture made of ethylbenzene (polarity = 3.15) and butylbenzene (polarity = 3.30). These results suggest that the separation mechanism is not simply governed by reversed phase mechanism. It is assumed that aniline moieties provide enhanced pi-pi interactions owing to the electron releasing effect of the primary amine on the phenyl through resonance. Further investigation will be carried out to elucidate the interaction mode involved with aniline-grafted monolith. The main achievement of this work relies on the use of Mirkhalaf's strategy to efficiently anchoring metallic nanoparticles on monolith pore surface *via* robust carbon-metal bond. Diazonium units were generated *in situ*, *i.e.* on the monolith surface, through the reaction between equimolar solution of tetrafluoroboric acid and sodium nitrite and the aniline-grafted monolith. Nanogold-decorated monolith was then applied as flow through catalytic microreactor for the hydride-mediated reduction of 4-nitrophenol into 4-amino-phenol. Yield of the reaction was directly governed by the flow rate and complete conversion of the nitro-derivative was obtained at 1 $\mu\text{L}/\text{min}$. We anticipate that this newly developed approach may be extended to other type of monolith surface functionalization such as the grafting of other metal nanoparticles or sp² carbon-rich nanostructures.

5. References

1. F. Mirkhalaf, J. Paprotny and D. J. Schiffrin, *Journal of the American Chemical Society*, 2006, **128**, 7400-7401.
2. M. S. Silverstein, N. R. Cameron and M. A. Hillmyer, *Porous polymers*, John Wiley & Sons, 2011.
3. D. Wu, F. Xu, B. Sun, R. Fu, H. He and K. Matyjaszewski, *Chemical reviews*, 2012, **112**, 3959-4015.
4. M. S. Silverstein, *progress in Polymer Science*, 2014, **39**, 199-234.
5. M. S. Silverstein, *Polymer*, 2014, **55**, 302-303.
6. F. Svec, *Journal of Chromatography B*, 2006, **841**, 52-64.
7. J. Krenkova and F. Svec, *Journal of separation science*, 2009, **32**, 706-718.
8. F. Svec, *Journal of separation science*, 2004, **27**, 747-766.
9. L. Geiser, S. Eeltink, F. Svec and J. M. Fréchet, *Journal of Chromatography A*, 2008, **1188**, 88-96.
10. M. R. Buchmeiser, *Polymer*, 2007, **48**, 2187-2198.
11. F. Gritti and G. Guiochon, *Journal of Chromatography A*, 2009, **1216**, 4752-4767.
12. M. Araya-Farias, M. Taverna, M. Woytasik, F. Bayle, M. Guerrouache, I. Ayed, H. H. Cao, B. Carbonnier and N. T. Tran, *Polymer*, 2015, **66**, 249-258.
13. K. Faure, M. Albert, V. Dugas, G. Crétier, R. Ferrigno, P. Morin and J. L. Rocca, *Electrophoresis*, 2008, **29**, 4948-4955.
14. F. Svec, *Journal of Chromatography A*, 2010, **1217**, 902-924.
15. M. Vázquez and B. Paull, *Analytica chimica acta*, 2010, **668**, 100-113.
16. C. Viklund, E. Pontén, B. Glad, K. Irgum, P. Hörstedt and F. Svec, *Chemistry of materials*, 1997, **9**, 463-471.
17. S. Xie, F. Svec and J. M. Fréchet, *Chemistry of materials*, 1998, **10**, 4072-4078.
18. S. I. Kebe, M. B. Boubaker, M. Guerrouache and B. Carbonnier, *New Journal of Chemistry*, 2016.
19. J. Wang, W. Jia, X. Lin, X. Wu and Z. Xie, *Electrophoresis*, 2013, **34**, 3293-3299.
20. M. Guerrouache, A. Pantazaki, M. C. Millot and B. Carbonnier, *Journal of separation science*, 2010, **33**, 787-792.
21. M. Guerrouache, M. C. Millot and B. Carbonnier, *Journal of separation science*, 2011, **34**, 2271-2278.
22. T. Mekhalif, S. I. Kebe, M. Guerrouache, N. Belattar, M. C. Millot and B. Carbonnier, *Chromatographia*, 2016, **79**, 1333-1341.
23. J. C. Masini, *Analytical and bioanalytical chemistry*, 2016, **408**, 1445-1452.
24. C. Bisjak, R. Bakry, C. W. Huck and G. Bonn, *Chromatographia*, 2005, **62**, s31-s36.
25. B. Preinerstorfer, W. Bicker, W. Lindner and M. Lämmerhofer, *Journal of Chromatography A*, 2004, **1044**, 187-199.
26. B. Preinerstorfer, W. Lindner and M. Lämmerhofer, *Electrophoresis*, 2005, **26**.
27. Y. Lv, F. M. Alejandro, J. M. Fréchet and F. Svec, *Journal of Chromatography A*, 2012, **1261**, 121-128.
28. D. Connolly, B. Twamley and B. Paull, *Chemical Communications*, 2010, **46**, 2109-2111.
29. M. Guerrouache, S. Mahouche-Chergui, M. M. Chehimi and B. Carbonnier, *Chemical Communications*, 2012, **48**, 7486-7488.
30. D. Connolly, S. Currivan and B. Paull, *Proteomics*, 2012, **12**, 2904-2917.

31. S. Mahouche-Chergui, M. Guerrouache, B. Carbonnier and M. M. Chehimi, *Colloids and Surfaces A: Physicochemical and Engineering Aspects*, 2013, **439**, 43-68.
32. Y. Pan, X. Wang, H. Zhang, Y. Kang, T. Wu and Y. Du, *Analytical Methods*, 2015, **7**, 1349-1357.
33. Y. Xu, Q. Cao, F. Svec and J. M. Frechet, *Analytical chemistry*, 2010, **82**, 3352-3358.
34. Q. Cao, Y. Xu, F. Liu, F. Svec and J. M. Frechet, *Analytical chemistry*, 2010, **82**, 7416-7421.
35. Y. Liang, C. Wu, Q. Zhao, Q. Wu, B. Jiang, Y. Weng, Z. Liang, L. Zhang and Y. Zhang, *Analytica chimica acta*, 2015, **900**, 83-89.
36. P. Floris, B. Twamley, P. N. Nesterenko, B. Paull and D. Connolly, *Microchimica Acta*, 2014, **181**, 249-256.
37. A. M. Khalil, V. Georgiadou, M. Guerrouache, S. Mahouche-Chergui, C. Dendrinou-Samara, M. M. Chehimi and B. Carbonnier, *Polymer*, 2015, **77**, 218-226.
38. Y. Ye, M. Jin and D. Wan, *Journal of Materials Chemistry A*, 2015, **3**, 13519-13525.
39. R. Msaadi, A. Gharsalli, S. Mahouche-Chergui, S. Nowak, H. Salmi, B. Carbonnier, S. Ammar and M. M. Chehimi, *Surface and Interface Analysis*, 2016.
40. S. Mahouche Chergui, A. Ledebt, F. Mammeri, F. Herbst, B. Carbonnier, H. Ben Romdhane, M. Delamar and M. M. Chehimi, *Langmuir*, 2010, **26**, 16115-16121.
41. S. Gam-Derouich, M. Gosecka, S. Lepinay, M. Turmine, B. Carbonnier, T. Basinska, S. Slomkowski, M.-C. Millot, A. Othmane and D. Ben Hassen-Chehimi, *Langmuir*, 2011, **27**, 9285-9294.
42. C. Fairman, J. Z. Ginges, S. B. Lowe and J. J. Gooding, *ChemPhysChem*, 2013, **14**, 2183-2189.
43. I. Bakas, Z. Salmi, M. Jouini, F. Geneste, I. Mazerie, D. Floner, B. Carbonnier, Y. Yagci and M. M. Chehimi, *Electroanalysis*, 2015, **27**, 429-439.
44. G. Liu, T. Böcking and J. J. Gooding, *Journal of Electroanalytical Chemistry*, 2007, **600**, 335-344.
45. A. A. Mohamed, Z. Salmi, S. A. Dahoumane, A. Mekki, B. Carbonnier and M. M. Chehimi, *Advances in colloid and interface science*, 2015, **225**, 16-36.
46. J. J. Gooding, *Electroanalysis*, 2008, **20**, 573-582.
47. I. Bakas, Z. Salmi, S. Gam-Derouich, M. Jouini, S. Lépinay, B. Carbonnier, A. Khelifi, R. Kalfat, F. Geneste and Y. Yagci, *Surface and Interface Analysis*, 2014, **46**, 1014-1020.
48. S. Mahouche-Chergui, S. Gam-Derouich, C. Mangeney and M. M. Chehimi, *Chemical Society Reviews*, 2011, **40**, 4143-4166.
49. B. D. Assresaegn, T. Brousse and D. Bélanger, *Carbon*, 2015, **92**, 362-381.
50. Z. Salmi, S. Gam-Derouich, S. Mahouche-Chergui, M. Turmine and M. Chehimi, *Chemical Papers*, 2012, **66**, 369-391.
51. M. Guerrouache, B. Carbonnier, C. Vidal-Madjar and M.-C. Millot, *Journal of Chromatography A*, 2007, **1149**, 368-376.
52. B. Carbonnier, M. Guerrouache, R. Denoyel and M. C. Millot, *Journal of separation science*, 2007, **30**, 3000-3010.
53. W. Zhang, Y. Feng, L. Zhang, T. Li and Y. Zhang, *Electrophoresis*, 2005, **26**, 2935-2941.
54. C. P. Bisjak, S. H. Lubbad, L. Trojer and G. K. Bonn, *Journal of Chromatography A*, 2007, **1147**, 46-52.

55. C. P. Bisjak, L. Trojer, S. H. Lubbad, W. Wieder and G. K. Bonn, *Journal of Chromatography A*, 2007, **1154**, 269-276.
56. S. Karenga and Z. El Rassi, *Electrophoresis*, 2010, **31**, 3200-3206.
57. Z. Zhang, H. Lin, J. Ou, H. Qin, R. a. Wu, J. Dong and H. Zou, *Journal of Chromatography A*, 2012, **1228**, 263-269.
58. T. X. Lav, D. Grande, C. Gaillet, M. Guerrouache and B. Carbonnier, *Macromolecular Chemistry and Physics*, 2012, **213**, 64-71.
59. T.-X. Lav, B. Carbonnier, M. Guerrouache and D. Grande, *Polymer*, 2010, **51**, 5890-5894.
60. R. Meinus, K. Hormann, R. Hakim, U. Tallarek and B. M. Smarsly, *RSC Advances*, 2015, **5**, 20283-20294.
61. S. Karenga and Z. El Rassi, *Electrophoresis*, 2010, **31**, 3192-3199.
62. H. Zhong and Z. El Rassi, *Journal of separation science*, 2009, **32**, 10-20.
63. S. Karenga and Z. El Rassi, *Journal of separation science*, 2008, **31**, 2677-2685.
64. M. Szumski, Z. Kučerova, P. Jandera and B. Buszewski, *Electrophoresis*, 2009, **30**, 583-588.
65. M. Guerrouache, S. Mahouche-Chergui, T. Mekhalif, T. T. H. Dao, M. M. Chehimi and B. Carbonnier, *Surface and Interface Analysis*, 2014, **46**, 1009-1013.
66. Ç. Gölgelioğlu and A. Tuncel, *Electrophoresis*, 2013, **34**, 331-342.
67. C. D. Iverson and C. A. Lucy, *Journal of Chromatography A*, 2014, **1373**, 17-24.
68. I. Canals, K. Valkó, E. Bosch, A. P. Hill and M. Rosés, *Analytical chemistry*, 2001, **73**, 4937-4945.
69. T. Cserhádi, B. Bordás and M. Szögyi, *Chromatographia*, 1986, **21**, 312-316.
70. X. Dong, J. Dong, J. Ou, Y. Zhu and H. Zou, *Electrophoresis*, 2006, **27**, 2518-2525.

Chapitre IV

Objectifs

Réaliser un ancrage de nanoparticules métalliques stable vis-à-vis de solutions aqueuses basiques et des conditions de température modérément élevées.

Elaborer des matériaux monolithiques hautement perméables et présentant des propriétés catalytiques gouvernées par la nature des nanoparticules immobilisées en surface.

Préparer des monolithes nanostructurés présentant une distribution homogène et dense de nanoparticules individuelles en surface.

Etudier l'effet de la méthode d'immobilisation des nanoparticules d'or sur les propriétés de perméabilité et catalytiques des microréacteurs.

Contrôler la morphologie des nanoparticules immobilisées en surface

Démontrer le potentiel catalytique de monolithes nanostructurés vis-à-vis de différents types de réactions catalytiques.

Méthodes

Chimie thiol-ène par voie photochimique pour le greffage de groupements chélatants.

Immobilisation de nanoparticules métalliques en surface par adsorption de solutions colloïdales et par réduction sur site de sels métalliques.

Réaction catalytiques en flux continu sur supports monolithiques nanostructurés.

Limites

Analyse quantitative des dépôts d'or.

Perte de perméabilité pour les monolithes préparés *via* l'adsorption de nanoparticules préformées.

Accès à la spectroscopie de photo-électrons X pour la caractérisation des monolithes nanostructurés.

Complexité de coupler les microréacteurs catalytiques avec un système de détection permettant un suivi en ligne et en temps réel des rendements de réactions.

Importance

Démonstration de la polyvalence de la chimie thiol-ène pour l'immobilisation de chélatants spécifiques de différentes nanoparticules métalliques.

Possibilité de contrôler la morphologie de nanoparticules d'or immobilisées en surface *via* la nature de l'agent réducteur.

Stabilité accrue des dépôts d'or permettant de mener des procédés catalytiques à des températures modérément élevées.

Metal nanoparticles @ monolithic supports as continuous-flow microreactor for the catalytic reduction of mono and disubstituted nitroaromatics, oxydation of benzyl alcohol and Suzuki-Miyaura carbon-carbon coupling reactions

Keywords: Catalytic reduction, Au-supported nanoparticles, Pd- supported nanoparticles, Monolithic microreactor, Photo-click chemistry

Abstract

In this work, microreactors based on metal nanoparticles-decorated monoliths were applied to the catalytic reduction of nitro-arenes, oxidation of benzyl alcohol and Suzuki-Miyaura carbon-carbon coupling reaction between phenyl boronic acid and bromobenzene. To this aim, monolith materials, based on N-acryloxysuccinimide and ethylene glycol dimethacrylate, were synthesized inside fused-silica capillary through radical photo-polymerization (365 nm). After the polymerization step, the monolith with optimal porous properties was successively modified with allylamine – through nucleophilic substitution of the N-hydroxysuccinimide units – and cysteamine – *via* DMPA-initiated photo-assisted thiol-ene click addition – with the aim to further immobilizing noble metal nanoparticles *via* primary amine-driven surface chelation. Herein, both adsorption of pre-formed metal nanoparticles and *in situ* synthesis of the said nanoparticles were explored with the aim the design permeable nanostructured monoliths with efficient catalytic activity. Success of the in-capillary polymerization and thiol-ene click chemistry was evidenced by Raman spectroscopy. Scanning electron microscopy complemented with energy dispersive X-ray analyses provided information about the morphology of the monolithic matrix, dispersion state of the metal nanoparticles on the monolith surface and surface chemical composition of the monolith. Catalytic reduction of the mono- and di-nitro-arenes was achieved under flow through conditions at room temperature and the reaction yields, as determined by UV-Vis, (reduction aromatic) were compared as a function of both size and immobilization method of the metal nanoparticles. As a general trend it was observed that decreasing the size of metal nanoparticles allows improving significantly the catalytic activity of the microreactor. Moreover, the *in situ* approach proved very appealing to prepare metal nanoparticle with tunable size beside typical commercially available range size (typically 5, 20 and 60 nm) while avoiding loss of permeability due to the clogging of preformed nanoparticles at the monolith inlet. For the benzyl alcohol oxidation and phenyl boronic-acid coupling, the flow process were achieved at

moderately high temperature. It was notably shown that temperature controls the nature of the oxidized compound obtained from benzyl alcohol, as benzaldehyde and benzoic acid were the major products for low (< 60°C) and high (> 60°C) reaction temperature, respectively. This work brings out the catalytic properties of noble metal nanoparticles and their interest in micro-technology.

1 Introduction

The combination of inorganic particles with length scales in the nanometer range with organic polymers offers unique opportunities for designing advanced composite materials with applications in various scientific and technological domains. Two main strategies can be found among the vast literature relying on either the embedding or the interfacial deposition of nanoparticles within or on the polymer.¹⁻⁶ Both strategies provided efficient solutions for analytical and synthetic chemists, material scientists and biologists interested in participating to the nanotechnology-driven scientific revolution. Electrospinning-assisted embedding of silver nanoparticles in polyvinyl alcohol nanofibers provided nanomaterials with dual functionality⁷. Indeed, robust antibacterial activity against both Gram-positive *Staphylococcus aureus* (*S. aureus*) and Gram-negative *Escherichia coli* (*E. coli*) microorganisms was observed in parallel to a surface-enhanced Raman spectroscopy activity towards mercaptophenol. Zhang et al. reported on enhancement of the photoresponse behavior of conductive polymer nanowires embedded with Au nanoparticle.⁸ The authors demonstrated clearly the crucial effect of the precise positioning of the gold nanoparticles *via* a modulation effect of the photoresponse behavior by excitation light wavelength or power due to a plasmon coupling effect. Guo et al discussed the effect of adding tubular nanoparticles, namely native and resorcinol diphenyl phosphate coated montmorillonite and halloysite nanotubes, on mechanical properties of biodegradable polymer blends.⁹ The authors showed that only the particles with very high surface area allowed reducing the size of the phase separated polymer domains based on poly(lactic acid) and (poly(butylene adipate-*co*-butylene terephthalate)). Thus, inorganic nanoparticles have been successfully combined to polymeric materials for sensitive sensing,¹⁰ medical diagnosis,¹¹ water treatment,¹² improvement of mechanical,¹³ barrier¹⁴ and flame retardancy¹⁵ properties of polymeric partner, catalysis applications¹⁶ ..., to cite but a few.

Considering catalytic applications, the adsorption of nanocatalyst onto polymeric materials' surface is well-suited affording catalytic sites with enhanced accessibility. Various polymers such as thermoplastic polyurethane,¹⁷ N-containing polymer nanospheres,¹⁸ polymer

nanocapsules,¹⁹ poly(*m*-phenylenediamine)²⁰ have been decorated with metal or metal oxide nanoparticles for the reduction of nitrophenol, oxidation of methanol, carbon-carbon and carbon-nitrogen bond-forming reactions. This approach also proved true using porous polymer although some successful examples of catalytically active porous polymer encapsulating metal nanoclusters have been reported. For instance, crosslinked polystyrene with rigid nanocavities²¹ or conjugated polymer networks made of rigid building blocks²² proved to be good candidates as supports for platinum and palladium nanostructures, respectively. The use of porous polymers as nanocatalyst supports has recently emerged as a very powerful strategy affording versatile platforms for the stabilization of metallic nanostructures.²³ Taking full advantage of intrinsic properties of both partners, one may design function composite materials with improved catalytic properties. On the one hand, permeability and easy surface chemical modification for polymers and, on the other hand, unique physical and chemical properties for nanoparticles arising from high surface-area-to-volume ratios and differing undoubtedly from both atoms and bulk materials. The formers enables the grafting of specific anchoring sites and fast diffusion of target molecules, respectively. The latter can be exploited for other purposes beyond heterogeneous catalysis and one may cite optical, solid phase extraction and separation purposes. Of particular interest to the context of our investigation is the use of porous polymer@metal-based nanoparticles for catalytic applications under flow through conditions. To this aim, porous polymers have been implemented in the form of monolithic materials synthesized within the confines of channels and further surface decorated with gold nanoparticles for catalyzing reduction reactions.^{24,25} Intermediate surface functionalization step was introduced to graft metal nanoparticles chelating groups. In the case of gold nanoparticles, strategies involving the surface grafting of thiol or amino groups have provided major contributions to the adsorption of gold colloids.²⁶⁻²⁸ The so-designed monolithic composites were successfully applied to catalytic reduction reactions. Owing to the numerous positive attributes of monolithic materials, and regarding their historical applications in the field of separation science, various research groups have discussed the use of related nanomaterials for detection, separation or sample treatment purposes²⁹⁻³⁵. One may also briefly mention the use of gold-modified monolith as enzymatic bioreactor.³⁶

Herein, we report on the preparation of functional monoliths serving as permeable supports for immobilizing metal nanoparticles. The results are discussed as a function of the nature of the metal nanoparticles and correspondingly the type of ligand surface anchored on the monolith *via* thiol-ene click chemistry. On-site approach for the preparation of metal

nanoparticles relying on the *in situ* reduction of metal salt precursors together with the adsorption of preformed nanoparticles are compared. The tested catalytic reactions concern the hydride-mediated reduction of mono- and dinitro-arenes, the oxidation of benzylic alcohol in the presence of hydrogen peroxide and the Suzuki-Miyaura carbon-carbon coupling reaction. The catalytic results are discussed, when possible, in terms of flow rate and temperature.

2 Materials and methods

2.1 Materials

N-acryloxysuccinimide (NAS) was obtained from TCI. Ethylene glycol dimethacrylate (EDMA), 3-(trimethoxysilyl) propyl methacrylate (γ -MAPS), 2,2'-azobisisobutyronitrile (AIBN), 2,2-dimethoxy-2-phenylacetophenone (DMPA), dodecane, allyllamine, cysteamine hydrochloride, hydrogen tetrachloroaurate(III) trihydrate ($\text{HAuCl}_4 \cdot 3\text{H}_2\text{O}$), gold nanoparticles colloids (20 & 60 nm diameter), p-nitrophenol and its derivatives, namely 4-nitroaniline, 2,4-dinitroaniline, and 2,5-dinitroaniline, sodium hydroxide (NaOH 1M), hydrochloric acid (HCl 0.1M), extra dry toluene, acetonitrile (ACN), ethanol, were obtained from Sigma-Aldrich. Fused silica capillaries with a UV-transparent external coating (100 μm I.D. x 325 μm O.D.) were purchased from InnovaQuartz (Phoenix, ZA, USA). The catalytic reactions were performed in ultrapure water from a Milli-Q system.

2.2 Instrumentation

Spectrolinker XL-1500 UV crosslinker (Spectronics, Westbury, NY, USA) equipped with six lamps (6x15 W) was used for the photopolymerization and the thiol-ene reactions at a wavelength of 365 nm. An HPLC pump (Dionex Ultimate 300, RSLC nano System) was used to flush monolithic columns with allyllamine, cysteamine, HAuCl_4 solutions and AuNP colloids. Raman measurements were used to analyse the monoliths chemical structures using an Xplora spectrometer (HoribaJobin Yvon) equipped with a laser emitting at 638 nm. .. UV-visible absorption spectra of the nitroaromatic compounds were recorded at room temperature on a Cary 60 UV-vis spectrophotometer (Agilent). A MERLIN scanning electron microscope (Carl Zeiss) integrated with an energy-dispersive X-ray spectrometer (EDX) was used to characterize the surface morphology and chemical composition of the monolith and its gold hybrids. The monolithic columns were cut into 1 cm length and sputtered with palladium or chromium prior to the SEM analysis in order to avoid subsequent charging.

2.3 Experimental methods details

2.3.1 Preparation internal surface of capillaries

To ensure good adhesion between the monolith and the inner wall of the fused silica capillaries, grafting of polymerizable silane coupling agent was performed prior to the *in situ* polymerization step. The capillaries were first washed with 1.0 M NaOH for 1 hour at room temperature and then heated under nitrogen flow at 100 °C for 2 hours. Then the capillaries were rinsed by flushing successively with 0.1M HCl, ultrapure water and acetone, each for 15 minutes at room temperature, and subsequently heated under nitrogen flow at 120°C for 2 hours. After the inner silanol groups activation, the capillaries were filled with a solution of 3-(trimethoxysilyl)propyl methacrylate in toluene (30%, v/v) for 1 night, followed by washing with toluene under nitrogen for 15 min. The monolithic materials were sealed with rubber septa and then stored at 4°C until polymerization.

2.3.2 *In situ* synthesis of generic monolith

The monolithic columns were prepared by *in situ* photopolymerization at 365 nm for 800 s of a homogeneous solution composed of N-acryloxysuccinimide (NAS), ethylene glycol dimethacrylate (EDMA) porogen (toluene and/or dodecanol), 2,2'-Azobis(2-methylpropionitrile) (AIBN, 1 wt-% with respect to monomers) confined inside the septa rubber sealed capillaries. The as-obtained monolithic columns were subsequently rinsed with ACN with a flow rate of 2 μ L/min for 1 hour to remove the residual reagents and the pore generator solvent.

2.3.3 Chemical functionalization of the generic monoliths

A two-step functionalization protocol was followed for the introduction of chelant free amine groups on the porous poly (NAS-co-EDMA) monolith. Firstly, a 1 M allylamine solution in ACN was flushed in the capillaries at flow rate=1mL/min for 2 h. The monolithic columns were then washed with ACN during 1 h in order to remove unreacted allylamine. Afterwards, the allyl-functionalized monoliths were post-functionalized via thiol-ene addition reaction by flushing with a solution containing 200 mg of cysteamine hydrochloride and 2mg of DMPA in 2 mL of ethanol and irradiated at 365 nm under continuous flow for 2 h. The amine-functionalized monoliths were rinsed with absolute ethanol for 1 hour.

2.3.4 Preparation of nanogold@amine-functionalized poly (NAS-co-EDMA) hybrids via *ex situ* and *in situ* methods

To prepare nanogold@amine-functionalized monoliths, two synthetic routes were performed, the *ex situ* and the *in situ* one. It's noteworthy that prior to the gold immobilization in both *ex situ* and *in situ* routes, the monolithic columns were washed with 0.1 M HCl solution for 15 min in order to protonate the grafted amine sites and thus generate ammonium groups. This would favor their interfacial electrostatic interactions with the citrate or borohydride stabilized gold nanoparticles. The pore channel of the monolithic columns were considered fully filled with the gold nanoparticles when its color change from white to dark purple or even black. In the case of the *ex situ* immobilization, the capillaries were flushed with commercial gold colloidal suspensions of 20 and 60 nm diameter. While, the *in situ* gold synthesis was carried out in two-step process. The first step consisted on adsorption of Au^{3+} by flushing the monolithic column with 0.1 M HAuCl_4 for 1h followed by washing with water for 30 min. The second one was the *in situ* reduction of the chelated chlorate ions to gold nanoparticles with a solution of NaBH_4 0.1 M at room temperature. The capillaries were then washed with water for 30 min.

2.3.5 Preparation of nanopalladium@amine-functionalized poly (NAS-co-EDMA) hybrids via *ex situ* method

To prepare nanopalladium@amine-functionalized monolith, the *ex situ* route was performed. The monolithic column were washed with 0.1 M HCl solution for 15 min in order to protonate the grafted amine sites. First, we by flushed the monolithic column with 0.1 M PdCl_2 for 1h followed by washing with water for 30 min. The second one step was to reduce Pd^{2+} to palladium nanoparticles with a solution of NaBH_4 0.1 M at room temperature. The capillary column was washed with water for 30 min.

2.4 Application of gold decorated-monolithic microreactors to flow catalysis

Exploring the scope of the nanogold@amine-functionalized monolith hybrids as catalytic microreactors, both reduction and oxidation catalytic reactions were tested. To do this, reduction of nitroromatics to their corresponding amines and oxidation of alcohol to its carboxylic acid were chosen as model reactions. All the catalytic experiments were carried out under continuous flow using monolithic columns of 7 cm length (if not otherwise mentioned). It is worth to mention that 4-nitrophenol was selected to optimize the catalytic experimental

conditions. Continuous-flow catalytic reduction of mono- and disubstituted nitroaromatics using AuNP@Amine-functionalized monoliths

2.4.1 Hydride mediated reduction of mono- and dinitroarenes

The catalytic reduction tests of the nitroaromatic toxic compounds through the monolithic columns were carried out at room temperature in presence of an excess of NaBH₄. Typically, a solution composed of 0.5 mL of nitroaromatic (4 mM), 0.5 mL of NaBH₄ (0.3 M) freshly prepared and 3 mL of water was flushed in the capillaries and the collected solutions at the outlet of the microreactors were monitored using UV-vis spectrophotometer in the range of 200-800 nm. To highlight the catalytic activity of the supported gold nanoparticles, similar experiments were conducted with the “blank” monolith, i.e. nanogold-free monolithic microreactor.

2.4.2 Hydrogen peroxide-assisted oxidation of benzyl alcohol

The catalytic oxidation of benzyl alcohol to benzoic acid or benzaldehyde was assisted oxidant agent hydrogen peroxide. To do so we prepared a solution of benzyl alcohol (16.7mg), potassium carbonate (90.5mg), hydrogen peroxide (30% weight, 750μL). All compounds were mixed and stirred in water (8.5mL). This solution was passed through the gold nanoparticles filled monolith using nitrogen gas at room temperature and 100°C using oven chromatographic. The product of the reaction was recovered at the end of the column and it was analyzed by gas chromatography.

2.4.3 Catalytic coupling Suzuki

To catalyze this reaction, palladium nanoparticles were used. Solutions of bromobenzene (1.49 g/L), phenylboronic acid (1.51 g/L) and potassium carbonate (3 g/L) were prepared in absolute ethanol. This solution was passed through monolithic capillaries containing palladium nanoparticles at temperature 80 °C. The reaction product was recovered at the end of the capillary and extracted with dichloromethane and water. The yields of the reaction were evaluated using gas phase chromatography.

3. Results and discussion

3.1 Monolith synthesis and surface grafting

The first step in preparing metal nanoparticles@monolith-based micro-reactors is the chemical modification of the inner wall of the microchannel to ensure the robust anchorage of the monolithic skeleton. 3-(trimethoxysilyl) propyl methacrylate was selected as a coupling agent as it allows, on the one hand, the formation of siloxane bond with the fused-silica capillary wall and permits, on the other hand, anchoring of the polymeric monolith. Indeed, trimethoxysilanes react quickly with silanol groups present on the surface of acid activated fused silica while the as-grafted methacrylate units may contribute to propagation steps in the course of the polymerization process providing the wall surface-attachment of the monolith.

Table 1: Composition of the polymerization mixtures applied to the preparation of monolith by photo-induced polymerization. The monomer ratio (NAS/EDMA) was kept constant at 63.5/36.5 (% , w/w) in all cases. Toluene or dodecanol was used as macroporogen either as unique porogenic agent or in combination with polar solvent, namely, DMF or DMSO.

Monolith	Macroporogen	Microporogen (wt-%)	Monomers/Porogen (%, w/w)	Homogeneity ^a	Permeability ^b (m ₂)
M1	Dodecanol	–	30/70	-	-
M2	Toluene	–	30/70	-	-
M3	Dodecanol	–	34/66	+	-
M4	Toluene	–	34/66	+	3.04×10 ⁻¹³
M5	Toluene	DMSO (15)	34/66	+	1.01×10 ⁻¹⁴
M6	Toluene	DMF (15)	30/70	+	6.32×10 ⁻¹⁵
M7	Toluene	DMSO (25)	34/66	-	-
M8	Toluene	DMF (25)	30/70	-	-

^{a)} The homogeneity of the capillary filling was evaluated by optical microscopy.

^{b)} The permeability was measured using monolithic column with 35 cm length.

To synthesize the monolithic skeleton, N-acryloxysuccinimide (NAS), ethylene glycol dimethacrylate (EDMA), toluene or dodecanol with eventually dimethylformamide or dimethylsulfoxide, and 2,2'-Azobis(2-methylpropionitrile) (AIBN) were initially mixed in dark conditions and degassed through nitrogen purging (20 min) at room temperature. Then the homogeneous reactive mixture was introduced at a controlled rate in the methacrylate-wall functionalized UV-transparent capillary. The polymerization was initiated under UV irradiation at 365 nm. Schematic representation of the synthesis path applied to prepare

monolithic microreactors is shown in Fig. 1 and compositions of the polymerization mixtures used for the preparation of polymer monoliths are shown in table 1.

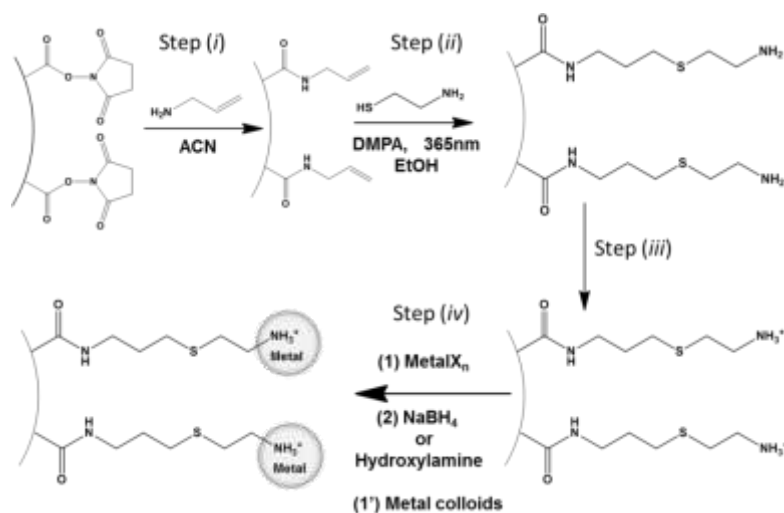


Figure 1: Schematic representation of the synthesis path applied to the preparation monolithic microreactors based on organic polymer skeleton surface-decorated with metal nanoparticles. Metal nanoparticles chelating are introduced on the monolith surface via photodriven thiol-ene click chemistry. The immobilization of metal nanoparticles is achieved either via on site reduction of metal salt precursors (step 1 and 2) or adsorption of colloid (step 1').

By comparing the back pressure measured during the rinsing step in the range 1-4 $\mu\text{l}/\text{min}$, we assumed that addition of polar solvent, namely dimethylformamide or dimethyl sulfoxide, provided less permeable polymeric monoliths. This was fully confirmed by qualitative SEM observations and quantitative mercury intrusion porosimetry measurements. The averaged pore size decreased from 2.2 μm for the monolith prepared with toluene as porogen, to 0.89 μm and 0.43 μm for the ones prepared with binary porogen containing 15% of DMSO and DMF, respectively. Consequently, a more compact monolithic structure was observed for M5 and M6 as illustrated in Fig 2a for the former case. Porous structure made of, in-between skeleton-forming globuli, channel-like pores is clearly observed for M4 (Fig 2b). As exemplified in the magnified SEM image (Fig 2c), the structure is made of fused-together microspheres with uniform size distribution and macropores with averaged size of 2 μm corroborating the 2.2 μm value determined by mercury intrusion porosimetry measurements. Furthermore, M4 fills homogeneously the whole capillary section and no defects could be observed for the different analyzed samples. The non-successful preparation of homogeneous and permeable monoliths using dodecanol as macroporogen was assumed to arise from the low solubility of the reactive mixture in dodecanol that required long mixing time and soft heating to provide homogeneous mixture.

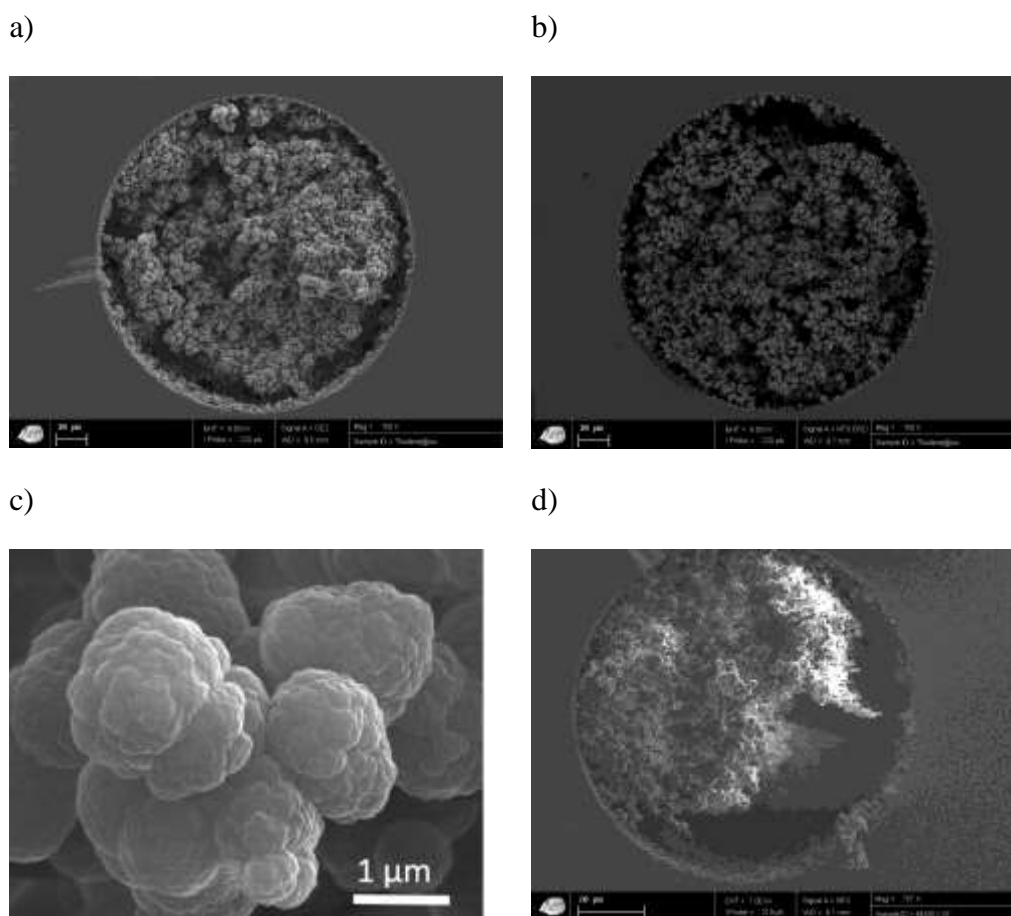


Figure 2: Scanning electron microscopy images showing the morphology of a) M5, b) and c) M4 and d) M8.

It is also seen that a dense polymer layer is formed at the interface with the fused silica capillary (Fig 2b). Such a feature confirms the effective participation of the surface-grafted methacrylate units in the free radical polymerization of the monolith precursors. This provides tight anchoring of the monolith to the inner surface of the capillary ensuring the stability of the monolithic support, which is a prerequisite to flow chemistry applications and to design reusable monolith-based materials. The decrease in pore size and structure densification upon addition of polar porogen result from porogen-triggered phase separation and is consistent with previous studies on preparation of polar ethylene glycol dimethacrylate-based monoliths using binary porogen mixtures including dimethylsulfoxide and water.³⁷ It was also noticed that for porogen content larger than 65 wt-% (with respect to the monomer and crosslinker amount), independently of the nature of the porogen, the section of the channel was not completely filled along the capillary column. As illustrated in Figure 2d showing a SEM micrograph of the monolith prepared from the reactive mixture 8, voids with size well over the average pore size are observed. Such filling characteristics will induce preferential paths

for fluids travelling through the column which are highly detrimental to the efficiency of any flow-through processes. Permeability values were calculated from the linear dependence of the drop pressure (in the range 10 – 140 bars) vs. flow rate (in the range 1-12 $\mu\text{L}/\text{min}$). Flow rates were converted into linear flow velocities and water was used as fluid because the main envisioned application will be performed with aqueous solution of sodium borohydride. The monolith M4 exhibited a permeability value of $3.04 \times 10^{-13} \text{ m}^2$ that is up to two orders of magnitude larger as compared to the values determined for monoliths M5 and M6 (Table 1). These pressure permeability tests ascertained both mechanical stability of the monolithic skeletons and robustness of the on-wall anchoring. Based on these characterization results after step 1 of the entire synthesis, we selected monolith M4 having the largest permeability and corresponding pore size for the design of the metal nanoparticles-decorated monolithic microreactors. Indeed, monolithic materials exhibiting a continuous interconnected network of pores with size above 1 μm are well-suited for surface functionalization with particulate objects and further flow chemistry applications where permeability plays a crucial role. It is assumed that large pores will facilitate the direct loading of colloidal nanogold preventing clogging effect. Hence the deliberate choice to apply M4 porous structure as a promising heterogeneous catalyst in continuous flow micro-reactor even at moderate pressures.

N-hydroxysuccinimide (NHS) groups are known to react readily and irreversibly with nucleophilic groups such as NH_2 , or SH . In the present study, the reaction of allylamine with the polymer surface bearing NHS moieties yielded monolith with alkene-functionalized pore surface, or M4-C=C (step (i) in figure 1). Success of the reaction was established on the basis of a comparative analysis of the Raman signatures of pristine and alkene monoliths (Figure 3). Raman spectrum of M4 reveals the presence of two absorption bands at 1725 and 1780 cm^{-1} which correspond to the characteristic absorption of imide asymmetric and symmetric stretching vibration bands, respectively. It is worthy to note that the 1725 cm^{-1} broad peak contains additional contribution from the stretching vibrations of the carbonyl arising from EDMA crosslinker. In addition, the native monolith M4 shows a peak at 1810 cm^{-1} , which is attributed to the stretching vibrations of NHS esters group.

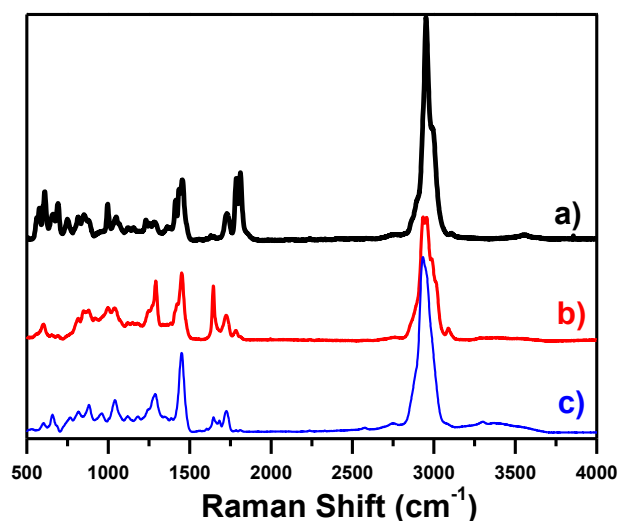


Figure 3: Raman spectra recorded *in situ* for monolith M4 with (a) pristine surface and surface grafted (b) alkene groups and (c) primary amine units via nucleophilic substitution and photo thiol-ene click chemistry, respectively.

In contrast, plot b in Fig. 3 shows the significant decrease in the imide absorption bands intensity confirming the conversion of the N-hydroxysuccimide groups as well as the appearance of a new strong band at 1646 cm^{-1} . The latter can be assigned to the formation of both amide group and C=C double bands as a result of the nucleophilic reaction between the activated ester on the monolith surface and the free amine functions arising from allylamine. Allyl-modified monolith spectrum revealed also additional bands at 2957 , 3017 and 3089 cm^{-1} corresponding to the vibration modes of sp^2 C-H stretching of alkene groups. The generated carbon-carbon double bonds were reacted with the cysteamine's thiol groups *via* thiol-ene photo click reaction (step (ii) in Figure 1). A thiol-ene radical addition reaction was selected because, being a part of the so-called click chemistry, it proceeds to high yields and is not accompanied with side reactions. Moreover, the thiol-mediated radical addition reaction does not require the use of toxic transition-metal catalysts and can be phototriggered. This latter feature is of particular interest because photochemical reactions generally provide faster reaction rates as compared to their thermal counterparts, are well-suited to achieve monolith synthesis or surface chemical functionalization within a confined space such as a microchannel. By using masks, the reaction can be restricted to the UV-exposed regions so that the microchannel can be photolithographically patterned, while reactants from the unexposed regions are simply washed out after the irradiation step. In the present study, we used 2,2-dimethoxy-2-phenylacetophenone as radical initiator, the decomposition of which is readily affected *via* UV light irradiation at a wavelength of 365 nm. Here again, *in situ* Raman

micro-spectroscopy brought evidence for the occurrence of the radical addition. Typical Raman spectrum of the monolith grafted cysteamine is shown in plot c in Fig. 3. The intensity of the peak at 1646 cm^{-1} decreased remarkably due to the addition of the thiyl radicals to the alkene groups. It should be mentioned that the remaining weak intensity peak should not be considered as an evidence for limited reaction yield as it is also assigned to the amide groups derived from the grafting of allylamine as described above. In addition, apparition of broad bands centered at 3250 cm^{-1} and 760 cm^{-1} corresponding to amine and thioether functionalities, respectively, provides the evidence for the successful thiol-ene radical addition reaction.

3.2 Surface deposition of nanogold on amino-functionalized monolith via deposition of gold colloids

Prior to flowing colloidal solution of gold with size 5nm, 20 nm and 60 nm, the surface-grafted amine groups were protonated by flushing HCl (0.1 M) during 30 min at a flow rate of $2\text{ }\mu\text{L}/\text{min}$. Indeed, electrostatic interactions between the positively charged monolith surface and the negatively charged citrate-stabilized gold colloids are assumed to act as the driving force for the robust surface immobilization of the metal nanoparticles providing further potentiality as microreactors for continuous flow heterogeneous catalysis.

Observing the progression of the gold nanoparticle elution front, as indicated by the purplish coloration of the in-microchannel monolith upon adsorption of gold nanoparticles, provided initial insight into the effect of the gold nanoparticles size on their adsorption onto protonated amine surface-functionality. Indeed, rather similar adsorption behavior was visually observed for the gold nanoparticles with size 20 and 60 nm, for which the 7 cm section of the monolith appeared purple after a loading time of 6 h. In contrast, the adsorption rate for the 5 nm sized gold nanoparticles was much slower, and only a 3 cm long section of the protonated amine-functionalized monolith appeared light purple for the same loading time. For the larger nanoparticles (20 and 60 nm) the progression speed of the coloration front was decreased as it was moving toward the outlet of the microchannel. Such an effect suggests strong interfacial interactions between protonated primary amines and carboxylated gold nanoparticles. *In situ* Raman spectroscopy analysis did not provide clear evidence of the interaction between the protonated amines and carboxylated gold nanoparticles mainly because of the broadness of the NH_2 band centered at 3250 cm^{-1} . Dynamic loading was continued over night until the

entire column length turned black, and a pink solution was observed to coming out from the capillary outlet.

SEM images in Figure 4 show the spatial distribution of the gold nanoparticles with size 20 and 60 nm on the monolith surface as either isolated nanoparticles (20 nm) or agglomerates (60 nm). Indeed, homogeneous and very dense coverage of the surface of the monolith's globuli was achieved in the former case providing monolith with gold-like surface. Such morphological features were previously reported for amino-functionalized polymeric monoliths and 20 nm-sized gold nanoparticles.^{27,28} Although tendency to agglomeration was observed in the latter case, individual nanoparticles can still be easily recognized in Fig 3c. From these results, it is expected that the morphology obtained for the hybrid M4 decorated with the 20 nm sized gold nanoparticles would favor its catalytic performances owing to enhanced accessibility of catalytic interactions sites with reactants.

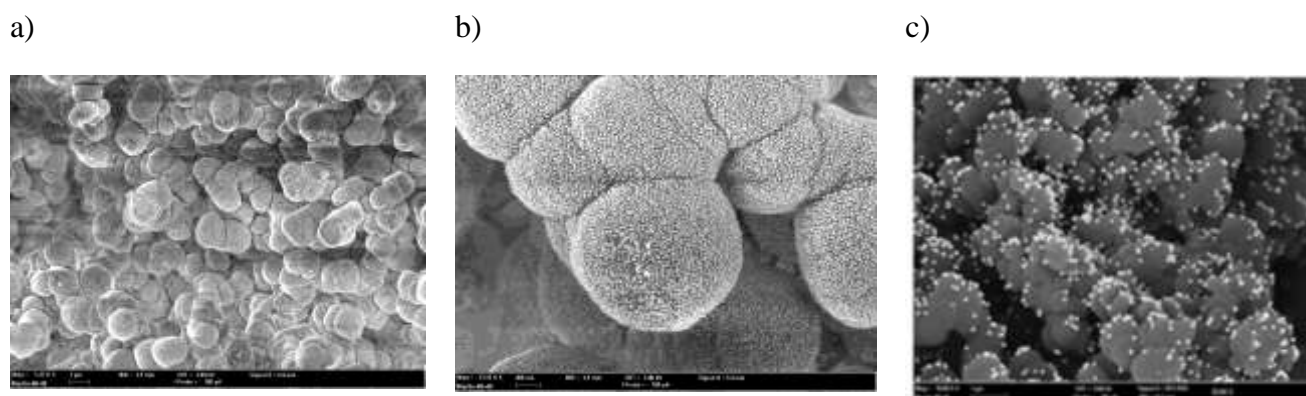


Figure 4: Scanning electron microscopy images recorded for gold-modified monolith M4 with gold colloids with size (a, b) 20 nm and (c) 60 nm.

Subsequently, energy-dispersive X-ray microanalysis spectroscopy revealed the presence of an intense peak centered at 2.1 KeV characteristic of nanocrystalline gold suggesting that the gold deposition occurred in quantitative amount in both monoliths loaded with 20 and 60 nm. The gold content was estimated to lie in the range 28-36 wt-%. It should be briefly mentioned that because of the aggregated morphology, the gold content was found to vary significantly in the case of monolith M4 60 nm depending on the measurement location on the sample. An example of EDX profile is given in figure 5 for the monolith M4 20 nm.

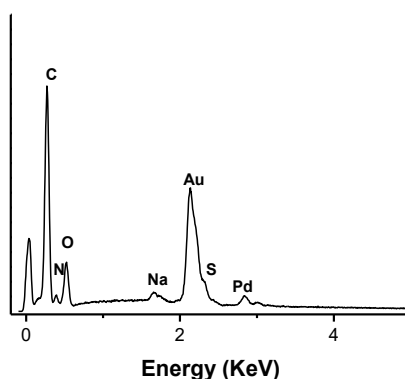


Figure 5: Energy dispersive X-ray analysis profile recorded for the nanogold-modified monolith prepared by adsorption of gold colloids with size 20 nm.

To evaluate the effect of the surface deposition of gold nanoparticles on permeability of the so-obtained hybrid monoliths, permeability of M4 60nm and M4 20nm was investigated (Fig 6). Independently of the gold nanoparticles' size, linear increase in the back pressure was obtained as the flow rate was increased, and the slope was much steeper as compared to the one observed for native M4, for which flow rate up to 12 $\mu\text{L}/\text{min}$ could be applied leading to a back pressure of 140 bars. Because of pressure limitation, the flow rate could not exceed 5 $\mu\text{L}/\text{min}$ for M4 20 nm and M4 60 nm as the back pressure reached values of 155 and 170 bars, respectively. For comparison purpose, the back pressure measured at 5 $\mu\text{L}/\text{min}$ for mono was as low as 50 bars that is at least three times lower than the value measured for the hybrid monoliths. This behavior is assigned to a clogging effect occurring mainly, if not exclusively, at the inlet of the monolith upon loading of gold nanoparticles. This effect is enhanced in the case of larger nanoparticles as shown in figure 6b for the M4 60 nm. It may be noticed that cutting the initial section of the gold nanoparticles-coated monolithic columns resulted, in some cases, in a decrease of the measured back pressure. Both M4 20 nm and M4 60 nm were applied as heterogeneous catalytic flow reactors and their activity was evaluated towards the hydride-mediated reduction of nitro-aromatics, using 4-nitrophenol as a model molecule. Indeed, despite the detrimental effect of the gold nanoparticles deposition on monoliths permeability, most of reported studies, if not all, dealing with the use of in-capillary (diameter = 100 μm) monolith materials decorated with metal nanoparticles for separation, capture or catalytic applications mentioned the use of flow rate lower than 2 $\mu\text{L}/\text{min}$.

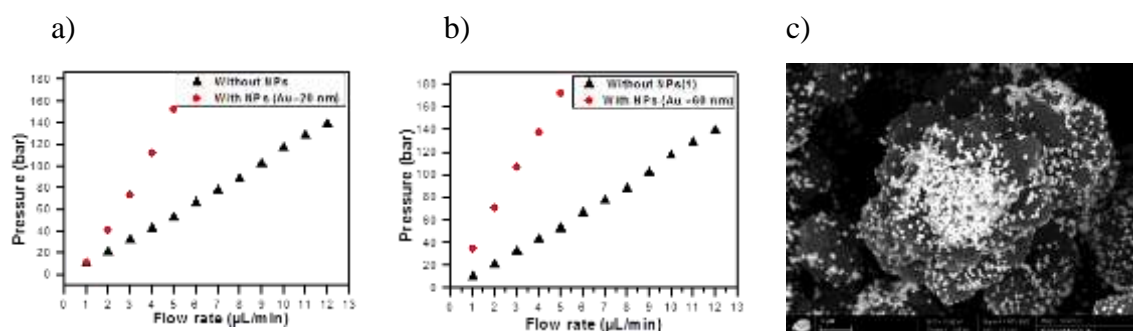


Figure 6: Dependences of the back pressure vs. flow rate measured for monoliths M4 decorated with gold nanoparticles (circle) with size a) 20 nm and b) 60 nm. For comparison purposes, the dependence is also shown for the monolith M4 with pristine surface (triangle). c) Scanning electron image recorded for monolith M4 decorated with gold nanoparticles with size 60 nm showing the formation of large aggregates inducing loss of the monolith permeability. Such aggregation effect was observed only at the inlet of the monolith.

3.3 Application of nanogold-modified monolithic microreactor prepared by gold colloids adsorption to the flow hydride-assisted reduction of nitroarenes

Aqueous solution of 4-nitrophenol appears light yellow with a corresponding UV_{vis} absorption peak measured at 317 nm, while its color is changed to dark yellow in the presence of sodium borohydride. This shift of the absorption peak to 400 nm is indicative of the conversion of the phenol groups “OH” to “O” phenolate ions by alkaline sodium borohydride. The reduction of 4-nitrophenol was achieved at room temperature in the presence of NaBH_4 , and an initial flow rate of 5 $\mu\text{L}/\text{min}$ was selected in correspondence to the permeability of both M4-60 nm and M4-20 nm. To highlight the catalytic effect of the immobilized gold nanoparticles, a blank test was performed using the gold-free amine-functionalized monolithic column. The reactive solution was loaded in the 20 μL loop of an Ultimate HPLC system and was injected in the 7 cm long capillary filled with the amino monolith using water as fluid at a flow rate of 9, 7, 5 and 3 $\mu\text{L}/\text{min}$. The solutions were collected at the outlet of the monolithic reactor and were analyzed by UV-spectroscopy in the range from 200 to 550 cm^{-1} . As expected, a UV absorption band centered at 400 nm was obtained and the value of the maximum of absorption was independent on the flow rate. The measurement was repeated 10 times at a flow rate of 5 $\mu\text{L}/\text{min}$ using both the same reactive solution and freshly prepared ones, and the value of absorption maximum was found to vary by less than 4%. These UV signatures are typical for the 4-nitrophenol and confirm that in the absence of surface immobilized gold-based nano-metals, the nitro-unit remains unaffected by chemical reducing agents such as hydrides. The UV profiles were changed significantly upon flowing the reactive solution through gold-

decorated monolithic reactors. Indeed, the absorption band at 400 nm decreased significantly confirming the change in the chemical structure of 4-nitrophenol. The intensity decrease obtained with a flow rate of 5 $\mu\text{L}/\text{min}$ was more pronounced for the M4 20 nm as compared to M4 60 nm (Fig 7). Concomitantly to the disappearance of the band at 400nm, a new absorption peak, with weak intensity, showed up at a wavenumber of about 300 nm. These two effects, intensity decrease and increase at 400 and 300 nm, respectively, clearly indicate the conversion of 4-nitrophenol in the corresponding amine, namely 4-aminophenol. The more pronounced intensity decrease at 400 nm observed for M4 20 nm as compared to M4 60 nm, can be rationalized on the basis of the surface distribution of the respective nanoparticles as observed by SEM. Finely dispersed and densely distributed gold nanoparticles on monolith surface are expected to enhance roughness providing larger contact surface *i.e.* catalytic activity. Contact time in catalytic process is a key towards high reaction yield. Herein, we hypothesized that the contact time can be easily controlled trough changing the flow rate of fluid pushing the reactive mixture through the monolithic reactor. This was confirmed to a large extend for M4 20 nm as decreasing the flow rate from 5 $\mu\text{L}/\text{min}$ to 3 $\mu\text{L}/\text{min}$ led to a total disappearance of the absorption band at 400 nm, that is a total conversion of 4-nitrophenol. Although similar trend was observed for M4-60 nm, the reduction reaction was not total even at a reduced flow rate of 2 $\mu\text{L}/\text{min}$ (part b in Fig 7).

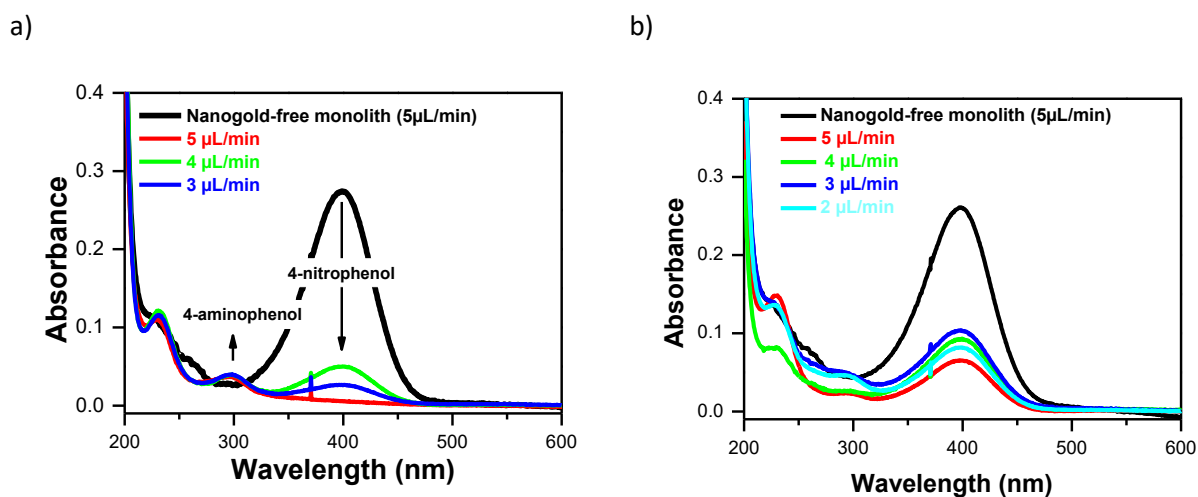


Figure 7: UV-Vis profiles recorded for the product solutions collected at the outlet of gold-modified monolithic microreactors prepared via the adsorption of gold colloids with size a) 20 nm and b) 60 nm. For comparison purpose and to fully highlight the catalytic effect of gold nanoparticles attached on the monolith surface the Uv-Vis plot recorded for a nanogold-free monolith is also shown. The flow rates are indicated in the figure.

3.4 Surface deposition of nanogold on amino-functionalized monolith via on site reduction of precursor gold salt and application to the catalytic reduction of nitroarenes.

With the aim to design high throughput catalytic micro-reactors with interesting nano-metal mediated catalytic properties, we envisioned a two-step approach for immobilizing gold nanoparticles on amino monoliths. This strategy implies first, the on-monolith's surface immobilization of gold metal precursor salt, HAuCl_4 , and second, the reduction of the surface adsorbed gold ion into metallic gold. For simplicity purpose, we used borohydride as reducing agent for gold. After loading aqueous solution of HAuCl_4 for 30 min at a flow rate of 2 $\mu\text{L}/\text{min}$, and thorough rinsing with water (15 min at 2 $\mu\text{L}/\text{min}$) the capillary appeared yellow indicating the effective chelation of gold ions on the amino surface. The capillary color turned dark purple after the reduction with aqueous solution of NaBH_4 suggesting the successful formation of Au^0 . This assumption was fully confirmed by SEM observations revealing the presence of well-dispersed and isolated nanoparticles with spherical shape (Figure 8) and separated by very regular inter-particle distance. The so-designed surface immobilized gold nanoparticles featured monomodal distribution with average size centered at 10 nm (part c in Fig 8).

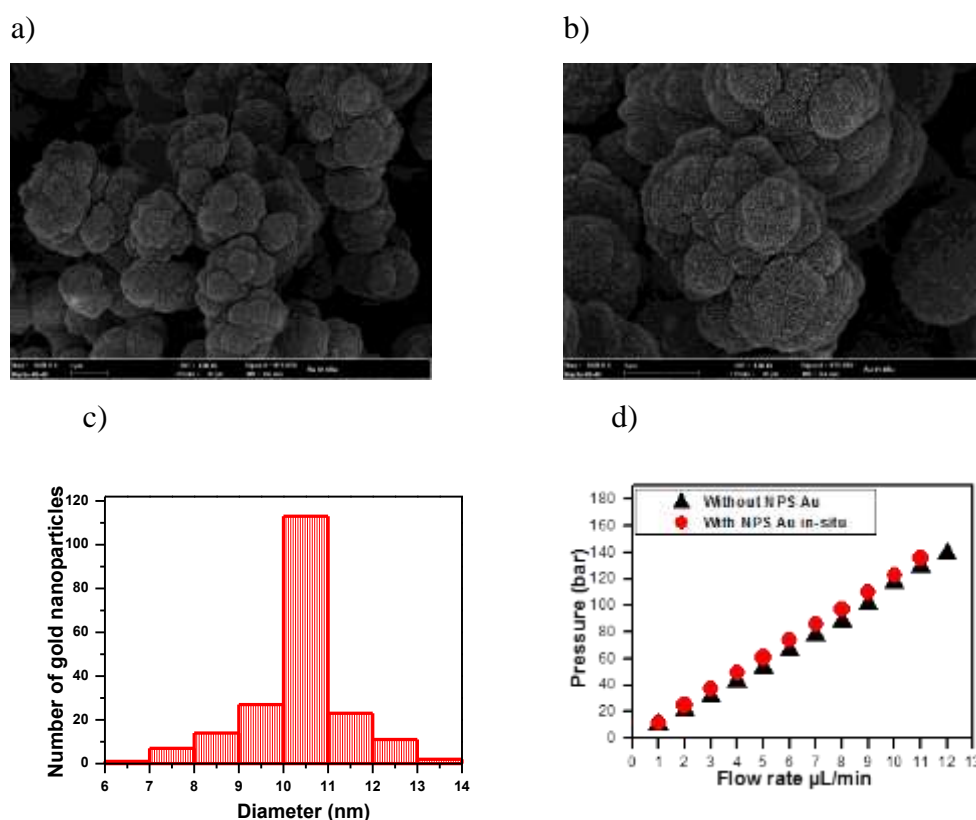


Figure 8: a) and b) Scanning electron microscopy images recorded for gold-modified monolith M4 prepared by on site reduction. c) Estimated size distribution of the gold nanoparticle on the monolith's surface. d) Dependence of the back pressure vs. flow rate measured for monolith M4 decorated with gold nanoparticles prepared by on site reduction (circle). For comparison purposes, the dependence is also shown for the monolith M4 with pristine surface (triangle).

The Au content was calculated in the range 38-43 %, depending on the analysis location (Fig 9).

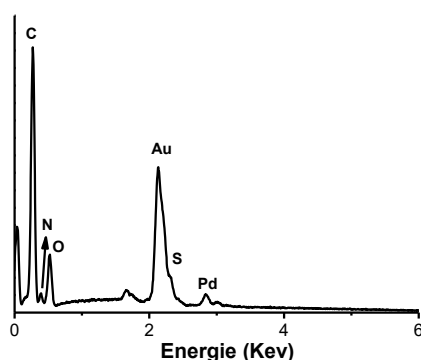


Figure 9: Energy dispersive X-ray analysis profile recorded for the nanogold-modified monolith prepared by on site reduction.

Another important characteristic/issue of the hybrid monolith prepared by the *in-situ* route is presented in Fig 8d. Indeed, it is seen that the back pressure increases linearly with the flow rate and, more importantly, the plot is superimposed to the one obtained for native monolith M4. This behavior evidences that the preparation of monolith bearing a dense layer of homogeneously distributed gold nanoparticles with well-defined shape and size can be successfully achieved without altering the permeability of the porous monolithic skeleton. As such, gold nanoparticles decorated monolith prepared *via* the *in-situ* reduction of surface concentrated Au^{3+} ions can be applied with high flow rate-up to 10 $\mu\text{L}/\text{min}$. By combining improved permeability and lower sized gold nanoparticles it is expected that catalytic reaction can be performed at higher flow rate. We thus also tested the catalytic activity of the monolith M4-*in situ* towards the reduction of 4-nitrophenol (Fig 10). The flow rate was initially set at 9 $\mu\text{L}/\text{min}$ providing a reaction yield of 86.4 %. Comparable reaction yield could be obtained with M4 20 nm using a half flow rate value as estimated from the plot in figure 7. In contrast, using monolith M4 60 nm the yields remained below 80%. Total conversion of 4-nitrophenol was achieved at the highest flow rate of 3 $\mu\text{L}/\text{min}$ with M4 *in situ*. For the three type of hybrid monoliths, the reaction yield increased linearly as the flow rate was decreased suggesting direct dependence on the reaction time (part b in Fig10). The beneficial effect of decreasing the flow rate evidences time-resolved character of the transformation of NO_2 into NH_2 as expected for flow process. All these results highlight the superiority of the *in situ* approach for preparing monolith-supported nanogold for the fast and efficient catalysis of hydride mediated reduction reaction.

To fully demonstrate the applicability of monolith@gold nanoparticles materials to the hydride-mediated catalysis of nitroarenes, we applied the micro-reactor M4-Au *in situ* to the reduction of other nitro derivatives bearing either one or two NO_2 group(s). 4-nitroaniline and 2,5-dinitrophenol were reduced quantitatively into para-phenylene diamine and 2,5-diaminophenol using a 7cm long micro-reactor and a flow rate of 3 $\mu\text{L}/\text{min}$ as attested by the total disappearance of their spectral signature in the solution collected after flowing through the micro-reactor (Fig 10c and 10d). It is worth to note that this concept based on the use of organic monolithic skeleton acting as solid support for metal gold nanoparticles has not yet been envisioned for the catalytic reduction of dinitroarenes. Indeed, previous report discussing the catalytic degradation of 2,4-dinitrophenol mentioned the use of hydroelectric plasma in the presence of TiO_2 as catalyst.³⁸

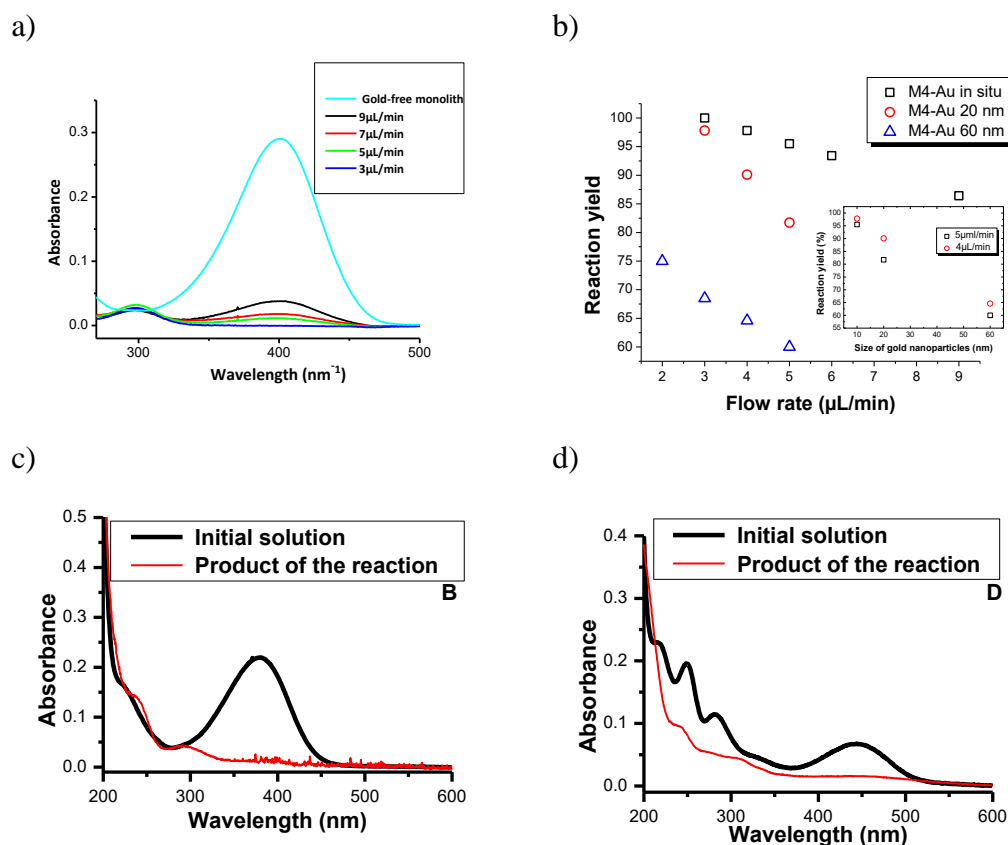


Fig 10: a) UV-Vis profiles recorded for the product solutions collected at the outlet of gold-modified monolithic microreactors prepared via on site reduction. b) Dependence of the reaction yield for the reduction of 4-nitrophenol vs flow rate for the monoliths M4 20 nm, M4 60 nm and M4 in situ. c) and d) UV-Vis profiles recorded for the product solutions collected at the outlet of gold-modified monolithic microreactors prepared via on site reduction for the reduction of 4-nitroaniline and 2,5-dinitrophenol, respectively.

Robust deposition of the nanocatalyst onto amine-containing monolith is crucial to long term application of the microreactor. Presence of gold nanoparticles in aqueous solutions can be easily evidenced as gold nanoparticles exhibit a distinct optical feature, referred to as localized surface plasmon resonance. The latter leads to a strong absorbance band in the visible region between 500 and 600 nm, which can be easily measured by UV-Vis spectroscopy. The product solution as collected at the outlet of the monolithic reactor after the catalytic reactions did not show such characteristic features as can be seen from figure 10c and 10d where the measured UV range was expanded up to 600 nm. This was further confirmed by inductively coupled plasma mass spectrometry.

3.5 Application of nanogold modified monolithic microreactor prepared by on site reduction to the catalytic oxidation of benzyl alcohol.

To enlarge the application range of gold-decorated monolithic microreactors prepared via on-site synthesis of the nanocatalyst, their use was extended to the opposite reaction of reduction, namely oxidation reaction. Herein, we considered the gold-catalyzed oxidation of benzylic alcohol using hydrogen peroxide as catalyst. The supported metal catalyst strategy has been well-described in the literature for the oxidation of benzyl alcohol and supports as diverse as ceria-zirconia mixed oxide,³⁹ graphene oxide,⁴⁰ carbon,⁴¹ nickel ion-modified hydrotalcite,⁴² mesoporous SBA-15,⁴³ carbon nanotubes,⁴⁴ alumina,⁴⁵ ... have been implemented. Numerous examples can also be found where the nature of the catalyst was different and one may cite copper and copper oxide,⁴³ gold,^{42,46}, palladium,^{41,47} bimetallic gold-palladium,^{39,48} nanoparticles. Although organic polymer supported catalysts have also been reported for the oxidation of benzyl alcohol,^{49,50} to the best of our knowledge, no report discussed the use of monolithic polymer applied under flow conditions. Al Badran et al. used newly designed pilot-scale continuous flow pharmaceutical fixed-bed catalytic reactor based on carbon for the partial oxidation of benzyl alcohol in benzaldehyde.⁵¹

The catalytic oxidation reaction was initially tested at room temperature and the progress of the reaction was evaluated by gas chromatography analysis. For the room temperature conditions, it was seen that no conversion occurred and that the benzyl alcohol remained unaffected, independently of the flow rate. Prior to testing the reaction at elevated temperature the thermal stability of the Poly (NAS-co-EDMA) prepared in bulk as evaluated by thermogravimetric analysis (Fig 11). It was found that as expected for highly crosslinked polymeric materials, the monolith skeleton remains nearly intact up to temperature of 100°C. Indeed weight losses of 0.4% and 1.1% were observed at 100°C and 200°C, respectively.

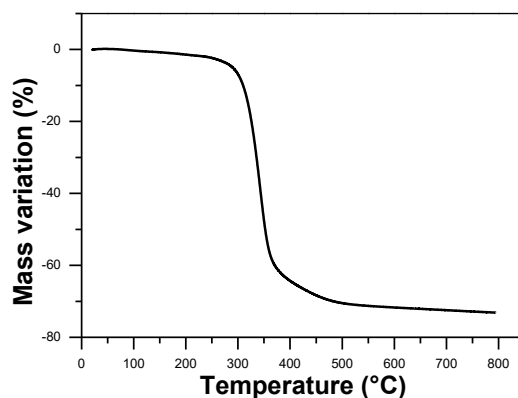


Figure 11: Thermogravimetric analysis of Poly(NAS-co-EDMA).

Based on these results, we opted for a maximum temperature of 100°C and we selected an intermediate temperature of 50°C for testing further the catalytic activity of M4 in situ towards oxidation reaction. The chromatogram obtained for these two conditions are shown in Fig 12. Clear effect of increasing the temperature can be noticed from these two chromatograms. Indeed, for the low temperature process we observed two peaks additionally to the ones characteristic of the solvent and the internal standard. The said peaks are detected at retention times of 5.49 min and 10.65 min corresponding to benzaldehyde and benzoic acid, respectively. The peak for the benzyl alcohol reactant is still seen. For the high temperature process, the situation is quite different. First, the peak of benzyl alcohol is not seen and only the product peak at 10.65 min is observed. Such chromatographic profile suggests that for a temperature of 100°C complete conversion of benzyl alcohol into benzoic acid is obtained. In contrast, in the case where the reaction was conducted at 50°C, both benzaldehyde and benzoic acid are obtained however the former is the major product of the reaction. These experimental observations suggest that the character of the oxidation, partial *versus* total, as performed under flow conditions using a microreactor filled with poly(NAS-co-EDMA) monolith surface-decorated with gold nanoparticles prepared directly onto the surface of the monolithic support via hydride-mediated reduction of the precursor gold salt can be controlled by changing the reaction temperature.

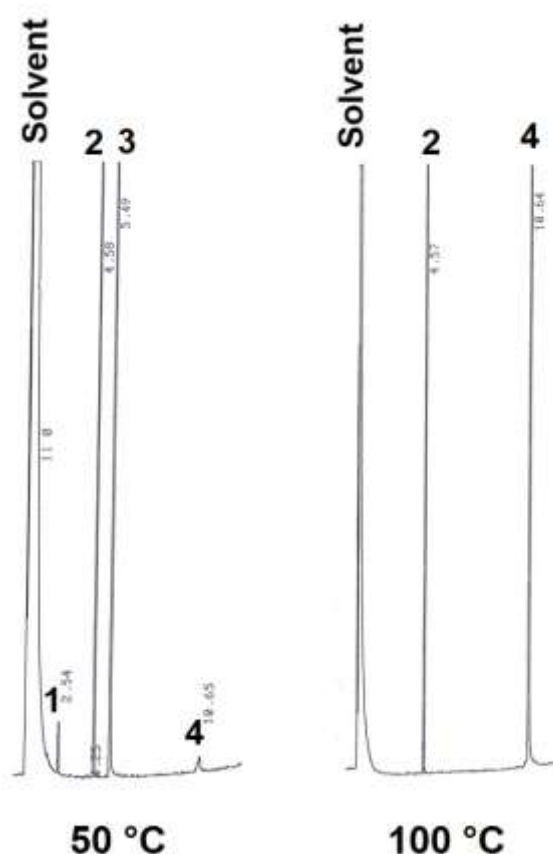


Figure 12: Chromatogram obtained for the product-solution as-collected at the outlet of the gold-decorated monolithic reactor M-4 in situ after the catalytic oxidation of benzyl alcohol. The reaction was performed at (left hand side) 50°C and (right hand side) 100°C. The peaks correspond to (1) benzyl alcohol, (2) dodecane, (3) benzaldehyde and (4) benzoic acid. Dodecane was used as internal standard. CPG conditions, column acid, H_e flow =1,5 mL/min, $T^{\circ}C=100^{\circ}C+10^{\circ}C/min$

3.6 Preparation of gold nanoflower-decorated monolith microreactor by on site reduction and application to flow catalytic reduction of pesticides

Catalytic activity of metal nanostructures is strongly related to the size, shape and assembly pattern, and thereby great efforts have been focused on their controlled synthesis with various morphologies.^{52,53} Highly branched Au flowers with sharp tips were synthesized as chemically stable substrate for surface-enhanced Raman scattering (SERS) allowing detection of 4-mercaptopyridine (4-MPy) down to 10^{-12} mol.dm⁻³.⁵⁴ In another implementation, highly branched gold nanodendrites with a narrow size and tuneable localized surface plasmon resonance signal from the visible (~530 nm) to the near-infrared region (~1100 nm) of the electromagnetic spectrum were synthesized using a multiamine as surfactant and further

evaluated towards the SERS of Rhodamine.⁵⁵ Besides the use of nanoflower, SERS-active substrates were also designed using gold nanorod-containing composites.⁵⁶ Gold nanoflowers⁵⁷ and nanorods⁵⁸ found also application in photothermal cancer therapy. Performance of gold nanocages-based composites were tested for the photoelectrochemical-assisted water oxidation,⁵⁹ trace level detection of nitro explosives,⁶⁰ Also in the field of catalysis, the possibility to finely tune the morphology of metal nanostructures has stimulated the imagination of scientists and gold nanoflowers have been implemented for the oxidation of alcohol,⁶¹ the reduction of nitroaromatics,^{62,63} Only few examples discussed the use of supported gold nanostructures with “exotic” morphology for catalysis application and to the best of our knowledge flow catalytic were not proposed. One may cite the study by Chao et al describing the effective synthesis of 3D palladium-gold nanoflower and the subsequent deposition of the resulting colloids onto magnesium-aluminium mixed metal oxide.⁶⁴ The as newly designed supported catalyst exhibited high activity, selectivity and stability in the catalytic partial hydrogenation of acetylene as compared to their counterparts with more traditional shape. Based on these statements, we intended to prepare gold nanoparticle with flower-like shape directly on the surface of amino-monolith prepared according to the protocol described here above. Briefly speaking, monolith M-4 was reacted successively with allylamine and cysteamine and then loaded with HAuCl_4 solution. After rinsing, the surface-immobilized gold salt was reduced into metallic gold using hydroxylamine as reducing agent. The SEM images in Fig 13 clearly indicate the success of the reduction process providing homogeneous dispersion of gold nanostructures on the monolithic material surface. High magnification images demonstrate undoubtedly the flower shape of the gold nanoparticle having tips with nanometric dimensions.

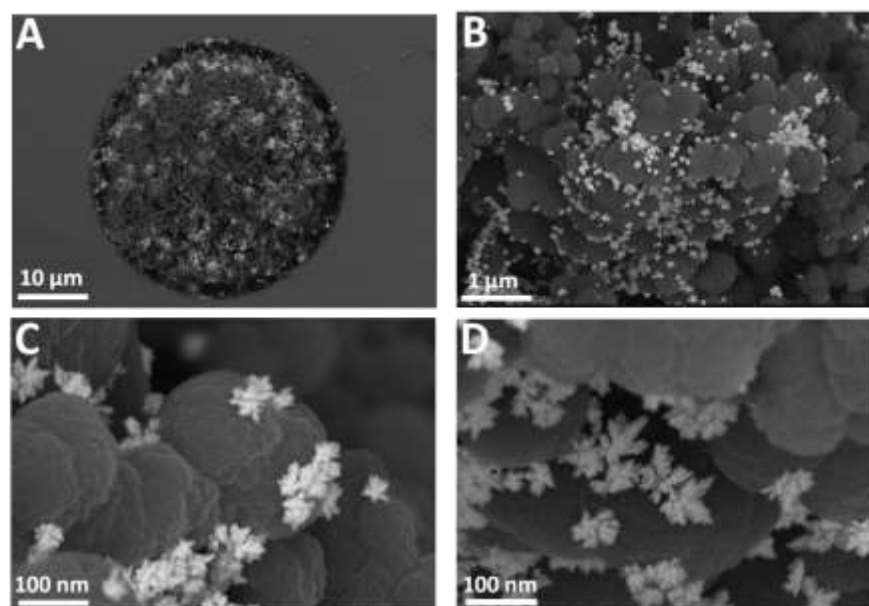


Figure 13: Scanning electron microscopy images recorded for monolith M4 decorated with gold nanoflower prepared by in situ hydroxylamine-mediated reduction of gold salt precursor. The images were recorded at different magnifications as indicated by the insets in the figure.

The Au⁰ nature of the structures seen in Fig 14 is further demonstrated by the EDX profile presented in Fig. Besides the signals assigned to the polymeric matrix, namely carbon, nitrogen and oxygen, the signal at about 2.1 eV is typical for metallic gold. The shoulder at the high energy side is assigned to the sulfur atom introduced in the course of the thiol-ene reaction.

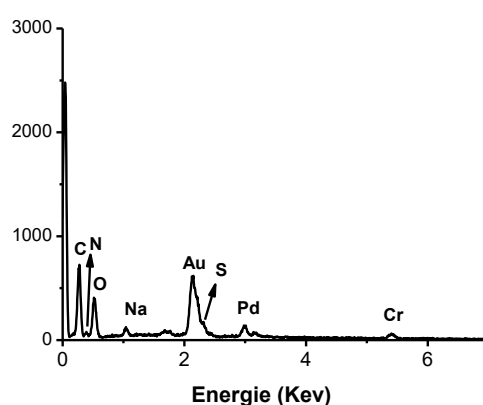


Figure 14: Energy dispersive X-ray analysis profile recorded for the gold nanoflower-modified monolith prepared by on site reduction.

The catalytic activity of the monolith M4 decorated with gold nanoflowers was evaluated towards the reduction of pesticides, namely pendimethalin and trifluralin (Fig 15). The reaction was performed in the presence of NaBH₄ as reducing agent in ACN. The reaction was conducting at a flow rate of 3 μL/min. The UV-vis plots in part 15a shows that no conversion occurs when the reactive mixture made of pendimethalin and hydride is passed through gold nanoflower-free monolith. In contrast, the presence of nanogold flowers induces a significant decrease of the major UV-vis absorbance peaks for the two pesticides. As such the for the conversion of pendimethalin was considered as quantitative with reaction yield above 98.5% while in the case of trifluralin the reaction yield was calculated to be equal to 86.5%. Further optimization of the reaction yield was possible upon decreasing the flow rate.

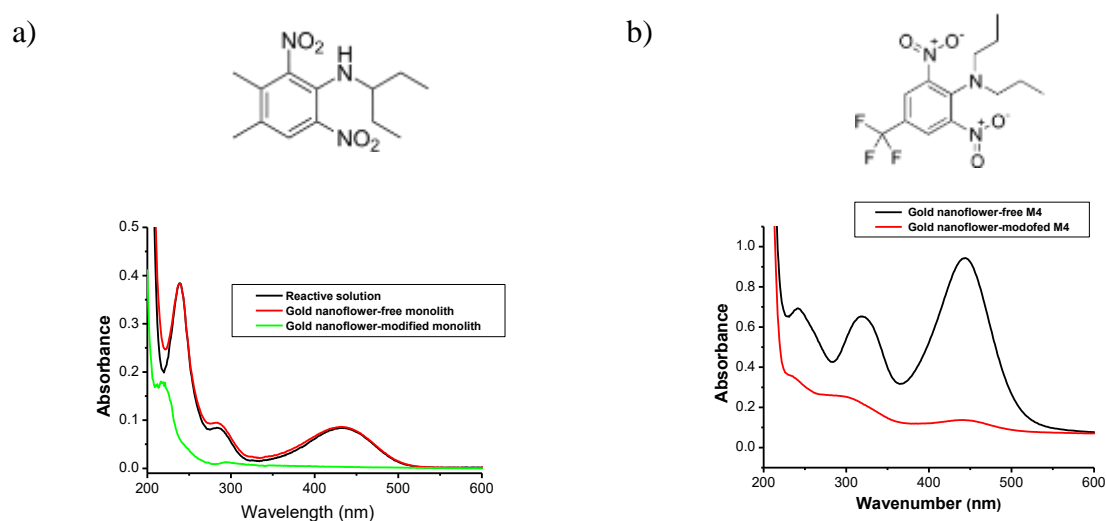


Figure 15: a) and b) UV-Vis profiles recorded for the product solutions collected at the outlet of gold nanoflower-modified monolithic microreactors prepared via on site reduction for the catalytic reduction of pesticides. The chemical structures of pesticides are also shown in a) and b).

3.7 Preparation of palladium-modified monolith microreactor by on site reduction and application to flow catalytic Suzuki-Miyaura carbon-carbon coupling reaction

After having successfully demonstrated the ability of amino-containing monolith prepared via the photo-initiated thiol-ene click grafting of cysteamine onto alkene-monolith, we have intended to explore the possibility to graft other types of noble metal nanoparticles. Palladium, platinum and silver were considered however we present herein only fragmentary results about palladium-modified regarding the widespread application of supported palladium nanoparticles to catalytic reactions. Palladium in the form of metallic nanoparticle has been supported on mesoporous polybenzimidazole for Suzuki cross-coupling reaction in

aqueous media,⁶⁵ highly porous carbon nanofibers for Heck Reaction,⁶⁶ silica for debromination of polybrominated diphenyl ethers.⁶⁷

Herein PdCl₂ was used as metal salt precursor and was immobilized on the amino-functionalized M-4 monolith following the same protocol as described for the case of gold salt. Then, monolith was flown with a reducing solution based on sodium borohydride. The SEM images on fig. 16 reveal the presence of nanostructures dispersed on the monolith surface whose metal nature was confirmed by EDX.

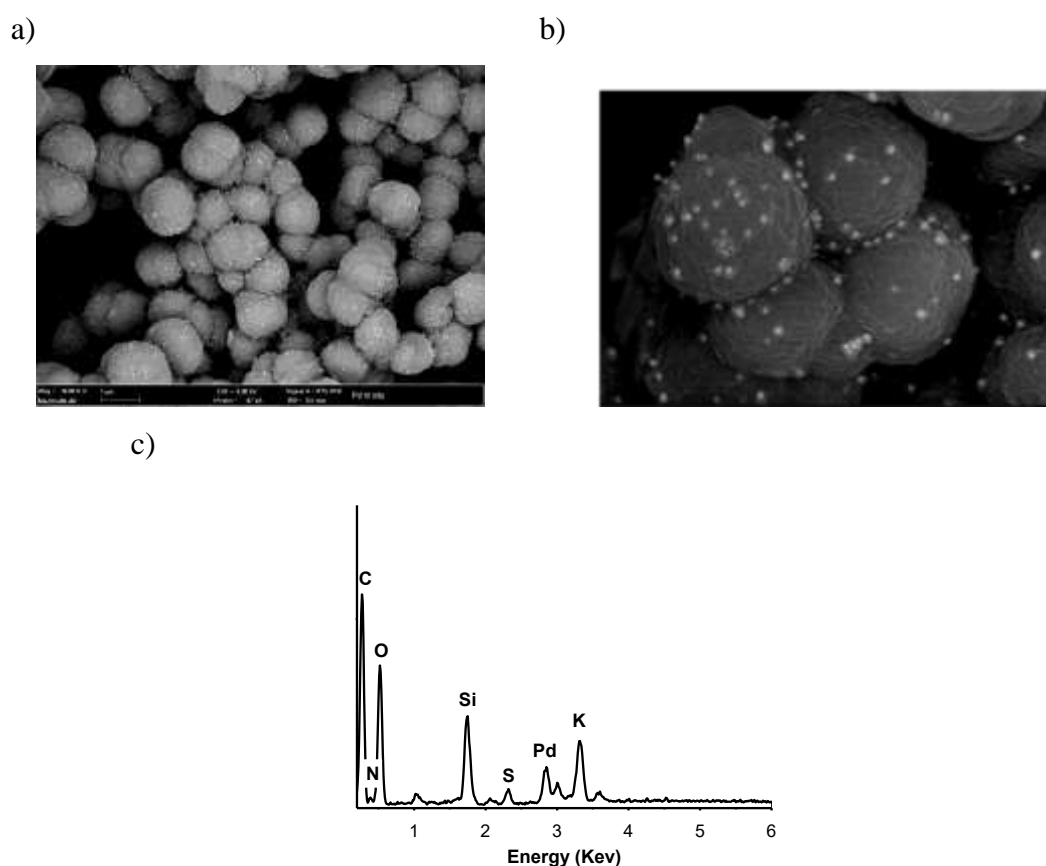


Figure 16: a) and b) Scanning electron microscopy images and c) energy dispersive X-ray analysis profile recorded for palladium-modified monolith microreactor by on site reduction and application

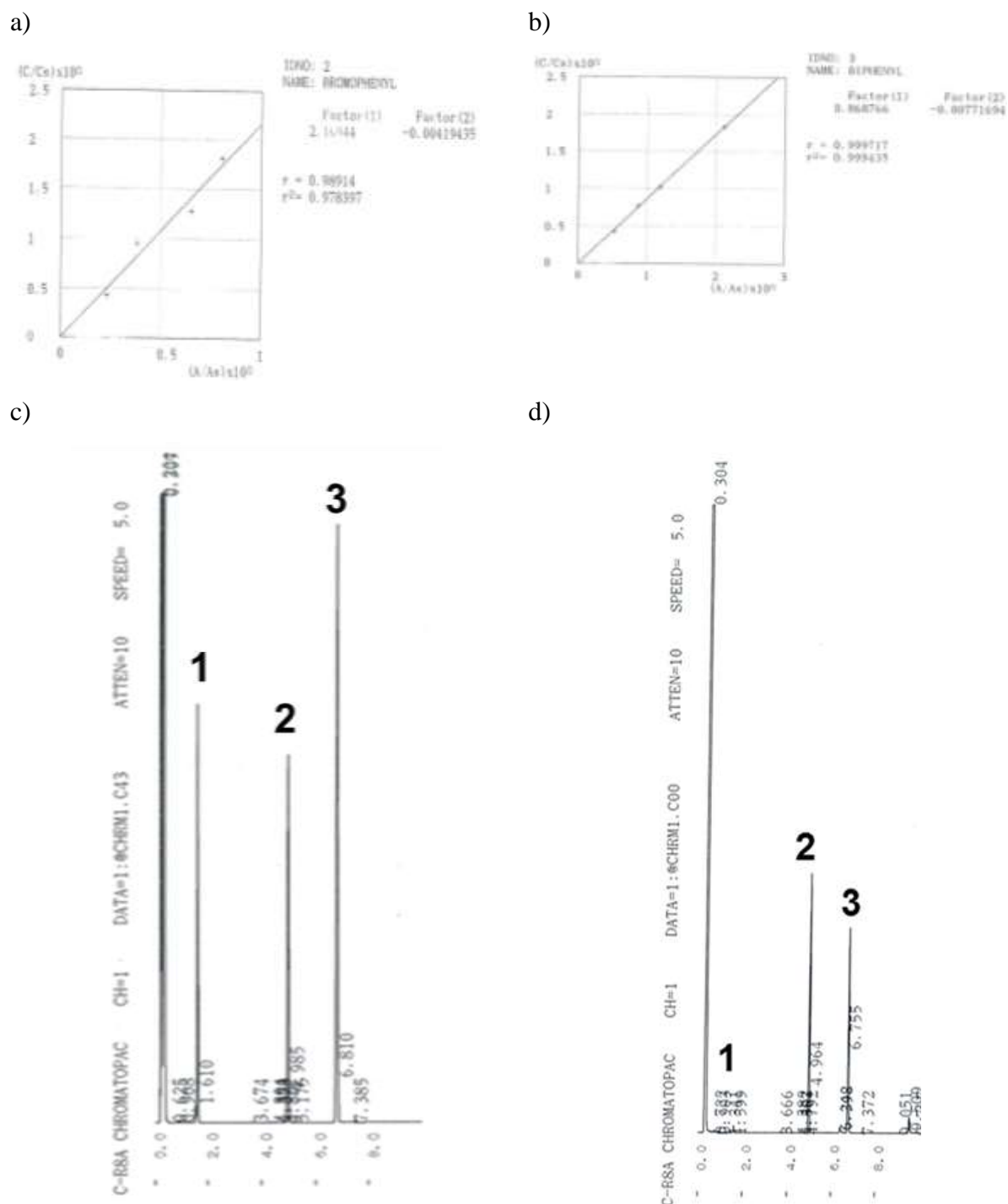


Figure 17: Calibration curve as-obtained for a) bromobenzene and b) biphenyl by gas chromatography analysis. C) Chromatogram showing an example of separation of bromobenzene, dodecanol and diphenyl. Chromatogram obtained for the product-solution as-collected at the outlet of the palladium-decorated monolithic reactor prepared by on site reduction after the catalytic coupling between bromobenzene and biphenyl at 80°C. The peaks correspond to (1) bromobenzene, (2) dodecane, (3) biphenyl. Dodecane was used as internal standard. CPG conditions, column acide, H_e flow = 1,5 mL/min, $T^\circ C = 100^\circ C + 10^\circ C/min \dots$

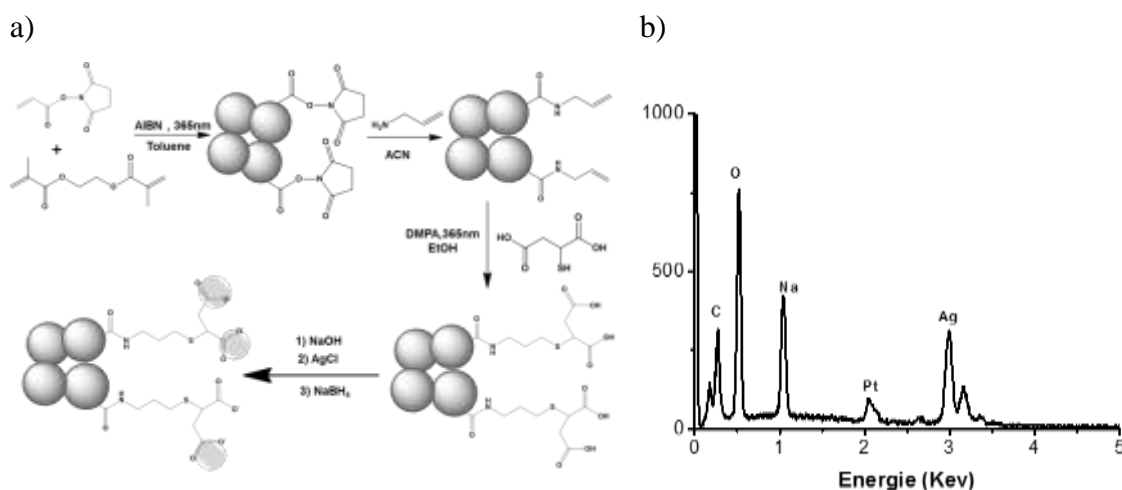
The palladium modified monolithic microreactor was used for the catalytic coupling reaction between phenyl boronic acid and bromobenzene. The reaction was performed under a pressure of 50 bars to allow for the reactive solution to flow over the catalytic support and a temperature of 80°C. The product solution was collected at the outlet of the microreactor and analysed by GC after appropriate sample treatment. The reaction yield was calculated based on the calibration curve determine for both bromobenzene and diphenyl using dodecane as internal standard. The chromatogram shown in Figure 17 shows that under these conditions, the bromobenzene (peak 1 in par c and d of the figure 17) is consumed to a large extent yielding the formation of diphenyl (peak 3 in parts c and d of the figure 17). We also proved that homocoupling did not occur under these conditions

From these results, we hypothesized that the Suzuky-Miyaura reaction was effective and a reaction yield above 95% was calculated.

5. Conclusions.

Permeable monoliths based on poly (N-acryloxysuccinimide-*co*-ethylene dimethacrylate) were prepared through the photo-initiated free radical polymerization of the respective monomers. Several parameters were investigated such as the nature and the content of porogens. The presence of nucleophile-sensitive N-hydroxysuccinimide allowed for the subsequent grafting of functional amines, namely allylamine, providing thiol-sensitive monolith. Indeed, reaction of thiols and alkene is known to proceed in high yield and selectivity upon radical addition mechanism, also referred to as thiol-ene click chemistry. Herein, a photo-triggered approach was selected to achieve such a reaction the using cysteamine as functional thiol and alkene-grafted monolith as reactive solid support. The amino groups were used as ligands to immobilize metal nanoparticles. We have in this contribution concentrated our efforts towards the immobilization of gold nanoparticles using either preformed and commercially available particles or gold salt precursors. The former proceed *via* simple adsorption of gold colloids upon dynamic conditions while the latter requires, after flowing a solution of H₂AuCl₄, a reducing step. It was shown that the morphology of the on-site prepared gold nanoparticles can be tuned from spherical to flower-like shape by changing the nature of the reducing agent. Interestingly also, is that the in situ approach does not affect the permeability of the monolithic providing nanostructure monolithic support compatible with high-throughput uses. Success of the synthesis and surface functionalization steps described here-above have been established on the basis characterization data collected by means of micro Raman spectroscopy, scanning electron microscopy and energy dispersive X-ray analysis. The catalytic hydride-mediated reduction of 4-nitrophenol into 4-amino-phenol was select as model reaction to compare the catalytic activity of gold nanospheres-modified monoliths. As expected, it was shown that decreasing the size of the nanoparticles enables enhancement of the catalytic support. Other parameters such as gold content, and nanoparticles aggregation are also key factors. The monolithic microreactor prepared *via* in situ reduction proved to provide the highest catalytic activity and was further applied to the firstly described reduction of dinitroarenes under flow conditions. Although the use of catalyst enables increases the rate of reaction through decreasing considerably the corresponding activation energy, some catalyzed reaction still do not proceed at room temperature. As such, we have shown that the monolithic support used herein, owing most probably to its highly crosslinked nature, is not only mechanically stable up to pressures of 120 bars, but also thermally stable up to the temperature range 100-120°C. This latter

positive feature motivated to test the application of monolithic microreactor with in situ prepared gold nanospheres to catalytic process conducted at moderately high temperature. The catalytic oxidation of benzyl alcohol was evaluated using hydrogen peroxide as oxidant as the function of the temperature. One of the major result of this study is that controlling the temperature enables to adjust the oxydation of the reaction product. In other words, low and high temperature processes yielded benzaldehyde and benzoic acid as major reaction product. Finally, and to fully demonstrate that this work can pave the way to new nanostructured monolithic materials we have presented some preliminary results on the preparation palladium-modified monolith and their catalytic activity towards the preparation of biphenyl via the well-known Suzuki-Miyaura carbon-carbon coupling reaction. At last but not least, we would like here to consolidate our choice to implement photo-initiated thiol-ene click chemistry. Indeed although full demonstration of the key character of such an approach was not demonstrated here, we would like to mention the possibility offered by photoclick. First, by using photomasks the chemical grafting can be limited to the irradiated zone, so that patterned distribution of the gold nanoparticles on the monolith surface is possible. This can be advantageously used to prepare at the inlet of the microreactor a gold-modified monolithic section while letting the following section gold free. As such, two steps can be included within unique microreactor, the first meant for the catalytic reduction of nitrophenol and the second one meant for the separation of the reaction products. As such, online monitoring of the catalytic process is feasible. Secondly, the thiol-ene reaction can be easily applied to a plethora of thiol molecule bearing end-functionalities with specific chelation ability towards other types on nanaoparticles.



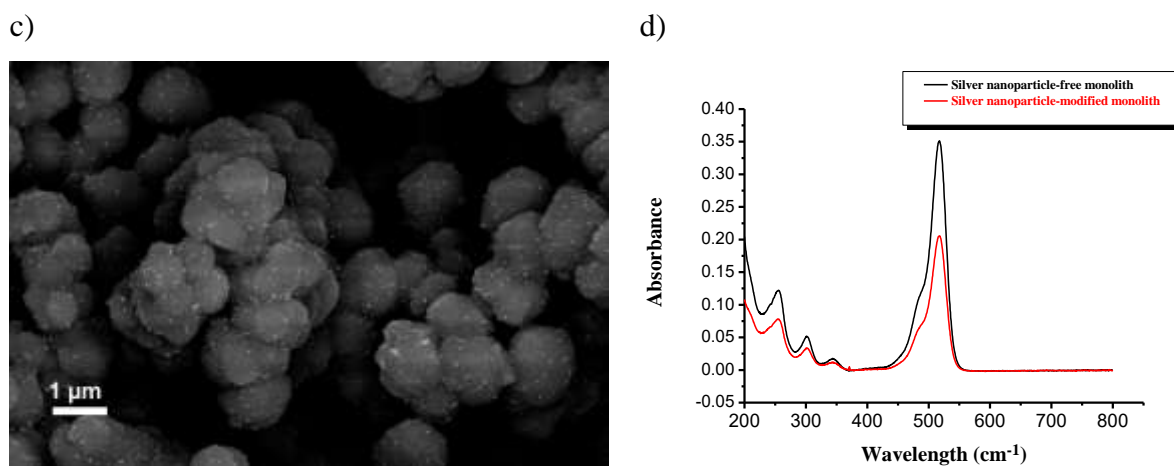


Figure 18: a) Schematic of the synthesis path applied to the preparation of silver modified monolithic microreactor via the surface-grating of mercaptosuccinic acid via photodriven thiol-ene click chemistry. b) Energy dispersive X-ray analysis profile and c) scanning electron microscopy image recorded for the silver nanoparticles-modified monolithic microreactor. d) UV-Vis profile recorded for the product solution collected at the outlet of gold nanosilver-modified monolithic microreactor prepared via on site reduction for the catalytic reduction of eosine using a 10 fold excess of sodium borohydride as reducing agent.

This is illustrated in Fig 18a where mercaptosuccinic acid was grafted on the monolith surface. The so-designed carboxylated monolith served as platform for the immobilization of silver nanoparticles (Fig 18 b and c). Our preliminary results inspired glimpse of portentiality as catalytic microreactor for the reduction of dye pollutants (Fig 18d)

6 References

1. Li, K.; Liu, B. *Chemical Society Reviews* **2014**, *43*, 6570-6597.
2. Kao, J.; Thorkelsson, K.; Bai, P.; Rancatore, B. J.; Xu, T. *Chemical Society Reviews* **2013**, *42*, 2654-2678.
3. Ramesh, G.; Porel, S.; Radhakrishnan, T. *Chemical Society Reviews* **2009**, *38*, 2646-2656.
4. Meer, S.; Kausar, A.; Iqbal, T. *Polymer-Plastics Technology and Engineering* **2016**, *55*, 826-861.
5. Rahman, I. A.; Padavettan, V. *Journal of Nanomaterials* **2012**, *2012*, 8.
6. Mahouche-Chergui, S.; Guerrouache, M.; Carbonnier, B.; Chehimi, M. M. *Colloids and Surfaces A: Physicochemical and Engineering Aspects* **2013**, *439*, 43-68.
7. Zhang, Z.; Wu, Y.; Wang, Z.; Zou, X.; Zhao, Y.; Sun, L. *Materials Science and Engineering: C* **2016**, *69*, 462-469.
8. Zhang, J.; Zhong, L.; Sun, Y.; Li, A.; Huang, J.; Meng, F.; Chandran, B. K.; Li, S.; Jiang, L.; Chen, X. *Advanced Materials* **2016**.
9. Guo, Y.; He, S.; Yang, K.; Xue, Y.; Zuo, X.; Yu, Y.; Liu, Y.; Chang, C.-C.; Rafailovich, M. H. *ACS Applied Materials & Interfaces* **2016**, *8*, 17565-17573.
10. Hussain, M.; Kotova, K.; Lieberzeit, P. A. *Sensors* **2016**, *16*, 1011.
11. Jeon, W.; Lee, S.; Manjunatha, D.; Ban, C. *Analytical biochemistry* **2013**, *439*, 11-16.
12. Fallah TAlooki, E.; Ghorbani, M.; Ghoreyshi, A. A. *Polymer Engineering & Science* **2015**, *55*, 2735-2742.
13. Singh, V. P.; Kapur, G.; Choudhary, V. *RSC Advances* **2016**, *6*, 59762-59774.
14. Murima, D.; Pfukwa, H.; Tiggelman, I.; Hartmann, P. C.; Pasch, H. *Macromolecular Materials and Engineering* **2016**.
15. LU, S.-W.; ZENG, X.-J.; ZHANG, C.-X.; WANG, J.-J.; NIE, P. *Journal of Inorganic Materials* **2014**, *6*, 004.
16. Farooqi, Z. H.; Naseem, K.; Begum, R.; Ijaz, A. *Journal of Inorganic and Organometallic Polymers and Materials* **2015**, *25*, 1554-1568.
17. Cheng, H. H.; Chen, F.; Yu, J.; Guo, Z. X. *Journal of Applied Polymer Science* **2017**, *134*.
18. Wang, S.; Zhang, J.; Yuan, P.; Sun, Q.; Jia, Y.; Yan, W.; Chen, Z.; Xu, Q. *Journal of Materials Science* **2015**, *50*, 1323-1332.
19. Yun, G.; Hassan, Z.; Lee, J.; Kim, J.; Lee, N. S.; Kim, N. H.; Baek, K.; Hwang, I.; Park, C. G.; Kim, K. *Angewandte Chemie International Edition* **2014**, *53*, 6414-6418.
20. Li, W.; Wu, H.; Chen, J.; Xue, H.; Kong, Y. *Synthetic Metals* **2013**, *185*, 56-60.
21. Bronstein, L. M.; Goerigk, G.; Kostylev, M.; Pink, M.; Khotina, I. A.; Valetsky, P. M.; Matveeva, V. G.; Sulman, E. M.; Sulman, M. G.; Bykov, A. V. *The Journal of Physical Chemistry B* **2004**, *108*, 18234-18242.
22. Schmidt, J.; Weber, J.; Epping, J. D.; Antonietti, M.; Thomas, A. *Advanced Materials* **2009**, *21*, 702-705.
23. Kaur, P.; Hupp, J. T.; Nguyen, S. T. *ACS Catalysis* **2011**, *1*, 819-835.
24. Floris, P.; Twamley, B.; Nesterenko, P. N.; Paull, B.; Connolly, D. *Microchimica Acta* **2014**, *181*, 249-256.
25. Khalil, A. M.; Georgiadou, V.; Guerrouache, M.; Mahouche-Chergui, S.; Dendrinou-Samara, C.; Chehimi, M. M.; Carbonnier, B. *Polymer* **2015**, *77*, 218-226.
26. Lv, Y.; Alejandro, F. M.; Fréchet, J. M.; Svec, F. *Journal of Chromatography A* **2012**, *1261*, 121-128.
27. Connolly, D.; Twamley, B.; Paull, B. *Chemical Communications* **2010**, *46*, 2109-2111.
28. Guerrouache, M.; Mahouche-Chergui, S.; Chehimi, M. M.; Carbonnier, B. *Chemical Communications* **2012**, *48*, 7486-7488.
29. Xu, Y.; Cao, Q.; Svec, F.; Frechet, J. M. *Analytical chemistry* **2010**, *82*, 3352-3358.
30. Cao, Q.; Xu, Y.; Liu, F.; Svec, F.; Frechet, J. M. *Analytical chemistry* **2010**, *82*, 7416-7421.
31. Liu, J.; White, I.; DeVoe, D. L. *Analytical chemistry* **2011**, *83*, 2119-2124.
32. Tang, S.; Guo, Y.; Xiong, C.; Liu, S.; Liu, X.; Jiang, S. *Analyst* **2014**, *139*, 4103-4117.
33. Hu, W.; Hong, T.; Gao, X.; Ji, Y. *TrAC Trends in Analytical Chemistry* **2014**, *61*, 29-39.
34. Connolly, D.; Currivan, S.; Paull, B. *Proteomics* **2012**, *12*, 2904-2917.
35. Wu, C.; Liang, Y.; Zhao, Q.; Qu, Y.; Zhang, S.; Wu, Q.; Liang, Z.; Zhang, L.; Zhang, Y. *Chemistry—A European Journal* **2014**, *20*, 8737-8743.
36. Lv, Y.; Lin, Z.; Tan, T.; Svec, F. *Biotechnology and bioengineering* **2014**, *111*, 50-58.
37. Buchmeiser, M. R. *Polymer* **2007**, *48*, 2187-2198.
38. Liu, Z. L.; Zeng, Y. F.; Sun, J. H.; Di Yang, K. *Environmental Chemistry Letters* **2009**, *7*, 149-153.
39. Olmos, C. M.; Chinchilla, L. E.; Villa, A.; Delgado, J. J.; Pan, H.; Hungría, A. B.; Blanco, G.; Calvino, J. J.; Prati, L.; Chen, X. *Applied Catalysis A: General* **2016**, *525*, 145-157.
40. Hu, Z.; Zhao, Y.; Liu, J.; Wang, J.; Zhang, B.; Xiang, X. *Journal of Colloid and Interface Science* **2016**, *483*, 26-33.
41. Savara, A.; Rossetti, I.; Chan-Thaw, C. E.; Prati, L.; Villa, A. *ChemCatChem* **2016**, *8*, 2482-2491.
42. Guo, D.; Wang, Y.; Zhao, P.; Bai, M.; Xin, H.; Guo, Z.; Li, J. *Catalysts* **2016**, *6*, 64.
43. Cruz, P.; Pérez, Y.; del Hierro, I.; Fajardo, M. *Microporous and Mesoporous Materials* **2016**, *220*, 136-147.

44. Zhou, C.; Guo, Z.; Dai, Y.; Jia, X.; Yu, H.; Yang, Y. *Applied Catalysis B: Environmental* **2016**, *181*, 118-126.
45. Gómez-Villarraga, F.; Radnik, J.; Martin, A.; Köckritz, A. *Journal of Nanoparticle Research* **2016**, *18*, 1-18.
46. Miao, M.; Feng, J.; Jin, Q.; He, Y.; Liu, Y.; Du, Y.; Zhang, N.; Li, D. *RSC Advances* **2015**, *5*, 36066-36074.
47. Yan, Y.; Chen, Y.; Jia, X.; Yang, Y. *Applied Catalysis B: Environmental* **2014**, *156*, 385-397.
48. Hong, Y.; Jing, X.; Huang, J.; Sun, D.; Odoom-Wubah, T.; Yang, F.; Du, M.; Li, Q. *ACS Sustainable Chemistry & Engineering* **2014**, *2*, 1752-1759.
49. Dell'Anna, M. M.; Mali, M.; Mastroilli, P.; Cotugno, P.; Monopoli, A. *Journal of Molecular Catalysis A: Chemical* **2014**, *386*, 114-119.
50. Weng, Z.; Wang, J.; Zhang, S.; Yan, C.; Jian, X. *Catalysis Communications* **2008**, *10*, 125-128.
51. Al Badran, F.; Awdry, S.; Kolaczowski, S. *Catalysis today* **2013**, *216*, 229-239.
52. Pud, S.; Kisner, A.; Heggen, M.; Belaine, D.; Temirov, R.; Simon, U.; Offenhäusser, A.; Mourzina, Y.; Vitusevich, S. *Small* **2013**, *9*, 846-852.
53. Narayanan, R.; Lipert, R. J.; Porter, M. D. *Analytical chemistry* **2008**, *80*, 2265-2271.
54. Pradhan, M.; Chowdhury, J.; Sarkar, S.; Sinha, A. K.; Pal, T. *The Journal of Physical Chemistry C* **2012**, *116*, 24301-24313.
55. Jia, W.; Li, J.; Jiang, L. *ACS applied materials & interfaces* **2013**, *5*, 6886-6892.
56. Vianna, P. G.; Grasseschi, D.; Costa, G. K.; Carvalho, I. C.; Domingues, S. H.; Fontana, J.; de Matos, C. J. *ACS Photonics* **2016**.
57. Wang, X.; Wang, H.; Zhang, Q.; Cheng, Y. *Nanomedicine: Nanotechnology, Biology and Medicine* **2016**, *12*, 505.
58. Ko, H.; Son, S.; Bae, S.; Kim, J.-H.; Yi, G.-R.; Park, J. H. *Nanotechnology* **2016**, *27*, 175102.
59. Chadha, T. S.; Park, J.; An, W. J.; Biswas, P. *Journal of Nanoparticle Research* **2014**, *16*, 1-9.
60. Kanchanapally, R.; Sinha, S. S.; Fan, Z.; Dubey, M.; Zakar, E.; Ray, P. C. *The Journal of Physical Chemistry C* **2014**, *118*, 7070-7075.
61. Imura, Y.; Furukawa, S.; Ozawa, K.; Morita-Imura, C.; Kawai, T.; Komatsu, T. *RSC Advances* **2016**, *6*, 17222-17227.
62. Bera, K.; Ghosh, T.; Basak, S. *The Journal of Physical Chemistry C* **2015**, *119*, 1800-1808.
63. Mao, K.; Chen, Y.; Wu, Z.; Zhou, X.; Shen, A.; Hu, J. *Journal of agricultural and food chemistry* **2014**, *62*, 10638-10645.
64. Ma, C.; Du, Y.; Feng, J.; Cao, X.; Yang, J.; Li, D. *Journal of Catalysis* **2014**, *317*, 263-271.
65. Chen, Z.; Yu, X.; Song, Y. *Ferroelectrics* **2016**, *494*, 200-207.
66. Meng, Q.; Bai, J.; Guo, S.; Li, C. *Chemical Research in Chinese Universities* **2015**, *31*, 1072-1077.
67. Ukisu, Y. *Environmental Chemistry Letters* **2015**, *13*, 211-216.

CHAPITRE V

Objectifs

Elaborer des films polymères ancrés de façon covalente sur des substrats de verre et présentant une structure monolithique.

Réaliser un dépôt homogène et dense de nanoparticules d'or de morphologie de type fleur.

Mettre à profit la haute surface spécifique de la morphologie fleur pour des applications en catalyse supportée et en spectroscopie Raman exaltée de surface.

Méthodes

Activation acide et silanisation de substrats en verre pour permettre un ancrage covalent de la structure polymère au cours de l'étape de polymérisation.

Photopolymérisation radicalaire en présence d'un porogène pour générer des films monolithiques présentant une forte porosité.

Réduction de sels d'or à la surface de films monolithiques pour générer des nanofleurs d'or.

Catalyse supportée en batch pour la réduction de composés nitrés.

Mise en œuvre d'un phénomène d'exaltation de surface du signal Raman en utilisant des supports monolithiques 2D modifiés par des nano dépôts d'or.

Limites

Démonstration de la validité de l'approche SERS pour l'analyse de matrices réelles. Toutefois, des essais préliminaires pour la détection de la mélamine dans le lait sont encourageants.

Adhésion robuste de supports monolithiques épais sur des substrats de verre.

Contrôle spatial du greffage des fonctions amine par chimie thiol-ène pour localiser *in fine* les dépôts d'or et préparer des capteurs SERS au format array.

Importance

Matériaux monolithiques nanostructurés à dualité de fonction.

Détection sensible de pesticides à des concentrations compatibles avec la législation en vigueur.

Réactions catalytiques de pesticides en utilisant des nanométaux de morphologie originale supportés sur support plan.

Gold Nano-flowers-decorated monolithic films as versatile platforms for catalysis and SERS Detection applications

Keywords: Monolithic film, Supported gold nano-flowers, Photochemical thiol-ene, SERS, Supported catalysis

Abstract

In this study, we have designed a nanostructured monolithic material with dual functionality with the aim to contribute to two fields of chemistry: namely heterogeneous catalysis and analytical chemistry using surface-enhanced Raman scattering (SERS). Nanostructured gold flowers (GNFs) were synthesized *in situ* and immobilized on the surface of amino-functionalized monolithic polymer. The latter, hereafter poly (NAS-co-EDMA), was synthesized through photo-chemically initiated radical polymerization. A two-step chemical modification strategy was applied involving successive by nucleophilic substitution via allylamine and thiol-ene click with cysteamine. Chemical analysis by Raman spectroscopy allowed us to monitor the success of the surface modification. Molecules with high pollutant potential such as *p*-nitrophenol, pendimethalin and trifluraline were chosen as to evaluate the catalytic activity of the on monolithic film-deposited GNFs for catalytic application into the corresponding amine-containing molecules and sensitive detection by SERS analysis.

1. Introduction

Surface enhanced Raman spectroscopy (SERS) is a powerful method towards the detection of trace level molecules without the need for labelling.^{1,2} Because of its numerous beneficial attributes, SERS has been to date applied for a plethora of applications ranging from the detection of pollutants in water^{3,4} to the detection of viruses⁵, bacteria⁶, vitamins⁷ and drug molecules⁸, defense applications⁹. Indeed SERS is a Raman Spectroscopic method providing great enhancement of the Raman signal through adsorption of Raman-active solutes onto specially prepared metal surfaces. Increases in the intensity of Raman signal allowing detection down to sub-femtomolar limit of detection has been claimed in some cases.¹⁰ SERS is a surface selective and highly sensitive phenomenon where the implementation of “simple” Raman spectroscopy is ineffective. This is because propagation of photons from the incident laser light is confined to the bulk so that it overcomes any Raman signal arising from the analytes at the surface. In other words, SERS selectivity is primarily due to surface-mediated mechanisms. In favourable SERS cases, the surface signal overwhelms the bulk signal, making bulk subtraction unnecessary. One of the major issues with SERS-based sensing systems is the lack of reproducibility and homogeneity of the molecule distribution on the SERS substrate, leading to problems in the quantification. A powerful approach for designing SERS-active substrates relies on the deposition of metal nanostructures on solid supports such as natural rubber latex,¹¹ filter paper,¹² plastic,¹³ metal oxide nanoplatelets¹⁴, porous polymer...to cite but a few. Monolithic supports were also proposed in the form permeable columns or films as supports for metal nanoparticles for SERS applications. Silver nanoparticles were aggregated on the surface of glycidyl-methacrylate (GMA) based monoliths through dynamic loading of the corresponding colloidal solution to design surface enhanced Raman spectroscopy microfluidic devices for trace-detection of proteins.¹⁵ In this case, although nucleophile-sensitive glycidyl-groups were present on the monolith surface, the monolith was used as-obtained after polymerization step without any specific surface treatment. In another implementation, poly(GMA-co-ethylene dimethacrylate) was prepared by UV-initiated polymerization in glass mold, followed by a functionalization step through epoxy-mediated reaction yielding to thiolated monolith and further surface attachment of gold nanoparticles.¹⁶ Living bacteria *Escherichia coli* were detected from highly dilute solution. Monolithic polymers in the form of layers have been also applied for planar chromatography,¹⁷ as platforms for protein¹⁸ and DNA¹⁹ microarray. Herein, we describe the preparation of polymer-gold nanoparticle composite films made of on-monolith surface

attached gold nanoflower and its use as catalytic- and SERS-active support for the reduction and detection of pesticides, respectively.

2. Apparatus

A spectrolinker (XL-1500 UV crosslinker) equipped with six lamps (6x15, 365 nm) obtained from Spectronics, Westbury, NY, USA was used for both photo polymerization and photo grafting steps. Raman microscope Xplora with a laser emitting at 638 nm and provided from Horiba Scientific was used for chemical analysis. Apparatus LEO Gemini 130 scanning electron microscopy (SEM) from Leo Elektronenmikroskopie, Oberkoche in Germany was used for morphology analysis. Structural characterization was performed by X-ray diffraction (XRD) using a D8 advanced Bruker diffractometer. Transmission electron microscopy (TEM, SX 100 CAMECA model) was used for further morphological analysis. UV-Visible spectrophotometer Cary 50 Bio developed by Varian was used for recorded the absorbance of pesticide solution in the UV-visible domain.

3. Chemical products

Slides glass 76 x 26mm x 1.1mm was obtained from Ghäasel. Sulfuric acid, hydrogen peroxide, allylamine, cysteamine, *p*-nitrophenol, pendimethalin, trifluraline, sodium borohydride (NaBH₄), 2, 2'-azobisisobutyronitrile (AIBN), ethylene glycol dimethacrylate, toluene, chloroauric acid, hydrochloric acid, 3-(trimethoxysilyl) propyl methacrylate (30%), acetonitrile (ACN), ethanol, were obtained from Sigma-Aldrich. N-acryloxysuccinimide (NAS) was providing by TCI.

4. Experimental

4.1 Activation and functionalization of glass slide

Glass slide activation was achieved through piranha solution treatment. The piranha solution was prepared by mixing sulfuric acid and hydrogen peroxide 35% in water (70/30: v/v). Firstly, the glass slide was washed with ethanol and dried under nitrogen for 5 min. Then, the slide was dipped in the piranha solution and heated during 1 hour at 100°C. Thereby, silanols groups were formed on the surface. Secondly, the glass slide was washed with ethanol and dried again under nitrogen flow. Finally the glass slide was immersed in a 3-(trimethoxysilyl) propyl methacrylate solution (30% v/v, in toluene) react overnight at room temperature to

allow reaction with silanols groups. At last, the slide was washed with toluene and heated at 70°C for 1 hour. Figure 1 shows the surface hydrophobicity as estimated by goniometry.

4.2 Monolithic film Synthesis

Monolithic polymer film was synthesized by photo-driven free radical polymerization initiated by 2, 2'-azobisisobutyronitrile. The polymerization mixture was composed of N-acryloxysuccinimide (600 mg), ethylene glycol dimethacrylate (400 μL), toluene (2100 μL) and 2, 2'-azobisisobutyronitrile (15 mg). This mixture was solubilized and homogenized under ultrasonic conditions for 15 min at room temperature to obtain a clear solution. Subsequently, it was degassed with nitrogen (15 min). Using a syringe, the solution was placed in a teflon mold deposited on the surface of a piranha-activated slide and covered with another untreated glass slide. The mold assembly was firmly hold by two pincers, and it was placed inside the Spectrolinker XL to initiate the free radical polymerization. The polymerization process was conducted at an overall intensity of 72 J/cm^2 (7200 s). The as-obtained monolith hereafter, poly (NAS-co-EDMA), was washed with acetonitrile for 1 hour in order to remove the porogen and eventually unreacted monomers. The Figure 2 provides schematic illustration of the reaction path.

4.3 Monolithic film functionalization

Surface functionalization included two steps. The first reaction was a nucleophilic substitution type with allylamine and the second was a thiol-ene click reaction with cysteamine. Allylamine solution in acetonitrile (1M) was allowed to react with the monolith during 1 hour at room temperature under gentle stirring. Thereafter, the monolith was washed with ethanol. The second step relied on the photochemical free radical addition of cysteamine (1M in absolute ethanol) using darocur 20% w/w as a photo-initiator. It was conducted at 365 nm. Kinetic of the thiol-ene reaction was studied to optimize the reaction conditions and to ensure high yield of surface functionalization. To do so, the intensity decrease of alkene group Raman signature typical for allylamine was monitored as a function of the reaction time. The Raman results are presented in Figure 3 and Figure 4.

4.4 Gold Nano flower synthesis

Gold Nano flower was immobilized through interaction with monolith bearing chelating primary amine groups as obtained after cysteamine thiol-ene click grafting. Herein, we implemented on *in situ* synthesis approach. To do this, NH₂-modified monolithic film was washed with hydrochloric acid 0.1M during 1hour under gentle stirring. Then, the protonated monolith film was immersed into a solution of HAuCl₄ (0.1 M) for 1 hour and then rinsed thoroughly with water. On site reduction of the surface immobilized metal salt was achieved using hydroxylamine 50% in H₂O as a reducing agent. The on-glass slide covalently attached gold-modified monolith was finally thoroughly washed with water and kept in a clean vial prior to further characterization, SERS and catalysis testing. Figure 5 shows the different steps for gold nanoflower synthesis on the monolithic support.

4.5 Catalytic reduction of nitro aromatic compounds:

To achieve this, aqueous solutions of *p*-nitrophenol (0.5g/L) and NaBH₄ (11g/L) in water were prepared separately and mixed under stirring. Solution of pendimethalin and trifluralin were prepared at a concentration 0,5g/L by solubilizing each compound in water-acetonitrile mixture (90/10). Thus, 300 μ L of the each solution were taken out and diluted in 4 mL of water in three different vials. To highlight the catalytic activities of gold nanoflowers-modified monolithic support, monolithic films (with similar dimensions) were placed in the pesticide solutions in UV cuve and maintained under constant stirring. The catalytic performances were evaluated through monitoring the UV-vis signature of the pesticide as a function of time.

5. Results

5.1 Activation of glass substrates

Success of the surface activation to the glass slide was evaluated through analyzing the shape of a water drop deposited on the surface after the various treatment steps. Such an analysis revealed that the native, untreated, slide as obtained after simple washing with ethanol and drying was rather hydrophilic. The contact angle of the corresponding glass surface was estimated to be about $37^\circ \pm 4^\circ$ (Picture A in Figure 1). On the other hand, the contact angle of the slide after treatment with the piranha solution exhibited a more pronounced hydrophilic character. Indeed, the measured contact angle was much lower and it was estimated to be equal to $13^\circ \pm 3^\circ$ (Picture B in Figure 1). These observations can be rationalized by the

hydrolysis of the silica network-forming siloxane bridges and the resulting presence of silanol units on the surface. Moreover, the glass slide after treatment by the piranha solution and functionalization with 3-(trimethoxysilyl) propyl methacrylate proved to exhibit a more hydrophobic character with a contact angle equal to $98^\circ \pm 3^\circ$ (Picture C in Figure 1). This changes in surface wettability behaviour can be considered, to our point of view, as a qualitative evidence that reaction between silanols groups and 3-(trimethoxysilyl) propyl methacrylate occurred successfully.

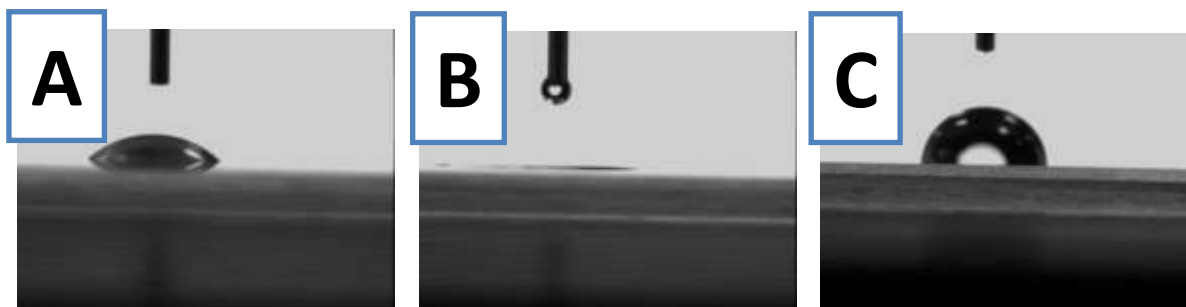


Figure 1: Surface hydrophobicity analysis as estimated by recording the shape of a water drop deposited on A) native glass slide, B) glass slide treated by piranha solution and C) glass slide functionalized with 3-(trimethoxysilyl) propyl methacrylate.

5.2 Synthesis and surface functionalization of monolithic film

The synthesis was carried out in a single step upon photo-polymerization during 2h. Poly(NAS-co-EDMA) monolith as-obtained directly after the polymerization process is characterized by the presence of succinimidyl esters groups, which are known as being very labile in the presence of a nucleophile molecule. The Figure 2 shows the overall synthesis for the preparation of monolith functionalized with gold nanoparticle-affinity ligands. After polymerization, the first functionalization step was a nucleophilic substitution using NHS as leaving group and allylamine as nucleophilic, whose amine end group attacks the electrophilic carbon of NHS ester group. The second surface functionalization step was based on a thiol-ene click radical addition using the intermediate alkene-functionalized monolith and cysteamine. Under the experimental condition, i.e. UV irradiation and radical initiator, thiol group of cysteamine is converted into C=C double bond-reactive sulfhydryl group. Gold nanoparticles were immobilized *via* hydroxylamine-assisted on site reduction of the gold precursor salt after protonation of the primary amine groups of cysteamine through treatment with hydrochloric acid solution (0,1M).

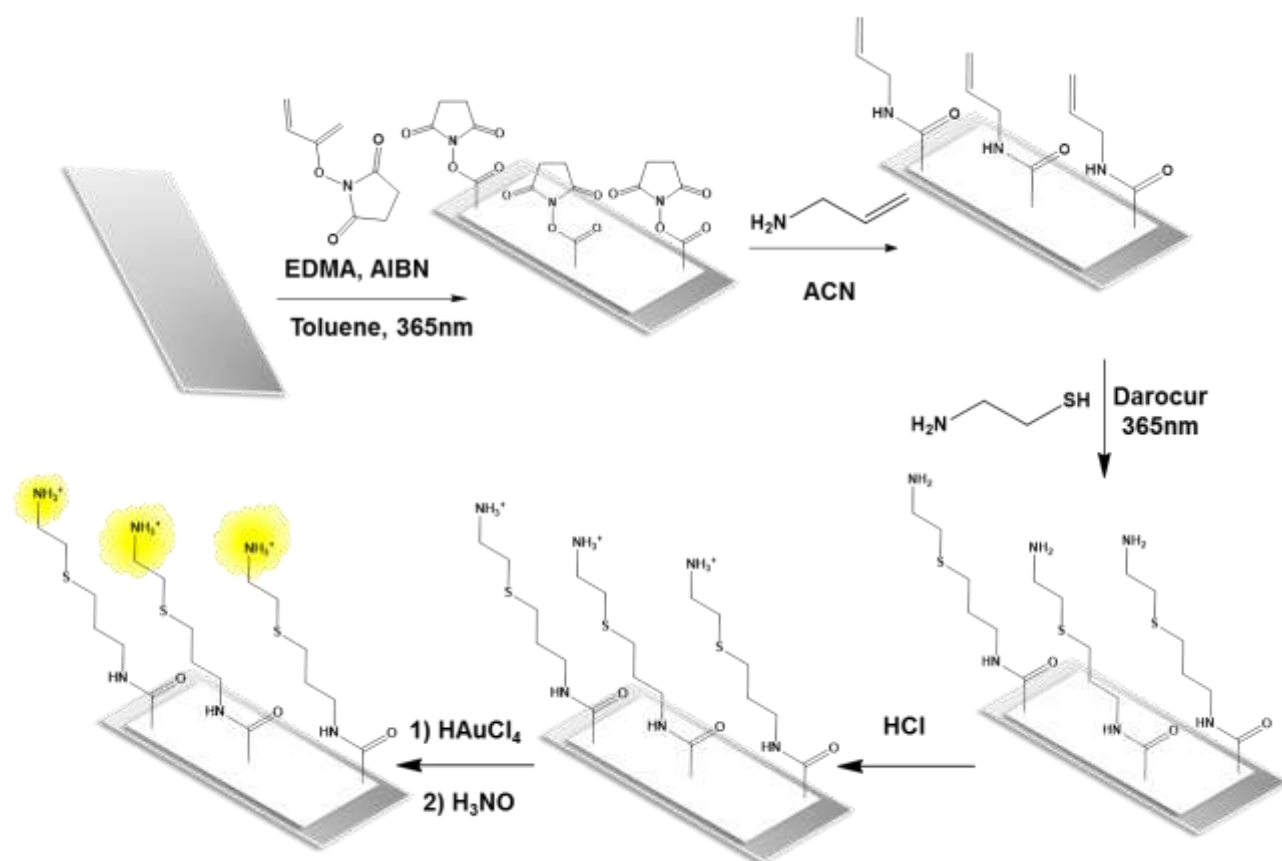


Figure 2: Schematic representation of the synthetic steps applies to the synthesis and further surface functionalization of monolithic films.

5.3 Characterization of the amino-modified monolithic film

Poly (NAS-co-EDMA)-based monolith was synthesized on slide glass. Raman spectroscopy was used as major method to determine the chemical structure of the said porous monolith. Raman spectrum recorded for pristine monolithic polymer as obtained after the photodriven free radical polymerization showed the presence of peaks characteristic for succinimidyl esters in the Raman shift range between 1750 cm^{-1} and 1850 cm^{-1} (Figure 3, line a). With the aim to immobilize metals nanoparticles, a two-step surface modification was implemented. Regarding the nucleophilic substitution step affording the surface grafting of allylamine, quantitative reaction was achieved after a reaction time of 1h. Indeed, the Raman spectrum indicates quantitative consumption of the peaks characteristic for NHS (Figure 3, line b). The Raman signal assigned to the double carbon-carbon bond of allylamine was visible at 1645 cm^{-1} . Upon UV irradiation at 365 nm in the presence of Darocur, thiol-ene radical addition with cysteamine proceeds leading to the intensity decrease of the peak at 1645 cm^{-1} . Raman spectrum (Figure 3, line c) confirms such assumption as it is observed the disappearance of allylamine signal and the appearance of a broad peak (at 3180 cm^{-1} to 3500 cm^{-1})

corresponding the primary amine group of cysteamine and a peak at 1050 cm^{-1} . The latter is attributed to the C-S bond resulting from the covalent surface attachment of cysteamine. Although all these observations evidence the effective occurrence of the grafting of cysteamine through a thiol-ene-like mechanism, the kinetics of the reaction was studied. The kinetic confirmed that progress of the reaction is strongly related to the reaction time. It was found that the consumption of the double bonds by radical-mediated cysteamine grafting reached an optimal reaction yield of 93%. Further increase in the reaction time does not provide further improvement in the yield of the reaction, and the conversion reaches a plateau regime. Plot B in Figure 3 shows the decrease of the Raman signal at 1645 cm^{-1} (corresponding to the double band signal) vs reaction time.

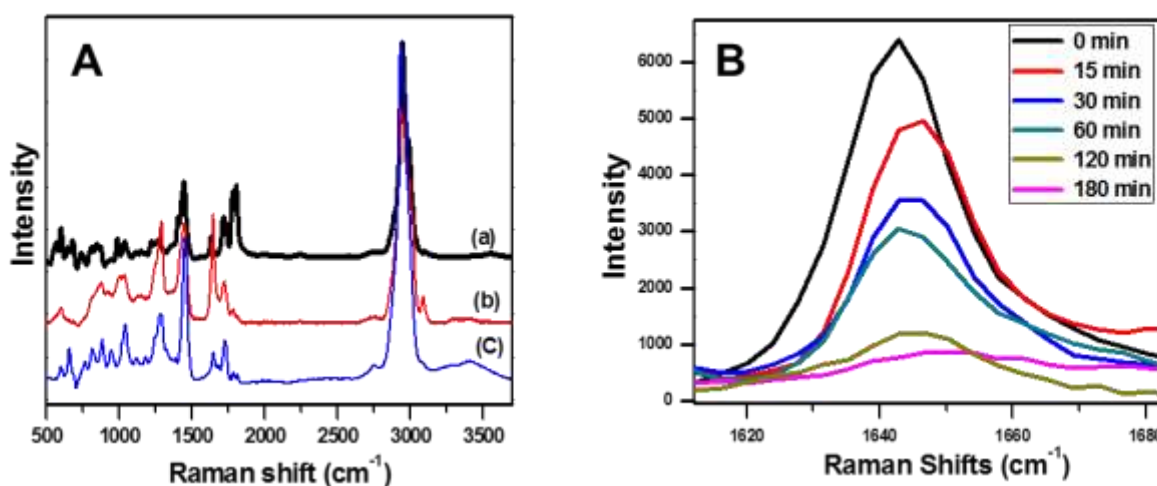


Figure 3: Raman spectra recorded A) for (a) native monolith, (b) allylamine- and (c) cysteamine -modified monoliths and B) for cysteamine-modified monoliths after different time of thiol-ene click reaction.

5.4 Synthesis of gold nanoflowers (GNFs) via on site reduction

After surface functionalization, the monolithic film was washed with hydrochloric acid solution 0,1 M to protonate the primary amine functions. The monolith still retains its initial texture and white color. Once the monolith with tertiary amines was put in contact with the HAuCl_4 solution the monolithic support exhibited yellowish appearance resulting from the chelation metal ions on the monolith surface. Reduction of gold ions by hydroxylamine 50% H_2O into metal gold with zero as oxidation state was optically visible. Indeed, upon reducing step, the monolith changed from yellow to black. The Figure 4 illustrates all these changes.

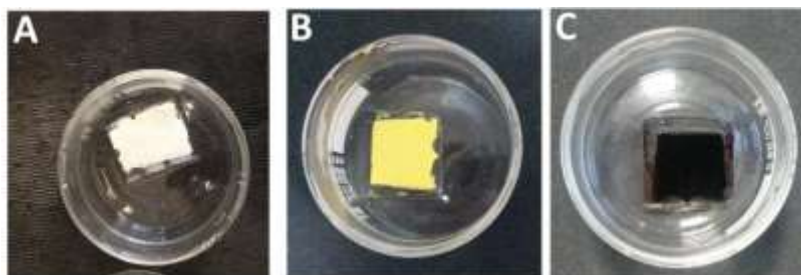


Figure 4: Images showing the change in optical appearance A) from the monolithic film as-obtained after free radical photopolymerization and B) upon chelation of gold metal salt precursor and C) gold nanoparticles synthesis through on site reduction with hydroxylamine.

5.5 Characterization of the gold nanoflower-modified monolithic film

In this part of our work, two types of electron microscopic analyses were used, namely scanning electron microscopy (SEM) and transmission electron microscopy (TEM). Image showing the cross section of the monolithic films (Figure 5 Pictures A) proved the good adhesion of the monolith onto the glass substrate. The monolith exhibits a thickness of about 314 μm which is fitting perfectly to the thickness of the teflon mold. Through enhancing the magnification, pores of the monolith film were clearly visible. Scheme B of Figure 5 shows the monolith with surface immobilized gold nanoflowers. Morphology of these nanostructures is clearly visible at a 200nm scale. The SEM presented in part B in Figure 5 shows a good dispersion of flowers on the monolith surface. No aggregation of the gold flowers was noticed. The size of the gold structure is around 100-200 nm. Herein, we do applied the nano terminology because the individual structures forming the flower structure The TEM images in part C of Figure 5 exhibits more clearly the flower-like morphology of the gold structures exhibiting typical nanometric dimensions. The EDX analysis confirmed the metal nature of gold structures.

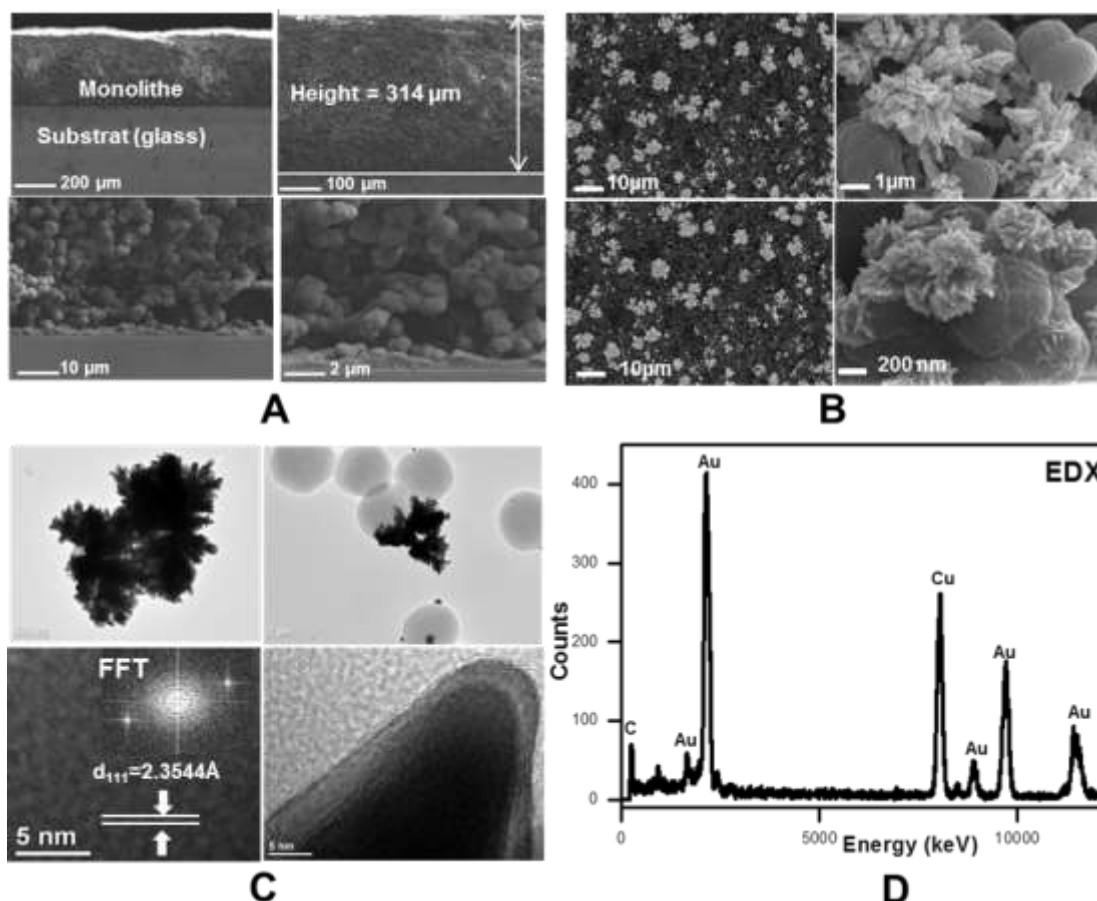


Figure 5: Scanning electron microscopy images of A) native and B) gold modified monolithic films. C) Transmission electron microscopy images of the gold-modified film detached from the glass substrate. D) Energy dispersive X-ray analysis of the gold modified monolithic film.

The as-prepared gold-monolith was also characterized by X-ray Diffraction (XRD). The carried out XRD analysis provided the spectrum shown in part A in the Figure 6 indicating four characteristic peaks at 38.1° , 44.5° , 64.6° and 77.5° for the indices (111), (200), (220) and (311), respectively. These results prove the gold crystal structure and corroborate the EDX analysis. A thermal analysis under nitrogen was done with the aim to quantify the amount of gold immobilized on the surface of the monolithic film. Two monolithic samples with dimension of 0.5 cm^2 were scraped off the glass substrate. One of the sample was a gold-free monolith while the second was gold-modified one. The samples were analyzed in the temperature range from 0°C to 800°C . The plots in part B in Figure 6, show a mass loss of 83, 2% for the gold-free monolith. On the other hand, the monolith decorated with gold exhibited a mass loss of only 57%. The difference between these two measurements allowed us to estimate the gold content to 26, 2%.

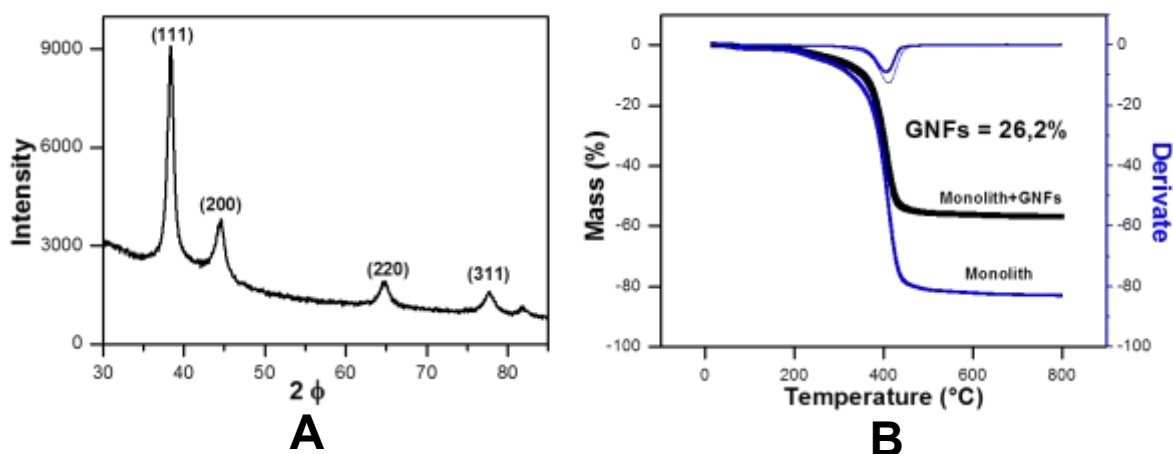


Figure 6: Characterization of the gold-modified monolith by A) X-ray diffraction and B) thermogravimetric analysis.

5.6 Catalytic application of gold nanoflower-modified monolith

The catalytic properties of gold-modified monolith was evaluated *via* the reduction of nitroarenes compounds to the corresponding amines in the presence of NaBH_4 as reducing agent. The compounds used for catalytic tests have been carefully selected. They are food pollutants used as a pesticide and dye currently used in textile industry, respectively. Pendimethalin and trifluraline are often used in agriculture as herbicide and *p*-nitrophenol is used in textile industry. The catalytic test was initially performed with the 4-nitrophenol. A kinetic study was performed. The solution of the 4-nitrophenol with NaBH_4 corresponding to a green yellow color was prepared as described in the experimental section and was added in the presence of the catalyst under stirring. A UV-vis analysis measurement was performed every 5 min. At each successive measurement, we noticed a change in the solution color corresponding to the decrease of the characteristic peak of 4-nitrophenol in sodium borohydride solution visible at 400 nm. Moreover a peak appeared at 300 nm corresponding to the aminophenol. After 15 minutes, we noticed a total disappearance of the peak of *p*-nitrophenol corresponding to a change from green yellow colored solution to a colorless solution which indicates complete conversion of all NO_2 to NH_2 (Figure 7A). Similarly to the case of *p*-nitrophenol, the two pesticides were reducing to a significant extent after 15 minutes

of reaction under stirring in the presence of the catalyst. Plots C and D in Figure 7 present the corresponding UV-vis spectra attesting the effective reduction of trifluraline and pendimethalin, respectively. However, we noted in the case of trifluraline that the reaction was not complete after 15 minutes.

The catalytic conversion efficiency of 4-NP (CE_{NP} (%)) was calculated by monitoring the absorbance decrease of the band at 400 nm using the following equation.

$$CE_{NP} (\%) = [(A_0 - A_t) \div A_0] \times 100$$

Where A_t is the absorbance of 4-NP ($\lambda=400$ nm) at any time t and A_0 is the initial absorbance of 4-NP measured at zero time

Time required to entire reduce compounds is 15 minutes with the rate catalyst activity parameter of $k = 0.275$ min.

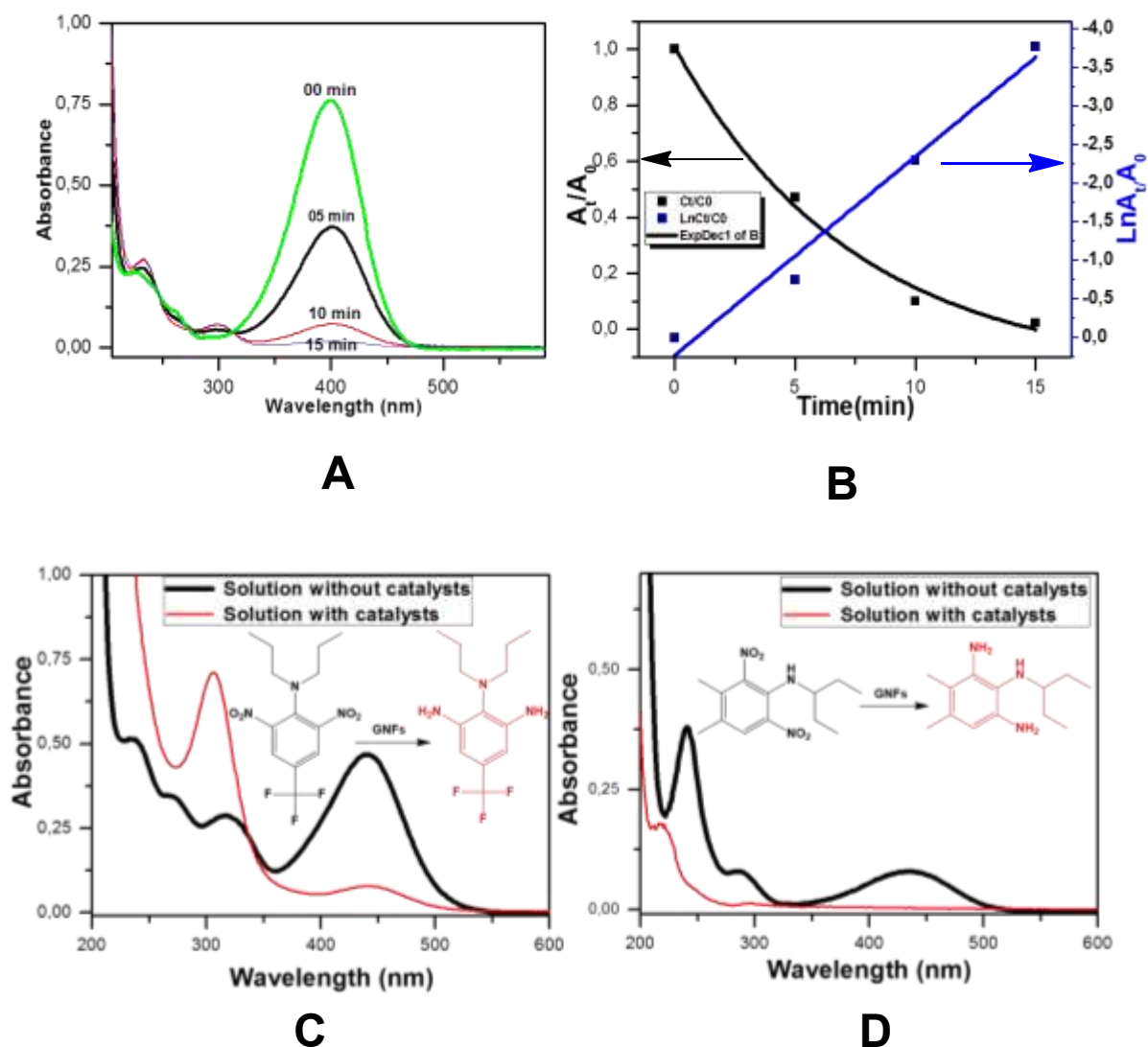


Figure 7: UV-vis absorption spectra recorded for the reduction of A) p-nitrophenol, C) trifluraline and D) pendimethalin using amino monolith-supported GNPs as nanocatalysts and NaBH₄ as reducing agent. The reaction was performed in aqueous solution and UV-Vis spectra were recorded every 5 min. B) plot of logarithm of (A/A₀) at 400 nm vs reduction time for the case of 4-nitrophenol.

5.7 Surface-enhanced Raman scattering (SERS) application of gold nanoflower-modified monolith

SERS is a powerful, non-destructive technique allowing to investigate the spectral signature of a molecule. The first parameter to take into account is the choice of enhancing substrate. In our case, the substrate was composed of monolith decorated with gold Nano-flower as described in the above part of this manuscript. We highlight here few exciting applications of SERS as a very sensitive technique for the detection of pollutant molecules with high toxic

potential at low concentration. Three molecules were chosen for this application such as: *p*-nitrophenol, pendimethalin and trifluraline. All are pollutants and frequently used in various fields. Four solutions of each compound mentioned above were prepared in different concentrations ranging from 10^{-5} M to 10^{-8} M through dilution of stock solutions. First, the spectral fingerprint of the monolithic matrix (enhancing subtract) was recorded in order to differentiate any other parasite spectra arising from the matrix surface. Although some changes can occur between the Raman spectroscopy and surface enhanced Raman spectroscopy variants each raw analyte was analyzed in solid state by Raman spectroscopy (Figure 8). Then, analysis was performed for highly diluted solutions deposited on the surface of the gold-modified monolith substrate. Henceforth the material was dried and placed under the Raman laser light for analysis. This protocol was repeated for the different samples at different concentration starting with the lowest concentration. Analysis of pure trifluraline showed a peak at 1092 cm^{-1} that was considered as a finger print of the molecule. The surface-enhanced analysis of this product showed a signal shifted to about 1000 cm^{-1} . Intensity of this signal decreases with the concentration but it was still visible to 10^{-8} M. As for the trifluraline analysis, a dilute solution of *p*-nitrophenol 10^{-8} M was analyzed. Here again, the detection was still possible with a solution diluted to 10^{-8} M. Finally, analysis was performed for pendimethalin the peak at 1002 cm^{-1} was visible at a pendimethalin concentration 10^{-8} M.

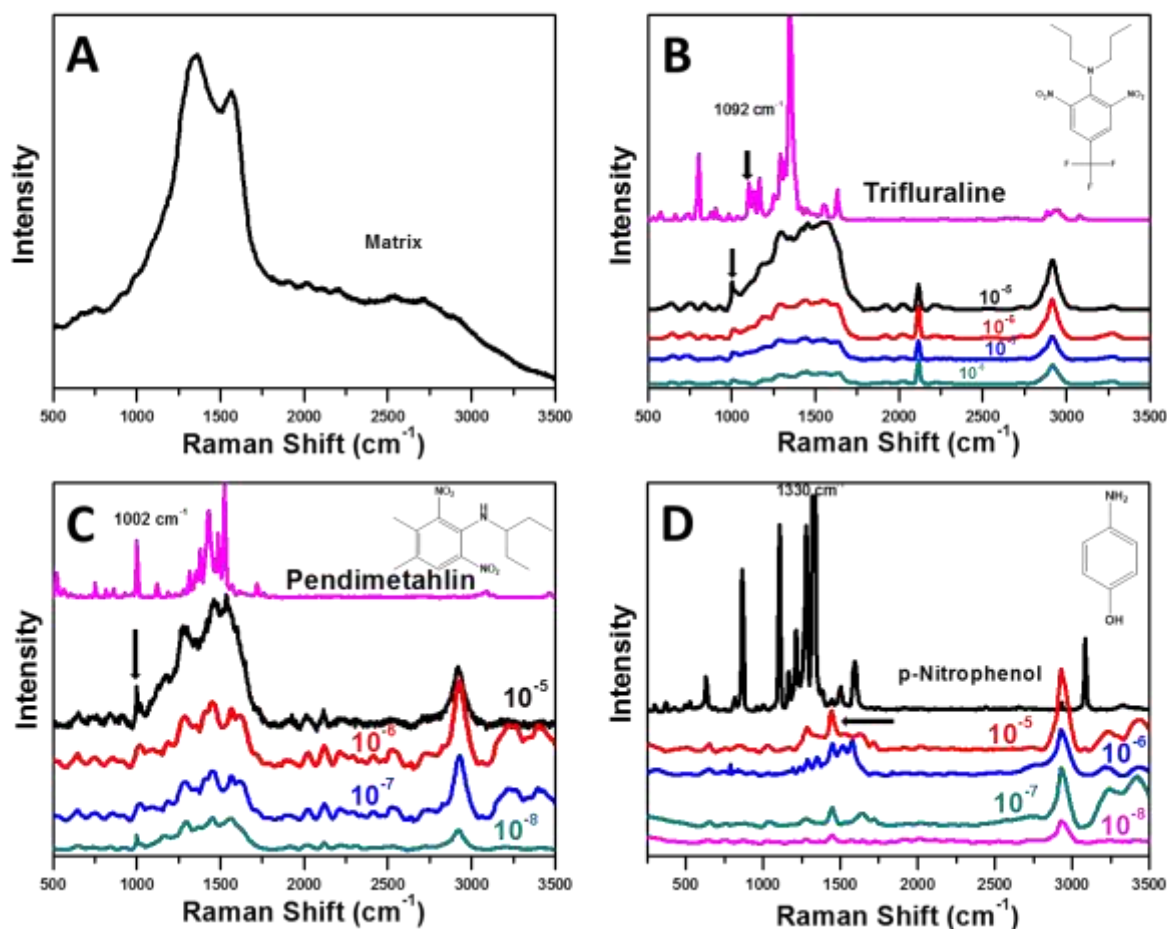


Figure 8: Surface-enhanced Raman scattering analysis of A) monolithic matrix, B) trifluraline, C) pendimethalin and D) p-nitrophenol. The concentrations are indicated in the figure.

6. Conclusion

Herein, we report on our preliminary results meant for the design of gold modified films with dual potentialities as supported catalytic supports and surface enhanced Raman spectroscopy (SERS) active substrate. The monolith was prepared by photoinitiated free radical polymerization on glass substrate bearing polymerizable methacrylate units. The monolith, incorporating N-acryloxysuccinimide as reactive monomer, was successfully functionalized to introduce amino groups. The latter served as anchoring sites for gold. Herein, we opted for a flower-like morphology of the gold to (i) enhance the surface area (ii) and roughness structure of the metal that are considered as beneficial to catalysis and SERS applications. Although further study is required to fully assess the properties of these materials, we have shown the successful detection and catalytic reduction of some toxic molecules.

7. References

1. Sun, X.; Li, H. *Current Nanoscience* **2016**, *12*, 175-183.
2. McNay, G.; Eustace, D.; Smith, W. E.; Faulds, K.; Graham, D. *Applied spectroscopy* **2011**, *65*, 825-837.
3. Hao, J.; Han, M.-J.; Han, S.; Meng, X.; Su, T.-L.; Wang, Q. K. *Journal of Environmental Sciences* **2015**, *36*, 152-162.
4. Zhou, N.; Meng, G.; Huang, Z.; Ke, Y.; Zhou, Q.; Hu, X. *Analyst* **2016**, *141*, 5864-5869.
5. Luo, S.-C.; Sivashanmugan, K.; Liao, J.-D.; Yao, C.-K.; Peng, H.-C. *Biosensors and Bioelectronics* **2014**, *61*, 232-240.
6. Qiu, L.; Wang, W.; Zhang, A.; Zhang, N.; Lemma, T.; Ge, H.; Toppari, J. J.; Hytönen, V. P.; Wang, J. *ACS Applied Materials & Interfaces* **2016**, *8*, 24394-24403.
7. Radu, A. I.; Kuellmer, M.; Giese, B.; Huebner, U.; Weber, K.; Cialla-May, D.; Popp, J. *Talanta* **2016**, *160*, 289-297.
8. Yang, L.; Gong, M.; Jiang, X.; Chen, Y.; Han, X.; Song, K.; Sun, X.; Zhang, Y.; Zhao, B. *Colloids and Surfaces A: Physicochemical and Engineering Aspects* **2016**, *508*, 142-149.
9. Nuntawong, N.; Eiamchai, P.; Limwichean, S.; Horprathum, M.; Patthanasettakul, V.; Chindaudom, P. In *Defence Technology (ACDT), 2015 Asian Conference on*; IEEE, 2015, pp 92-96.
10. Tabatabaei, M.; Najiminaini, M.; Davieau, K.; Kaminska, B.; Singh, M. R.; Carson, J. J.; Lagugné-Labarhet, F. o. *ACS Photonics* **2015**, *2*, 752-759.
11. Tao, J.; He, D.; Tang, B.; Kong, L.; Luo, Y.; Zhao, P.; Gong, W.; Peng, Z. *RSC Advances* **2015**, *5*, 49168-49174.
12. Raza, A.; Saha, B. *Forensic science international* **2014**, *237*, e42-e46.
13. Bianco, G. V.; Losurdo, M.; Giangregorio, M. M.; Capezzuto, P.; Bruno, G. *Plasmonics* **2013**, *8*, 159-165.
14. Yang, H.; Ni, S.-Q.; Jiang, X.; Jiang, W.; Zhan, J. *CrystEngComm* **2012**, *14*, 6023-6028.
15. Liu, J.; White, I.; DeVoe, D. L. *Analytical chemistry* **2011**, *83*, 2119-2124.
16. Cao, Y.; Lv, M.; Xu, H.; Svec, F.; Tan, T.; LV, Y. *Analytica Chimica Acta* **2015**, *896*, 111-119.
17. Maksimova, E.; Vlakh, E.; Tennikova, T. *Journal of Chromatography A* **2011**, *1218*, 2425-2431.
18. Sinitsyna, E.; Vlakh, E.; Rober, M. Y.; Tennikova, T. *Polymer* **2011**, *52*, 2132-2140.
19. Sinitsyna, E. S.; Walter, J. G.; Vlakh, E. G.; Stahl, F.; Kasper, C.; Tennikova, T. B. *Talanta* **2012**, *93*, 139-146.

Conclusion Générale

Le but de notre étude était l'utilisation de monolithes organiques comme phases stationnaires pour des applications en électrochromatographie et comme supports de nanoparticules métalliques pour des applications en catalyse. Le squelette monolithique utilisé se caractérise par la présence (i) de macropores conférant des propriétés de perméabilité remarquables, et (ii) des fonctions réactives en surface permettant une fonctionnalisation chimique de surface aisée. (i) permet d'envisager ces matériaux monolithiques à différents domaines de la chimie en flux telle que la chimie analytique pour la séparation électrochromatographique de phénols, anilines, hydrocarbures aromatiques polycycliques, bases pyrimidiques, parabènes, polychlorobiphényles et la catalyse supportée. En effet, même après immobilisation de nanoparticules à la surface des pores des monolithes, ces derniers demeurent hautement perméables, notamment lorsque l'immobilisation des nanoparticules a été réalisée par réduction sur site de sels métalliques précurseurs. (ii) permet de contrôler les propriétés de surface des monolithes par la nature des greffons moléculaires immobilisés en surface. Des monolithes polaires ont été simplement préparés par immobilisation de fonctions diol via une réaction de chimie click de type thiol-ène. Le greffage de segments moléculaires riches en unités phényle transforme le monolithe en matériau apolaire et capable d'interagir *via* le recouvrement des orbitales pi entre sélecteur et soluté. L'immobilisation de groupes porteurs de fonctions amine primaires génère des sites de chélation assurant la fixation de nanoparticules métalliques (or et palladium). En fonction de la nature des nanoparticules, des nitro-phénols peuvent être convertis en nitro-amines par action de borohydrure de sodium, de l'alcool benzylique peut, en présence de peroxyde d'hydrogène, être oxydé en benzaldéhyde ou en acide benzoïque en fonction de la température de réaction, le bromobenzène et le acide phénylboronique peuvent former le produit de couplage selon le mécanisme dit de Suzuki-Miyaura pour donner le diphenyle.

La méthode de réduction *in situ* des nanoparticules d'or mentionnée ci-dessous offre la possibilité de varier la morphologie des nanoparticules depuis des formes classiques sphériques vers des morphologies plus exotiques telles que des nanofleurs d'or. Ces morphologies sont obtenues en utilisant respectivement le borohydrure de sodium et l'hydroxylamine comme agents réducteurs. Ces morphologies déposées à la surface de films monolithiques permettent d'induire une exaltation du signal Raman, permettant de détecter des pesticides à de très faibles concentrations.

Une des nouveautés portée par ce document est l'utilisation de la chimie interfaciale des sels de diazonium pour immobiliser de façon covalente des nanoparticules d'or. La stabilité du dépôt a permis des applications en catalyse hétérogène. L'intermédiaire de synthèse, un monolithe modifié en surface par des groupements aniline a démontré par ailleurs des propriétés intéressantes en électrochromatographie capillaire.

Au cours de ce travail de thèse, un nouveau monomère a été envisagé pour la préparation de monolithes génériques. Ce monomère est la thiolactone. Les résultats obtenus n'ont pas fait l'objet d'un chapitre dans ce document même si les résultats ont déjà apporté la preuve de concept.

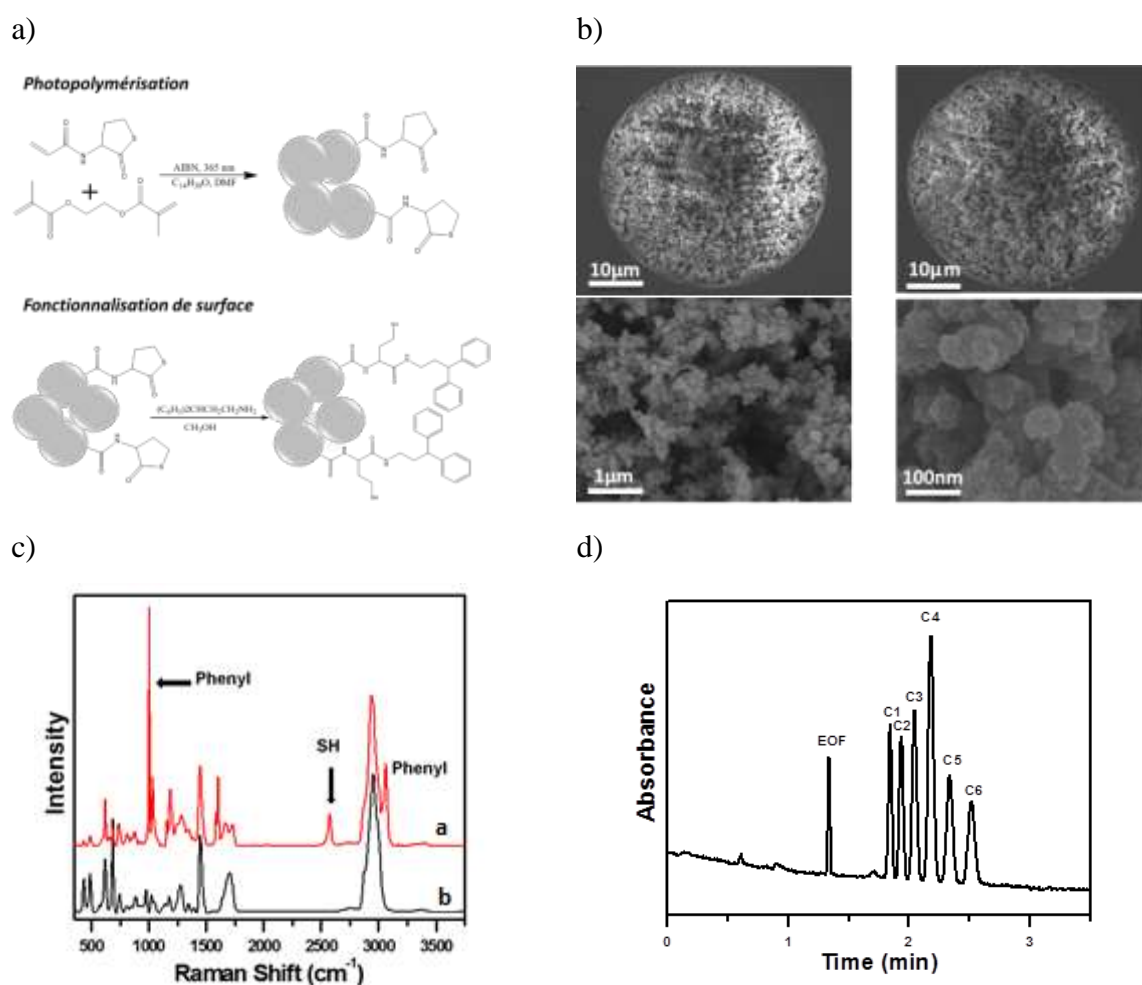


Figure 1 : a) Représentation schématique des voies de synthèse et de fonctionnalisation d'un monolithe à base de thiolactone. b) Images de microscopie électronique à balayage obtenues à différents grossissements pour le monolithe à base de thiolactone. c) Spectres Raman obtenus pour le monolithe à base de thiolactone a) directement après la photopolymérisation et b) après la fonctionnalisation de surface. d) Exemple de séparation électrochromatographique obtenue avec le monolithe à base de thiolactone fonctionnalisé par le 3,3-diphenylpropylamine. Conditions CEC : pH 8, phase mobile : 60/40 (ACN/PBS 5mM),

tension 15 kV, injection 5 kV, 5 s, 25°C, detection 214 nm. C1 :Toluène, C2 : Ethylbenzène, C3 : Propylbenzène, C4 : Butylbenzène, C5 : Pentylbenzène, C6 : Phénylhexane.

La thiolactone (110 mg) peut être polymérisée sous irradiation UV à 365 nm avec le diméthacrylate d'éthylène glycol (50 µL), en présence de diméthylformamide (250 µL) et de tétradodécanol (150 mg) comme porogènes et d'AIBN comme amorceur (Figure 1a, panel du haut). La structure ainsi obtenue est caractéristique des monolithes et présente une macroporosité compatible avec des applications en flux continu. Un premier essai de fonctionnalisation a été réalisé avec un composé modèle, le 3,3-diphénylpropylamine qui peut facilement être mis en évidence par sa signature spectrale typique des cycles aromatiques. La figure 1c atteste du succès de l'étape de fonctionnalisation. Le monolithe greffé par des sélecteurs diphényle a pu être utilisé en électrochromatographie pour la séparation de six alkylbenzènes (Fig 1d). Les solutés sont séparés en fonction de leur hydrophobie, i.e. le temps de rétention augmente lorsque la longueur de la chaîne aliphatique augmente. Une perspective au travail proposé dans ce manuscrit serait d'utiliser cette nouvelle matrice monolithique qui permet d'envisager une double fonctionnalisation *via* l'ouverture du cycle comme montré dans la Fig 1a pour 3,3-diphénylpropylamine mais aussi *via* la fonction thiol qui en résulte. Des réactions de chimie Click de type thiol-ène tout comme l'immobilisation de nanoparticules d'or stabilisées par des liaisons Au-S peuvent être envisagées. Une autre voie serait d'oxyder la fonction thiol en sulfate ce qui générerait des fonctions au caractère acide fort et donc une possibilité de générer un flux électro-osmotique indifféremment de la valeur du pH du milieu environnant.

Résumé

Les matériaux polymères ont connu un engouement considérable avec l'avènement de l'ère du pétrole et connaissent aujourd'hui encore un succès considérable notamment au travers de la valorisation de ressources naturelles mais également d'applications spécifiques à haute valeur ajoutée, liées à des domaines aussi divers que la chimie analytique, l'exploration spatiale, la médecine où l'enjeu premier est souvent la conception d'objet miniaturisés. Dans ce travail de thèse nous avons développé des matériaux polymères à taille micrométrique, immobilisés soit dans des microcanaux (diamètre interne = 75 μm) ou à la surface de substrats de verre (épaisseur de quelques centaines de μm). Une morphologie de type monolithique a été choisie afin de conférer auxdits matériaux des propriétés de perméabilité, résistance mécanique et thermique compatibles avec des applications dans le domaine de la chimie en flux. Afin de contrôler les propriétés d'interaction aux interfaces des matériaux, un monolithe générique, présentant des unités ester de N-hydroxysuccinimide en surface, a été préparé et fonctionnalisé à façon. Ainsi ont été immobilisés des segments moléculaires jouant le rôle de sélecteurs – *pour des applications en électrochromatographie* – ou de ligands de nanoparticules métalliques – *pour applications en catalyse supportée* – via des méthodes classiques (substitution nucléophile) ou originales (photo-addition radicalaire thiol-ène) de greffage.

Les matériaux ont été caractérisés par une combinaison de méthodes spectroscopiques, microscopiques, de diffraction, de thermogravimétrie permettant de corréler les propriétés électrochromatographiques ou catalytiques avec la structure interfaciale des matériaux monolithiques. A titre d'exemples d'application, nous pouvons citer la séparation électrochromatographiques de molécules toxiques tels les polluants organiques (aniline, phénols, hydrocarbures aromatiques polycycliques, polychlorobiphényles) et les conservateurs pour les crèmes cosmétiques (parabènes), de biomarqueurs (hydrocarbures aromatiques polycycliques, bases pyrimidiques). Ces analyses ont été réalisées avec des solutions modèles de laboratoire mais aussi des matrices réelles (crèmes cosmétiques, analogues d'échantillons extraterrestres). Aussi les réactions catalytiques de réduction de nitroarènes, d'oxydation d'alcool aromatique, de couplage carbone-carbone et la détection par spectroscopie Raman exaltée de surface de pesticides (trifuraline) et d'intermédiaires de synthèse (para-nitrophénol) ont été réalisées.

Abstract

Polymeric materials have gained immense popularity with the golden age of petroleum and they still today meet with great success through Green polymer chemistry approaches and numerous high added value dedicated application in scientific domains such as analytical chemistry, medicine, space investigations, where one of the key for success is the design of miniaturized objects. In this contribution, micro-sized monolithic materials have been designed though either in microchannel immobilization (I.D. = 75 μm) or surface attachment on glass substrates (hundredths of microns in thickness). Polymers exhibiting monolithic morphology were considered to benefit of high permeability, mechanical and thermal resistances which are mandatory to flow chemistry applications. With the aim to control the interfacial interaction ability, a generic monolith having N-hydroxysuccinimide ester groups was used and on purpose functionalized. Molecular segments acting as selector – *for electrochromatographic applications* – of metal nanoparticles ligands – *for supported catalysis applications* – have been immobilized on the monolith surface via classical (nucleophilic substitution) or original (photo-induced thiol-ene click) grafting reactions.

The so-designed materials were characterized through spectroscopic, microscopic, diffraction, thermogravimetric methods providing insight into correlation between the observed separation and catalytic abilities and the interfacial structure of the monolith. As representative examples of application, one may cite the electrochromatographic separation of toxic molecules such as organic pollutants (phenols, anilines, polycyclic aromatic hydrocarbons, polychlorobiphenyls), preservatives in cosmetics (parabens) and biomarkers (polycyclic aromatic hydrocarbons, pyrimidic bases). The analyses were conducted on model solutions and complex matrices (cosmetics, extraterrestrial analog samples). Flow catalytic reaction meant for the reduction of nitroarenes, the oxidation of aromatic alcohol, the carbon-carbon coupling and the sensitive detection of pesticides and synthesis intermediates (para-nitrophenol) have been achieved.